SELECTED
TOPICS
IN

Identification Modelling and Control

Volume 7, 1994

Edited by O.H. Bosgra and P.M.J. Van den Hof

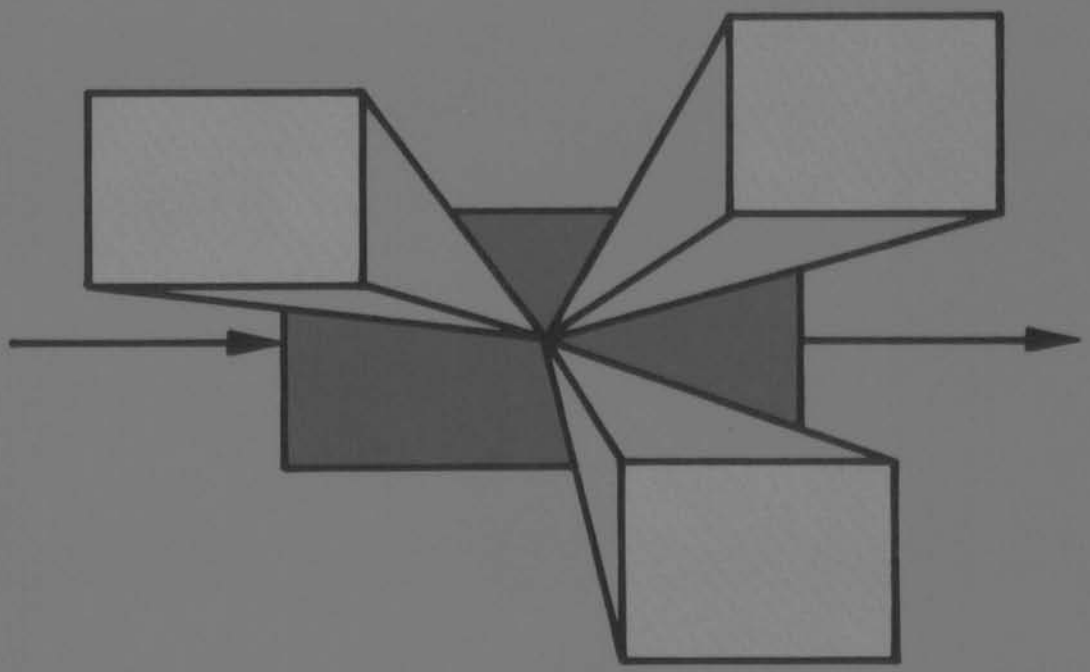

Delft University Press

IDENTIFICATION, MODELLING AND CONTROL

SELECTED TOPICS IN IDENTIFICATION, MODELLING AND CONTROL

Progress Report on Research Activities in the Mechanical Engineering Systems and Control Group

Edited by O.H. Bosgra and P.M.J. Van den Hof

Volume 7, December 1994

Mechanical Engineering Systems and Control Group
Delft University of Technology

Delft University Press/1994

Published and Distributed by

Delft University Press
Stevinweg 1
2628 CN Delft
The Netherlands
Tel.: (0)15 - 783254
Telefax: (0)15 - 781661

By order of

Mechanical Engineering Systems and Control Group
Delft University of Technology
Mekelweg 2, 2628 CD Delft
The Netherlands
Tel.: +31-15-786400; Telefax: +31-15-784717
email: arkesteijn @tudw03.tudelft.nl

CIP-GEGEVENS KONINKLIJKE BIBLIOTHEEK, DEN HAAG

Selected

Selected topics in identification, modelling and control:
progress report on research activities in the mechanical engineering
systems and control group. - Delft:Mechanical Engineering Systems and Control Group,
Delft University of Technology, Vol. 7-ed. by O.H. Bosgra and
P.M.J. Van den Hof.-ill. Met lit.opg.
ISBN 90-407-1077-5
SISO 656 UDC 531.7 + 681.5 NUGI 841

Cover design by Ruud Schrama

Contents

Volume 7, December 1994

Editorial

This is the seventh volume in the series *Selected Topics in Identification, Modelling, and Control* reporting on current research projects in the *Mechanical Engineering Systems and Control Group* at Delft University of Technology, Delft, The Netherlands. This volume contains 13 papers, of which 6 address engineering modelling and control problems and the other 7 consider methods and techniques for control design and system identification. This reflects the general pattern of activity in our group, where the research is both addressing theoretical issues in control theory and system identification, as well as control engineering issues in the fields of process control and motion servo systems.

An industrial *glass tube manufacuring process* is considered in the paper by *Richard Hakvoort* and *Dick de Roover*, where issues of system identification-based model uncertainty are studied in their relevance to robust control. A full scale *wind turbine power generating system* is considered by *Gregor van Baars*, where the validation of dynamic system models on the basis of closed-loop system identification experiments is discussed. A large pilot-scale *industrial crystallizer* is considered in the paper by *Rob Eek, Jaap Both* and *Paul Van den Hof*. The research reported here is part of a collaborative project, jointly with the Particle Technology, Process Equipment, and Crystallization groups at Delft University, and co-sponsored by European and US industrial process industries. Here, system identification experiments are used not only to obtain dynamic models for control purposes, but the experimental evidence also reveals important information on the actual physical mechanisms taking place in a continuous crystallizer.

The paper by *Hans Heintze* and *Ton Van der Weiden* considers the feedback design of impedance control for a hydraulically actuated robot. The project is part of a collaborative effort with industry to develop a *brick-laying robot*. The experimental work reported has been performed on a large scale prototype 3-DOF SCARA robot available in our laboratory. The paper by *Gert van Schothorst, Piet Teerhuis* and *Ton van der Weiden* considers a hydraulic servo system which is designed as an actuation mechanism for the *SIMONA Flight Simulator* to be located at the Simona Research Center operated by the Department of Aerospace Engineering at Delft University. This simulator is a large 6-DOF Stewart platform, now under construction and planned to be available by the end of 1995. The research project is a collaborative effort between three university research groups of Delft University, industry and the national aerospace research laboratory *NLR*. Finally, the paper by *Henk Huisman* discusses a new approach to torque ripple minimization in brushless DC motors. In precision drive systems such as video scanners, it is of utmost importance to have mass produced, cheap motors displaying high servo control performance.

Robust control issues are discussed in several papers. Some preliminary results on an uncompromised $\mathcal{H}_2/\mathcal{H}_\infty$ optimal control problem are given in the paper by *Maarten Steinbuch* and *Okko Bosgra*. As a contribution to the recent interest in *LMI-based robust control* problem formulations, the paper by *Carsten Scherer* has results on the solvability of Lyapunov inequalities. The issue of model reduction for control design is considered in the paper by *Pepijn Wortelboer* and *Okko Bosgra*, where frequency weighted versions of the $\mathcal{H}_2$ optimal reduction problem are studied. Some unifications of robust stability theory for fractional uncertainty models are presented in the paper by *Raymond de Callafon, Paul Van den Hof* and *Peter Bongers*. Finally, in the paper by *Dick de Roover* the servomechanism problem with finite horizon is considered, using an approach in which ideas of feedforward three-degrees-of-freedom control, predictive control, the internal model principle, and repetitive control, are combined.

In the present issue there finally are two contributions on the methodology of *system identification*. The paper by *Ramond de Callafon* and *Paul Van den Hof* discusses a feedback relevant identification approach using coprime fractional model representations. The assessment of frequency domain uncertainty bounds from system identification experiments is discussed in the paper by *Richard Hakvoort* and *Paul Van den Hof*.

We wish to acknowledge the important contributions to the work in the group made by colleagues from industry. In this issue we have contributions by *Maarten Steinbuch* and *Pepijn Wortelboer* from *Philips Research*, and by *Peter Bongers* from *Unilever Research*.

If you wish to react to any of the papers in this volume, please do not hesitate to contact us.

Okko Bosgra bosgra@tudw03.tudelft.nl
Paul Van den Hof vdhof@tudw03.tudelft.nl
Editors

Selected Topics in Identification, Modelling and Control
Vol. 7, December 1994

Robust performance H_2/H_∞ optimal control[‡]

Maarten Steinbuch [§] and Okko H. Bosgra[♯]

[§] *Philips Research Laboratories, Prof. Holstlaan 4, 5656 AA Eindhoven, The Netherlands.*
[♯] *Mechanical Engineering Systems and Control Group,*
Delft University of Technology, Mekelweg 2, 2628 CD Delft, The Netherlands.

Abstract. This paper considers the robust performance mixed H_2/H_∞ optimal control problem formulation. An explicit parametrization of H_∞ norm bounded, causal, real-rational uncertainties is used, based on LMIs. This leads to a constrained H_2 optimal control problem. In case the uncertainty can be considered to lie on its bound, a new parametrization for lossless bounded real functions can be used. Using this parametrization, it is possible to formulate an unconstrained optimization problem for the solution of the robust performance mixed H_2/H_∞ optimal control problem. The theory is applied to a Compact Disc robust control problem.

Keywords. H_2/H_∞ control; optimal control; robust control; compact disc player; uncertainty; optimization.

1 Introduction

In the sixties the optimal LQG control approach provided a systematic solution to the control design problem of multivariable systems, see for instance Anderson and Moore (1971), Kwakernaak and Sivan (1972) and Levine and Athans (1970). Despite of its relevance in the formulation of performance requirements, LQ optimal control was shown to possess no guaranteed robustness margins if applied in conjunction with an observer or Kalman filter, see Doyle and Stein (1981). The robustness issue has attracted a lot of attention during the last decade, resulting in the development of H_∞ control theory, see for instance Francis (1987), Doyle and Glover (1988), Maciejowski (1989) and Doyle *et al.* (1989). Robust control based on the H_∞ norm of a weighted closed-loop transfer function is capable of handling the design problem for systems with uncertainties. However, the use of one single number, albeit frequency dependent, to address robustness and performance for multivariable systems is rather restrictive. The design problem of stating performance and robustness objectives in both the H_2 and H_∞ framework has recently been stated by several authors, see Bernstein and Haddad (1989), Doyle *et al.* (1989), Mustafa (1989), Rotea and Khargonekar (1991), Scherer (1995), Steinbuch and Bosgra (1991a, 1991b), Stoorvogel (1993), Paganini *et al.* (1994), Yeh *et al.* (1992), Zhou *et al.* (1994). In general one can define the problem as follows. Suppose the plant is given by its transfer function G(s) with three sets of inputs and outputs.

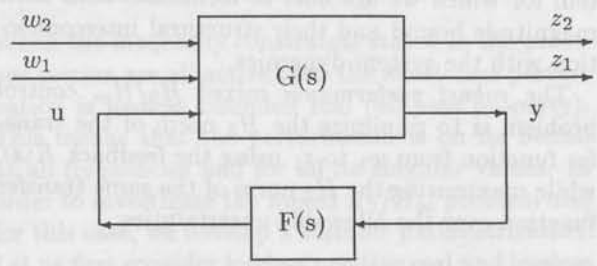

Fig. 1: Standard H_2/H_∞ control problem

[‡]This paper is presented at the 33rd IEEE Conference on Decision and Control, Orlando, FL, USA, December 14-16, 1994.

The manipulated variables are u, the measured outputs are y. The signal sets (w_1, z_1) are related to H_2 or LQ type of performance criteria, whereas (w_2, z_2) are related to H_∞ norm requirements. Doyle and Zhou (1989) and Zhou *et al.* (1994) posed the problem $z_1 = z_2, w_1 \neq w_2$ and gave a very nice interpretation for an induced semi-norm on the transfer function. Their work showed that the H_2/H_∞ control problem definition can be stated precisely in terms of signal sets. Bernstein and Haddad (1989) have considered the dual mixed H_2/H_∞ problem for the situation where $w_1 = w_2, z_1 \neq z_2$. They used a performance criterion relating $w(= w_1 = w_2)$ with z_1, under the constraint of an H_∞ norm bound on the transfer function from w to z_2. They derived necessary conditions for reduced order controllers and necessary and sufficient conditions for the full order case. Mustafa (1989) showed that if $w_1 = w_2$ and $z_1 = z_2$ the auxiliary performance index of Bernstein and Haddad can be interpreted nicely as an entropy expression, yielding the central H_∞ controller for the full order case.

In all these cases, the problem solved does not address the true robust performance control problem relevant in practical applications: only a very restricted class of problems do have the same inputs (or dually outputs) for the H_2 performance measures as for the H_∞ norm-bounded uncertainties.

The mixed H_2/H_∞ problem with minimizing the transfer function in the H_2 sense from w_1 to z_1, while constraining the H_∞ norm of the transfer function from w_2 to z_2 to some bound is unsolved. However, this problem does not address *robust* H_2 performance.

In contrast to the aforementioned results, in this paper a robust performance mixed H_2/H_∞ optimal control problem (or 'robust H_2 problem' as called by Stoorvogel (1993) and Paganini *et al.* (1994)) is considered including a parametrization of the worst case H_∞ norm bounded uncertainty relating the signals w_2 and z_2 (Steinbuch and Bosgra (1991b)), see Fig. 2.

In this problem, the worst-case norm-bounded uncertainty represents unmodeled dynamics of the system for which we are able to formulate both their magnitude bound and their structural interconnection with the system dynamics.

The *robust performance* mixed H_2/H_∞ control problem is to minimize the H_2 norm of the transfer function from w_1 to z_1 using the feedback $K(s)$, while maximizing the H_2 norm of the same transfer function over the allowable uncertainties:

$$\sup_{\|\Delta\|_\infty < \gamma} \min_{K(s)} \| T_{w_1 \to z_1}(K, \Delta) \|_2 \qquad (1)$$

In the literature there exist various formulations for performance optimization problems involving worst-case disturbances, resulting in a minimax formulation, e.g. Mills and Bryson (1994) and Sweriduk and Calise (1993).

From an application point of view this *robust performance* mixed H_2/H_∞ control problem addresses many design problems in which H_2 performance is the optimization criterion, subject to (un)structured H_∞ norm-bounded uncertainties. This problem is hard to solve, but because of the possible implications for use in practice, it seems worthwhile to further investigate the problem. Note also the interesting work of Paganini *et al.* (1994) in which the behavioral framework is used to asymptotically calculate the worst-case uncertainty for the robust performance H_2/H_∞ control problem. In this paper we will explore the validity and usefulness of this mixed H_2/H_∞ problem formulation using numerical tools. In earlier work we considered the calculation of the worst-case uncertainty, see Steinbuch and Bosgra (1994). In this paper we will extend the calculation of the worst case uncertainty and investigate the related control design. A numerical approach will be presented and applied to a mixed H_2/H_∞ Compact Disc control problem.

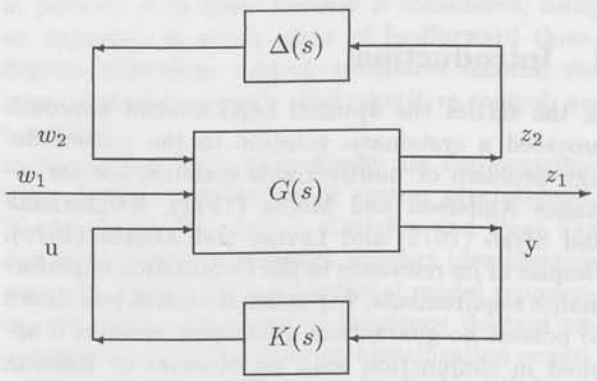

Fig. 2: Robust performance H_2/H_∞ control problem.

2 Preliminaries

Given a stable strictly proper transfer function matrix $G(s)$ with state space realization $C(sI-A)^{-1}B$, then the following performance measures can be defined.

Definition 2.1 *The H_2 norm of a transfer function $G(s)$ is defined as:*

$$\| G \|_2 = \left(\frac{1}{2\pi} \int_{-\infty}^{\infty} tr(G^T(-j\omega)G(j\omega))d\omega \right)^{1/2} \quad (2)$$

with tr(.) the trace matrix operator.

The 2-norm can be computed with Lyapunov equations:

$$\| G \|_2 = tr(SC^TC) = tr(PBB^T) \quad (3)$$

where S is the controllability Gramian and P is the observability Gramian solving:

$$AS + SA^T + BB^T = 0 \qquad A^TP + PA + C^TC = 0 \quad (4)$$

Definition 2.2 *The H_∞ norm of a transfer function $G(s)$ is defined as:*

$$\| G \|_\infty = \max_{\omega \in \mathbf{R}} \bar{\sigma}(G(j\omega)) \quad (5)$$

with $\bar{\sigma}$ the maximum singular value.

3 Parametrization of H_∞ norm bounded transfer functions

In Steinbuch and Bosgra (1991b) a parametrization was introduced for stable strictly proper H_∞ norm-bounded uncertainty models. In this paper we will extend this parametrization to proper H_∞ norm-bounded uncertainties using Linear Matrix Inequalities (LMIs), see Section 3.1. Based on numerical experiences with this parametrization it seems worthwhile to exploit the boundary conditions, i.e. when the worst-case perturbation is lossless bounded real, see Section 3.2.

3.1 Inequality formulation

Theorem 3.1 *Let (F, G, H, J) be an asymptotically stable minimal realization of the transfer function $\Delta(s) = H(sI - F)^{-1}G + J$. Then the following statements are equivalent.*

1. $\| \Delta \|_\infty < 1$ (6)

2. $\exists X > 0$ such that (7)

$$\begin{bmatrix} F^TX + XF & XG & H^T \\ G^TX & -I & J^T \\ H & J & -I \end{bmatrix} < 0 \quad (8)$$

3. $\exists X > 0$ such that (9)

$$(i)\ F^TX + XF + \begin{bmatrix} XG & H^T \end{bmatrix} \mathcal{J}^{-1} \begin{bmatrix} G^TX \\ H \end{bmatrix} < 0 \quad (10)$$

$$(ii)\ \mathcal{J} > 0 \quad (11)$$

with

$$\mathcal{J} = \begin{bmatrix} I & -J^T \\ -J & I \end{bmatrix} \quad (12)$$

Proof: Follows directly from the Bounded Real Lemma as formulated in Petersen *et al.* (1991). □

In the sequel we will denote the set of all transfer functions $\Delta(s)$ with $\| \Delta \|_\infty < 1$ as $\mathcal{D}$.

This result directly leads to the following parametrization which characterizes all real rational causal stable transfer functions $\Delta(s)$ of order n having $\| \Delta \|_\infty < 1$:

1. Choose J such that

$$\mathcal{J} > 0 \quad (13)$$

2. Let G and H be matrices of appropriate dimensions containing free parameters, and let $F = F_s + F_k$ with $F_s = F_s^T$ and $F_k = -F_k^T$, such that

$$F_s < -\frac{1}{2} \begin{bmatrix} G & H^T \end{bmatrix} \mathcal{J}^{-1} \begin{bmatrix} G^T \\ H \end{bmatrix} \quad (14)$$

and

$$F_k = diag \begin{bmatrix} 0 & -a_i \\ a_i & 0 \end{bmatrix}, \qquad i = 1, 2, ..., \frac{1}{2}n \quad (15)$$

for n even, and

$$F_k = \begin{bmatrix} diag \begin{bmatrix} 0 & -a_i \\ a_i & 0 \end{bmatrix} & 0 \\ 0 & 0 \end{bmatrix}, \quad i = 1, 2, ..., \frac{1}{2}(n-1) \quad (16)$$

for n uneven.

These equations follow from the theorem above by selecting a coordinate frame such that $X = I$ and by utilizing an additional orthogonal transformation that brings F_k into modal from.

3.2 Lossless bounded real formulation

When the inequality constraints stated in the previous section are all active then the worst-case perturbation is lossless bounded real (all-pass property). This means that the perturbation is on its bound at all frequencies and for all its singular values. In order to investigate the mixed H_2/H_∞ problem also for this case, we develop a suitable parametrization. Let us first consider lossless positive real and lossless bounded real transfer functions, see also Anderson and Vongpanitlerd (1973).

Definition 3.2 *The real rational function* $\Gamma(s)$, $s \in \mathbb{C}$, *is lossless positive real if* $\Gamma(s) + \Gamma^T(-s) = 0$.

Definition 3.3 *The real rational function* $\Delta(s)$, $s \in \mathbb{C}$, *is lossless bounded real if* $\Delta^T(-s)\Delta(s) = \mathrm{I}$. *The set of all such* $\Delta(s)$ *is denoted* $\mathcal{D}_a$.

Lemma 3.4 *Let* $\Delta(s) = (\mathrm{I}-\Gamma(s))(\mathrm{I}+\Gamma(s))^{-1}$, *then* $\Delta(s)$ *is lossless bounded real iff* $\Gamma(s)$ *is lossless positive real.*

Proof: $\Delta^T(-s)\Delta(s) =$
$(\mathrm{I}+\Gamma^T(-s))^{-1}(\mathrm{I}-\Gamma^T(-s))(\mathrm{I}-\Gamma(s))(\mathrm{I}+\Gamma(s))^{-1} =$
$(\mathrm{I}+\Gamma^T(-s))^{-1}(\mathrm{I}+\Gamma^T(-s)\Gamma(s))(\mathrm{I}+\Gamma(s))^{-1} = (\mathrm{I}+$
$\Gamma^T(-s))^{-1}(\mathrm{I}+\Gamma^T(-s))(\mathrm{I}+\Gamma(s))(\mathrm{I}+\Gamma(s))^{-1} = \mathrm{I}$, and conversely. □

Lemma 3.5 *Let* $\Gamma(s) = \bar{H}(s\mathrm{I} - \bar{F})^{-1}\bar{G} + \bar{J}$, *with* $\bar{F} + \bar{F}^T = 0$, $\bar{G} = \bar{H}^T$ *and* $\bar{J} + \bar{J}^T = 0$, *with* $\bar{F} \in \mathbb{R}^{n\times n}$ *and* $\bar{J} \in \mathbb{R}^{m\times m}$, *and with* $\bar{H}$ *and* $\bar{G}$ *of compatible dimensions. Then the real matrices* $\bar{F}$, $\bar{H}$ *and* $\bar{J}$ *parametrizes all lossless positive real transfer functions* Γ *with state dimension* n.

Proof: follows by direct application of Definition 3.2. □

Lemma 3.6 *Let* $\Delta(s) = (\mathrm{I}-\Gamma(s))(\mathrm{I}+\Gamma(s))^{-1}$ *with* $\Gamma(s) = \bar{H}(s\mathrm{I} - \bar{F})^{-1}\bar{G} + \bar{J}$, *with* $\bar{F}$, $\bar{H}$ *and* $\bar{J}$ *as defined in the previous lemma. Then a state space realization for* $\Delta(s) = H(s\mathrm{I} - F)^{-1}G + J$ *is given by:*

$$\begin{aligned} F &= \bar{F} - \bar{H}^T(\mathrm{I}+\bar{J})^{-1}\bar{H} \\ G &= -\sqrt{2}\bar{H}^T(\mathrm{I}+\bar{J})^{-1} \\ H &= \sqrt{2}(\mathrm{I}+\bar{J})^{-1}\bar{H} \\ J &= (\mathrm{I}-\bar{J})(\mathrm{I}+\bar{J})^{-1} \end{aligned} \tag{17}$$

And this is a parametrization for all stable lossless bounded real $\Delta(s)$.

Proof: follows by some matrix manipulations and is omitted here. □

Since matrices $\bar{F}$ and $\bar{J}$ are defined as skew-symmetric (see Lemma 3.5), we further reduce the number of free variables and end this section with the main result.

Theorem 3.7 *Define the matrices* θ *and* ϕ *as upper triangular real matrices, with zero on their diagonal, and with appropriate dimensions, such that* $\bar{F} = \theta - \theta^T$, *and* $\bar{J} = \phi - \phi^T$, *then the triple* (θ, ϕ, $\bar{H}$) *parametrizes all stable lossless bounded real transfer functions* $\Delta(s) = H(s\mathrm{I} - F)^{-1}G + J$, *with* H,F,G *and* J *defined by (17).*

4 Worst case perturbations

Consider Fig. 3. The noise disturbances w_1 have unit noise intensity, and the uncertainty $\Delta(s)$ represents unstructured H_∞ norm bounded perturbations of the nominal closed-loop system ($M(s)$ includes $G(s)$ and $K(s)$).

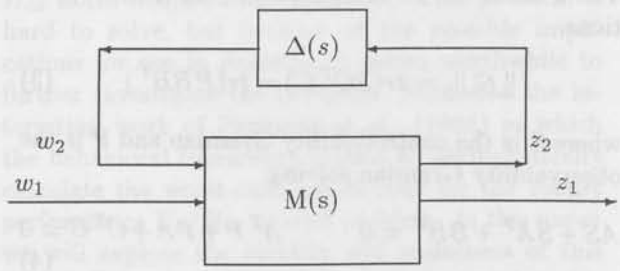

Fig. 3: H_2 worst case uncertainty.

In contrast to Stoorvogel (1993), causality of the perturbation is assumed as an implicit and necessary ingredient to pose the true problem. Thus we consider a set $\mathcal{D}$ of real-rational causal stable transfer function matrices $\Delta(s)$ satisfying $\| \Delta \|_\infty < 1$, and $\mathcal{D}_a$ if $\Delta^T(-s)\Delta(s) = I$. As performance indicator we use the variance of the signal z_1, i.e. the H_2 norm of the closed-loop transfer function from w_1 to z_1. Let $M(s)$ have the state space realization

$$\begin{aligned} \dot{x} &= Ax + B_1 w_1 + B_2 w_2 \\ z_1 &= C_1 x + \qquad D_{12} w_2 \\ z_2 &= C_2 x + D_{21} w_1 \end{aligned} \tag{18}$$

and let $\Delta(s) = H(s\mathrm{I} - F)^{-1}G + J$. Then the closed-loop system is:

$$\begin{aligned} \begin{pmatrix} \dot{x} \\ \dot{p} \end{pmatrix} &= \begin{pmatrix} A + B_2 J C_2 & B_2 H \\ G C_2 & F \end{pmatrix} \begin{pmatrix} x \\ p \end{pmatrix} + \\ &\quad \begin{pmatrix} B_1 + B_2 J D_{21} \\ G D_{21} \end{pmatrix} w_1 \\ z_1 &= \begin{pmatrix} C_1 + D_{12} J C_2 & D_{12} H \end{pmatrix} \begin{pmatrix} x \\ p \end{pmatrix} \end{aligned} \tag{19}$$

denoted as $[A],[B],[C]$. Notice that $D_{12}JD_{21} = 0$ for $\| T_{w_1 \to z_1}(\Delta) \|_2 < \infty$.

Let the system (19) be stable and consider the *constrained* optimization problem

$$\sup_{\Delta\in\mathcal{D}} \| T_{w_1\to z_1}(\Delta) \|_2 = \sup_{\Delta\in\mathcal{D}} tr[C]^T[C]S \tag{20}$$

or

$$\max_{(F_s,F_k,G,H,J)} tr[C]^T[C]S \tag{21}$$

with F_s, F_k, G, H, J according to (13)-(16), and with the state-variance matrix $S = S^T$ the solution to:

$$[A]S + S[A]^T + [B][B]^T = 0 \qquad (22)$$

In case of Δ being lossless bounded real, i.e. $\Delta \in \mathcal{D}_a$ the optimization problem can be reformulated as an *unconstrained* optimization problem:

$$\max_{(\theta,\phi,\bar{H})} tr[C]^T[C]S \qquad (23)$$

with S the solution to (22), and with (F, G, H, J) defined by (17), where $\bar{F} = \theta - \theta^T$, $\bar{J} = \phi - \phi^T$.

5 Numerical exploration of the control design problem

In the preceding section we have considered worst-case perturbations $\Delta(s)$ for the fixed system $M(s)$. As $M(s)$ includes the feedback controller $K(s)$, we have to investigate how $\Delta(s)$ and $K(s)$ are related.

Recall the set $\mathcal{D}$ of all stable norm-bounded uncertainties. Let $\Delta_k(s) \in \mathcal{D}$ be the worst-case disturbance, i.e. a disturbance attaining

$$\sup_{\Delta\in\mathcal{D}} \| T_{w_1\to z_1}(K, \Delta) \|_2 \qquad (24)$$

for a certain feedback controller $K(s)$. Although the underlying problem may show a much more complicated structure, we assume here that (at least locally) there exists a unique maximizing $\Delta_k(s)$. Now consider all such $\Delta_k(s)$, and determine the feedback law K^* that would be H_2-optimal in case $\Delta_k(s)$ indeed would qualify as worst-case uncertainty. By assigning an H_2-optimal K^* to each $\Delta_k(s)$, we iterate over $\Delta_k(s)$ until it satisfies the conditions for a worst-case disturbance, i.e. the gradients with respect to its parameters are zero for a fixed H_2-optimal K^*.

Using the parametrization of the worst case uncertainty we are now able to rewrite the control design problem in a numerically tractable way. Consider Fig. 2, with the noise disturbances w_1 having unit noise intensity and uncertainty $\Delta(s) \in \mathcal{D}$ or $\Delta(s) \in \mathcal{D}_a$ respectively. The design problem is

$$\sup_{\Delta\in\mathcal{D}_{(a)}} \min_{K(s)} \| T_{w_1\to z_1}(K, \Delta) \|_2 \qquad (25)$$

Let $G(s)$ have the state space realization

$$\begin{aligned} \dot{x} &= Ax + B_1 w_1 + B_2 w_2 + B_3 u \\ z_1 &= C_1 x + D_{12} w_2 + D_{13} u \\ z_2 &= C_2 x + D_{21} w_1 + D_{23} u \\ y &= C_3 x + D_{31} w_1 + D_{32} w_2 \end{aligned} \qquad (26)$$

and let $\Delta(s) = H(sI - F)^{-1}G + J$, then the perturbed system is given by:

$$\begin{aligned} \dot{x}_p &= A_p x_p + B_{p1} w_1 + B_p u \\ z_1 &= C_{p1} x_p + D_{p1} u \\ y &= C_p x_p + D_{1p} w_1 \end{aligned} \qquad (27)$$

with

$$x_p = \begin{pmatrix} x \\ p \end{pmatrix}$$

$$A_p = \begin{pmatrix} A + B_2 J C_2 & B_2 H \\ G C_2 & F \end{pmatrix}$$

$$B_{p1} = \begin{pmatrix} B_1 + B_2 J D_{21} \\ G D_{21} \end{pmatrix}$$

$$B_p = \begin{pmatrix} B_3 + B_2 J D_{23} \\ G D_{23} \end{pmatrix}$$

$$C_{p1} = \begin{pmatrix} C_1 + D_{12} J C_2 & D_{12} H \end{pmatrix}$$

$$D_{p1} = \begin{pmatrix} D_{13} + D_{12} J D_{23} \end{pmatrix}$$

$$C_p = \begin{pmatrix} C_3 + D_{32} J C_2 & D_{32} H \end{pmatrix}$$

$$D_{1p} = \begin{pmatrix} D_{31} + D_{32} J D_{21} \end{pmatrix}$$

Notice that $D_{12} J D_{21} = 0$ for $\| T_{w_1\to z_1}(\Delta) \|_2 < \infty$ and that $D_{32} J D_{23} = 0$ is assumed for simplicity. The feedback controller $K(s)$ connects the measured variables y with the inputs u.

Let the system (27) be stable and assume for the moment that the uncertainty parameters (F, G, H, J) are fixed. Then the optimization problem

$$\min_K \| T_{w_1\to z_1}(u = K(s)y) \|_2 \qquad (28)$$

can be solved as a standard H_2 or LQG type of problem:

$$\begin{aligned} &(A_p^T - C_{p1}^T D_{p1} B_p^T) X + X(A_p - B_p D_{p1}^T C_{p1}) - \\ &\quad X B_p B_p^T X + C_{p1}^T (I - D_{p1} D_{p1}^T) C_{p1} = 0 \end{aligned} \qquad (29)$$

$$\begin{aligned} &(A_p - B_{p1} D_{1p}^T C_p) Y + Y(A_p^T - C_p^T D_{1p} B_{p1}^T) - \\ &\quad Y C_p^T C_p Y + B_{p1} (I - D_{1p}^T D_{1p}) B_{p1}^T = 0 \end{aligned} \qquad (30)$$

and the H_2 optimal control law $u = K^*(s)y$ is defined by

$$\begin{aligned} \dot{v} &= (A_p - B_p(B_p^T X + D_{p1}^T C_{p1}))v + \\ &\quad (Y C_p^T + B_{p1} D_{1p}^T)y \\ u &= -(B_p^T X + D_{p1}^T C_{p1})v \end{aligned} \tag{31}$$

The optimization problem including the uncertainty $\Delta \in \mathcal{D}$ can now be formulated as a *constrained* optimization problem over a standard H_2 optimal control problem:

$$\max_{(F_s,F_k,G,H,J)} \| T_{w_1 \to z_1}(u = K^*(s)y) \|_2 \tag{32}$$

with K^* the solution to (29) - (31), and F_s, F_k, G, H, J according to (13) - (16).

If $\Delta \in \mathcal{D}_a$ the optimization problem can be formulated as an *unconstrained* optimization problem:

$$\max_{(\theta,\phi,\bar{H})} \| T_{w_1 \to z_1}(u = K^*(s)y) \|_2 \tag{33}$$

with K^* the solution to (29)-(31).

6 Example: Compact Disc player robust control problem

In Fig.4 a schematic view of a Compact Disc mechanism is shown. The mechanism is composed of a turn-table DC-motor, and a balanced radial arm for track-following. An optical element is mounted at the end of the radial arm. A diode located in this element generates a laser beam that passes through a series of optical lenses to give a spot on the information layer of the disc. An objective lens, suspended by two parallel leaf springs, can be actuated vertically for focussing.

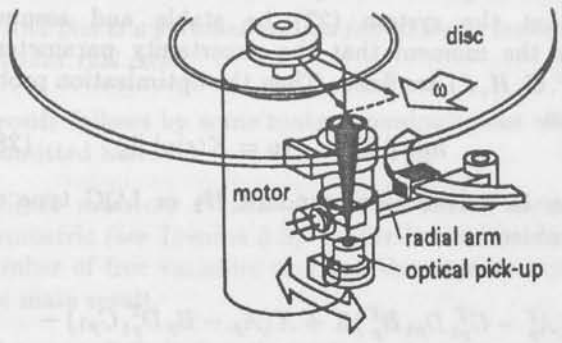

Fig. 4: Schematic view of a rotating arm Compact Disc mechanism.

Both the radial and the vertical (focus) position of the laser spot, relative to the track of the disc, have to be controlled actively. To accomplish this, the controller uses position-error information provided by four photo diodes. As input to the system the controller generates control currents to the radial and focus actuator, which both are permanent-magnet/coil systems.

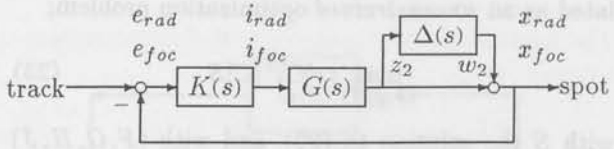

Fig. 5: Configuration of the CD MIMO control loop.

In Fig.5 a block-diagram of the control loop is shown. The difference between the radial (x_{rad}) and vertical (x_{foc}) spot position and the reference track is detected by an optical pick-up which generates a radial error signal (e_{rad}) and a focus error signal (e_{foc}). A controller $K(s)$ feeds the system with the currents i_{rad} and i_{foc}, see also Steinbuch *et al.* (1994).

In the numerical experiments a MIMO 2×2 model (G) of order 10 is used. We will consider two types of uncertainties. The first is a multiplicative output uncertainty. The uncertainty Δ is 50 %. The noise disturbances w_1 acting on the multivariable control loop enter the loop at the input of the system and measurement noise act on the feedback loop. The performance measures z_1 are the input to the plant and the output of the plant ('spot'). Our interest is in how the uncertainty $\Delta(s)$ can disturb the H_2 performance from w_1 to z_1, and how the H_2 optimal controller $K(s)$ counteracts this. By using a general purpose optimization program the results are obtained, using the formulation of the previous section. The inputs w_1 and w_2 have been scaled such that the nominal performance equals 1 and such that $\| \Delta \|_\infty = 1$ corresponds to 50 % model uncertainty. The results are presented in the table below, and have been obtained with a first order (2×2) uncertainty; see Steinbuch and Bosgra (1994) for investigations with respect to the number of states in a worst-case Δ. The results obtained using the LMI formulation showed that all the boundary conditions were met, and after application of the lossless bounded real formulation it appeared that identical solutions were obtained. It should be noted that this result holds for this example. It is not clear whether more general statements can be made. This is subject of future research.

The results are summarized in Table 1. In the Table the column 'nominal, K_{nom}, $\Delta = 0$' denotes the value of the objective function for the unperturbed

	$\| T_{w_1 \to z_1} \|_2$
nominal: K_{nom}, $\Delta = 0$	1.00
nominal: K^*, $\Delta = 0$	1.06
perturbed: K^*, Δ_k^*	1.38
perturbed: K_{nom}, Δ_k^*	1.48

Table 1: H_2 performance for CD player with output uncertainty

case with the standard H_2 optimal control K_{nom}. The second column 'nominal, K^*, $\Delta = 0$' means the robust performance optimal controller solving (32) or (33) and with which the H_2 performance is evaluated without a perturbation. The third column 'perturbed , K^*, Δ_k^*' means the robust performance optimal controller solving (32) or (33) and with which the H_2 performance is evaluated with the worst case perturbation, i.e. this number is the value of (32) or (33). Finally, the last column 'perturbed , K_{nom}, Δ_k^*' means the nominal performance optimal controller K_{nom} for which the H_2 performance is evaluated for the worst case perturbation, i.e. this number is the value of (32) or (33) with $K = K_{nom}$ fixed.

The results shown in the Table indicate that the worst case variance of the performance variables z_1 increases with a factor 1.48 if the nominal optimal H_2 controller is used. In case of the optimized controller for the uncertainty, the nominal performance degrades with 6%. The worst-case performance is 1.38, which is about 10% better than with the nominal feedback. In the following figure the nominal and perturbed transfer functions are shown from the input i_{rad} to the radial spot position.

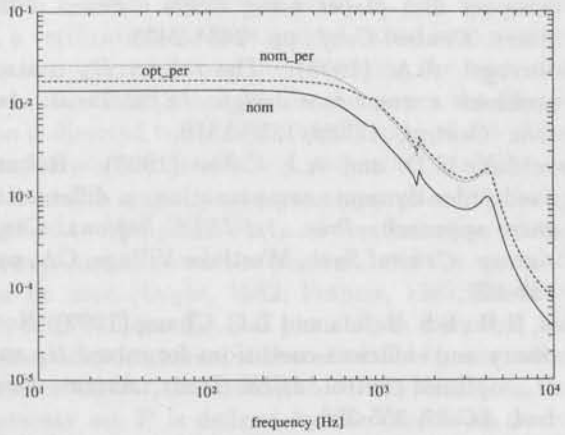

Fig. 6: Nominal (–) and worst case perturbed (- -, ...) transfer function from w_1 to z_1

The second example considers the same Compact Disc player MIMO control loop, but now with an uncertainty affecting the resonance at 860 Hz. The uncertainty perturbs especially the damping of the resonance, with an amount almost equal to 100% [1]. Again, the noise disturbances w_1 acting on the multivariable control loop enter the loop at the input of the system and measurement noise act on the feedback loop. The performance measures z_1 are the input to the plant and the output of the plant. The results of the calculations are presented in Table 2.

	$\| T_{w_1 \to z_1} \|_2$
nominal: K_{nom}, $\Delta = 0$	1.00
nominal: K^*, $\Delta = 0$	1.01
perturbed: K^*, Δ_k^*	1.01
perturbed: K_{nom}, Δ_k^*	17.90

Table 2: H_2 performance for CD player with resonance uncertainty

The variance of the performance variables z_1 increases with a factor of almost 18 (!) if the nominal optimal H_2 controller is used, while in case of the optimized controller for the uncertainty, the robust performance is only 1% less than the nominal performance. Analysis of the worst-case uncertainty revealed that it is equal to a proportional term (J) driving the damping of the system close to zero. The H_2/H_∞ optimal controller counteracts this effectively. In the following figure the nominal and perturbed transfer functions are shown.

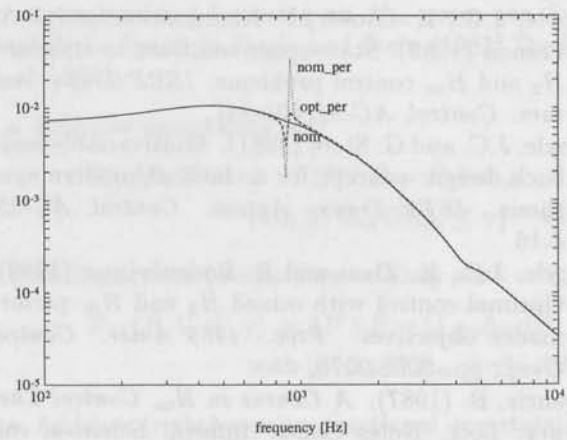

Fig. 7: Nominal (–) and worst case perturbed (- -, ...) transfer function from w_1 to z_1

[1] Although this can be described as a parametric uncertainty (real-valued) it is treated here as a complex uncertainty.

Conclusions

A new formulation of the robust performance H_2/H_∞ optimal control problem has been proposed in this paper, and an explicit parametrization for a worst-case norm-bounded uncertainty has been used, yielding an (un)constrained optimization problem. A Compact Disc system with an unstructured uncertainty has been discussed. Using a numerical algorithm we have shown that it is possible to calculate worst case uncertainties and to robustify the controller to counteract with the worst case perturbation. The robust performance obtained in these examples shows that it is worthwhile to further explore the theory of the robust performance mixed H_2/H_∞ control problem.

References

Anderson, B.D.O. and J.B. Moore (1971). *Linear Optimal Control.* Prentice-Hall, Englewood Cliffs, N.J.

Anderson, B.D.O. and S. Vongpanitlerd (1973). *Network Analysis and Synthesis'.* Prentice Hall, Englewood Cliffs.

Bernstein, D.S. and W.M. Haddad (1989). LQG control with an H_∞ performance bound: a Riccati equation approach. *IEEE Trans. Autom. Control, AC-34*, 293-305.

Doyle, J.C. and K. Glover (1988). State space formulae for all stabilizing controllers that satisfy an H_∞-norm bound and relations to risk sensitivity. *Syst. Control Lett., 11*, 167-172.

Doyle, J.C., K. Glover, P. Khargonekar and B.A. Francis (1989). State-space solutions to standard H_2 and H_∞ control problems. *IEEE Trans. Autom. Control, AC-34*, 831-847.

Doyle, J.C. and G. Stein (1981). Multivariable feedback design: concept for a classical/modern synthesis. *IEEE Trans. Autom. Control, AC-25*, 4-16.

Doyle, J.C., K. Zhou and B. Bodenheimer (1989). Optimal control with mixed H_2 and H_∞ performance objectives. *Proc. 1989 Amer. Control Conf.*, pp. 2065-2070.

Francis, B. (1987). *A Course in H_∞ Control Theory.* Lect. Notes Contr. Inform. Sciences, vol. 88, Springer Verlag, Berlin.

Kwakernaak, H. and R. Sivan (1972). *Linear Optimal Control Systems.* Wiley-Interscience, New-York.

Levine, W.S. and M. Athans (1970). On the determination of the optimal constant output feedback gains for linear multivariable systems. *IEEE Trans. Autom. Control, AC-15*, 44-48.

Maciejowski, J.M. (1989). *Multivariable Feedback Design.* Addison-Wesley Publ. Comp., Workingham, UK.

Mills, R.A. and A.E. Bryson (1994). Calculus of variations derivation of the minimax linear-quadratic (H_∞) controller. *J. Guidance Control and Dynamics, 17*, 153-160.

Mustafa, D. (1989). Relations between maximum entropy/H_∞ control and combined H_∞/LQG control. *Syst. Control Lett., 12*, 193-203.

Paganini, F., R. D'Andrea and J.C. Doyle (1994). Behavioral approach to robustness analysis. *Proc. 1994 Amer. Control Conf.*, pp. 2782-2786.

Petersen, I.R., B.D.O. Anderson and E.A. Jonckheere (1991). A first principles solution to the non-singular H_∞ control problem. *Intern. J. Robust and Nonlinear Control, 1*, 171-185.

Rotea, M.A. and P.P. Khargonekar (1991). H_2-optimal control with an H_∞-constraint, the state-feedback case. *Automatica, 27*, 307-316.

Scherer, C.W. (1995). Multiobjective H_2/H_∞ control. Preprint 1993, to appear in *IEEE Trans. Autom. Control.*

Steinbuch, M. and O.H. Bosgra (1991a). Necessary conditions for static and fixed order dynamic mixed H_2/H_∞ optimal control. *Proc. 1991 Amer. Control Conf.*, pp.1137-1143.

Steinbuch, M. and O.H. Bosgra (1991b). Robust performance in H_2/H_∞ optimal control. *Proc. 31st IEEE Conf. Decision and Control*, Brighton, UK, pp. 539-550.

Steinbuch, M. and O.H. Bosgra (1994). H_2 performance for unstructured uncertainties. *Proc. IMACS Symp. Mathem. Modelling '1. MATHMOD VIENNA'*, Feb 2-4, 1994, pp. 265-268.

Steinbuch, M., P.J.M. van Groos, G. Schootstra and O.H. Bosgra (1994). Multivariable control of a compact disc player using DSPs. *Proc. 1994 Amer. Control Conf.*, pp. 2434-2438.

Stoorvogel, A.A. (1993). The robust H_2 control problem: a worst case design. *IEEE Trans. Autom. Control, AC-38*, 1358-1370.

Sweriduk, G.D. and A.J. Calise (1993). Robust fixed order dynamic compensation: a differential game approach. *Proc. 1st IEEE Regional Conf. Aerosp. Control Syst.*, Westlake Village, CA, pp. 458-462.

Yeh, H.H., S.S. Banda and B.C. Chang (1992). Necessary and sufficient conditions for mixed H_2 and H_∞ optimal control. *IEEE Trans. Autom. Control, AC-37*, 355-358.

Zhou, K., K. Glover, B. Bodenheimer and J.C. Doyle (1994). Mixed H_2 and H_∞ performance objectives I+II. *IEEE Trans. Autom. Control, AC-39*, 1564-1587.

Selected Topics in Identification, Modelling and Control
Vol. 7, December 1994

A unified approach to stability robustness for uncertainty descriptions based on fractional model representations

Raymond de Callafon[‡], Paul Van den Hof and Peter Bongers[§]

Mechanical Engineering Systems and Control Group
Delft University of Technology, Mekelweg 2, 2628 CD Delft, The Netherlands.

Abstract. The powerful standard representation for uncertainty descriptions in a basic perturbation model as introduced by Doyle can be used to attain necessary and sufficient conditions for stability robustness within various uncertainty descriptions. In this paper these results are employed to formulate necessary and sufficient conditions for stability robustness of several uncertainty sets based on simple additive coprime factor uncertainty, gap-metric uncertainty as well as the recently introduced and less conservative Λ-gap uncertainty.

Keywords. Stability robustness, coprime factorizations, gap-metric

1 Introduction

In a model-based control design paradigm, the design is based on a (necessarily) approximative model $\hat{P}$ of a plant to be controlled. An apparently successful control design leads to a controller C, having some desired closed loop properties for the feedback controlled model $\hat{P}$, but due to the possible mismatch between the actual plant P_o and the model $\hat{P}$, a verification of these desired closed loop properties is preferred before implementing the controller C on the actual plant P_o. In this paper the discussion is directed towards the verification of one of the most important closed loop properties: stability.

To evaluate stability when the controller C is being applied to the plant P_o, a characterization of the discrepancy between the plant P_o and the model $\hat{P}$ can be used (Doyle, 1982; Francis, 1987; Doyle *et al.*, 1992). Since the real plant P_o is *unknown*, the discrepancy in general is characterized by a so called *uncertainty set*, denoted with $\mathcal{P}$. Typically an uncertainty set $\mathcal{P}$ is defined by the (nominal) model $\hat{P}$, which is found by physical modelling or identification techniques, and some bounded 'area' around it (Doyle *et al.*, 1992). The uncertainty set $\mathcal{P}$ itself reflects all possible perturbations of the (nominal) model $\hat{P}$ that may occur. Some typical examples of commonly used *unstructured* uncertainty sets that are norm-bounded by using an H_∞-norm can for example be found in Doyle and Stein (1981),Doyle *et al.* (1992):

- Additive uncertainty set:

$$\mathcal{P}_A(\hat{P},V,W,\gamma) := \{P \mid P = \hat{P} + \Delta_A, \text{ with } \|V\Delta_A W\|_\infty \leq \gamma\}. \quad (1)$$

- Multiplicative (output) uncertainty set:

$$\mathcal{P}_M(\hat{P},V,W,\gamma) := \{P \mid P = [I + \Delta_M]\hat{P}, \text{ with } \|V\Delta_M W\|_\infty \leq \gamma\}. \quad (2)$$

- Additive (right) coprime fractional uncertainty set, where $\hat{P}$ has been factorized first in a right coprime factorization $\hat{P} := \hat{N}\hat{D}^{-1}$ and the set is defined as

$$\mathcal{P}_{CF}(\hat{N},\hat{D},V_D,V_N,W,\gamma) := \{P \mid P = [\hat{N} + \Delta_N][\hat{D} + \Delta_D]^{-1}, \text{ with } \left\| \begin{bmatrix} V_D & 0 \\ 0 & V_N \end{bmatrix} \begin{bmatrix} \Delta_D \\ \Delta_N \end{bmatrix} W \right\|_\infty \leq \gamma\}. \quad (3)$$

[‡]The work of Raymond de Callafon is sponsored by the Dutch Systems and Control Theory Network.

[§]Now with Unilever Research, Technical Application Unit, Vlaardingen, The Netherlands.

Clearly, by defining the uncertainty set in such a way that at least the plant $P_o \in \mathcal{P}$, stability robustness results for the set $\mathcal{P}$ will reflect sufficient conditions under which the plant P_o will be stabilized by C, (Doyle *et al.*, 1992). In this perspective, special attention will be given in this paper to an uncertainty set $\mathcal{P}_{CF}$ which is characterized by perturbations on an additive coprime factor description of the nominal model $\hat{P}$, like in (3). The specific application of the uncertainty set description of (3) will be motivated by the favourable properties it has over a standard additive (1) or multiplicative (2) uncertainty set description.

Stability robustness results for uncertainty sets employing weighted and unstructured additive perturbations on a coprime factorization, gap-metic based uncertainty sets and the recently introduced Λ-gap uncertainty sets will be shown to be closely related to each other. The contribution of this paper is in the unified treatment of the situations of the different uncertainty sets, by employing the weighting and the factorization used in an uncertainty $\mathcal{P}_{CF}$ as given in (3). While stability robustness results for uncertainty sets using additive perturbations on normalized (left) coprime factorizations (Glover and McFarlane, 1989) and gap-metric based uncertainty sets (Georgiou and Smith, 1990*a*) have separately been derived before, this paper amplifies their relation, as well as the extension to a less conservative Λ-gap (Bongers, 1991; Bongers, 1994) uncertainty set description.

The outline of this paper will be as follows. In section 2 some preliminary notations and definitions will be given, while in section 3 the basic stability robustness result using the powerful perturbation model (Doyle, 1982) will be summarized. This perturbation model gives rise to an unified approach to handle stability robustness for various uncertainty descriptions, including additive weighted perturbations on a coprime factorization. Section 4 contains the results of applying this unified approach to additive uncertainty descriptions on fractional model representations like in (3) and favourable properties are illuminated. The link with gap and Λ-gap based stability robustness results is discussed in sections 5 and 6, the latter one being less conservative than the former one, as shown in section 7. The paper ends with some concluding remarks.

2 Preliminaries

Throughout this paper, the feedback configuration of a plant P and a controller C is denoted by $\mathcal{T}(P,C)$ and defined by the feedback connection structure depicted in figure 1.

P and C are represented by real rational (discrete time) transfer function matrices, and it will be assumed that the feedback connection is well-posed, i.e. that $\det[I + CP] \not\equiv 0$.

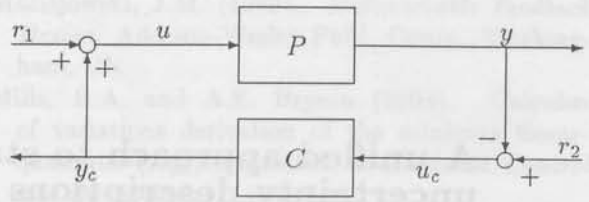

Fig. 1: Feedback connection structure $\mathcal{T}(P,C)$ of a plant P and a controller C

In figure 1 the signals u and y reflect respectively the inputs and outputs of the plant P. The signals u_c and y_c are respectively the inputs and outputs of the controller $C_{\hat{P}}$, and r_1 and r_2 are external reference signals. The feedback system $\mathcal{T}(P,C)$ is defined to be internally stable if the mapping from $col(r_2, r_1)$ to $col(u_c, u)$ is BIBO stable, i.e. if the corresponding transfer function is in $\mathbb{RH}_\infty$, being the Hardy space of real rational transfer function matrices with bounded $\mathcal{H}_\infty$-norm (Francis, 1987):

$$\|G\|_\infty := \sup_{\omega \in [0,\pi)} \bar{\sigma}\{G(e^{i\omega})\} \qquad (4)$$

with $\bar{\sigma}$ the maximum singular value.

The dynamics of the closed loop system $\mathcal{T}(P,C)$ will also be described by the mapping from $col(r_2, r_1)$ to $col(y, u)$ which is given by the transfer function matrix $T(P,C)$:

$$T(P,C) := \begin{bmatrix} P \\ I \end{bmatrix} [I + CP]^{-1} \begin{bmatrix} C & I \end{bmatrix}. \qquad (5)$$

Using the theory of fractional representations, as e.g. presented in Vidyasagar (1985), a plant P is expressed as a ratio of two stable transfer functions N and D. For two transfer functions $N, D \in \mathbb{RH}_\infty$ the pair (N, D) is called right coprime over $\mathbb{RH}_\infty$ if there exist $X, Y \in \mathbb{RH}_\infty$ such that $XN + YD = I$. The pair (N, D) is a right coprime factorization (rcf) of P if additionally $\det\{\mathrm{D}\} \not\equiv 0$ and $P = ND^{-1}$. A right coprime factorization (N, D) is called normalized (nrcf) if it satisfies $N^*N + D^*D = I$, where * denotes complex conjugate transpose. For (normalized) left coprime factorizations (lcf) dual definitions exist. With respect to internal stability of the feedback system $\mathcal{T}(P,C)$ the following lemma will be used.

Lemma 2.1 *Let P have rcf (N, D) and lcf $(\tilde{D}, \tilde{N})$, and let C have rcf (N_c, D_c) and lcf $(\tilde{D}_c, \tilde{N}_c)$. The following statements are equivalent*

i. the feedback system $\mathcal{T}(P,C)$ given in figure 1 is internally stable

ii. $T(P,C) \in \mathbb{R}\mathcal{H}_\infty$, *with* $T(P,C)$ *defined in* (5).

iii. $\Lambda^{-1} \in \mathbb{R}\mathcal{H}_\infty$, *with* $\Lambda := \begin{bmatrix} \tilde{D}_c & \tilde{N}_c \end{bmatrix} \begin{bmatrix} D \\ N \end{bmatrix}$

iv. $\tilde{\Lambda}^{-1} \in \mathbb{R}\mathcal{H}_\infty$, *with* $\tilde{\Lambda} := \begin{bmatrix} \tilde{D} & \tilde{N} \end{bmatrix} \begin{bmatrix} D_c \\ N_c \end{bmatrix}$

Proof: *i* $\Leftrightarrow$ *ii*: From figure 1 and lemma 2.1 it can be seen that

$$\begin{aligned} \begin{bmatrix} y \\ u \end{bmatrix} &= \begin{bmatrix} -I & 0 \\ 0 & I \end{bmatrix} \begin{bmatrix} u_c \\ u \end{bmatrix} + \begin{bmatrix} r_2 \\ 0 \end{bmatrix} \\ &= \begin{bmatrix} -I & 0 \\ 0 & I \end{bmatrix} H(P,C) \begin{bmatrix} r_2 \\ r_1 \end{bmatrix} + \begin{bmatrix} r_2 \\ 0 \end{bmatrix} \\ &= T(P,C) \begin{bmatrix} r_2 \\ r_1 \end{bmatrix} \end{aligned}$$

Hence $T(P,C) \in \mathbb{R}\mathcal{H}_\infty$ if and only if $H(P,C) \in \mathbb{R}\mathcal{H}_\infty$ which is equivalent to $\mathcal{T}(P,C)$ being internally stable.
i $\Leftrightarrow$ *iii,iv*: See Vidyasagar (1985), Bongers (1994) or Schrama (1992). □

Fractional representations have a close relation with approximation in the graph topology. The graph topology is the weakest topology[1] in which a variation of the elements of a stable feedback configuration around their nominal values, preserves stability of that closed loop system (Vidyasagar *et al.*, 1982). The graph topology is known to be induced by several metrics, as e.g. the graph metric introduced in Vidyasagar (1984) or the gap metric introduced in Zames and El-Sakkary (1980), being expressed in the following way (Georgiou, 1988).

Definition 2.2 *Consider the two plants P_1, P_2 with nrcf's (N_1, D_1) of P_1 and (N_2, D_2) of P_2. Then the gap between P_1 and P_2 is expressed by*

$$\begin{aligned} \delta(P_1,P_2) &:= \max\{\vec{\delta}(P_1,P_2), \vec{\delta}(P_2,P_1)\}, \text{ with} \\ \vec{\delta}(P_i,P_j) &:= \inf_{Q \in \mathbb{R}\mathcal{H}_\infty} \left\| \begin{bmatrix} D_i \\ N_i \end{bmatrix} - \begin{bmatrix} D_j \\ N_j \end{bmatrix} Q \right\|_\infty \end{aligned}$$

3 Stability robustness in standard form

For describing the stability robustness of several uncertainty sets based on fractional model representations, the standard results on stability robustness for a general situation as depicted in Figure 2 will be used.

[1] Given two topologies $\mathcal{O}_1$ and $\mathcal{O}_2$, $\mathcal{O}_1$ is said to be weaker than $\mathcal{O}_2$ if $\mathcal{O}_1$ is a subcollection of $\mathcal{O}_2$, see also Vidyasagar *et al.* (1982)

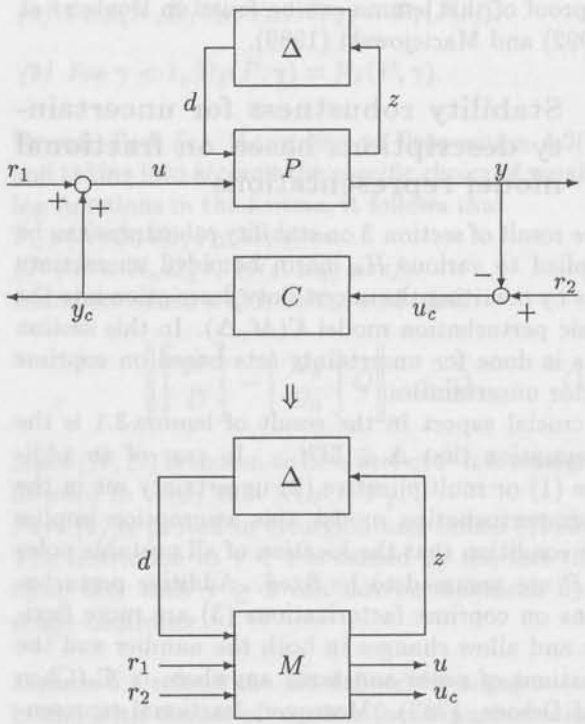

Fig. 2: (a) Feedback connection structure of a perturbed plant P_Δ and a controller C; (b) general feedback connection structure $\mathcal{K}(M,\Delta)$.

It is well known that the feedback system depicted in Figure 2(a) can be recasted into the situation given in Figure 2(b), where the uncertainty Δ has been pulled out (Doyle *et al.*, 1992) using the artificial signals d and z. Provided that the transfer M is BIBO stable, internal stability of the configuration in Figure 2(a) is equivalent to BIBO stability of the feedback system $\mathcal{K}(M,\Delta)$ in Figure 2(b), where M_{11} will denote the map from from d onto z only.
The small gain theorem can now be applied to characterize stability results for the connection structure of Figure 2(b) and has been summarized in the following lemma.

Lemma 3.1 *Let the stable transfer functions $M, \Delta \in \mathbb{R}\mathcal{H}_\infty$ construct a feedback connection $\mathcal{K}(M,\Delta)$. Then*

(a) A sufficient condition for BIBO stability of $\mathcal{K}(M,\Delta)$ is given by

$$\|M_{11}\Delta\|_\infty < 1 \tag{6}$$

(b) $\mathcal{K}(M,\Delta)$ is BIBO stable for all Δ with $\|\Delta\|_\infty \leq \gamma$ if and only if

$$\|M_{11}\|_\infty < \gamma^{-1} \tag{7}$$

A proof of this lemma can be found in Doyle *et al.* (1992) and Maciejowski (1989).

4 Stability robustness for uncertainty descriptions based on fractional model representations

The result of section 3 on stability robustness can be applied to various H_∞-norm bounded uncertainty sets by rewriting the uncertainty description into the basic perturbation model $\mathcal{K}(M,\Delta)$. In this section this is done for uncertainty sets based on coprime factor uncertainties.

A crucial aspect in the result of lemma 3.1 is the assumption that $\Delta \in \mathbb{RH}_\infty$. In case of an additive (1) or multiplicative (2) uncertainty set in the basic perturbation model, this assumption implies the condition that the location of all unstable poles of P are assumed to be fixed. Additive perturbations on coprime factorizations (3) are more flexible and allow changes in both the number and the locations of poles and zeros anywhere in $\mathbb{C}$ (Chen and Desoer, 1982). Moreover, fractional representations have a close relation with approximation in the graph topology. Distance measures (or metrics) like the graph and gap metric given in definition 2.2 induce this same graph topology and can also be used to evaluate stability robustness properties of a closed loop system (Vidyasagar, 1984; El-Sakkary, 1985; Vidyasagar and Kimura, 1985).

Firstly, the uncertainty set $\mathcal{P}_{CF}$ (3), as mentioned in the introduction, will be discussed.

Corollary 4.1 *Consider a plant $\hat{P}$ with rcf $(\hat{N},\hat{D})$, stabilized by a given controller C, and consider the uncertainty set*
$\mathcal{P}_{CF}(\hat{N},\hat{D},V_D,V_N,W,\gamma) :=$

$$\{P \mid P=[\hat{N}+\Delta_N][\hat{D}+\Delta_D]^{-1}, \text{ with } \left\| \begin{bmatrix} V_D & 0 \\ 0 & V_N \end{bmatrix} \begin{bmatrix} \Delta_D \\ \Delta_N \end{bmatrix} W \right\|_\infty \leq \gamma\}. \quad (8)$$

for stable and stably invertible filters V_D, V_N, W. Then the feedback system $\mathcal{T}(P,C)$ is internally stable for all $P \in \mathcal{P}_{CF}$ if and only if

$$\gamma < \left\| W^{-1}[\hat{D}+C\hat{N}]^{-1} \begin{bmatrix} I & C \end{bmatrix} \begin{bmatrix} V_D^{-1} & 0 \\ 0 & V_N^{-1} \end{bmatrix} \right\|_\infty^{-1}.$$

Proof: Defining

$$\Delta := \begin{bmatrix} V_D & 0 \\ 0 & V_N \end{bmatrix} \begin{bmatrix} \Delta_D \\ \Delta_N \end{bmatrix} W, \text{ such that } \|\Delta\|_\infty \leq \gamma, \quad (9)$$

the basic perturbation structure of the uncertainty set $\mathcal{P}_{CF}$ can be written into a form that corresponds to $\mathcal{K}(M,\Delta)$ for a specific form of M_{11}. Denoting $col(d_1,d_2) = \Delta z$ with the appropriate signals defined as indicated in figure 3, the corresponding stable transfer function M_{11} satisfying $z = M_{11} col(d_1,d_2)$ can be written as

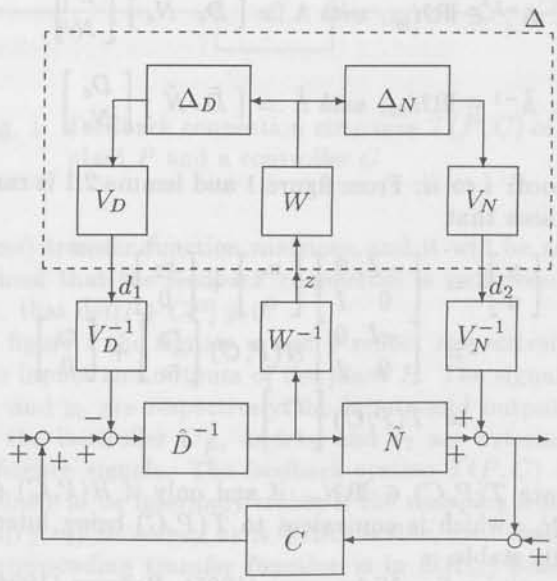

Fig. 3: Additive perturbations on a right coprime factorization

$$\begin{aligned} M_{11} &= -W^{-1}[\hat{D}+C\hat{N}]^{-1} \begin{bmatrix} I & C \end{bmatrix} \begin{bmatrix} V_D^{-1} & 0 \\ 0 & V_N^{-1} \end{bmatrix} \\ &= -W^{-1}\Lambda^{-1} \begin{bmatrix} \tilde{D}_c & \tilde{N}_c \end{bmatrix} \begin{bmatrix} V_D^{-1} & 0 \\ 0 & V_N^{-1} \end{bmatrix} \quad (10) \end{aligned}$$

with $\Lambda = [\tilde{D}_c\hat{D} + \tilde{N}_c\hat{N}]$ and $(\tilde{D}_c, \tilde{N}_c)$ a lcf of C. As the weighting functions are stable and stably invertible, and Λ^{-1} is stable according to Lemma 2.1 it follows that M_{11} is stable. Application of Lemma 3.1 then proves the result. □

In the next section it will be shown how these results can be exploited to derive stability robustness conditions for gap-metric uncertainty sets as well as for uncertainty sets based on further generalizations of the gap-metric. To this end, the result on the equivalence between several formulations of the same uncertainty sets will be presented first.

Proposition 4.2
The uncertainty set $\mathcal{P}_{CF}(\hat{N},\hat{D},V_D,V_N,W,\gamma)$ as defined in Corollary 4.1 can alternatively be written in the following equivalent forms:

(a) $\mathcal{P}_{CF}(\hat{N},\hat{D},V_N,V_D,W,\gamma) = \{P \mid$

$$P = (\hat{N}W + V_N^{-1}\Delta N)(\hat{D}W + V_D^{-1}\Delta D)^{-1},$$

$$\left\| \begin{bmatrix} \Delta N \\ \Delta D \end{bmatrix} \right\|_\infty \leq \gamma\}; \qquad (11)$$

(b) $\mathcal{P}_{CF}(\hat{N}, \hat{D}, V_N, V_D, W, \gamma) =$
$\{P \mid P = N_n D_n^{-1},\ (N_n, D_n)$ nrcf, *and there exists a* $Q \in \mathbb{R}\mathcal{H}_\infty$ *such that*

$$\left\| \begin{bmatrix} V_N & 0 \\ 0 & V_D \end{bmatrix} \left[\begin{bmatrix} \hat{N} \\ \hat{D} \end{bmatrix} W - \begin{bmatrix} N_n \\ D_n \end{bmatrix} Q \right] \right\|_\infty \leq \gamma\}. \qquad (12)$$

Proof: Part (a) follows by simple calculation. The proof of part (b) is more involved. In this derivation the freedom in (11) is used to denote:

$$\begin{aligned} (\hat{N}W + V_N^{-1}\Delta N) &= N_n Q \\ (\hat{D}W + V_D^{-1}\Delta D) &= D_n Q \end{aligned}$$

with (N_n, D_n) a nrcf and $Q \in \mathbb{R}\mathcal{H}_\infty$. Such factors can always be found. It follows then that

$$\begin{aligned} \Delta N &= V_N[N_n Q - \hat{N}W] \\ \Delta D &= V_D[D_n Q - \hat{D}W]. \end{aligned}$$

which proves the result. Note that the factor Q cancels in the representation of P. □

5 Stability robustness based on distance measures

In this section stability robustness results for gap-metric uncertainty sets are formulated. The main result of this section is not new, but already proven separately in Georgiou and Smith (1990*a*). The close relation of the stability robustness result here with the formulation in the previous section concerning general coprime factor uncertainty sets will be illuminated. This relation will be employed in the next section to formulate similar results for uncertainty sets based on the so-called Λ-gap, as recently introduced in Bongers (1991) and Bongers (1994).

The following uncertainty sets are being considered

$$\mathcal{P}_{\vec{\delta}}(\hat{P}, \gamma) := \{P \mid \vec{\delta}(\hat{P}, P) \leq \gamma\} \qquad (13)$$

$$\mathcal{P}_{\delta}(\hat{P}, \gamma) := \{P \mid \delta(\hat{P}, P) \leq \gamma\}, \qquad (14)$$

for which the following relation with the coprime factor uncertainty sets can be shown, as presented before.

Lemma 5.1 *Let a plant* $\hat{P}$ *and a controller* C *constitute an internally stable feedback system* $T(\hat{P}, C)$. *Consider the uncertainty set* $\mathcal{P}_{CF}(\hat{N}, \hat{D}, V_N, V_D, W, \gamma)$ *under the additional conditions that* $(\hat{N}, \hat{D})$ *is a nrcf of* $\hat{P}$, *and* $V_D = I$, $V_N = I$, *and* $W = I$. *Then*

(a) $\mathcal{P}_{CF}(\hat{N}, \hat{D}, V_N, V_D, W, \gamma) = \mathcal{P}_{\vec{\delta}}(\hat{P}, \gamma)$;

(b) For $\gamma < 1$, $\mathcal{P}_{\vec{\delta}}(\hat{P}, \gamma) = \mathcal{P}_{\delta}(\hat{P}, \gamma)$.

Proof: *Part (a).* According to Proposition 4.2(b) and taking into account the specific choice of weighting functions in the lemma, it follows that
$\mathcal{P}_{CF}(\hat{N}, \hat{D}, V_N, V_D, W, \gamma) =$
$\{P \mid P = N_n D_n^{-1},\ (N_n, D_n)$ *nrcf,*
and there exists a $Q \in \mathbb{R}\mathcal{H}_\infty$ such that

$$\left\| \begin{bmatrix} \hat{N} \\ \hat{D} \end{bmatrix} - \begin{bmatrix} N_n \\ D_n \end{bmatrix} Q \right\|_\infty \leq \gamma\}. \qquad (15)$$

Since $(\hat{N}, \hat{D})$ is chosen to be a nrcf of $\hat{P}$ it is straightforward to verify that $\mathcal{P}_{CF} = \mathcal{P}_{\vec{\delta}}$.
Part (b) is proven in Georgiou and Smith (1990*a*). The restriction to $\gamma < 1$ is caused by the fact that these sets with $\gamma \geq 1$ can not be stabilized by a single controller. □

Lemma 5.1 relates the set defined by a gap metric bound with the set of coprime factor purturbations by a special choice of the weighting functions V_D, V_N, W and the coprime factorization $(\hat{N}, \hat{D})$ of the model $\hat{P}$. This gives rise to an unified approach to handle sets of plants that are bounded by a gap metric, and the stability robustness result for these sets follows now directly from Corollary 4.1.

Corollary 5.2
Consider the situation of Lemma 5.1 with $\gamma < 1$. *Then for each of the three sets of plants* $\mathcal{P}_{CF}$, $\mathcal{P}_{\vec{\delta}}$ *and* $\mathcal{P}_{\delta}$, $T(P, C)$ *is internally stable for all* $P \in \mathcal{P}$ *if and only if*

$$\gamma < \|T(\hat{P}, C)\|_\infty^{-1}. \qquad (16)$$

Proof: The proof follows simply by substituting the specific weightings in the result of Corollary 4.1, employing the fact that premultiplication of the expression within the norm by $[\hat{N}^T \ \hat{D}^T]^T$ leaves the norm invariant, due to the normalization of the rcf. □

Note that the result of this corollary is not new. It was shown already in Georgiou and Smith (1990*a*), where a complete proof of the stability robustness result is given. It has been shown here that the stability robustness results in the standard form has simply be exploited, as formulated in section section 3. Restricting attention to the situation that $\gamma < 1$ is natural, as Bode's sensitivity integral shows that $\|T(\hat{P}, C)\|_\infty > 1$, (Maciejowski, 1989), showing that stability robustness can only be achieved for sets with $\gamma < 1$.

Finally it should be noted that the gap and graph metric are induced by the same topology and are uniformly equivalent (Georgiou, 1988; Packard and Helwig, 1989). Therefore stability robustness in the graph metric yields a similar result as mentioned in corollary 5.2.

6 Stability robustness in the Λ-gap

The results obtained in the previous section for gap-based stability robustness can be further extended for uncertainty sets based on the recently introduced Λ-gap, (Bongers, 1991; Bongers, 1994).

Definition 6.1 *Let two plants P_1, P_2 have nrcf's (N_1, D_1), (N_2, D_2) respectively. Let C be a controller with nlcf $(\tilde{D}_c, \tilde{N}_c)$ such that $\mathcal{T}(P_1, C)$ is internally stable. Then the Λ-gap between the plants P_1, P_2 is defined to be expressed by*

$$\vec{\delta}_\Lambda(P_1, P_2) = \inf_{Q \in \mathbb{RH}_\infty} \left\| \begin{bmatrix} D_1 \\ N_1 \end{bmatrix} \Lambda^{-1} - \begin{bmatrix} D_2 \\ N_2 \end{bmatrix} Q \right\|_\infty$$

with $\Lambda = [\tilde{D}_c D_1 + \tilde{N}_c N_1]$.

The difference between $\vec{\delta}(P_1, P_2)$ and $\vec{\delta}_\Lambda(P_1, P_2)$ is the additional shaping of the nrcf of P_1 with Λ^{-1} into a rcf $(\bar{N}, \bar{D})$. In this way $\bar{\Lambda} := \tilde{D}_c \bar{D} + \tilde{N}_c \bar{N} = I$, with $\bar{N} = N_1 \Lambda^{-1}$, $\bar{D} = D_1 \Lambda^{-1}$, which is used to consider the closed loop operation of P_1 induced by the controller C being employed. This makes the distance between P_1 and P_2 dependent on the nrcf of the controller C. Note that the distance measure $\vec{\delta}_\Lambda(P_1, P_2)$ is not a metric since $\vec{\delta}_\Lambda(P_1, P_2) \neq \vec{\delta}_\Lambda(P_2, P_1)$ due to the influence of the controller C (Bongers, 1994).
Accordingly, an uncertainty set based on Λ-gap uncertainty can be defined as:

$$\mathcal{P}_{\vec{\delta}_\Lambda}(\hat{P}, \gamma) := \{P \mid \vec{\delta}_\Lambda(\hat{P}, P) \leq \gamma\}.$$

This uncertainty set can also be shown to be equivalent to an uncertainty set of coprime factor uncertainties, provided appropriate weighting functions are chosen.

Lemma 6.2 *Let a plant $\hat{P}$ and a controller C with nlcf $(\tilde{D}_c, \tilde{N}_c)$ constitute an internally stable feedback system $\mathcal{T}(\hat{P}, C)$. Consider the uncertainty set $\mathcal{P}_{CF}(\hat{N}, \hat{D}, V_N, V_D, W, \gamma)$ under the additional conditions that $(\hat{N}, \hat{D})$ is a nrcf of $\hat{P}$, and $V_D = I$, $V_N = I$, and $W = \Lambda^{-1}$ with $\Lambda = [\tilde{D}_c \hat{D} + \tilde{N}_c \hat{N}]$. Then*

(a) $\mathcal{P}_{CF}(\hat{N}, \hat{D}, V_N, V_D, W, \gamma) = \mathcal{P}_{\vec{\delta}_\Lambda}(\hat{P}, \gamma)$;

(b) $\mathcal{T}(P, C)$ is internally stable for all $P \in \mathcal{P}_{CF}$ if and only if $\gamma < 1$.

Proof: The proof of (a) is straightforward, along the same lines as the proof of Lemma 5.1(a). Result (b) then follows directly from Corollary 4.1, employing the fact that $\Lambda[\hat{D} + C\hat{N}]^{-1}[I\ C] = [\tilde{D}_c\ \tilde{N}_c]$ having an ∞-norm of 1 due to the fact that it is a normalized left coprime factorization. □

As said before, in case of the Λ-gap, the uncertainty set defined accordingly considers perturbations of the nominal plant $\hat{P}$ that are controller dependent. The introduction of weightings in the gap metric has also been studied in Geddes and Postlethwaite (1992), Georgiou and Smith (1990*b*) or Qui and Davidson (1992). In Geddes and Postlethwaite (1992) a multiplicative uncertainty description on the nrcf $(\hat{N}, \hat{D})$ of the model $\hat{P}$ is being used, leading to an uncertainty structure Δ having a diagonal form. Due to the diagonal form only necessary and sufficient conditions based on the structured singular value $\mu\{\cdot\}$ can be obtained. The weightings in the weighted gap of Georgiou and Smith (1990*b*) have to be defined *a posteriori* which makes the choice of the weighting functions, to access robustness issues on the basis of a weighted gap, not a trivial task. Information on the size of the coprime factor perturbations can be used in the weighted pointwise gap metric defined in Qui and Davidson (1992), but still an efficient computational method for pointwise gap metric is not available yet.

7 Conservatism issues

All stability robustness results in this paper reflect necessary and sufficient conditions of an uncertainty set to be stabilized by a single controller. As such no conservatism is introduced in the test for checking stability robustness itself. However, for a single given controller, different of such uncertainty sets contain a different portion of the set of all systems that is stabilized by the controller. In this perspective the concept of conservatism is an intrinsic property of the uncertainty set being used. As a result an uncertainty set will be called more conservative than another if one controller stabilizes both sets, while the former set is contained in the latter.

Theorem 7.1 (Bongers, 1991) *Consider a plant $\hat{P}$ and a stabilizing controller C with nlcf $(\tilde{D}_c, \tilde{N}_c)$. Consider the following two uncertainty sets resulting from the stability robustness results in the previous sections:*

$$\mathcal{S}_\delta(\hat{P}, C) := \{\cup\, \mathcal{P}_\delta(\hat{P}, b),\ b < \|T(\hat{P}, C)\|_\infty^{-1}\}$$
$$\mathcal{S}_{\vec{\delta}_\Lambda}(\hat{P}, C) := \{\cup\, \mathcal{P}_{\vec{\delta}_\Lambda}(\hat{P}, c),\ c < 1\}$$

then

$$\mathcal{S}_\delta(\hat{P}, C) \subset \mathcal{S}_{\vec{\delta}_\Lambda}(\hat{P}, C). \qquad (17)$$

Proof: The following implication will be proven:

$$\bar{P} \in \mathcal{S}_\delta(\hat{P}, C) \Rightarrow \bar{P} \in \mathcal{S}_{\bar{\delta}_\Lambda}(\hat{P}, C). \qquad (18)$$

As $\bar{P} \in \mathcal{S}_\delta(\hat{P}, C)$ there exists a $\bar{U} \in \mathbb{RH}_\infty$ such that

$$\| \begin{bmatrix} \hat{D}_n \\ \hat{N}_n \end{bmatrix} - \begin{bmatrix} \bar{D} \\ \bar{N} \end{bmatrix} \bar{U} \|_\infty \leq \frac{1}{\|T(\hat{P}, C)\|_\infty}. \qquad (19)$$

This implies that

$$\| \begin{bmatrix} \hat{D}_n \\ \hat{N}_n \end{bmatrix} - \begin{bmatrix} \bar{D} \\ \bar{N} \end{bmatrix} \bar{U} \|_\infty \cdot \|\Lambda^{-1}\|_\infty \leq \frac{\|\Lambda^{-1}\|_\infty}{\|T(\hat{P}, C)\|_\infty}. \qquad (20)$$

As $\|T(\hat{P}, C)\|_\infty = \|\Lambda^{-1}\|_\infty$, this implies that

$$\| \begin{bmatrix} \hat{D}_n \\ \hat{N}_n \end{bmatrix} - \begin{bmatrix} \bar{D} \\ \bar{N} \end{bmatrix} \bar{U} \|_\infty \cdot \|\Lambda^{-1}\|_\infty \leq 1. \qquad (21)$$

Lower bounding the left hand term of this expression implies that

$$\| \begin{bmatrix} \hat{D}_n \\ \hat{N}_n \end{bmatrix} \Lambda^{-1} - \begin{bmatrix} \bar{D} \\ \bar{N} \end{bmatrix} \bar{U} \Lambda^{-1} \|_\infty \leq 1 \qquad (22)$$

which proves the result. □

The result shows the the Λ-gap uncertainty set is less conservative than the gap uncertainty set. Intuitively this is also clear, since the gap metric does not take into account the closed loop operation of the plants P in the set, induced by the controller C being used, see e.g. also Hsieh and Safonov (1993). This drawback has been rectified by the use of the Λ-gap.

Conclusions

The powerful standard representation for uncertainty descriptions in a basic perturbation model as introduced in Doyle (1982) can be used to attain necessary and sufficient conditions for stability robustness within various uncertainty descriptions. In this paper these results are applied to uncertainty descriptions based on fractional model representations, leading to necessary and sufficient conditions for stability robustness in case of additive coprime factor uncertainties.

In this way a unified approach to handle additive coprime factor perturbations can be derived which yields a manageable and comprehensive way to relate gap and Λ-gap based uncertainty sets to (weighted) additive coprime factor perturbations. Based on this framework necessary and sufficient conditions for gap and Λ-gap based uncertainty sets are presented and it is shown that in terms of stability robustness, the Λ-gap uncertainty set is less conservative than the gap uncertainty set.

Acknowledgement

The authors would like to thank Carsten Scherer and Ruud Schrama for fruitful discussions that contributed to the results of this paper.

References

Bongers, P.M.M. (1991). On a new robust stablity margin. *Recent Advances in Mathematical Theory of Systems, Control, Networks and Signal Processing, Proc. of the Int. Symposium MTNS-91.* pp. 377–382.

Bongers, P.M.M. (1994). Modeling and Identification of Flexible Wind Turbines and a Factorizational Approach to Robust Control. PhD thesis. Delft Univ. Techn., Mech. Eng. Systems and Control Group.

Chen, C.T. and C.A. Desoer (1982). Algebraic theory for robust stability of interconnected systems: necessary and sufficient conditions. In *Proc. IEEE Conf. Decision and Control*, pp. 491–494.

Doyle, J.C. (1982). Analysis of feedback systems with structured uncertainties. *IEE Proc. on Control Theory and Applications, part D*, Vol. *129*, pp. 242–250.

Doyle, J.C. and G. Stein (1981). Multivariable feedback design: concepts for a classical/modern synthesis. *IEEE Trans. Autom. Control, AC-26*, 4–16.

Doyle, J.C., B.A. Francis and A.R. Tannenbaum (1992). *Feedback Control Theory.* MacMillan Publishing Company, NY, USA.

El-Sakkary, A.K. (1985). The gap metric: Robustness of stabilization of feedback systems. *IEEE Trans. Autom. Control, AC-30*, 240–247.

Francis, B.A. (1987). *A Course in H_∞ Control Theory.* Lect. Notes Contr. Inform. Sc., Vol. 88, Springer Verlag, Berlin.

Geddes, E.J.M. and I. Postlethwaite (1992). The weigthed gap metric and structured uncertainty. *Proc. Amer. Control Conf.*, Chicago, IL, pp. 1138–1142.

Georgiou, T.T. (1988). On the computation of the gap metric. *Syst. Control Lett., 11*, 253–257.

Georgiou, T.T. and M.C. Smith (1990*a*). Optimal robustness in the gap metric. *IEEE Trans. Autom. Control, AC-35*, 673–686.

Georgiou, T.T. and M.C. Smith (1990*b*). Robust control of feedback systems with combined plant and controller uncertainty. In *Proc. Amer. Control Conf.*, pp. 2009–2013.

Glover, K. and D. McFarlane (1989). Robust stabilization of normalized coprime factor plant descriptions with H_∞-bounded uncertainty. *IEEE Trans. Autom. Control, AC-34*, 821–830.

Hsieh, G.C. and M.G. Safonov (1993). Conservatism of the gap metric. *IEEE Trans. Autom. Control, AC-38*, 594–598.

Maciejowski, J.M. (1989). *Multivariable Feedback Design*. Addison–Wesley Publishing Company, Wokingham, UK.

Packard, A. and M. Helwig (1989). Relating the gap and graph metrics via the triangle inequality. *IEEE Trans. Autom. Control, AC-34*, 1296–1297.

Qui, L. and E.J. Davidson (1992). Pointwise gap metrics on transfer matrices. *IEEE Trans. Autom. Control, AC-37*, 741–758.

Schrama, R.J.P. (1992). *Approximate Identification and Control Design with Application to a Mechanical System*. PhD Thesis. Delft Univ. Techn., Mech. Eng. Systems and Control Group.

Vidyasagar, M. (1984). The graph metric for unstable plants and robustness estimates for feedback stability. *IEEE Trans. Autom. Control, AC-29*, 403–418.

Vidyasagar, M. (1985). *Control System Synthesis: A Factorization Approach*. Cambridge, MIT Press.

Vidyasagar, M and H. Kimura (1985). Robust controllers for uncertain multivariable systems. *Automatica, 22*, 85–94.

Vidyasagar, M., H. Schneider and B.A. Francis (1982). Algebraic and topological aspects of feedback stabilization. *IEEE Trans. Autom. Control, AC-27*, 880–894.

Zames, G. and A.K. El-Sakkary (1980). Unstable systems and feedback: The gap metric. *Proc. Allerton Conference*, pp. 380–385.

Selected Topics in Identification, Modelling and Control
Vol. 7, December 1994

Solvability tests for the Lyapunov inequality[‡]

Carsten W. Scherer[§]

Mechanical Engineering Systems and Control Group
Delft University of Technology, Mekelweg 2, 2628 CD Delft, The Netherlands.

Abstract. For *arbitrary* complex A and Q (Q Hermitian), this paper provides an algebraic test for verifying the existence of a Hermitian solution X of the nonstrict Lyapunov inequality

$$A^*X + XA + Q \geq 0.$$

If existing we exhibit how to construct a solution. Moreover, a necessary condition for the existence of a positive definite solution is presented which is most likely to be sufficient as well. Our approach involves the validation problem for the linear matrix inequality

$$\sum_{j=1}^{k}(A_j^* X_j B_j + B_j^* X_j^* A_j) + Q > 0$$

in X_j for which we provide a (constructive) algebraic solvability test if the kernels of A_j or, dually, those of B_j form an isotonic sequence.

Keywords. Lyapunov inequality, linear matrix inequality, Riccati inequality.

Notation. $\mathcal{C} = \mathcal{C}^- \cup \mathcal{C}^0 \cup \mathcal{C}^+$ is the complex plane, the open left-half plane, the imaginary axis and the open right-half plane. For $A \in \mathcal{C}^{n\times m}$, $A^{-\nu}\mathcal{S}$ denotes the preimage $\{x \in \mathcal{C}^m \mid A^\nu x \in \mathcal{S}\}$ of $\mathcal{S} \subset \mathcal{C}^n$ under A^ν. For a Hermitian $Q \in \mathcal{C}^{n\times n}$, $Q_{\mathcal{S}}$ denotes the sesquilinear form $\mathcal{S} \times \mathcal{S} \ni (x, y) \to x^*Qy \in \mathcal{C}$. Then $Q_{\mathcal{S}} > 0$ (Q is positive definite on $\mathcal{S}$) iff $x^*Qx > 0$ for $x \in \mathcal{S} \setminus \{0\}$, $Q_{\mathcal{S}} \geq 0$ (Q is positive semidefinite on $\mathcal{S}$) iff $x^*Qx \geq 0$ for $x \in \mathcal{S}$, and $\ker(Q_{\mathcal{S}}) = \{x \in \mathcal{S} : x^*Qx = 0\}$ (the annihilating set of Q on $\mathcal{S}$).

1 Introduction

The Lyapunov equation and inequality is one of the most studied objects in the control literature. In particular, it arises in stability theory where the interest is on inertia relations rather than on solvability questions. The present work is mainly motivated by state-space H_∞-theory (Petersen (1989), Doyle *et al.* (1989), Scherer (1994)). It has been shown in Scherer (1994) that the optimal value in the general state-feedback H_∞-problem is attained iff a certain algebraic Riccati inequality has a positive definite solution. In Scherer (1993,1994) we present a technique which reduces this problem, under a mild regularity assumption, to the solvability problem for a nonstrict Lyapunov inequality (LI)

$$A^*X + XA + Q \geq 0$$

where A and Q can be computed from the system's state-space representation. Here Q is generally indefinite and the eigenvalues of A correspond to invariant system zeros in $\mathcal{C}^0 \cup \mathcal{C}^+$. Hence eigenvalues in $\mathcal{C}^0$ can only be excluded by *assuming* the absence of system zeros on the imaginary axis.
If A has *no eigenvalues* in $\mathcal{C}^0$ then it is a consequence of the reduction principles in Scherer (1993, 1994) (but easily proved directly) that the LI is always solvable, although the corresponding equation might not have a solution. Hence the main difficul-

[‡]This paper is presented at the 33rd IEEE Conf. Decision and Control, Lake Buena Vista, FL, December 14-16, 1994.

[§]supported by Deutsche Forschungsgemeinschaft, grant Wi 1219/1-1.

ties arise if A indeed has eigenvalues in $\mathcal{C}^0$. If the $\mathcal{C}^0$-Jordan blocks of A with respect to $\mathcal{C}^0$ are diagonal, it has been pointed out that the LI is solvable iff $Q_{\ker(A-\lambda I)} \geq 0$ for each $\lambda \in \mathcal{C}^0$ (Scherer (1994)). If the $\mathcal{C}^0$-eigenstructure of A is nonderogatory, solvabilty tests have been obtain in Scherer (1995a). However, the general case with an unrestricted $\mathcal{C}^0$-Jordan structure is considerably more difficult to handle. In this paper we extend results from Scherer (1993) and show how to verify the solvability of the LI in complete generality. In view of the recent progress in solving more general *strict* linear matrix inequalities (Nesterov, Nemirovsky (1994)), our work is intended to clarify, for a specific inequality of independent importance, that the algebraic approach leads to deep insights into the structure of the solution set and into the possibly tremendous difference between *strict* and *nonstrict* inequalities. We work throughout with complex matrices and spaces. If A and Q are real symmetric, our results allow to verify the existence and to construct a complex Hermitian solution X. Then $\frac{1}{2}(X+\bar{X})$ is a real symmetric solution of the LI. Hence the present results apply to real data as well.

The paper is structured as follows. In Section 2 we present some auxiliary results of independent interest. In Section 3 we motivate and formulate the solvability characterization, and in Section 4 it is shown how to construct a solution. For reasons of space the proofs are given in the full version of the paper which will appear elsewhere.

2 Auxiliary Linear Matrix Inequalities

We first recall a key result in Scherer (1992) for the strict Lyapunov inequality (SLI)

$$A^*X + XA + Q > 0.$$

Theorem 2.1 *The SLI has a Hermitian solution iff $Q_{\ker(A-\lambda I)} > 0$ for all $\lambda \in \mathcal{C}^0$. If solvable, the SLI has arbitrarily large (and thus positive definite) solutions iff $\sigma(A) \subset \mathcal{C}^0 \cup \mathcal{C}^+$.*

Remark. In Scherer (1995b), the last part has been generalized to the nonstrict Lyapunov inequality: The LI has arbitrarily large solutions iff $\sigma(A) \subset \mathcal{C}^0 \cup \mathcal{C}^+$, $Q_{\ker(A-\lambda I)} \geq 0$ and $\ker(Q_{\ker(A-\lambda I)}) \cap \mathrm{im}(A-\lambda I) = \{0\}$ for all $\lambda \in \mathcal{C}^0$.

If we drop the structural constraint $X = X^*$, we can even consider the more general inequality

$$A^*XB + B^*X^*A + Q > 0 \qquad (1)$$

which has recently proved important in the H_∞-problem and variations thereof (Gahinet, Apkarian (1994), Iwasaki, Skelton (1994)).

Theorem 2.2 *The inequality (1) is (constructively) solvable iff $Q_{\ker(A)} > 0$ and $Q_{\ker(B)} > 0$.*

In this paper we need a generalization to the LMI

$$\sum_{j=1}^{k} (A_j^* X_j B_j + B_j^* X_j^* A_j) + Q > 0 \qquad (2)$$

for which we can indeed give an algebraic solvability test and a procedure to construct a solution if the kernels of A_j form a nondecreasing sequence.

Theorem 2.3 *Suppose* $\ker(A_1) \subset \cdots \subset \ker(A_k)$. *Then the LMI (2) is (constructively) solvable iff Q is* positive definite *on*

$$\bigcap_{\nu=0}^{j-1} \ker(B_\nu) \cap \ker(A_j)$$

for all $j = 1, \ldots, k+1$ where setting $B_0 = 0$ and $A_{k+1} = 0$.

Clearly, a dual result holds if the kernels of B_j form a nondecreasing sequence and, by reordering, one can easily translate all this to nonincreasing kernel sequences as well.

3 The Lyapunov Inequality

A key step will consist of identifying the largest subspace on which $A^*X + XA + Q$ *vanishes* for every X in the solution set

$$\mathcal{X} := \{X : \ X = X^*, \ A^*X + XA + Q \geq 0\}$$

of the LI. It will turn out that we can indeed compute

$$\mathcal{K} := \bigcap_{X \in \mathcal{X}} \ker(A^*X + XA + Q) \qquad (3)$$

on the basis of the data matrices A and Q without having a solution available! The space $\mathcal{K}$ will be shown to be A-invariant. Moreover, it might happen that for each individual $X \in \mathcal{X}$ the kernel of $A^*X + XA + Q$ is larger than $\mathcal{K}$. Luckily enough this is not the case since we are able to prove the existence of an $X \in \mathcal{X}$ with $\ker(A^*X + XA + Q) = \mathcal{K}$. All this will be essential for the test whether $\mathcal{X}$ is empty or not.

For formulating the main result we need the following notations. For any $\lambda \in \mathcal{C}^0$ define

$$A_\lambda := A - \lambda I$$

and the linear map

$$\mathcal{L}_\lambda^j(Q) := \sum_{\nu=0}^{j} (-1)^\nu (A_\lambda^*)^{j-\nu} Q A_\lambda^\nu.$$

Note that $\mathcal{L}_\lambda^0(Q) = Q$ and that $\mathcal{L}_\lambda^j$ is just the j-fold composition of $\mathcal{L}_\lambda(Q) = A_\lambda^* Q - Q A_\lambda$. We exploit $\lambda \in \mathcal{C}^0$ to infer $A^*X + XA = A_\lambda^* X + X A_\lambda$ which implies $\mathcal{L}_\lambda^j(A^*X+XA) = (A_\lambda^*)^{j+1}X+(-1)^j X A_\lambda^{j+1}$. For any $j = 0, 1, \ldots$, this shows that $A^*X + XA + Q = P$ implies

$$(A_\lambda^*)^{j+1}X + (-1)^j X A_\lambda^{j+1} + \mathcal{L}_\lambda^j(Q) = \mathcal{L}_\lambda^j(P). \quad (4)$$

Let us now motivate the computation of (3) under the hypothesis $\mathcal{X} \neq \emptyset$. Choose $X \in \mathcal{X}, \lambda \in \mathcal{C}^0 \cap \sigma(A)$ and define the *positive semidefinite* $P := A^*X + XA + Q$.
Look at (4) for $j = 0$. $A_\lambda x = 0$ yields $x^*Qx = x^*Px \geq 0$. If, in addition, $x^*Qx = 0$ then $x^*Px = 0$ and thus $Px = 0$. Hence Q is positive semidefinite on $A_\lambda^{-1}\{0\}$ and $\mathcal{N}_1^\lambda = \{x \in A_\lambda^{-1}\{0\} : x^*Qx = 0\}$ is a subspace with $\mathcal{N}_1^\lambda \subset \ker(P)$. We proceed with $\mathcal{K}_1^\lambda = \{0\} + A_\lambda^0 \mathcal{N}_1^\lambda = \mathcal{N}_1^\lambda$.
To increase the space $\mathcal{N}_1^\lambda$, the central trick is to exploit (4) for $j = 2$ which leads to

$$[(A_\lambda^*)^3 X + X A_\lambda^3] + \mathcal{L}_\lambda^2(Q) = (A_\lambda^*)^2 P - A_\lambda^* P A_\lambda + P A_\lambda^2.$$

If x satisfies $A_\lambda^2 x \in \mathcal{K}_1^\lambda$ then $A_\lambda^3 x = 0$ (since $A_\lambda \mathcal{K}_1^\lambda = \{0\}$) and $PA_\lambda^2 x = 0$ (since $P\mathcal{K}_1^\lambda = \{0\}$). We infer

$$x^* \mathcal{L}_\lambda^2(Q) x = -x^* A_\lambda^* P A_\lambda x.$$

Hence $-\mathcal{L}_\lambda^2(Q)$ is positive semidefinite on $A_\lambda^{-2}\mathcal{K}_1^\lambda$. Moreover, the annihilating set $\mathcal{N}_2^\lambda = \{x \in A_\lambda^{-2}\mathcal{K}_1^\lambda : x^*\mathcal{L}_\lambda^2(Q)x = 0\}$ is a subspace with $A_\lambda \mathcal{N}_2^\lambda \subset \ker(P)$. We proceed with $\mathcal{K}_2^\lambda = \mathcal{K}_1^\lambda + A\mathcal{N}_2^\lambda$.
Now we can turn to a formal definition of this algorithm. Since we do not require the LI to have a solution, certain positivity conditions (as appearing in the above motivation) need not be verified. If they are not true, we allow the algorithm to stop irregularly since then, as can be proved, the LI has no solution.

Definition 3.1 *Fix $\lambda \in \mathcal{C}^0$ and $\mathcal{K}_0^\lambda := \{0\}$. Suppose $\mathcal{K}_j^\lambda$ has been constructed. Then the algorithm* stops irregularly *if $(-1)^j \mathcal{L}_\lambda^{2j}(Q)$ is* not positive semidefinite *on $A_\lambda^{-(j+1)}\mathcal{K}_j^\lambda$. Otherwise define the neutralizing* subspace

$$\mathcal{N}_{j+1}^\lambda := \{x \in A_\lambda^{-(j+1)}\mathcal{K}_j^\lambda \mid x^*\mathcal{L}_\lambda^{2j}(Q)x = 0\}$$

and iterate with

$$\mathcal{K}_{j+1}^\lambda := \mathcal{K}_j^\lambda + A_\lambda^j \mathcal{N}_{j+1}^\lambda.$$

Remark. To clarify the behavior of $\mathcal{K}_j^\lambda$ under transformations of (A, Q) we will sometimes stress the dependence on the data by writing $\mathcal{K}_j^\lambda(A, Q)$ and $\mathcal{N}_j^\lambda(A, Q)$.

The inclusion $\mathcal{K}_j^\lambda \subset \mathcal{K}_{j+1}^\lambda$ is obvious. If the algorithm does not stop irregularly then $\mathcal{K}_j^\lambda$ is well-defined for all $j = 0, 1, \ldots$ and there exists a (smallest) k with $\mathcal{K}_{k+1}^\lambda = \mathcal{K}_k^\lambda$ which implies $\mathcal{K}_0^\lambda \subset \mathcal{K}_1^\lambda \subset \cdots \subset \mathcal{K}_k^\lambda = \mathcal{K}_{k+1}^\lambda = \mathcal{K}_{k+2}^\lambda = \cdots$. The limiting subspace $\mathcal{K}_k^\lambda$ is denoted by $\mathcal{K}_*^\lambda$.

Definition 3.2 *We say that $\mathcal{K}_*^\lambda$ exists iff the algorithm does not stop irregularly for λ. We say that $\mathcal{K}_*$ exists iff $\mathcal{K}_*^\lambda$ exists for each $\lambda \in \mathcal{C}^0$, and define*

$$\mathcal{K}_* := \sum_{\lambda \in \mathcal{C}^0} K_*^\lambda.$$

Remarks.

- If existing, all $\mathcal{K}_j^\lambda$ and hence also $\mathcal{K}_*$ are A-invariant.
- For $\lambda \in \mathcal{C}^0 \setminus \sigma(A)$ it is clear that $\mathcal{K}_*^\lambda$ exists and equals $\{0\}$. Only if λ is an *eigenvalue of A on the imaginary axis*, the space $\mathcal{K}_*^\lambda$ might not exist or might be nontrivial. However, if $Q_{\ker(A_\lambda)} > 0$ (as appearing in Theorem 2.1) then, again, $\mathcal{K}_*^\lambda = \{0\}$.

We can now state in generality what has been motivated above.

Lemma 3.3 *If $\mathcal{X} \neq \emptyset$ then $\mathcal{K}_*$ exists and satisfies $(A^*X + XA + Q)\mathcal{K}_* = \{0\}$ for all $X \in \mathcal{X}$.*

Hence the existence of $\mathcal{K}_*$ and of some Hermitian X with $(A^*X+XA+Q)\mathcal{K}_* = \{0\}$ are necessary conditions for the solvability of the LI. The first condition amounts to the algorithm not stopping irregularly for each $\lambda \in \sigma(A) \cap \mathcal{C}^0$, and the second is a validation problem for a linear *equation* whose solution can be constructed if existing - both conditions are algebraically verifiable.
It is the new core result of the present paper that these conditions are also sufficient for the existence of solutions of the LI. As an important structural result we prove that not only $\mathcal{K}_* \subset \mathcal{K}$ but in fact equality holds. Hence the subspace $\mathcal{K}$ is exactly computable without having a solution of the LI available.

Theorem 3.4 *The Lyapunov inequality $A^*X + XA + Q \geq 0$ has a solution iff $\mathcal{K}_*$ exists and there is a Hermitian X with $(A^*X + XA + Q)\mathcal{K}_* = \{0\}$. Suppose $\mathcal{X} \neq \emptyset$. Then $\mathcal{K}_* \subset \ker(A^*X+XA+Q)$ for all $X \in \mathcal{X}$ and there exists a special solution such that equality holds.*

For testing the existence of a positive definite element in $\mathcal{X}$ we try to find a large subspace on which the quadratic form x^*Xx remains fixed if X varies in $\mathcal{X}$. The following can be shown to be a candidate.

Definition 3.5 *For each $\lambda \in \mathcal{C}^0$ define the subspace*

$$\mathcal{P}_*^\lambda := \sum_{j=1}^{\infty} \ker(A_\lambda^j) \cap im(A_\lambda^j) \cap \mathcal{K}_*^\lambda$$

and then

$$\mathcal{P}_* := \sum_{\lambda \in \mathcal{C}^0} \mathcal{P}_*^\lambda.$$

Theorem 3.6 *If the Hermitian X_1, X_2 satisfy $(A^*X_j + X_jA + Q)\mathcal{K}_* = \{0\}$, $j = 1, 2$, then $x^*X_1x = x^*X_2x$ holds for all $x \in \mathcal{P}_*$. If $\mathcal{X}$ contains positive definite elements then one/all Hermitian X satisfying $(A^*X + XA + Q)\mathcal{K}_* = \{0\}$ is/are positive definite on $\mathcal{P}_*$.*

Remarks. This necessary condition for the existence of positive definite solutions to the LI is verifiable. It can be shown constructively that it is also sufficient if A has precisely one Jordan block for each $\mathcal{C}^0$-eigenvalue. We conjecture that sufficiency also holds for a general A.

4 Construction of Solutions

From now on we assume that $\mathcal{K}_*$ exists and that we have found an $\tilde{X}$ with $\ker(A^*\tilde{X} + \tilde{X}A + Q)\mathcal{K}_* = \{0\}$. To prove sufficiency in Theorem 3.4, we intend to construct an $X = X^*$ with

$$A^*X + XA + Q \geq 0, \ker(A^*X + XA + Q) = \mathcal{K}_*. \quad (5)$$

With $\tilde{Q} := A^*\tilde{X} + \tilde{X}A + Q$, we can instead determine a Hermitian solution of $A^*Z + ZA + \tilde{Q} \geq 0$ with $\ker(A^*Z + ZA + \tilde{Q}) = \mathcal{K}_*$ since then $X := Z + \tilde{X}$ satisfies (5). It is not difficulty to prove that $\mathcal{K}_*(A, Q)$ exists iff $\mathcal{K}_*(A, \tilde{Q})$ exists, and that both spaces coincide. Hence we can work w.l.o.g. with the hypotheses that

$$\mathcal{K}_* \text{ exists and } Q\mathcal{K}_* = \{0\}. \quad (6)$$

By changing coordinates, we can also assume A in the shape

$$A = \operatorname{diag}(A_0 \; A_1 \; \cdots \; A_l)$$

with $\sigma(A_0) \subset \mathcal{C}^- \cup \mathcal{C}^+$, $\sigma(A_\nu) = \{\lambda_\nu\} \subset \mathcal{C}^0$, $\lambda_\nu \neq \lambda_\mu$ for $\nu, \mu = 1, \ldots, l$, $\nu \neq \mu$ and partition X, Q accordingly. Noting $A_{\lambda_\nu}^j \mathcal{K}_j^{\lambda_\nu} = \{0\}$, it is very simple to see that $\mathcal{K}_j^{\lambda_\nu}(A, Q)$ exists iff $\mathcal{K}_j^{\lambda_\nu}(A_\nu, Q_{\nu\nu})$ exists and

$$\mathcal{K}_j^{\lambda_\nu}(A, Q) = \{x_\nu \in \mathcal{K}_j^{\lambda_\nu}(A_\nu, Q_{\nu\nu}), x_\mu = 0, \mu \neq \nu\}.$$

Hence $\mathcal{K}_*^{\lambda_\nu}(A_\nu, Q_{\nu\nu}) = \mathcal{K}_*^0(A_\nu - \lambda_\nu I, Q_{\nu\nu})$ exists and satisfies $Q_{\nu\nu}\mathcal{K}_*^0(A_\nu - \lambda_\nu I, Q_{\nu\nu}) = \{0\}$. Note that these are just the properties (6) for the *nilpotent* matrix $A_\nu - \lambda_\nu I$ and $Q_{\nu\nu}$. Suppose that, under the assumption (6) with A being nilpotent, we can construct an X satisfying (5). Then one can compute $X_{\nu\nu}$ for $\nu = 1, \ldots, l$ with $A_\nu^* X_{\nu\nu} + X_{\nu\nu}A_\nu + Q_{\nu\nu} \geq 0$ and $\ker(A_\nu^* X_{\nu\nu} + X_{\nu\nu}A_\nu + Q_{\nu\nu}) = \mathcal{K}_*^0(A_\nu - \lambda_\nu I, Q_{\nu\nu})$. Let us choose X_{00} as $A_0^* X_{00} + X_{00}A_0 + Q_{00} > 0$. For all other indices we take $X_{\nu\mu}$ as the solution of $A_\nu^* X_{\nu\mu} + X_{\nu\mu}A_\mu + Q_{\nu\mu} = 0$ (which exists by $\sigma(A_\nu^*) \cap \sigma(-A_\mu) = \emptyset$). Then $A^*X + XA + Q = \operatorname{diag}(A_\nu^* X_{\nu\nu} + X_{\nu\nu}A_\nu + Q_{\nu\nu})$ implies that $X \in \mathcal{X}$. Moreover, $\ker(A^*X + XA + Q) = \{x : (A_\nu^* X_{\nu\nu} + X_{\nu\nu}A_\nu + Q_{\nu\nu})x_\nu = 0\} = \{x : x_0 = 0, x_\nu \in \mathcal{K}_*^0(A_\nu - \lambda_\nu I, Q_{\nu\nu})\} = \mathcal{K}_*(A, Q)$ finishes the proof.

We have reduced the general problem to the case that

$$A \text{ is nilpotent.}$$

From now on we drop the index $\lambda = 0$ in Definition 3.1. After a further coordinate change we assume w.l.o.g.

$$\mathcal{K}_* = \{\begin{pmatrix} x_1 \\ x_2 \end{pmatrix} \mid x_2 = 0\}$$

to obtain (recalling $A\mathcal{K}_* \subset \mathcal{K}_*$ and $Q\mathcal{K}_* = \{0\}$)

$$A = \begin{pmatrix} K & M \\ 0 & L \end{pmatrix} \text{ and } Q = \begin{pmatrix} 0 & 0 \\ 0 & P \end{pmatrix} \quad (7)$$

where K and L are in Jordan canonical form partitioned as

$$\begin{aligned} K &= \operatorname{diag}(K_0, K_1, \ldots, K_m), \\ L &= \operatorname{diag}(L_1, \ldots, L_m, L_{m+1}) \end{aligned} \quad (8)$$

and

- all blocks in K_0 are smaller than those in L,
- all blocks in K_k and L_k have the same size m_k, $k = 1, \ldots, m$, with $m_k < m_{k+1}$,
- all blocks in K are smaller than those in L_{m+1}.

We stress that extreme cases are not excluded: K_0 or L_{m+1} or all $K_1, \ldots, K_m$ might be empty matrices! We also need notations for the refinement of this partition into

$$\begin{aligned} K_k &= \operatorname{diag}(K_k^1 \; \cdots \; K_k^{\kappa_k}), \\ L_l &= \operatorname{diag}(L_l^1 \; \cdots \; L_l^{\lambda_l}) \end{aligned} \quad (9)$$

with single *upper* Jordan blocks K_k^κ, L_l^λ. This induces on a vector x compatible to the size of K, a vector y compatible to the size of L, and on any matrix Z of the same size as M the partitions $x = (x_k)_k$, $y = (y_l)_l$, $Z = (Z_{kl})_{kl}$ according to (8) and $x_k = (x_k^\kappa)_\kappa$, $y_l = (y_l^\lambda)_\lambda$, $Z_{kl} = (Z_{kl}^{\kappa\lambda})_{\kappa\lambda}$ according to (9).

Indeed we will fulfill (5) with X structured as $\begin{pmatrix} 0 & Y \\ Y^* & Z \end{pmatrix}$ such that $A^*X + XA + Q$ equals

$$\begin{pmatrix} 0 & K^*Y + YL \\ * & L^*Z + ZL + Y^*M + M^*Y + P \end{pmatrix}. \quad (10)$$

In the remainder of this section we clarify how to

> compute a $Y \in \mathcal{Y} := \{Y : K^*Y + YL = 0\}$ for which $L^*Z + ZL + Y^*M + M^*Y + P > 0$ has a Hermitian solution Z.

By Theorem 2.1, we hence need to guarantee, for any basis matrix E of the kernel of L, the existence of $Y \in \mathcal{Y}$ with $E^*(Y^*M + M^*Y + P)E > 0$ or

$$(YE)^*(ME) + (ME)^*(YE) + E^*PE > 0. \quad (11)$$

Note that this is a linear matrix inequality with a *structural* constraint on Y and hence generally very difficult to handle. Luckily enough the present case is indeed tractable.

We choose E (in our coordinates) as simple as possible. With $e_l^\lambda := (1\ 0\ \cdots\ 0)^T$ of length equal to the size of L_l^λ, $E_l := \mathrm{diag}(e_l^1\ \cdots\ e_l^{\lambda_l})$ is a basis matrix of $\ker(L_l)$ and hence $E := \mathrm{diag}(E_1\ \cdots\ E_m\ E_{m+1})$ is one of L.

If we partition Y as M, we now intend to identify the structure of $(ME)^*(YE)$ for $Y \in \mathcal{Y}$. Clearly $Y \in \mathcal{Y}$ iff

$$Y_{kl}^{\kappa\lambda} \in \mathcal{Y}_{kl}^{\kappa\lambda} := \{W : (K_k^\kappa)^* W + W L_l^\lambda = 0\}$$

for all indices. For our purposes it suffices to find $\mathcal{Y}_{kl}^{\kappa\lambda} e_l^\lambda$ which is pretty simple since the structure of $Y_{kl}^{\kappa\lambda} \in \mathcal{Y}_{kl}^{\kappa\lambda}$ is easily described explicitly (Gantmacher (1986)) (with $d(.)$ denoting the size of a square matrix):

$$\mathcal{Y}_{kl}^{\kappa\lambda} e_l^\lambda = \begin{pmatrix} 0 \\ \vdots \\ 0 \\ y_{kl}^{\kappa\lambda} \end{pmatrix} \begin{cases} y_{kl}^{\kappa\lambda} = 0 & , d(K_k^\kappa) < d(L_l^\lambda) \\ y_{kl}^{\kappa\lambda} \text{ free} & , d(K_k^\kappa) \geq d(L_l^\lambda) \end{cases} \quad (12)$$

As for $Y_{kl}^{\kappa\lambda} e_l^\lambda$ we introduce a notation for the last element in $M_{kl}^{\kappa\lambda} e_l^\lambda = (*\ \cdots\ *\ m_{kl}^{\kappa\lambda})^T$ and collect as $\hat{M}_{kl} := (m_{kl}^{\kappa\lambda})_{\kappa\lambda}$, $\hat{M} := (\hat{M}_{kl})_{kl}$, $\hat{Y}_{kl} := (y_{kl}^{\kappa\lambda})_{\kappa\lambda}$, $\hat{Y} := (\hat{Y}_{kl})_{kl}$. Because of the leading zeros in (12), we infer for any $Y \in \mathcal{Y}$ that

$$(ME)^*(YE) = \hat{M}^* \hat{Y}. \quad (13)$$

Here is the reason for introducing the partitions (8): By (12), if Y varies in $\mathcal{Y}$ then $\hat{Y}_{kl}$ vanishes identically if $k < l$ and $\hat{Y}_{kl}$ is a *free full block* for $k \geq l$.

Therefore $(ME)^*(YE)$ equals

$$\begin{pmatrix} \hat{M}_{01} & \dots & \hat{M}_{0,m+1} \\ \hat{M}_{11} & \dots & \hat{M}_{1,m+1} \\ \vdots & & \vdots \\ \hat{M}_{m,1} & \dots & \hat{M}_{m,m+1} \end{pmatrix}^* \begin{pmatrix} 0 & \dots & 0 & 0 \\ \hat{Y}_{11} & \dots & 0 & 0 \\ \vdots & & \vdots & \vdots \\ \hat{Y}_{m1} & \dots & \hat{Y}_{mm} & 0 \end{pmatrix}$$

where

$$\hat{Y}_{kl} \text{ is free for } k \geq l.$$

With $\hat{P} := E^*PE$, we hence need to prove that the constraint LMI

$$\hat{M}^* \hat{Y} + \hat{Y}^* \hat{M} + \hat{P} > 0,\ \hat{Y}_{kl} = 0 \text{ for } k < l \quad (14)$$

is solvable. Here is the point where we apply Theorem 2. With

$$A_j := \begin{pmatrix} \hat{M}_{j1} & \cdots & \hat{M}_{j,m+1} \\ \vdots & & \vdots \\ \hat{M}_{m1} & \cdots & \hat{M}_{m,m+1} \end{pmatrix},\ X_j := \begin{pmatrix} \hat{Y}_{jj} \\ \vdots \\ \hat{Y}_{mj} \end{pmatrix}$$

and

$$B_j := (\underbrace{0\ \cdots\ 0}_{j-1 \text{ blocks}}\ I\ 0\ \cdots\ 0)$$

(whose columns are partitioned as those of A_j), the LMI (14) is equivalent to $\sum_{j=1}^m (A_j^* X_j B_j + B_j^* X_j^* A_j) + \hat{P} > 0$ with *free* X_j. Since A_{j+1} results from A_j by canceling a block row, we have $\ker(A_j) \subset \ker(A_{j+1})$. For applying Theorem 2, we hence need to show for $j = 1, \dots, m+1$ (with $A_{m+1} := 0$) that

$$A_j \hat{z} = 0,\ \hat{z}_1 = 0,\ \dots,\ \hat{z}_{j-1} = 0,\ \hat{z} \neq 0 \Rightarrow \hat{z}^* \hat{P} \hat{z} > 0.$$

A pretty involved chain of arguments reveals that this is a consequence of the existence of $\mathcal{K}_*$ and the resulting nonnegativity conditions in Definition 3.1. We conclude that we can determine a solution $\hat{Y}$ of (14). Then it is possible to compute a $Y \in \mathcal{Y}$ with (13). Hence (11) holds and implies that $L^*Z + ZL + Y^*M + M^*Y + P > 0$ is solvable what finishes the construction.

References

Doyle, J., K. Glover, P. Khargonekar, B. Francis (1989). State-space solutions to standard H_∞ and H_2 control problems. *IEEE Trans. Automat. Control, AC-34*, 831-847.

Gahinet, P. and P. Apkarian (1994). A linear matrix inequality approach to H_∞ control, *Int. J. of Robust and Nonlinear Control, 4*, 449-455.

Gantmacher, F.R. (^{3}1986). *Matrizentheorie*. Springer-Verlag, Berlin.

Iwasaki, T. and R.E. Skelton (1994). A complete solution to the general H_∞ control problem: LMI existence conditions and state-space formulas. *Automatica, 34*, 1307-1317.

Kučera, V. (1974). The matrix equation $AX + XB = C^*$. *SIAM J. Appl. Math., 26*, 15-25.

Nesterov, Y. and A. Nemirovsky (1994). *Interior Point Polynomial Methods in Convex Programming: Theory and Applications.* SIAM Studies in Applied Mathematics, Vol. 13.

Petersen, I.R. (1989). Complete Results for a class of H_∞-control problems. *IEEE Trans. Autom. Control, AC-34*, 1196-1199.

Scherer, C.W. (1992). H_∞-control by state-feedback for plants with zeros on the imaginary axis. *SIAM J. Contr. Optim., 30*, 123–142.

Scherer, C.W. (1993). Algebraic solvability tests for linear matrix inequalities. *Proc. 32nd IEEE Conf. Decision and Control*, San Antonio, TX, pp. 349-354.

Scherer, C.W. (1994). The state-feedback H_∞-problem at optimality. *Automatica, 30*, 293–305.

Scherer, C.W. (1995a). The general nonstrict algebraic Riccati inequality. To appear in *Linear Algebra. Appl.*.

Scherer, C.W. (1995b). The algebraic Riccati equation and inequality for systems with uncontrollable modes on the imaginary axis. To appear in *SIAM J. Matrix Anal. Appl.*.

Snyders, J. and M. Zakai (1970). On nonnegative solutions of the equation $AD+DA' = -C$. *SIAM J. Appl. Math., 18*, 704–714.

Selected Topics in Identification, Modelling and Control
Vol. 7, December 1994

An iterative algorithm for frequency-weighted H_2-norm optimal reduction and centering

Pepijn M.R. Wortelboer [‡] and Okko H. Bosgra [§]

[‡] *Philips Research Laboratories,*
Prof. Holstlaan 4, 5656 AA Eindhoven, The Netherlands.
[§] *Mechanical Engineering Systems and Control Group*
Delft University of Technology, Mekelweg 2, 2628 CD Delft, The Netherlands.

Abstract. The H_2-norm frequency-weighted optimal model reduction problem is analysed. Necessary optimality conditions are derived for the general case with input and output weights. For non-dynamic weights the optimal reduction problem is reformulated as a specific projection of dynamics problem which is solved numerically by a new algorithm that forces each new iterate to be a balanced approximation. The paper shows the difficulty with formulating the dynamically weighted problem as a direct projection problem. The proposed algorithm shows remarkably fast convergence for the non-dynamic case. Convergence and global optimality are not analysed analytically. This paper also derives a method to create a central approximation within a set of models. The fixed-order central approximation requires the solution of an optimal order reduction problem. Optimal centering and reduction play an important role in the design process of a limited-order controller yielding well-specified performance and robustness properties. The algorithm is tested on two examples, one of which shows the existence of a non-global minimum.

Keywords. Model reduction; H_2-norm optimal; frequency-weighted reduction; nominal modelling; optimal central approximation; numerical algorithm.

1 Introduction

Order reduction is an important issue in model-based control design, both for deriving manageable plant models that can be used in computer programs for controller computation, and for reducing the resulting controller for reasons of implementation, robustness and cost. In order to avoid lengthy or non-converging iterations in the design process of high-performance controllers, order reduction is often used to diminish these numerical problems. When and where order reduction should be applied depends highly on the defined control problem and the properties of the available model. Answers to these questions only arise in the course of the design. This means that order reduction is not a well-defined stand-alone problem and it explains the effort to limit the amount of work (and time) involved in reduction steps.

Existing model reduction methods can be very valuable, but each has to be tested in an appropriate framework. *Modal reduction* and *balanced reduction* (Moore, 1981) don't need any further introduction nowadays since these methods have gained a firm position in today's control design education and practice. These simple and very direct methods can be tried a number of times without wasting much time. *Optimal Hankel-norm reduction* (see Glover 1984) is considered computationally more demanding, yet it is the only method that provides a straightforward construction of a reduced-order model that in fact is optimal in a sense (the Hankel-norm is the maximum Hankel singular value of a system).

The search for a construction of the H_∞-norm optimal approximation is ongoing (Kavranoğlu, 1994) and is most wanted in relation with H_∞-control design. Optimal reduction in H_2-norm has been studied in many areas. One of the first applications was

in the area of network synthesis to approximate desired transient response (Aigrain & Williams, 1949). The transfer function necessary conditions were generalized to the multivariable case by Krajewski *et al.* (1993). State-space necessary conditions can be found in Wilson (1970). These conditions were transformed into the optimal projection equations by Hyland & Bernstein (1985). The solution of these conditions is difficult. A large effort is directed towards homotopy solution of the optimal projection equations (see for instance Žigić *et al.*, 1992). There does not yet exist a complete theory that characterizes the existence, uniqueness and properties of the optimal solution (Baratchart *et al.*, 1992). Especially the solutions to the necessary conditions for an optimum are not completely understood. These equations may well have multiple solutions and it is not clear how to characterize the global optimum analytically. Thus one has to rely on numerical approaches. Current algorithms to solve the necessary conditions seem to be little used in practice, which is probably due to the computational complexity (homotopy methods) or the strong dependence on good initial approximations (for iterative methods).

This paper contributes a relatively simple iterative algorithm to solve the necessary conditions. Although we cannot prove any convergence properties, only a few iterations suffice to find solutions of the optimal projection equations in the majority of test cases considered. The consistent usage of projections that are factored such that the reduced-order models are balanced in each step, are believed to be crucial for convergence.

It is important to realize that these optimal solutions are not directly relevant in feedback systems: these require the solution of so-called frequency weighted closed-loop reduction problems. One of the first extensions of order reduction to controlled systems was due to Enns (1984), who developed *frequency weighted balanced reduction*, and who applied it to closed-loop systems.

Other extensions of the balancing idea to closed-loop relevant reduction problems are *Graph or fractional balanced reduction* (Meyer, 1988) and *LQG-balanced reduction* (Jonckheere & Silverman, 1983). Two other methods that embed order reduction in a relevant way in the control design process are described in Villemagne & Skelton (1988) and Wortelboer & Bosgra (1994). In the last method, iterations with model and controller reduction are exploited based on *closed-loop balanced reduction*, which generalizes frequency-weighted balanced reduction. Non of these methods is optimal however.

A first step to optimality was the solution of specific *frequency-weighted optimal Hankel-norm reduction* problems (Latham & Anderson 1985, Anderson & Liu 1989, and Zhou 1993). The objective has always been to get close to the frequency-weighted optimal solution in H_∞-norm. As Zhou (1993) remarks, the optimal Hankel-norm solution is no guarantee for small weighted H_∞-norm errors. Another approach to limit these errors could be the development of weighted H_2-norm optimal reduction. There has not been much interest in such a form of H_2-norm optimal reduction. In Halevi (1992) the minimization of a squared single-sided frequency-weighted error is addressed. This is equivalent to H_2-norm optimal reduction with either input weight or output weight. The general case of input *and* output weight is treated in Wortelboer (1994). This paper tries to present a full and transparent derivation of the coupled equations that the optimal solution has to satisfy. It will be shown that the nice structure that exists for unweighted H_2-norm optimal solutions is corrupted by dynamic frequency weights. This has severe implications for the implementation of numerical algorithms.

Once we have an efficient algorithm for H_2-norm optimal reduction, we can sharpen many results that have previously been obtained by balanced reduction: the reduction errors are always smaller measured in H_2-norm, and often also smaller measured in H_∞-norm.

An important issue in robust control is the characterization of the robustness objective. In other words, what variations are to be coped with by the controller? A mathematical elegant objective is to meet well-defined closed-loop specifications for a *set* of models using a constant feedback controller. This set may consist of a finite number of models, it can also be defined as a 'ball' around a central model. In robust control the central model is often called 'nominal model', and the ball represents the uncertainty. The issue here is to find an appropriate nominal model based on a discrete set of models. This paper contributes the following: a specific central approximation is the best nominal model from both an H_2-norm and an H_∞-norm point of view and limitation of the order of the nominal model requires the solution of an H_2-norm optimal reduction and an H_∞-norm optimal reduction problem respectively. This also holds in the frequency-weighted case.

The organisation of this paper is as follows. First, some preliminaries are summarized (Section 2). These include properties of projections, H_2-norm, H_∞-norm, and Lagrange functions. Section 3 derives the conditions for the H_2-norm optimal solution in the frequency-weighted case and links these conditions to the optimal projection equations for

the unweighted case. The new algorithms are presented in Section 4. Section 5 describes the optimal fixed-order central approximation of a model set. In Section 6 numerical examples is given, and a discussion is given in Section 7.

2 Preliminaries

Let $G = (A, B, C, D)$ represent a minimal realization of a linear stable finite-dimensional system, $\dot{x} = Ax + Bu$, $y = Cx + Du$. The associated transfer function matrix is $G(s) = C(sI - A)^{-1}B + D$. We use $G = (A, B, C, D)$ to denote a *specific* realization, not the associated transfer function matrix $G(s)$. The order of G (the McMillan degree of $G(s)$) is the size of A and will be denoted by n. A minimal n^{th}-order realization can be written in the following form

$$G_n = \left[\begin{array}{c|c} A & B \\ \hline C & D \end{array}\right].$$

Reduction can be achieved by operating on the row and column dimension of the state-space matrices. Let L_r, $R_r \in \mathbb{R}^{n\times r}$ with $0 \leq r \leq n$. We define

$$G_r = \left[\begin{array}{c|c} L_r^* A R_r & L_r^* B \\ \hline C R_r & D \end{array}\right] \triangleq \mathcal{R}_{[L_r,\, R_r]}(G_n) \qquad (1)$$

If $L_r^* R_r = I_r$, then the reduction is in fact governed by a *projection of dynamics* with projection matrix $\Pi_r = R_r L_r^*$. We refer to Wortelboer (1994) for a detailed description and analysis of the projection of dynamics principle. Here we just state that any projection matrix has a factorization $\Pi = RL^*$ of which the factors satisfy $L^*R = I$. The property $\Pi^2 = \Pi$ can also be used as a definition of a projection matrix. The matrix pair $[L_r,\, R_r]$ fully defines the projection of dynamics. In the sequel we will often use the term 'projection' when we mean 'projection of dynamics'.

Definition 2.1 (H_2-norm of $G_n(s)$) *The H_2-norm of a strictly stable and strictly proper system $G_n(s)$ is*

$$\|G\|_2 = \left(\frac{1}{2\pi}\int_{-\infty}^{\infty} \mathrm{tr}(G_n^*(j\omega)G_n(j\omega))\,\mathrm{d}\omega\right)^{\frac{1}{2}} \qquad (2)$$

with $G_n^*(j\omega) = G_n^T(-j\omega)$.

With $H(t) = Ce^{At}B$ the impulse response of G_n we also have due to Parseval's relation (see for instance Rudin 1966)

$$\|G\|_2 = \left(\int_0^{\infty} \mathrm{tr}(H^*(t)H(t))\,\mathrm{d}t\right)^{\frac{1}{2}}$$

The H_2-norm of a SISO system can be interpreted as the square root of the energy of the output due to an impulsive input. For MIMO systems a similar interpretation requires the notion of an impulse with random input direction (Zhou *et al.* 1993), $w(t) = \eta\delta(t)$ satisfying $E(\eta\eta^*) = I_{n_w}$ where $E(\cdot)$ the expectation operation. Then the H_2-norm is the expectation of the output energy.

Lemma 2.2 (Properties of the H_2-norm) *Let $G(s)$ and $H(s)$ be strictly stable and strictly proper square transfer function matrices. Then the following two properties hold:*

$$\left\|\begin{bmatrix} G & H \end{bmatrix}\right\|_2^2 = \left\|\begin{bmatrix} G \\ H \end{bmatrix}\right\|_2^2 = \|G\|_2^2 + \|H\|_2^2 \qquad (3)$$

$$\|G+H\|_2^2 + \|G-H\|_2^2 = 2\|G\|_2^2 + 2\|H\|_2^2 \qquad (4)$$

Proof: We can prove (3) by exploiting the fact that

$$\mathrm{tr}\left(\begin{bmatrix} G \\ H \end{bmatrix}\begin{bmatrix} G^* & H^* \end{bmatrix}\right) = \mathrm{tr}(GG^*) + \mathrm{tr}(HH^*).$$

Property (4) is also known as the 'parallelogram law' in an inner product space (Luenberger 1984). To prove (4) we first introduce the inner product underlying the H_2-norm:

$$\langle G, H\rangle = \frac{1}{2\pi}\int_{-\infty}^{\infty} \mathrm{tr}(G^*(j\omega)H(j\omega))\,\mathrm{d}\omega \qquad (5)$$

Then the following is immediate

$$\|X+Y\|_2^2 = \frac{1}{2\pi}\int_{-\infty}^{\infty} \mathrm{tr}((X(j\omega)+Y(j\omega))^*(X(j\omega)+Y(j\omega)))\,\mathrm{d}\omega =$$

$$\langle X, X\rangle + \langle Y, Y\rangle + 2\,\mathrm{Re}\,\langle X, Y\rangle =$$

$$\|X\|_2^2 + \|Y\|_2^2 + 2\,\mathrm{Re}\,\langle X, Y\rangle$$

If we take $-Y(s)$ instead of $Y(s)$, the last term changes sign and disappears in the addition. □

Notice that the above lemma does not hold for the H_∞-norm. The H_2-norm can be computed as

$$\|G\|_2 = \sqrt{\mathrm{tr}(CPC^*)} \qquad (6)$$

with P the controllability Gramian of G solved from the linear matrix equation (the controllability Lyapunov equation)

$$AP + PA^* + BB^* = O. \qquad (7)$$

We can also use (6, 7) as the definition of the H_2-norm. This definition will prove convenient in establishing the dependence of $\|G\|_2$ on state-space

parameters of $G(s)$. We remind that $\|G\|_2$ does not depend on the realization that is used to compute the H_2-norm. To find stationary values of the H_2-norm of $G(s)$ with respect to varying system parameters in $(A,\ B,\ C,\ O)$ we want to express the variation of $\|G\|_2$ in terms of variations in A, B, and C. In the sequel we will take the squared H_2-norm as a starting point in order to get rid of the square root in (6). The way in which variations in A, B, and C affect $\frac{1}{2}\|G\|_2^2$ cannot be determined directly since we cannot explicitly express the variation of P in terms of variations in A and B; this is due to the fact that we cannot solve the linear matrix equation (7) for P explicitly. From the variational theory of Lagrange we know that we can incorporate the set of $\frac{1}{2}n(n+1)$ independent constraint equations from (7) into the scalar function $\frac{1}{2}\|G\|_2^2 = \frac{1}{2}\mathrm{tr}(CPC^*)$ using a Lagrange multiplier vector in an inner product (Luenberger 1984). We define the so-called *Lagrangian* in matrix form:

$$\begin{aligned}\pounds(A,B,C,P,Q) \triangleq\ & \tfrac{1}{2}\mathrm{tr}(CPC^*)+ \\ & \tfrac{1}{2}\mathrm{tr}(Q(AP+PA^*+BB^*))\end{aligned} \tag{8}$$

with Q a matrix of Lagrange multipliers. The inner product in this matrix formulation is represented by the trace operation on the product between Q and $AP+PA^*+BB^*$. The Lagrange formulation is based on the assumption that a local extremum point $(\mathring{A},\mathring{B},\mathring{C},\mathring{P})$ of $\frac{1}{2}\mathrm{tr}(CPC^*)$ satisfying (7) is a *regular point* (Luenberger 1984). For our smooth problem, this regularity condition is satisfied for (A,B) a strictly stable controllable pair [1]. Now, first-order necessary conditions for an H_2-norm minimum can be derived from $\pounds(A,B,C,P,Q)$. Instead of looking for $\mathring{A},\mathring{B},\mathring{C}$ that can be varied infinitesimally without causing a change in $\frac{1}{2}\|G\|_2^2$, we are now looking for $\mathring{A},\mathring{B},\mathring{C},\mathring{P},\mathring{Q}$ for which infinitesimal variations do not change the Lagrangian $\pounds$. The idea is that we can allow independent variations of P and Q in (8) as long as we are looking for $\delta\pounds = 0$: the constraint equations for P and Q result from the requirement that neither δP nor δQ may change $\pounds$. We rewrite (8) using standard trace operations to obtain

$$\pounds = \tfrac{1}{2}\mathrm{tr}(CPC^*+QBB^*+2QPA^*). \tag{9}$$

Next consider (independent) first-order variations δA, δB, δC, δP, and δQ. We then find

$$\begin{aligned}\delta\pounds\ =\ & \mathrm{tr}(CP\delta C^*+QB\delta B^*+QP\delta A^* \\ & +\tfrac{1}{2}\delta P(A^*Q+QA+C^*C) \\ & +\tfrac{1}{2}\delta Q(AP+PA^*+BB^*)).\end{aligned} \tag{10}$$

[1] the authors thank an anonymous referee for pointing to the importance of this condition.

We see that the introduction of Lagrange multiplier matrix Q allows independent variations in P and returns a new constraint equation resulting from the required invariability of $\pounds$ for δP:

$$A^*Q+QA+C^*C=O \tag{11}$$

This is precisely the observability Lyapunov equation and thus Q can be identified as the observability Gramian.

From now on we identify P and Q as the controllability and observability Gramian of $G = (A,\ B,\ C,\ D)$. This simplifies (10) to

$$\delta\pounds = \mathrm{tr}(CP\delta C^*+QB\delta B^*+QP\delta A^*) \tag{12}$$

Finally we give the definition of the H_∞-norm of a transfer function matrix. The H_∞-norm of $G(s)$ is

$$\|G\|_\infty = \sup_\omega \lambda_{\max}(G(j\omega)^*G(j\omega))^{\frac{1}{2}} \tag{13}$$

3 Necessary conditions for H_2-norm optimal weighted reduction

This section is concerned with the construction of G_r that achieves a minimum of $\|W(G_n-G_r)V\|_2$. Transfer function matrices $V(s)$ and $W(s)$ play the role of frequency weights. Model reduction in a weighted setting can be very effective to simplify models that intend to describe the transition from ($V(s)$-)filtered signals to new signals (that may be filtered additionally by $W(s)$). In Wortelboer (1994), the derivation of necessary conditions to solve the *H_2-norm optimal frequency-weighted reduction* problem

$$\min_{G_r}\|W(G-G_r)V\|_2$$

has been given for the first time. This section gives a more detailed derivation and besides, shows that in the unweighted case the optimum is governed by projection of dynamics.

3.1 The square weighted case

Let $W = (A_W,\ B_W,\ C_W,\ D_W)$ be any minimal realization of $W(s)$ and similarly let $V = (A_V,\ B_V,\ C_V,\ D_V)$ be any minimal realization of $V(s)$. We consider $G_r = (A_r,\ B_r,\ C_r,\ D)$, i.e. we do not allow the D-term to change in the reduction. This presupposes that D_W and D_V satisfy certain rank conditions (Halevi 1992), and in case both D_W and D_V are *square*, this presupposes that D_W and D_V are invertible, which does not imply a severe practical restriction. Next, define

$$\Delta \triangleq W(G-G_r)V = \left[\begin{array}{c|c} \hat{A} & \hat{B} \\ \hline \hat{C} & \end{array}\right].$$

Following the convention of Wortelboer (1994) we have (empty entries refer to zero matrices)

$$\Delta = \left[\begin{array}{ccc|c} A_W & B_W C & -B_W C_r & \\ & A & & B C_V \quad B D_V \\ & & A_r & B_r C_V \quad B_r D_V \\ & & & A_V \quad B_V \\ \hline C_W & D_W C & -D_W C_r & \end{array}\right].$$

Let the controllability Gramian of Δ be partitioned as

$$\hat{\hat{P}} = \begin{bmatrix} P_W & P_{WG} & P_{Wr} & P_{WV} \\ P_{GW} & P_G & P_{Gr} & P_{GV} \\ P_{rW} & P_{rG} & P_r & P_{rV} \\ P_{VW} & P_{VG} & P_{Vr} & P_V \end{bmatrix}.$$

The same partitioning is applied to the observability Gramian $\hat{Q}$. Further let

$$\hat{\hat{E}}_W = \begin{bmatrix} I_W \\ O \\ O \\ O \end{bmatrix}, \quad \hat{\hat{E}}_r = \begin{bmatrix} O \\ O \\ I_r \\ O \end{bmatrix}, \quad \hat{\hat{E}}_V = \begin{bmatrix} O \\ O \\ O \\ I_V \end{bmatrix}. \tag{14}$$

We can also partition matrix products. A similar notation is used. The following matrix product parts will be needed in the sequel:

$$\begin{aligned} [\hat{\hat{Q}}\hat{\hat{P}}]_r &= \hat{\hat{E}}_r^* \hat{\hat{Q}} \hat{\hat{P}} \hat{\hat{E}}_r \\ [\hat{\hat{Q}}\hat{\hat{P}}]_{rV} &= \hat{\hat{E}}_r^* \hat{\hat{Q}} \hat{\hat{P}} \hat{\hat{E}}_V \\ [\hat{\hat{Q}}\hat{\hat{P}}]_{Wr} &= \hat{\hat{E}}_W^* \hat{\hat{Q}} \hat{\hat{P}} \hat{\hat{E}}_r \\ [\hat{\hat{Q}}\hat{\hat{B}}]_r &= \hat{\hat{E}}_r^* \hat{\hat{Q}} \hat{\hat{B}} \\ [\hat{\hat{C}}\hat{\hat{P}}]_r &= \hat{\hat{C}} \hat{\hat{P}} \hat{\hat{E}}_r \end{aligned}$$

The only possible variations in $\hat{\hat{A}}$, $\hat{\hat{B}}$, and $\hat{\hat{C}}$ are due to δA_r, δB_r and δC_r:

$$\delta\hat{\hat{A}} = \hat{\hat{E}}_r \delta A_r \hat{\hat{E}}_r^* + \hat{\hat{E}}_r \delta B_r C_V \hat{\hat{E}}_V^* - \hat{\hat{E}}_W B_W \delta C_r \hat{\hat{E}}_r^* \tag{15.a}$$

$$\delta\hat{\hat{B}} = \hat{\hat{E}}_r \delta B_r D_V \tag{15.b}$$

$$\delta\hat{\hat{C}} = -D_W \delta C_r \hat{\hat{E}}_r^* \tag{15.c}$$

Substitution of (15) in (12) gives

$$\begin{aligned} \delta\hat{\hat{\mathcal{L}}} &= \mathrm{tr}(\hat{\hat{C}}\hat{\hat{P}}\delta\hat{\hat{C}}^* + \hat{\hat{Q}}\hat{\hat{B}}\delta\hat{\hat{B}}^* + \hat{\hat{Q}}\hat{\hat{P}}\delta\hat{\hat{A}}^*) \\ &= \mathrm{tr}((\hat{\hat{E}}_r\hat{\hat{Q}}\hat{\hat{P}}\hat{\hat{E}}_r)\delta A_r^*) + \\ &\quad \mathrm{tr}((\hat{\hat{E}}_r^*\hat{\hat{Q}}\hat{\hat{B}}D_V^* + \hat{\hat{E}}_r^*\hat{\hat{Q}}\hat{\hat{P}}\hat{\hat{E}}_V C_V^*)\delta B_r^*) + \\ &\quad \mathrm{tr}((-D_W^*\hat{\hat{C}}\hat{\hat{P}}\hat{\hat{E}}_r - B_W^*\hat{\hat{E}}_W^*\hat{\hat{Q}}\hat{\hat{P}}\hat{\hat{E}}_r)\delta C_r^*) \end{aligned}$$

For $G_r = (A_r, B_r, C_r, D)$ to be the minimizing solution we need to have $\delta\hat{\hat{\mathcal{L}}} = 0$. This means that the following matrix equations have to be satisfied:

$$[\hat{\hat{Q}}\hat{\hat{P}}]_r = O \tag{16.a}$$

$$[\hat{\hat{Q}}\hat{\hat{B}}]_r D_V^* + [\hat{\hat{Q}}\hat{\hat{P}}]_{rV} C_V^* = O \tag{16.b}$$

$$D_W^*[\hat{\hat{C}}\hat{\hat{P}}]_r + B_W^*[\hat{\hat{Q}}\hat{\hat{P}}]_{Wr} = O \tag{16.c}$$

The matrices P_r and Q_r are symmetric positive definite if W, G, V and G_r are all strictly stable and G_r is minimal. We define

$$R_R \triangleq \begin{bmatrix} R_W \\ R_r \\ R_V \end{bmatrix} = \begin{bmatrix} P_{Wr} \\ P_{Gr} \\ P_{Vr} \end{bmatrix} P_r^{-1} \tag{17.a}$$

$$L_R \triangleq \begin{bmatrix} L_W \\ L_r \\ L_V \end{bmatrix} = -\begin{bmatrix} Q_{Wr} \\ Q_{Gr} \\ Q_{Vr} \end{bmatrix} Q_r^{-1} \tag{17.b}$$

such that (16.a) can be rewritten as

$$L_R^* R_R = I_r. \tag{18}$$

To derive compact formulas for A_r, B_r, and C_r, we introduce

$$\dot{C}_V = C_V^* D_V^{-*} D_V^{-1} \tag{19.a}$$

$$\dot{B}_W = D_W^{-1} D_W^{-*} B_W^*. \tag{19.b}$$

Then (16.b) can be rewritten as

$$\begin{aligned} B_r = (L_W^* P_{WV} - P_{rV})\dot{C}_V + [\, L_r^* \quad L_V^* \,] \times \\ \left(\begin{bmatrix} B \\ B_V D_V^{-1} \end{bmatrix} + \begin{bmatrix} P_{GV} \\ P_V \end{bmatrix} \dot{C}_V \right). \end{aligned} \tag{20}$$

Similarly, (16.c) yields

$$\begin{aligned} C_r = \dot{B}_W(Q_{WV}R_V + Q_{Wr}) + ([\, D_W^{-1}C_W \quad C \,] + \\ \dot{B}_W[\, Q_W \quad Q_{WG} \,]) \begin{bmatrix} R_W \\ R_r \end{bmatrix}. \end{aligned} \tag{21}$$

As derived in the previous section, the necessary conditions also include the following two Lyapunov equations

$$\hat{\hat{A}}\hat{\hat{P}} + \hat{\hat{P}}\hat{\hat{A}}^* + \hat{\hat{B}}\hat{\hat{B}}^* = O \tag{22.a}$$

$$\hat{\hat{A}}^*\hat{\hat{Q}} + \hat{\hat{Q}}\hat{\hat{A}} + \hat{\hat{C}}^*\hat{\hat{C}} = O. \tag{22.b}$$

We use these to derive an implicit solution for A_r. Premultiplying (22.a) by $[\, L_W^* \quad L_r^* \quad -I_r \quad L_V^* \,]$ and postmultiplying by $[\, O \quad O \quad P_r^{-1} \quad O \,]^*$ yields

$$\begin{aligned} A_r = L_W^* A_W R_W + L_r^* A R_r + L_V^* A_V R_V + \\ L_W^* B_W (C R_r - C_r) + (L_r^* B - B_r) C_V R_V. \end{aligned} \tag{23}$$

The result given in (23) can also be derived by premultiplication of (22.b) by $[\, O \quad O \quad Q_r^{-1} \quad O \,]$ and postmultiplication by $[\, R_W^* \quad R_r^* \quad I_r \quad R_V^* \,]^*$.

Summarizing, the necessary conditions for an optimum are given by (18, 20, 21, 22). These equations are strongly coupled. Once they are solved,

the reduced order model follows from (23, 20, 21). It remains to be checked if this reduced order model is a minimum. In order to find solution strategies, we first study the easiest case in which the weights are all static.

3.2 Static weights and optimal projections

For $W(s) = D_W$ and $V(s) = D_V$ (18) and (23, 20, 21) specialize to

$$L_r^* R_r = I_r \tag{24}$$

and

$$\begin{aligned} A_r &= L_r^* A R_r && \text{(25.a)} \\ B_r &= L_r^* B && \text{(25.b)} \\ C_r &= C R_r. && \text{(25.c)} \end{aligned}$$

respectively. This means that a necessary condition for statically weighted H_2-norm optimal reduction is that the reduced-order model is a projection of the full-order model. The projection is governed by the projection matrix $\Pi_r = R_r L_r^*$. Notice that the reduced-order model depends on D_W and D_V (which cannot be concluded from (25) directly), due to the fact that the optimal projection solution also has to satisfy the two Lyapunov equations for $\hat{P}$ and $\hat{Q}$ which include both D_W and D_V.

For the constant weighting case, the Lyapunov equations for $\hat{P}$ and $\hat{Q}$ can be divided into three parts each: a part associated with G, a part associated with G_r, and a part in which the coupling is expressed. The coupling equations form the crucial part:

$$\begin{aligned} A P_{Gr} + P_{Gr} A_r^* + B B_r^* &= O \\ A^* Q_{Gr} + Q_{Gr} A_r - C^* C_r &= O. \end{aligned}$$

Substituting $P_{Gr} = R_r P_r$ and $Q_{Gr} = -L_r Q_r$ (see (17)), we obtain

$$\begin{aligned} A R_r P_r + R_r P_r A_r^* + B B_r^* &= O && \text{(26.a)} \\ A^* L_r Q_r + L_r Q_r A_r + C^* C_r &= O. && \text{(26.b)} \end{aligned}$$

Note that P_r and Q_r are the Gramians of G_r. Without loss of generality, we may assume that the optimal reduced-order approximation $\mathring{G}_r$ is in balanced coordinates. Thus we can always ensure that $P_r = Q_r = \mathrm{diag}(\sigma_r)$. Similarly, we can assume that G is a balanced realization such that $P_G = Q_G = \mathrm{diag}(\sigma_G)$. Notice that the optimal projection matrix $\mathring{\Pi}_r$ only defines the *transfer function matrix* $\mathring{G}_r(s)$, the realization emerges after a factorization: with $\mathring{\Pi}_r = \mathring{R}_r \mathring{L}_r^*$ we find the *realization* $\mathring{G}_r = (\mathring{L}_r A \mathring{R}_r, \mathring{L}_r B, C \mathring{R}_r, D)$. In order to arrive at a balanced optimal approximation we thus need a 'balancing factorization' of the optimal projection matrix: $\mathring{\Pi}_r = \check{R}_r \check{L}_r^*$ with $(\check{L}_r^* A \check{R}_r, \check{L}_r^* B, C \check{R}_r, O)$ a *balanced* optimal r^{th}-order realization.

In this context it is also interesting to analyse the influence of the original realization on the projection matrix. In Wortelboer (1994) it was shown that there exists a realization of $G(s)$ such that the optimal reduction is a mere truncation. Then the associated optimal projection is orthogonal. This contrasts with Hyland & Bernstein who characterize their optimal projection as 'oblique'.

3.3 Reexamination of the weighted case

At this point we can explain the main difference between the weighted and unweighted (or statically weighted) case. The absence of states x_W and x_V in the statically weighted case enabled the reformulation of the necessary conditions into the projection form. We cannot prove that the optimal solution in the dynamically weighted case can also be obtained by a projection.

4 Algorithms

In this section we describe the algorithmic approach to find H_2-norm optimal approximations. The idea was first introduced in Wortelboer (1994) and the computer code developed by the author is freely available in the form of a toolbox for use with MATLAB™ (version 4). The so-called Wor-toolbox for *W*eighted *O*rder *R*eduction can be obtained by anonymous ftp[2].

In this section we first give the algorithm for the unweighted case. The succes of this algorithm stimulated the search for a similar algorithm for the weighted case, but the absence of a projection foundation seems to hamper a reliable implementation. Nevertheless, solutions for weighted problems with smooth weights are numerous.

4.1 The unweighted case

The main idea is to use an iterative scheme in which current reduced-order matrices A_r, B_r, and C_r (together with P_r and Q_r) are substituted in (26) which is solved subsequently for L_r and R_r after which new A_r, B_r, and C_r can be computed (25). The key modification to this rather simple scheme is a (minor) adjustment of R_r such that L_r, $\tilde{R}_r$ forms a projection (i.e. satisfy (24)). A further modification is that instead of arbitrary realizations, all intermediate results are rewritten in balanced form.

[2] ftp: **ftp-mr.wbmt.tudelft.nl**
username: **anonymous**
password: *your e-mail address*
directory: **/pub/wortelboer**

Now suppose we have preliminary $L_r^{(0)}, R_r^{(0)}$ satisfying (24) and a preliminary approximation $\tilde{G}_r^{(0)}$. For $k > 0$, we can solve for $L_r^{(k)}, R_r^{(k)}$ from

$$AR_r^{(k)}\tilde{\Sigma}_r^{(k-1)} + R_r^{(k)}\tilde{\Sigma}_r^{(k-1)}\tilde{A}_r^{(k-1)^*} + B\tilde{B}_r^{(k-1)^*} = O$$
$$A^*L_r^{(k)}\tilde{\Sigma}_r^{(k-1)} + L_r^{(k)}\tilde{\Sigma}_r^{(k-1)}\tilde{A}_r^{(k-1)} + C^*\tilde{C}_r^{(k-1)} = O$$

Only when the solution has converged $L_r^{(k)^*}R_r^{(k)} = I_r$ holds. The crucial step in the algorithm is to adjust the pair L_r, R_r such that

- $\tilde{L}_r^{(k)^*}\tilde{R}_r^{(k)} = I_r$
- $\tilde{G}_r^{(k)}$ is balanced

The following approach is a slight modification of the approach proposed in Wortelboer (1994).

Proposition 4.1 (Reorthonormalization) *Let $R_r \in \mathbb{R}^{n\times r}$ and $L_r \in \mathbb{R}^{n\times r}$ then*

$$\begin{aligned}\tilde{L}_r &= L_r\breve{T}_r^{-*}\\ \tilde{R}_r &= R_r(L_r^*R_r)^{-1}\breve{T}_r\end{aligned}$$

satisfy $\tilde{L}_r^*\tilde{R}_r = I_r$, while $\breve{T}_r$ can be chosen such that $\tilde{G}_r = (\tilde{L}_r^*A\tilde{R}_r,\ \tilde{L}_r^*B,\ C\tilde{R}_r,\ D)$ is an r^{th}-order balanced realization.

In the iteration we can replace $L_r^{(k)}$ by $L_r^{(k+1)}$ (and $R_r^{(k)}$ by $R_r^{(k+1)}$), but this is not very robust. Especially in the first iterations it is better to use part of the previous solutions $(0 \le \alpha \le 1)$

$$\hat{L}_r^{(k+1)} = \alpha\, L_r^{(k+1)} + (1-\alpha)\, L_r^{(k)} \quad (27.a)$$
$$\hat{R}_r^{(k+1)} = \alpha\, R_r^{(k+1)} + (1-\alpha)\, R_r^{(k)}. \quad (27.b)$$

Of course we have to adjust $\hat{L}_r^{(k+1)}$ and $\hat{R}_r^{(k+1)}$ again such that $\breve{L}_r^{(k+1)}$ and $\breve{R}_r^{(k+1)}$ define a new balanced approximation (see (1))

$$\breve{G}_r^{(k+1)} = \mathcal{R}_{[\breve{L}_r^{(k+1)}, \breve{R}_r^{(k+1)}]}(G),$$

with $\breve{L}_r^{(k+1)^*}\breve{R}_r^{(k+1)} = I_r$. If this iteration converges then this r^{th}-order balanced realization will eventually satisfy the necessary conditions. There is not (yet) a formal proof of convergence, but the remarkable results obtained so far suggest that the formulation of the problem in terms of balancing projections avoids most of the numerical problems encountered in alternative algorithms. Again it is stressed that convergence does not imply that the global minimum is found.

4.2 The dynamically weighted case

This scheme can also be extended for weighted optimal H_2-norm reduction (see Section 3). In each iteration step we compute $\hat{\tilde{P}}$ and $\hat{\tilde{Q}}$ for a given G_r, calculate R_R and L_R and apply a small modification to get $\tilde{R}_R$ and $\tilde{L}_R$ that satisfy (18). With this projection pair and current values for P_{WV}, P_{rV}, P_{GV}, P_V Q_{WV}, Q_{Wr}, Q_{WG}, and Q_W, new B_r, C_r and A_r can be computed. Similarly as in the unweighted case (27), the modification of R_R and L_R is damped. This is also done for the updates of B_r and/or C_r. The toolbox function `weighH2R` applies to optimal H_2-norm frequency-weighted reduction. For the unweighted case we have `optproj`. Both functions have restart facilities. To check the optimality we can use `gradH2R` for both cases: it computes the derivatives $\partial\mathfrak{L}/\partial A_r$, $\partial\mathfrak{L}/\partial B_r$, and $\partial\mathfrak{L}/\partial C_r$.

It is also straightforward to apply optimal H_2-norm reduction to the Graph of a system (Vidyasagar 1985). Recall that balanced reduction of the Graph of a system is used to define Graph-balanced reduction. The corresponding toolbox functions are `goptH2R`, and `gbalR`.

5 Reduced-order central approximation

Here we discuss a method to obtain a nominal model from a discrete set of models. As we have said in the introduction, robust control is often pursued by deriving a controller with a guaranteed performance level on a set of models around a nominal model. The variations that the controller can cope with are often characterized by an H_∞-norm distance measure with respect to the nominal model and a maximum distance value. In the ideal situation for robust H_∞-control design the centering should be performed in an H_∞-norm setting. Let the H_∞-norm distance measure be

$$\hat{\delta}_\infty(\mathcal{G}, G_{\text{nom}}) = \max_i \|G_{(i)} - G_{\text{nom}}\|_\infty \quad (28)$$

for $G_{(i)} \in \mathcal{G}$ any model from the discrete model set $\mathcal{G}$. The best nominal model then minimizes $\hat{\delta}_\infty(\mathcal{G}, G_{\text{nom}})$. This minimization problem cannot yet be solved in a structured way.

We can also adopt the point of view of Miyazawa & Dowell (1989) and cast the problem in an H_2-norm setting. Then we use the following distance measure

$$\delta_2(\mathcal{G}, G_{\text{nom}}) = \left\| \begin{bmatrix} \vdots \\ G_{(i)} \\ G_{(i+1)} \\ \vdots \end{bmatrix} - \begin{bmatrix} \vdots \\ I \\ I \\ \vdots \end{bmatrix} G_{\text{nom}} \right\|_2$$

First we consider the simplest case with two models: $\mathcal{G} = \{G_a, G_b\}$. We are interested in constructing a third model that is close to both G_a and G_b. More

precisely we look for a new model G_m that minimizes $\hat{\delta}_\infty(\mathcal{G}, G_m)$ or $\delta_2(\mathcal{G}, G_m)$. A straightforward centering, $G_m = \frac{1}{2}(G_a + G_b)$ achieves

$$\|G_a - G_m\|_p = \|G_b - G_m\|_p = \tfrac{1}{2}\|G_a - G_b\|_p$$

with p any system norm. This means $\hat{\delta}_\infty(\mathcal{G}, G_m) = \frac{1}{2}\|G_a - G_b\|_\infty$, whereas $\hat{\delta}_\infty(\mathcal{G}, G_a) = \hat{\delta}_\infty(\mathcal{G}, G_b) = \|G_a - G_b\|_\infty$. Similarly we have

$$\delta_2(\mathcal{G}, G_m) = \tfrac{1}{2}\sqrt{2}\,\|G_a - G_b\|_2$$

which is an improvement compared to

$$\delta_2(\mathcal{G}, G_a) = \delta_2(\mathcal{G}, G_b) = \|G_a - G_b\|_2.$$

The price we pay is an increased order. For simulation and control design, we want to have a low-order model G_r with small distance measures $\delta_2(\mathcal{G}, G_r)$ and $\hat{\delta}_\infty(\mathcal{G}, G_r)$. We formulate the following fixed-order centering problems ($p \in \{2, \infty\}$):

$$\min_{G_r} \delta_p(\mathcal{G}, G_r) \tag{29}$$

with

$$\delta_p(\mathcal{G}, G_r) = \left\| \begin{bmatrix} G_a \\ G_b \end{bmatrix} - \begin{bmatrix} I \\ I \end{bmatrix} G_r \right\|_p. \tag{30}$$

The minimization problem (29, 30) can be reformulated as an optimal reduction problem. Therefore we write

$$G_r = G_m + \Delta \tag{31}$$

with

$$G_m = \tfrac{1}{2}(G_a + G_b).$$

First consider $p = 2$. The following expression can be derived straightforwardly:

$$\begin{aligned} \delta_2^2(\mathcal{G}, G_r) &\overset{(3)}{=} \|G_a - G_r\|_2^2 + \|G_b - G_r\|_2^2 \\ &\overset{(31)}{=} \|\tfrac{1}{2}(G_a - G_b) - \Delta\|_2^2 + \\ &\quad \|\tfrac{1}{2}(G_b - G_a) - \Delta\|_2^2 \\ &\overset{(4)}{=} \tfrac{1}{2}\|G_a - G_b\|_2^2 + 2\|\Delta\|_2^2. \end{aligned}$$

Since G_a and G_b are given, optimal centering implies a minimization of $\|\Delta\|_2$. The optimal centering solution with unconstrained order is $G_r = G_m$. For fixed-order centering, the optimal G_r can be solved from the following optimal reduction problem

$$\min_{G_r} \|G_m - G_r\|_2.$$

Note that a similar derivation can be given for problem (29, 30) with $p = \infty$. This will be shown next for the three model case: $\mathcal{G} = \{G_a, G_b, G_c\}$. We make $G_m = \frac{1}{3}(G_a + G_b + G_c)$ and set $G_r = G_m + \Delta$. The centering objective is the same as in (29, 30), but here we formulate it as a search for the minimizing Δ:

$$\min_{\Delta} \delta_p(\mathcal{G}, G_m + \Delta)$$

Let

$$H(\mathcal{G}, \Delta) = \Gamma \begin{bmatrix} G_a \\ G_b \\ G_c \end{bmatrix} - \begin{bmatrix} I \\ I \\ I \end{bmatrix} \Delta. \tag{32}$$

and

$$\Gamma = \begin{bmatrix} \frac{2}{3}I & -\frac{1}{3}I & -\frac{1}{3}I \\ -\frac{1}{3}I & \frac{2}{3}I & -\frac{1}{3}I \\ -\frac{1}{3}I & -\frac{1}{3}I & \frac{2}{3}I \end{bmatrix},$$

then $\delta_p(\mathcal{G}, G_m + \Delta) = \|H(\mathcal{G}, \Delta)\|_p$. A crucial property of Γ is

$$[\, I \;\; I \;\; I \,]\,\Gamma = [\, O \;\; O \;\; O \,]. \tag{33}$$

Using (33) we can derive

$$H(\mathcal{G}, \Delta)^* H(\mathcal{G}, \Delta) = S(\mathcal{G}, \Delta)^* S(\mathcal{G}, \Delta) \tag{34}$$

$$S(\mathcal{G}, \Delta) = \begin{bmatrix} G_a - G_m \\ G_b - G_m \\ G_c - G_m \\ \sqrt{3}\Delta \end{bmatrix}. \tag{35}$$

From the definition of $\|H\|_2$ (2) and $\|H\|_\infty$ (13), we see that both norms have a kernel H^*H. Using (34) we conclude that $\|H(\mathcal{G}, \Delta)\|_p = \|S(\mathcal{G}, \Delta)\|_p$ for both $p = 2$ and $p = \infty$. Since the only free parameters for minimizing these norms are within Δ, we can conclude that the central *full-order* approximation G_m is optimal in both H_2-norm sense ($\delta_2(\mathcal{G}, G_m)$), and H_∞-norm sense ($\delta_\infty(\mathcal{G}, G_m)$). If the approximation has to be of a fixed order, we have to find a $\Delta = G_r - G_m$ with minimum $\|\Delta\|_p$ such that r does not exceed the maximum allowable value. Thus the best fixed-order central approximations are optimal reduced-order approximations of G_m.

For the general case of centering an arbitrary number of models we state the following.

Proposition 5.1 (Center of k models) *Let $G_{(i)}$, $i \in [1, \ldots, k]$, form a model set $\mathcal{G}$ with strictly stable and strictly proper models, and let G_r be an r^{th}-order strictly stable and strictly proper model. The r^{th}-order solution to the following nominal modelling problem,*

$$\min_{G_r} \left\| \begin{bmatrix} G_{(1)} \\ \vdots \\ G_{(k)} \end{bmatrix} - \begin{bmatrix} I \\ \vdots \\ I \end{bmatrix} G_r \right\|_p, \tag{36}$$

for $p \in \{2, \infty\}$, is the solution of the optimal model reduction problem

$$\min_{G_r} \|G_m - G_r\|_p \tag{37}$$

with

$$G_m = \frac{1}{k}\sum_{i=1}^{k} G_{(i)}. \tag{38}$$

Proof: Let $G_r = G_m + \Delta$, substititute this in the p-norm expression of (36), giving

$$\left\| \Gamma \begin{bmatrix} G_{(1)} \\ \vdots \\ G_{(k)} \end{bmatrix} - \begin{bmatrix} I \\ \vdots \\ I \end{bmatrix} \Delta \right\|_p \tag{39}$$

with

$$\Gamma = \begin{bmatrix} I & & \\ & \ddots & \\ & & I \end{bmatrix} - \frac{1}{k}\begin{bmatrix} I & \cdots & I \\ \vdots & & \vdots \\ I & \cdots & I \end{bmatrix}.$$

For $p \in \{2, \infty\}$, we can invoke the Γ-property

$$[\, I \ \cdots \ I \,]\,\Gamma = [\, O \ \cdots \ O \,]$$

and rewrite (39) as

$$\left\| \begin{bmatrix} G_{(1)} - G_m \\ \vdots \\ G_{(k)} - G_m \\ \sqrt{k}\,\Delta \end{bmatrix} \right\|_p = \left\| \begin{bmatrix} \Gamma \begin{bmatrix} G_{(1)} \\ \vdots \\ G_{(k)} \end{bmatrix} \\ \sqrt{k}\,\Delta \end{bmatrix} \right\|_p. \tag{40}$$

Minimization of (40) implies minimization of $\|\Delta\|_p$. □

The optimal solution can be interpreted as the optimal reduced-order approximation of the *mean* model G_m. The result of Miyazawa & Dowell (1989) is covered for $p = 2$. Note that the ultimate goal in centering for robust H_∞ control design is the minimization of $\hat{\delta}_\infty(\mathcal{G}, G_r)$ (28) which is different from the minimization of $\delta_\infty(\mathcal{G}, G_r)$ treated in the proposition above. Notice that the centering is restricted to stable models.

The centering problem can also be posed in a frequency-weighted setting. It can be shown easily that the full-order central approximation (38) is also the minimizing solution of

$$\left\| \begin{bmatrix} WG_{(1)} \\ \vdots \\ WG_{(k)} \end{bmatrix} V - \begin{bmatrix} W \\ \vdots \\ W \end{bmatrix} G_m V \right\|_2$$

with $W(s)$ an output weight and $V(s)$ an input weight. The difference with the unweighted case is that the fixed-order central approximation has to be solved from a *weighted* optimal reduction problem:

$$\min_{G_r} \|W(G_m - G_r)V\|_2$$

6 Numerical examples

First we test our algorithm for weighted reduction on a test problem defined in literature, and second we look at the problem of finding a single nominal model from two slightly different models of the same order.

6.1 Frequency weighted reduction of a sixth-order filter

As a first example we take the system and weights as in Latham & Anderson (1985). $G(s)$ is a sixth-order Butherworth filter with 3dB point at $\omega = 1$ (low-pass filter).

$$\begin{aligned} G_6(s) &= \frac{1}{n(s)} \\ n(s) &= s^6 + 3.8637s^5 + 7.4641s^4 + \\ &\quad 9.1416s^3 + 7.4641s^2 + 3.8637s + 1 \end{aligned}$$

To have a good approximation for frequencies around $\omega = 1$, Latham & Anderson proposed a frequency-weighted optimal Hankel-norm reduction technique using the following type of second-order weighting functions

$$W(s) = \frac{(s+1)^2}{s^2 + 2\alpha s + 1}$$

with $0 < \alpha \leq 1$. Primarily it was their objective to make $\|W(G_6 - G_4)\|_\infty$ as small as possible for $G_4(s)$ a stable fourth-order approximation. Here we also take $\|W(G_6 - G_4)\|_2$ in consideration. We take $\alpha = 0.1$. For this case, Latham & Anderson found a weighted Hankel-norm optimum ($\hat{G}_4(s)$) with $\|W(G_6 - \hat{G}_4)\|_\infty = 0.031$. The authors did not provide the model data nor the H_2-norm of the weighted error. For this weighted reduction problem we have computed the following fourth-order approximations (see Wortelboer 1994 for a full account of the notation):

balanced:	$\mathrm{bal}\mathcal{R}_4(G_6) = \breve{G}_4$
weighted balanced:	$\mathrm{bal}\mathcal{R}_4(W\underline{G_6}) = \underline{\breve{G}_4}$
H_2 optimal:	$\mathrm{optH}_2\mathcal{R}_4(G_6) = \mathring{G}_4$
weighted H_2 optimal:	$\mathrm{optH}_2\mathcal{R}_4(W\underline{G_6}) = \underline{\mathring{G}_4}$

The computational cost to find

$$\underline{\mathring{G}_4} = \frac{-0.0474s^3 + 0.1591s^2 - 0.3339s + 0.3749}{s^4 + 1.3834s^3 + 1.7926s^2 + 1.0764s + 0.3891}$$

was considerable compared to the others. The convergence to the (unweighted and weighted) optimal solutions $\mathring{G}_4$ and $\underline{\mathring{G}_4}$ is shown in Fig 1. Table 6.1 shows that the weighted solutions (underlined) are indeed better than the unweighted ones and that the H_2-norm optimal solutions are better than the

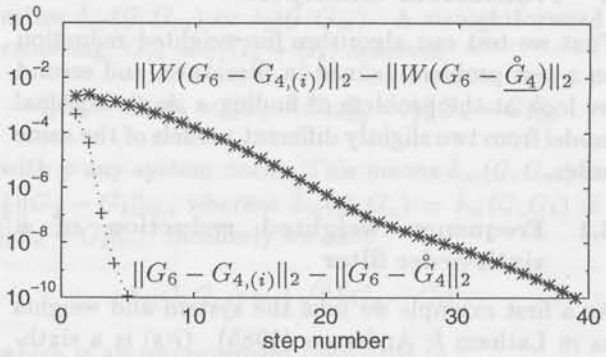

Fig. 1: Convergence to optimal solutions

G_4	$\|\Delta\|_2$	$\|\Delta\|_\infty$
$\mathrm{bal}\mathcal{R}_4(G_6)$	0.064	0.209
$\mathrm{bal}\mathcal{R}_4(W\underline{G_6})$	<u>0.037</u>	<u>0.050</u>
$\mathrm{optH}_2\mathcal{R}_4(G_6)$	0.058	0.182
$\mathrm{optH}_2\mathcal{R}_4(W\underline{G_6})$	<u>0.034</u>	<u>0.040</u>

Table 1: Frequency-weighted reduction errors: $\Delta = W(G_6 - G_4)$

balanced solutions. Finally it is remarked that the weighted reduction error measured in H_∞-norm can be reduced by exploiting the freedom in the D-term of the reduced model. This is common practice in frequency-weighted optimal Hankel-norm reduction, but should not be recommended in case the weighted H_2-norm is of concern.

6.2 In between two second-order models

Here we introduce the problem of finding a single model that is close to two other models with the restriction that all three models have the same order. Let

$$G_a = \frac{k_a}{s^2 + 2\beta_a\omega_a s + \omega_a^2} \qquad (41.a)$$

$$G_b = \frac{k_b}{s^2 + 2\beta_b\omega_b s + \omega_b^2} \qquad (41.b)$$

with $k_a = 0.8$, $k_b = 1.2$, $\beta_a = 0.005$, $\beta_b = 0.02$, $\omega_a = 1.1$, and $\omega_b = 0.9$. Let $d \triangleq \|\frac{1}{2}(G_a - G_b)\|_2$. In this example we have $d = 4.9291$. The objective is to find a second-order G such that

$$\mathcal{J}(\mathcal{G}, G) = \delta_2(\mathcal{G}, G)/d \qquad (42)$$

is minimal. We also define

$$\mathcal{J}_a(\mathcal{G}, G) = \|G - G_a\|_2/d \qquad (43.a)$$

$$\mathcal{J}_b(\mathcal{G}, G) = \|G - G_b\|_2/d. \qquad (43.b)$$

The optimal *full*-order central solution $G_m = \frac{1}{2}(G_a + G_b)$ gives $\mathcal{J}(\mathcal{G}, G_m) = \sqrt{2}$ and $\mathcal{J}_a(\mathcal{G}, G_m) = \mathcal{J}_b(\mathcal{G}, G_m) = 1$. We compare two methods to construct a line of second-order models in between G_a and G_b. The first is a mere linear parameter vector interpolation:

$$\grave{G}_{r,q} = \frac{k_q}{s^2 + 2\beta_q\omega_q s + \omega_q^2} \qquad (44)$$

with $k_q = (1-q)\,k_a + q\,k_b$, $\beta_q = (1-q)\,\beta_a + q\,\beta_b$, and $\omega_q = (1-q)\,\omega_a + q\,\omega_b$. The second method is the one advocated in this paper: centering followed by optimal reduction. In order to visualize the optimality of this solution, we first derive a line of second-order approximations

$$\mathring{G}_{r,q} = \mathrm{optH}_2\mathcal{R}_2(G_{m,q}) \qquad (45)$$

with

$$G_{m,q} = (1-q)\,G_a + q\,G_b. \qquad (46)$$

The central solution ($q = 0.5$) is the optimal one. Figure 2.a shows that $\grave{G}_{q=0}$ and $\grave{G}_{q=1}$ are the

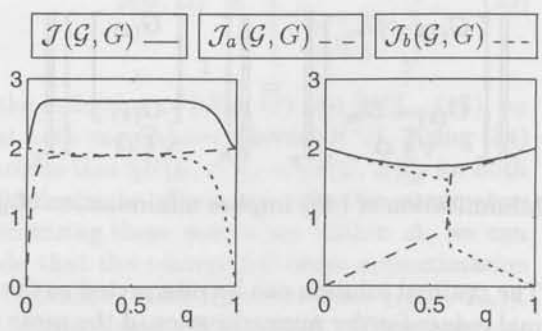

Fig. 2: Scaled distance measures for two interpolation methods
a: $G = \grave{G}_{r,q}$ b: $G = \mathring{G}_{r,q}$

best approximations for the parameter interpolation method, meaning that interpolation in this way does not give a clue for decreasing $\mathcal{J}(\mathcal{G}, G)$. Figure 2.b shows that the optimum on the line of approximations is indeed $\mathring{G}_{r,q=0.5}$. Moreover $\mathcal{J}(\mathcal{G}, \mathring{G}_{r,q}) < 2$ for all $0 < q < 1$, whereas for $q = 0$ and $q = 1$ the maximum value 2 is attained which means that the trivial fixed-order solutions G_a and G_b are worst.

This example also exhibits an important phenomenon in reduction problems. From Fig 2.b we see that for increasing values of q, $\mathcal{J}_a(\mathcal{G}, \mathring{G}_{r,q})$ increases and $\mathcal{J}_b(\mathcal{G}, \mathring{G}_{r,q})$ decreases; the steepest change occurs at

$$q \approx \hat{q} = 0.62.$$

This proved to be due to the fact that $G_{m,\hat{q}}$ has two resonance peaks of approximately the same magnitude. The Hankel singular values of $G_{m,\hat{q}}$ are:

$$\sigma(G_{m,\breve{q}}) = \begin{bmatrix} 25.18 \\ 25.03 \\ 23.15 \\ 22.70 \end{bmatrix}. \quad (47)$$

This suggests that reduction is not appropriate, and indeed balanced reduction gives bad results. Starting from the balanced approximation, $\breve{G}_{r,\breve{q}} = \text{bal}\mathcal{R}_2(G_{m,\breve{q}})$, our optimal H_2-norm reduction algorithm converges to

$$\overset{\times}{G}_{r,\breve{q}} = \frac{-0.04161\,s + 0.3096}{s^2 + 0.005707\,s + 1.2109} \quad (48)$$

with $\overset{\times}{\omega}_r = 1.1004$, and $\overset{\times}{\beta}_r = 0.0025932$. Since $\overset{\times}{\omega}_r \approx \omega_a = 1.1$ and $\overset{\times}{\beta}_r \approx \beta_a = 0.002$, $\overset{\times}{G}_{r,\breve{q}}$ essentially fits the resonance of $(1-\breve{q})G_a$. Since we know that for $q \to 1$ the resonance of G_b becomes the dominant one, there has to be a switch point for some q. To see if there exists another extremum that essentially fits the resonance of $\breve{q}G_b$, we restarted the iteration from $\breve{q}G_b$. After a few iteration steps we found

$$\mathring{G}_{r,\breve{q}} = \frac{0.05439\,s + 0.7484}{s^2 + 0.01821\,s + 0.8090} \quad (49)$$

with $\omega_r = 0.89942$, and $\beta_r = 0.010125$ which is indeed close to $\omega_b = 0.9$ and $\beta_b = 0.01$. Let $\breve{\Delta} = G_{m,\breve{q}} - \breve{G}_{r,\breve{q}}$, $\overset{\times}{\Delta} = G_{m,\breve{q}} - \overset{\times}{G}_{r,\breve{q}}$, and $\mathring{\Delta} = G_{m,\breve{q}} - \mathring{G}_{r,\breve{q}}$. Since $\|\breve{\Delta}\|_2 = 5.1808$, $\|\overset{\times}{\Delta}\|_2 = 4.3481$ and $\|\mathring{\Delta}\|_2 = 2.6272$, $\overset{\times}{G}_{r,\breve{q}}$ can only be a local minimum. Figure 3 compares the square reduction errors $\Delta^*(j\omega)\Delta(j\omega)$ as a function of frequency. The scales are linear in Fig 3, such that the enclosed area of the curves is proportional to $\|\Delta\|_2^2$. We see

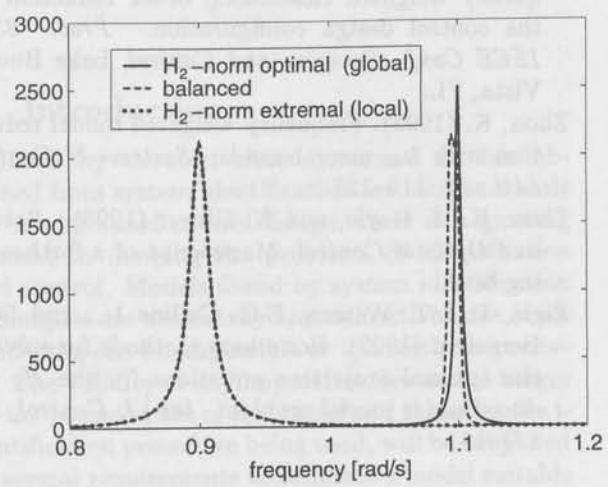

Fig. 3: Squared reduction errors for $q = \breve{q} = 0.62$

that the global optimum fits the $\omega_b = 0.9$-resonance, the balanced approximation fits neither of the two resonances, and the local optimum fits the $\omega_a = 1.1$-resonance. Summarizing, the reduction of a fourth-order model to an optimal second-order model is not completely characterized by the necessary optimality conditions: *at least two* local minima of the H_2-norm reduction error exist.

Finally we pose the following question: are the reduction errors involved in the second-order approximation of $G_{m,\breve{q}}$ truly larger than the reduction errors involved in the second-order approximation of $G_{m,\bar{q}}$ with $\bar{q} = 0.5$? The answer is no, and this contradicts the common confidence in the importance of Hankel singular values. The Hankel singular values of $G_{m,\bar{q}}$ are

$$\sigma(G_{m,\bar{q}}) = \begin{bmatrix} 33.11 \\ 32.95 \\ 18.67 \\ 18.30 \end{bmatrix}. \quad (50)$$

Comparison with (47) usually leads to the conclusion that it is more appropriate to reduce $G_{m,\bar{q}}$ to order two than to reduce $G_{m,\breve{q}}$ to order two. Table 2 shows that in fact $G_{m,\breve{q}}$ can be reduced at the cost of a lower error than $G_{m,\bar{q}}$, provided we use optimal H_2-norm reduction instead of balanced reduction.

q	$\|G_{m,q}\|_2$	$\|G_{m,q} - \mathring{G}_{r,q}\|_2$	$\|G_{m,q} - \breve{G}_{r,q}\|_2$
0.5	4.943	3.507	3.511
0.62	5.098	2.627	5.181

Table 2: Optimal and balanced reduction errors for two 4^{th}-order systems $G_{m,\bar{q}}$ and $G_{m,\breve{q}}$

7 Discussion of usage

The algorithm for optimal H_2-norm reduction proved very powerful in the unweighted case. The choice of the initial projection of G_n is very important. In most cases a balanced projection will give good convergence. As we have seen, there exist examples for which balanced reduction does not give good reduction results, and precisely in these cases optimal H_2-norm reduction should be preferred. The difficulty then is to construct a good initial projection. In this respect the interactive tool introduced in Wortelboer (1994) to monitor frequency response changes as a function of user supplied interval-based frequency penalty functions is crucial to initialize a promising projection. The user iterates towards a 'visually' good approximation and the algorithm discussed here iterates from there to the optimal approximation. The weighted case is considerably harder to solve numerically. The main advantage above balanced reduction is the optimality. Yet balanced reduction remains a valuable method since it is computationally less demanding

and often achieves both small H_2-norm and H_∞-norm errors. As we have said before, such simple reduction methods are very appropriate in iterative control design procedures.

8 Conclusion

Necessary conditions have been derived for obtaining a reduced-order model that minimizes a frequency weighted reduction error measured in H_2-norm (both input and output weights are allowed). This new derivation has been specialized to a known result for unweighted optimal H_2 reduction, resulting in the optimal projection formulation and a new numerical algorithm. Results for unweighted optimal reduction are often close to balanced approximations and can be obtained in only a few iterations. The weighted case is considerably harder to solve numerically. Existence of multiple local minima for our non convex minimization problem has been shown in an example. The proposed solutions can play a role in model-based control design. A special application of optimal reduction is the straightforward construction of a fixed-order central approximation of multiple models. This central approximation can be used as a nominal model for controller design, and the minimized distance to all other models allows a formal robustification of this controller.

References

Aigrain, P.R. and E.M. Williams (1949). Synthesis of n-reactance networks for desired transient response. *J. Applied Physics, 20*, 587–600.

Baratchart, L., M. Olivi and F. Wielonsky (1992). On a rational approximation problem in the real Hardy space H_2. *Theoretical Computer Science, 94*, 175–197.

Enns, D.F. (1984). Model reduction with balanced realization: an error bound and a frequency weighted generalization. *Proc. 23rd IEEE Conf. Decision and Control*, pp. 127–132.

Glover, K. (1984). All optimal Hankel-norm approximations of linear multivariable systems and their L_∞-error bounds. *Int. J. Contr., 39*, 1115–1193.

Halevi, Y. (1992). Frequency weighted model reduction via optimal projection. *IEEE Trans. Automat. Contr., AC-37*, 1537–1542.

Hyland, D.C. and D.S. Bernstein (1985). The optimal projection equations for model reduction and the relationships among the methods of Wilson, Skelton and Moore. *IEEE Trans. Automat. Contr., AC-30*, 1201–1211.

Kavranoğlu, D. (1994). A computational scheme for H_∞ model reduction. *IEEE Trans. Automat. Contr., AC-39*, 1447-1451.

Krajewski, W., A. Lepschy, G.A. Mian and U. Viaro (1993). Optimality conditions in multivariable L_2 model reduction. J. Franklin Inst., 330, 431-439.

Latham, G.A. and B.D.O. Anderson (1985). Frequency-weighted optimal Hankel-norm approximation of stable transfer functions. *System & Control Lett., 5*, 229–236.

Luenberger, D.G. (1984). *Linear and Nonlinear Programming.* Second edition, Addison-Wesley Publ. Comp.

Meyer, D.G. (1988). A fractional approach to model reduction, *Proc. American Control Conf.*, 1041–1047.

Miyazawa, Y. and E.H Dowell (1989). Approach to modeling and estimation for uncertain systems. *J. Guidance, Control, and Dynamics, 12*, 672–680.

Moore, B.C. (1981). Principal component analysis in linear systems: controllability, observability, and model reduction. *IEEE Trans. Automat. Contr., AC-26*, 17–32.

Rudin, W. (1966). *Real and Complex Analysis.* Second Edition, McGraw-Hill Book Co., New York.

Vidyasagar, M. (1985). *Control System Synthesis.* MIT Press, London.

Wilson, D.A. (1970). Optimum solution of model-reduction problem. *Proc. IEE, vol.117*, 1161–1165.

Wortelboer, P.M.R. (1994). *Frequency-Weighted Balanced Reduction of Closed-Loop Mechanical Servo-Systems: Theory and Tools.* Dr. Dissertation, Delft University of Technology.

Wortelboer, P.M.R. and O.H. Bosgra (1994). Frequency weighted closed-loop order reduction in the control design configuration. *Proc. 33rd IEEE Conf. Decision and Control*, Lake Buena Vista, FL.

Zhou, K. (1993). Frequency weighted model reduction with L_∞ error bounds. *Systems & Control Lett., 21*, 115–125.

Zhou, K., J. Doyle, and K. Glover (1993). *Robust and Optimal Control.* Manuscript of a forthcoming book.

Žigić, D.,L.T. Watson, E.G. Collins Jr., and D.S. Bernstein (1992). Homotopy methods for solving the optimal projection equations for the H_2 reduced order model problem. *Int. J. Control, 56*, 173–191.

Selected Topics in Identification, Modelling and Control
Vol. 7, December 1994

Filtering and parametrization issues in feedback relevant identification based on fractional model representations

R.A. de Callafon[‡§] and P.M.J. Van den Hof [§]

[§] *Mechanical Engineering Systems and Control Group*
Delft University of Technology, Mekelweg 2, 2628 CD Delft, The Netherlands.

Abstract. This paper discusses filtering and parametrization issues involved in the usage of fractional representations in multivariable, approximate and feedback relevant identification of a possibly unstable plant operating under closed loop conditions. The knowledge of the controller is used to access any stable right coprime factorization of the plant by measuring and filtering the signals present in the closed loop system. By exploiting a specific class of parametrizations in the estimation of the stable coprime factorization with a prespecified McMillan degree, a linear time invariant model having the same McMillan degree will be obtained. In addition the approximate and feedback relevant estimation of a *fixed order* linear time invariant model based on coprime factor identification leads to an additional constraint, which can be written down explicitly as a relation between the filtering of the signals present in the closed loop system and the coprime factors of the model being estimated. A possible solution to deal with this constraint based on an update algorithm is presented.

Keywords. System identification; robust control; coprime factors; filtering; parametrization.

1 Introduction

Induced by the fact that dynamical models obtained from system identification are used as a basis for model based control design, there is a growing interest in merging the problems of identification and control. Models found by system identification techniques are necessarily approximative since exact modelling can be impossible or too costly to perform. The validity of any approximative model hinges on the intended use of the model and therefore the identification procedure being used, will be subjected to several requirements to estimate a model suitable for control design thoughtfully. This has been the motivation to develop methods for a feedback relevant identification, which implies that the feedback relevant dynamical behaviour of a plant operating in a closed loop configuration has to be estimated in order to design enhanced controllers (Gevers, 1993; Van den Hof and Schrama, 1994).

To perform a feedback relevant identification, experiments from the real plant, denoted with P_o, operating in a closed configuration are needed to come up with a model, denoted with $\hat{P}$, suitable for control design (Lee *et al.*, 1992; Hakvoort *et al.*, 1994; Hjalmarsson *et al.*, 1994*a*). Since the controller to create the closed loop configuration can (yet) be unknown, a simultaneous optimization of identification and control design has been proposed in Bayard *et al.* (1992) or Hjalmarsson *et al.* (1994*b*). Furthermore, it has been widely motivated to separate the two stages of identification and control design and to use an iterative scheme of identification and model based control design (Schrama, 1992*a*). One of the first papers using this separation can be found in Farison *et al.* (1967) or Schwartz and Steiglitz (1971) and more recent examples of iterative

[‡]The work of Raymond de Callafon is sponsored by the Dutch Systems and Control Theory Network

schemes can be found in Zang *et al.* (1992), Rivera and Bhatnagar (1993), Bitmead (1993) or Lee *et al.* (1993). In such an iterative scheme the controller of step $i-1$, is used to perform closed loop experiments with the plant P_o and to estimate a feedback relevant model $\hat{P}$. The model $\hat{P}$ is used to design an improved model based controller, denoted by $C_{\hat{P}}$, again to perform closed loop experiments with in step i.

In this paper the *identification stage* in such an iterative scheme will be discussed. The identification is based on the algebraic theory of fractional representations (Vidyasagar, 1985) and involves the feedback relevant identification of a coprime factor realization of a model $\hat{P}$ based on closed-loop observations of the plant P_o using a controller C from the previous iteration (Hansen, 1989; Schrama, 1992*b*; Van den Hof *et al.*, 1993). In order to control the McMillan degree of the linear time invariant model $\hat{P}$, a specific class of parametrizations is used to parametrize the coprime factorization being estimated. Furthermore, the approximate and feedback relevant estimation of a *fixed order* linear time invariant model gives rise to an additional constraint, which can be written down explicitly in case of the coprime factor identification.

The outline of this paper is as follows. In section 2 some preliminary notations and definitions used in the sequel will be given. Section 3 discusses the relation between identification and control design. To deal with the closed loop identification problem, in section 4 the framework of equivalent open-loop identification of a coprime factor representation of the plant P_o will be summarized. Section 5 contains the parametrization aspects on the identification of a coprime factorization itself and the results of performing the identification in a feedback relevant way, leading to an additional parametrization constraint. Possible solutions to cope with this parametrization constraint are summarized. Finally, section 6 contains some concluding remarks.

2 Preliminaries

2.1 Feedback configuration

Throughout this paper the feedback configuration of a plant P and a controller C is denoted with $\mathcal{T}(P,C)$ and defined as the connection structure depicted in figure 1.

In figure 1 the signals u and y reflect respectively the inputs and outputs of the plant P, where v is an additive noise on the output y of the plant. The signals u_c and y_c are respectively the inputs and outputs of the controller C, and r_1 and r_2 are external reference signal that are uncorrelated with

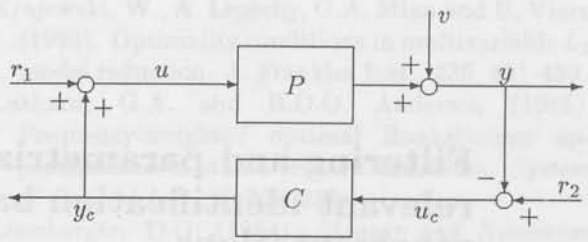

Fig. 1: feedback connection structure $\mathcal{T}(P,C)$

the additive noise v. From an identification point of view the signals u and y are being measured, v is unknown and r_1, r_2 (and consequently u_c, y_c) are possibly at our disposal.

It is assumed that the feedback connection structure is well posed, that is $\det[I+CP] \not\equiv 0$. In this way the closed loop dynamics of the closed loop system $\mathcal{T}(P,C)$ can be described by the mapping of $[r_2\ r_1]^T$ to $[y\ u]^T$ which is given by the transfer function matrix $T(P,C)$:

$$T(P,C) := \begin{bmatrix} P \\ I \end{bmatrix} [I+CP]^{-1} \begin{bmatrix} C & I \end{bmatrix}. \quad (1)$$

and describing the data coming from the closed loop system $\mathcal{T}(P,C)$ in the following way

$$\begin{bmatrix} y \\ u \end{bmatrix} = T(P,C) \begin{bmatrix} r_2 \\ r_1 \end{bmatrix} + \begin{bmatrix} I \\ -C \end{bmatrix} [I+PC]^{-1} v \quad (2)$$

where the additive noise $v := He$ can be modelled by a monic, stable and stably invertible noise filter H having a white noise input e (Ljung, 1987). In case of an *internally* stable closed loop system $\mathcal{T}(P,C)$, all four transfer function matrices in $T(P,C)$ will be stable (Desoer and Chan, 1975; Schrama, 1992*b*; Bongers, 1994) which implies $T(P,C) \in \mathbb{RH}_\infty$, where $\mathbb{RH}_\infty$ denotes the set of all rational stable transfer functions.

The controller C will be applied to both the real plant P_o and the model $\hat{P}$, according to the feedback connection structure given in figure 1. The corresponding closed loop dynamics of the two different feedback configurations will be described respectively by the two transfer function matrices $T(P_o,C)$ and $T(\hat{P},C)$.

2.2 Coprimeness and stability

Using the theory of fractional representations, an arbitrary plant P is expressed as a ratio of two stable mappings N and D. Following Vidyasagar (1985) the following definitions for coprimeness and coprime factorization will be used, where $\mathbb{RH}_\infty$ denotes the set of all rational stable transfer functions.

Definition 2.1 *Let $N, D \in \mathbb{RH}_\infty$, then the pair (N, D) is called right coprime over $\mathbb{RH}_\infty$ if there exist right Bezout factors $X, Y \in \mathbb{RH}_\infty$ such that*

$$XN + YD = I.$$

The pair (N, D) is a right coprime factorization (rcf) of P if $\det\{D\} \not\equiv 0$ and $P = ND^{-1}$ and (N, D) is right coprime over $\mathbb{RH}_\infty$.

Based on the theory of fractional representations and the usage of left and right coprime factorizations given in definition 2.1 the following result for internal stability of a closed loop system $\mathcal{T}(P, C)$ can be derived.

Theorem 2.2 *Let $P = ND^{-1} = \tilde{D}^{-1}\tilde{N}$ where (N, D) is a rcf and $(\tilde{D}, \tilde{N})$ a lcf of P. Let $C = N_c D_c^{-1} = \tilde{D}_c^{-1}\tilde{N}_c$ where (N_c, D_c) is a rcf and $(\tilde{D}_c, \tilde{N}_c)$ a lcf of C. Now the following statements are equivalent*

i. the feedback system $\mathcal{T}(P, C)$ given in figure 1 is internally stable

ii. $T(P, C) \in \mathbb{RH}_\infty$

iii. $\Lambda^{-1} \in \mathbb{RH}_\infty$, *with* $\Lambda := \begin{bmatrix} \tilde{D}_c & \tilde{N}_c \end{bmatrix} \begin{bmatrix} D \\ N \end{bmatrix}$

iv. $\tilde{\Lambda}^{-1} \in \mathbb{RH}_\infty$, *with* $\tilde{\Lambda} := \begin{bmatrix} \tilde{D} & \tilde{N} \end{bmatrix} \begin{bmatrix} D_c \\ N_c \end{bmatrix}$

Proof: Vidyasagar (1985) and Bongers (1994). □

3 Merging identification and control

3.1 Norm based control design

In the analysis of feedback relevant identification, the characterization of a closed loop performance criterion plays an important role. This criterion is usually characterized by an objective function, which depends on a plant P and the controller C that assemble the closed loop configuration (Van den Hof and Schrama, 1994).

Definition 3.1 *Let $\mathcal{X}$ denote a complete normed space, where $\|\cdot\|_\mathcal{X}$ is the norm function defined on $\mathcal{X}$. Let a plant P and a controller C form a well posed feedback connection structure $\mathcal{T}(P, C)$ according to figure 1, and let $J(P, C) \in \mathcal{X}$ be a any function depending on a plant P and the controller C. Then the objective function is defined by the norm $\|J(P, C)\|_\mathcal{X}$*

Unfortunately the plant P_o under consideration is unknown and the control design method will be based on minimization of a closed loop performance criterion $\|J(\hat{P}, C)\|_\mathcal{X}$ using a model $\hat{P}$. In this way the control design will be model based and can be interpreted by the computation of a so called model based controller, denoted with $C_{\hat{P}}$, such that

$$C_{\hat{P}} = \arg \min_C \|J(\hat{P}, C)\|_\mathcal{X}. \tag{3}$$

This minimization gives rise to a value of the objective function given by $\|J(\hat{P}, C_{\hat{P}})\|_\mathcal{X}$ and can be classified as the *design cost* (Gevers, 1993). Applying the model based controller $C_{\hat{P}}$ to the real plant P_o gives rise to the value $\|J(P_o, C_{\hat{P}})\|_\mathcal{X}$ which is characterized as the *achieved cost*. In this perspective the controller $C_{\hat{P}}$ is said to *satisfy* the design objective for the corresponding model $\hat{P}$ if

$$\|J(\hat{P}, C_{\hat{P}})\|_\mathcal{X} \leq \gamma, \text{ with } \gamma > 0 \tag{4}$$

holds, which is a nominal performance specification. Related examples can for example be found in Bitmead (1993), Gevers (1993) or Van den Hof and Schrama (1994) for ∞- or 2-norm based minimization.

In this paper the normed space $\mathcal{X}$ is chosen to be the space $\mathbb{RH}_\infty$. The function $J(P, C) \in \mathbb{RH}_\infty$ is taken to be a weighted form of the closed loop dynamics described by the transfer function matrix $T(P, C) \in \mathbb{RH}_\infty$ given in (1). In this way $J(P, C) = W_o T(P, C) W_i \in \mathbb{RH}_\infty$ if W_o and W_i in (5) are weighting filters satisfying $W_o, W_i \in \mathbb{RH}_\infty$, making

$$\|J(P, C)\|_\infty := \|W_o T(P, C) W_i\|_\infty \tag{5}$$

The objective function given in (5) represents a large class of ∞-norm based control design schemes and the usage of the weightings is inspired by the ability to create a trade off between conflicting requirements and constraints always present (Horowitz, 1963; Boyd and Barrat, 1991). In case of diagonal weighting filters, the weighting can be seen as an additional loop-shaping in the control design (Bongers, 1994).

3.2 A feedback relevant criterion

From an identification point of view, a model $\hat{P}$ can only be an approximation of the real plant P_o. The quality of any approximative model depends on the intended use of the model. In this perspective, the question wether a model $\hat{P}$ is good for model based control design gives rise to a so called feedback relevant identification, since the quality of the model $\hat{P}$ should be evaluated under feedback or closed loop conditions (Schrama, 1992*b*).

A successful controller $C_{\hat{P}}$, found by the norm based minimization given in (3) and based on a

model $\hat{P}$, gives rise to a value of objective function $\|J(\hat{P}, C_{\hat{P}})\|_{\mathcal{X}}$, which is said to satisfy the control objective (4) for the nominal model $\hat{P}$. From this perspective, the quality of the model $\hat{P}$ can be evaluated by considering the value of the objective function $\|J(P_o, C_{\hat{P}})\|_{\mathcal{X}}$ when applying the controller $C_{\hat{P}}$, to the real plant P_o.

Unfortunately, the real plant P_o is unknown and the following triangular inequalities (Schrama, 1992*b*) can be used to lower and upper bound $\|J(P_o, C_{\hat{P}})\|_{\mathcal{X}}$.

$$\|J(P_o, C_{\hat{P}})\|_{\mathcal{X}} \leq \|J(\hat{P}, C_{\hat{P}})\|_{\mathcal{X}} + \|J(P_o, C_{\hat{P}}) - J(\hat{P}, C_{\hat{P}})\|_{\mathcal{X}}$$

$$\|J(P_o, C_{\hat{P}})\|_{\mathcal{X}} \geq \left| \|J(\hat{P}, C_{\hat{P}})\|_{\mathcal{X}} - \|J(P_o, C_{\hat{P}}) - J(\hat{P}, C_{\hat{P}})\|_{\mathcal{X}} \right|$$

From the first inequality it can be seen that

$$\|J(\hat{P}, C_{\hat{P}})\|_{\mathcal{X}} + \|J(P_o, C_{\hat{P}}) - J(\hat{P}, C_{\hat{P}})\|_{\mathcal{X}} \leq \gamma \quad (6)$$

is a sufficient condition in order to have a model based controller $C_{\hat{P}}$ which satisfies the control objective (4) on the real plant P_o. From an identification point of view the performance degradation $\|J(P_o, C_{\hat{P}}) - J(\hat{P}, C_{\hat{P}})\|_{\mathcal{X}}$ for the controller $C_{\hat{P}}$ should be minimized in order to find a model $\hat{P} = P(\hat{\theta})$ such that (6) holds and can be seen as a feedback relevant identification of the plant P_o.

However, the model $\hat{P}$ and thus the controller $C_{\hat{P}}$ is not available (yet), which give rise to an iterative scheme wherein the controller C (from the previous iteration) is used to evaluate $\|J(P_o, C)\|_{\mathcal{X}}$. With the choice of the objective function given in (5), the minimization of the performance degradation $\|J(P_o, C) - J(\hat{P}, C)\|_{\mathcal{X}}$ then becomes

$$\min_{\theta} \|W_o[T(P_o, C) - T(P(\theta), C)]W_i\|_{\infty}. \quad (7)$$

By minimizing (7) such that (6) holds, the current controller C, applied to the plant P_o, is guaranteed to give a similar performance when applying it to the model $P(\hat{\theta})$ found by the minimization and the model $P(\hat{\theta})$ can be used for subsequent control design.

4 Closed loop identification

4.1 Identification of stable factorizations

Approximate identification on the basis of closed loop experiments could easily be defective due to the correlation between noise v and input u, (Ljung, 1987). Moreover, an explicit expression for the approximation of the plant P_o, independent of the noise contribution during the experiments, is needed to tune the bias of the model $\hat{P}$ in a feedback relevant way (7). Additionally, an unified approach to handle the identification of both stable and unstable plants P_o, that are stabilized during the closed loop experiments, is preferred. These demands can be handled by using the algebraic theory of fractional representations and to estimate stable (coprime) factorization of the plant P_o. Several authors have worked on this topic, see for example Hansen (1989), Van den Hof *et al.* (1993) or Lee *et al.* (1993).

To have access to a factorization of the plant P_o, the following approach can be followed. Consider the closed loop data generating system given in figure 1 and define $r := r_1 + Cr_2$. With (2) this yields

$$r = r_1 + Cr_2 = u + Cy \quad (8)$$

and (2) reduces to

$$\begin{bmatrix} y \\ u \end{bmatrix} = \begin{bmatrix} P_o S_i \\ S_i \end{bmatrix} r + \begin{bmatrix} S_o \\ -CS_o \end{bmatrix} He \quad (9)$$

where $S_i := [I + CP_o]^{-1}$ is the input sensitivity function and $S_o := [I + P_oC]^{-1}$ is the output sensitivity function. Since the controller C is used for the closed loop experiments, the closed loop system $\mathcal{T}(P_o, C)$ is assumed to be internally stable. With theorem 2.2 this yields $T(P_o, C) \in \mathbb{R}\mathcal{H}_{\infty}$ making both P_oS_i, $S_i \in \mathbb{R}\mathcal{H}_{\infty}$ in (9) but not necessarily coprime, which is summarized in the following corollary.

Corollary 4.1 *Let a plant P and a controller C create an internally stable feedback system $\mathcal{T}(P, C)$ then (PS_i, S_i) is a rcf of P if and only if $C \in \mathbb{R}\mathcal{H}_{\infty}$.*

Proof: See de Callafon (1994). □

Hence P_oS_i, S_i can be considered to be a stable right, but not necessarily coprime, factorization (N_o, D_o) of the plant P_o, with $N_o := P_oS_i$ and $D_o := S_i$.

4.2 Identification of coprime factorizations

To avoid the presence and estimation of unstable zeros in the factorization (PS_i, S_i), which gives rise to hidden unstable modes in the representation of the plant P_o, the factorization needs to be coprime. For an unstable controller C, the factorization (PS_i, S_i) is not coprime, as mentioned in corollary 4.1, while the operation given in (8) yields an unbounded signal. Furthermore, a rcf is not unique and access to factorizations different from (P_oS_i, S_i) would be preferable. In order to fulfil these requirements, an additional filtering of the signal r is introduced with $x := Fr$, similar as in Van den Hof *et al.* (1993) or

de Callafon *et al.* (1994). With (2) and (8) this yields

$$x = F \begin{bmatrix} C & I \end{bmatrix} \begin{bmatrix} r_2 \\ r_1 \end{bmatrix} = F \begin{bmatrix} C & I \end{bmatrix} \begin{bmatrix} y \\ u \end{bmatrix} \quad (10)$$

and (2) now reduces to

$$\begin{bmatrix} y \\ u \end{bmatrix} = \begin{bmatrix} P_o S_i F^{-1} \\ S_i F^{-1} \end{bmatrix} x + \begin{bmatrix} S_o \\ -C S_o \end{bmatrix} He \quad (11)$$

where (PS_iF^{-1}, S_iF^{-1}) again is a (right) factorization of the plant P_o.

In Van den Hof *et al.* (1993) the freedom in choosing the filter F is found by restricting both the factorization (PS_iF^{-1}, S_iF^{-1}) and the map $F[C\ I]$ in (10) to be stable. However, stability of the map $F[C\ I]$ is not necessary in general. In the case that $r_2(t) = 0\ \forall t$, $x = Fr_1$, hence stability of F is required only. By restricting (PS_iF^{-1}, S_iF^{-1}) to be a rcf, stability of $F[C\ I]$ is implied directly and is summarized in the following lemma.

Lemma 4.2 *Let a plant P and a controller $C := \tilde{D}_c^{-1}\tilde{N}_c$, where $(\tilde{D}_c, \tilde{N}_c)$ is a lcf of C, form an internally stable feedback system $\mathcal{T}(P, C)$ then the following conditions are equivalent*

(i) *(PS_iF^{-1}, S_iF^{-1}) is a rcf.*

(ii) *$F = W\tilde{D}_c$ with W, $W^{-1} \in \mathbb{RH}_\infty$*

and imply $F \begin{bmatrix} C & I \end{bmatrix} \in \mathbb{RH}_\infty$.

Proof: See Van den Hof *et al.* (1993) or de Callafon (1994). □

Lemma 4.2 is a generalisation of corollary 4.1 and characterizes the freedom in choosing the filter F by the choice of any stable and stably invertible filter W. The choice of W however can be related to the choice of an auxiliary model P_x and an auxiliary controller C_x with $T(P_x, C_x) \in \mathbb{RH}_\infty$ (de Callafon, 1994). Since C_x can be any controller, it can be chosen to be equal to the controller C that the controls the plant P_o under consideration. In this way the filter F in lemma 4.2 can be characterized as follows.

Corollary 4.3 *Let a plant P and a controller C create an internally stable feedback system $\mathcal{T}(P, C)$ and let (N_x, D_x) be any rcf of any auxiliary model P_x, then*

$$F = [D_x + CN_x]^{-1} \quad (12)$$

satisfies the conditions of lemma 4.2 if and only if $T(P_x, C) \in \mathbb{RH}_\infty$.

Proof: See Van den Hof *et al.* (1993). □

With the result of lemma 4.2 the following proposition for the open loop identification of a right coprime factor can be given.

Proposition 4.4 *Let the plant P_o and a controller C create a stable feedback system $\mathcal{T}(P_o, C)$, then the closed loop data $[y\ u]^T$ in (2) can be rewritten into*

$$\begin{bmatrix} y \\ u \end{bmatrix} = \begin{bmatrix} N_o \\ D_o \end{bmatrix} x + \begin{bmatrix} I \\ -C \end{bmatrix} [I + P_o C]^{-1} v$$

where x is given in (10), F is any filter satisfying lemma 4.2 and (N_o, D_o) is a rcf of the plant P_o given by

$$\begin{aligned} \begin{bmatrix} N_o \\ D_o \end{bmatrix} &= \begin{bmatrix} P_o \\ I \end{bmatrix} S_i F^{-1} = \\ &= \begin{bmatrix} P_o \\ I \end{bmatrix} [I + CP_o]^{-1} [I + CP_x] D_x \end{aligned} \quad (13)$$

Proof: By use of (11) with $N_o := P_o S_i F^{-1}$ and $D_o := S_i F^{-1}$ and direct application of corollary 4.3. Equation (13) is found by substituting (12). □

The specific rcf (N_o, D_o) in (13) of the plant P_o to be identified is related to the filter F since $N_o = P_o S_i F^{-1}$ and $D_o = S_i F^{-1}$. With F given by (12) in corollary 4.3, the rcf (N_o, D_o) is related to the rcf (N_x, D_x) of the auxiliary model P_x, used to create the filter F and is summarized in the following corollary.

Corollary 4.5 *The rcf (N_o, D_o) of the plant P_o given in proposition 4.4 and based on the realization of F given in corollary 4.3, satisfies*

$$[D_o + CN_o] = F^{-1} = [D_x + CN_x]. \quad (14)$$

Proof: With $N_o = P_o S_i F^{-1}$ and $D_o = S_i F^{-1}$, $[D_o + CN_o] = [I + CP_o] S_i F^{-1} = F^{-1}$ proving equation (14), where F is given in (12). □

The transfer function matrix $[D_o + CN_o]$ is unknown, since it contains the specific rcf (N_o, D_o) of the unknown plant P_o, but (14) indicates that this can be replaced by the filter operation F^{-1}, which is completely known. From corollary 4.5 it can also be seen that (N_o, D_o) can be of high order, containing redundant dynamics. A sensible choice of the model P_x may lead to cancelling of redundant dynamics, which is used in Van den Hof *et al.* (1993) to estimate possibly low order (normalized) factorizations of the plant P_o.

The same approach of filtering signals present during the closed loop experiments is also being used in the two stage method described in Van den Hof

and Schrama (1993). In this method the filter F is given by an accurate estimate of the input sensitivity function $S_i = [I + CP_o]^{-1}$. The specific factorization (N_o, D_o) to be identified becomes approximately (P_o, I) and an estimate of P_o is found by estimating N_o only. It should be noted that $F = [I + CP_o]^{-1}$ does not satisfy the conditions mentioned in lemma 4.2 and clearly, the factorization (P_o, I) is not coprime over $\mathbb{R}\mathcal{H}_\infty$ for an unstable plant P_o. Moreover, if the filter F is given by an *approximation* of the input sensitivity function $[I + CP_o]^{-1}$, the situation can become even worse since both $N_o := P_o S_i F^{-1}$ and $D_o = S_i F^{-1}$ can become unstable. This is due to the fact that F^{-1}, which is the inverse of the estimated input sensitivity function, can be unstable and the unstable modes will not be cancelled completely in the operation $P_o S_i F^{-1}$ or $S_i F^{-1}$.

The estimate of the right coprime factorization (N_o, D_o) in Van den Hof *et al.* (1993) and de Callafon *et al.* (1994) is found by a 2-norm minimization based on a prediction error method with an OE (output error) model structure (Ljung, 1987). However, for sake of analysis and to maintain generality, it is assumed here that an identification procedure based on the data given in proposition 4.4 is able to come up with an estimate $\hat{\theta}$ given by

$$\hat{\theta} = \arg\min_{\theta} \left\| W_1 \left(\begin{bmatrix} N_o \\ D_o \end{bmatrix} - \begin{bmatrix} N(\theta) \\ D(\theta) \end{bmatrix} \right) W_2 \right\|_{\mathcal{X}} \quad (15)$$

where W_1, W_2 are arbitrary weighting functions and $\|\cdot\|_{\mathcal{X}}$ is a norm function to be specified. The role of the weighting functions W_1, W_2, the norm function $\|\cdot\|_{\mathcal{X}}$ to be used and the parametrization of the factorization $(N(\theta), D(\theta))$ will be scrutinized in the following section.

5 Estimation of coprime factors

5.1 Feedback relevant identification

In order to perform a feedback relevant identification, the norm of the difference $\Delta T(P_o, \hat{P}, C) := W_o[T(P_o, C) - T(\hat{P}, C)]W_i$ introduced in section 3.2, needs to be minimized for a *fixed order* model $\hat{P}$. Using the filter F of corollary 4.3 the mismatch $\Delta T(P_o, \hat{P}, C)$ can be expressed in terms of the weighted difference between the rcf (N_o, D_o) and $(\hat{N}, \hat{D})$ respectively of the plant P_o and the model $\hat{P}$, along with an *additional* constraint, depending on the filter F being used. This is summarized in the following lemma.

Lemma 5.1 *Let the plant P_o with rcf (N_o, D_o) given in corollary 4.5 and a controller C create an internally stable feedback system $\mathcal{T}(P_o, C)$. Consider a model $\hat{P}$ with rcf $(\hat{N}, \hat{D})$ and any filter F satisfying lemma 4.2 then*

$$\Delta T(P_o, \hat{P}, C) = W_o[T(P_o, C) - T(\hat{P}, C)]W_i$$

equals

$$W_o \left(\begin{bmatrix} N_o \\ D_o \end{bmatrix} - \begin{bmatrix} \hat{N} \\ \hat{D} \end{bmatrix} \right) F \begin{bmatrix} C & I \end{bmatrix} W_i \Big|_{\hat{D}+C\hat{N}=F^{-1}}$$

Proof: With (N_o, D_o) as rcf of P_o the matrix $T(P_o, C)$ can be rewritten as

$$T(P_o, C) = \begin{bmatrix} N_o \\ D_o \end{bmatrix} [D_o + CN_o]^{-1} \begin{bmatrix} C & I \end{bmatrix}$$

and using the fact $[D_o + CN_o] = F^{-1}$ from (14) in corollary 4.5, this can be rewritten into

$$T(P_o, C) = \begin{bmatrix} N_o \\ D_o \end{bmatrix} F \begin{bmatrix} C & I \end{bmatrix}.$$

With $(\hat{N}, \hat{D})$ as rcf of $\hat{P}$, the matrix $T(\hat{P}, C)$ equals

$$\begin{bmatrix} \hat{N} \\ \hat{D} \end{bmatrix} [\hat{D} + C\hat{N}]^{-1} \begin{bmatrix} C & I \end{bmatrix}$$

and under the constraint $[\hat{D}+C\hat{N}] = F^{-1}$ this yields

$$T(\hat{P}, C) = \begin{bmatrix} \hat{N} \\ \hat{D} \end{bmatrix} F \begin{bmatrix} C & I \end{bmatrix}$$

making $T(P_o, C) - T(\hat{P}, C)$ equal to

$$\left(\begin{bmatrix} N_o \\ D_o \end{bmatrix} - \begin{bmatrix} \hat{N} \\ \hat{D} \end{bmatrix} \right) F \begin{bmatrix} C & I \end{bmatrix} \Big|_{\hat{D}+C\hat{N}=F^{-1}}$$

□

Clearly, lemma 5.1 reflects an additional constraint on the parametrized coprime factorization $(N(\theta), D(\theta))$ of the model $\hat{P}$ to be identified. In case the choice of the filter F is replaced by the choice of a rcf (N_x, D_x) of an auxiliary model P_x as in corollary 4.3, the constraint equals

$$[D(\theta) + CN(\theta)] = F^{-1} = [D_x + CN_x] \quad (16)$$

which has to be incorporated in the feedback relevant identification of a model $\hat{P}$.

With the result of lemma 5.1 the following observations can be made for the weightings W_1, W_2 and the norm function $\|\cdot\|_{\mathcal{X}}$ in (15), in order to minimize the feedback relevant criterion given in (7).

Proposition 5.2 *The feedback relevant criterion of* (7) *and the estimation problem of* (15) *can be made compatible by taking* $W_1 = W_o$, $W_2 = F[C\ I]W_i$, $\|\cdot\|_{\mathcal{X}} = \|\cdot\|_\infty$ *and satisfying the constraint given in* (16), *which yields*

$$\hat{\theta} = \arg\ \min_\theta \left\| W_o \left(\begin{bmatrix} N_o \\ D_o \end{bmatrix} - \begin{bmatrix} N(\theta) \\ D(\theta) \end{bmatrix} \right) \cdot F \begin{bmatrix} C & I \end{bmatrix} W_i \right\|_\infty \Big|_{\hat{D}+C\hat{N}=F^{-1}} \tag{17}$$

Proof: With $W_1 = W_o$, $W_2 = F[C\ I]W_i$ the argument of $\|\cdot\|_{\mathcal{X}}$ in (15) equals the argument of $\|\cdot\|_\infty$ in (7), by substituting the results of lemma 5.1. Since the argument $\Delta T(P_o, \hat{P}, C) \in \mathbb{RH}_\infty$, the norm function $\|\cdot\|_{\mathcal{X}}$ in (15) can be chosen to be $\|\cdot\|_\infty$ and both (7) and (15) are equal. □

5.2 Minimization with constraint

According to proposition 5.2, the minimization of

$$\min_\theta \|W_o[T(P_o, C) - T(P(\theta), C)]W_i\|_{\mathcal{X}}$$

for any norm function $\|\cdot\|_{\mathcal{X}}$ can be replaced by the minimization given in (17) and involves basically a non-linear minimization for a model $P(\theta)$ with a specified McMillan degree, even if the model is parametrized linearly.

To avoid the use of the constraint (16) in the minimization, an iterative scheme of minimization without the constraint in step $i-1$ and updating the constraint in step i was proposed in de Callafon *et al.* (1994) and was based on the estimation of normalized coprime factors. However, updating the constraint involves only the update of the filter F, used to create the signal x in (10). In case the filter F is defined via a rcf (N_x, D_x) of any auxiliary model P_x as in corollary 4.3, (N_x, D_x) can be computed directly and is given in the following proposition.

Proposition 5.3 *Let the filter* F *in* (10) *be given by corollary 4.3 then the rcf* (N_x, D_x) *given by*

$$\begin{bmatrix} N_x \\ D_x \end{bmatrix} = T(P_x, C) \begin{bmatrix} N(\theta) \\ D(\theta) \end{bmatrix}$$

satisfies the constraint given in (16).

Proof: Similar as in corollary 4.5. □

Clearly, the estimate of the rcf $(N(\theta), D(\theta))$ in proposition 5.3 is not available (yet). Taking any rcf (N_x, D_x) such that $P_x := N_x {D_x}^{-1}$ satisfies $T(P_x, C) \in \mathbb{RH}_\infty$, this gives rise to an update algorithm to handle the minimization given in (17) for performing a feedback relevant identification of the plant P_o as indicated in proposition 5.2 and can be summarized as follows.

1. In step i, create F_i from corollary 4.3.
2. Estimate a rcf $(N(\hat{\theta}_i), D(\hat{\theta}_i))$ based on a parametrization given in theorem 5.4 and the minimization given in proposition 5.2 *without* the constraint (16).
3. Update the rcf (N_x, D_x) with proposition 5.3 according to

$$\begin{bmatrix} N_{xi+1} \\ D_{xi+1} \end{bmatrix} = T(P_x, C) \begin{bmatrix} N(\hat{\theta}_i) \\ D(\hat{\theta}_i) \end{bmatrix}$$

   making $D(\hat{\theta}_i) + CN(\hat{\theta}_i) = D_{xi+1} + CN_{xi+1}$ and $P_x = N_{xi+1} D_{xi+1}^{-1}$ with $T(P_x, C) \in \mathbb{RH}_\infty$ remains fixed for all i.
4. $i := i + 1$ and go to 1.

If the iteration converges then $D(\hat{\theta}_i) + CN(\hat{\theta}_i) = D_{xi} + CN_{xi}$ is independent of i and the constraint (16) has been satisfied, thus a feedback relevant estimate $\hat{P}$ of the plant P_o has been obtained according to proposition 5.2. A rigorous proof of the convergence of the iteration is not available (yet) but extensive simulations reveal promising results.

5.3 Parametrization

To control the McMillan degree of the model $\hat{P} = P(\theta) = N(\theta)D(\theta)^{-1}$ being estimated, the factorization $(N(\theta), D(\theta))$ has to be parametrized in a special way and boils down to the fact that both $N(\theta)$ and $D(\theta)$ should have *common* stable modes. Furthermore, any common unstable zeros should be avoided to ensure coprimeness of the factorization $(N(\theta), D(\theta))$. The result has been stated in the following theorem.

Theorem 5.4 *Let* $(\hat{N}, \hat{D}) \in \mathbb{RH}_\infty$ *be given by a minimal and stable state space representation*

$$\left(\bar{A}, \bar{B}, \begin{bmatrix} \bar{C}_N \\ \bar{C}_D \end{bmatrix}, \begin{bmatrix} \bar{E}_N \\ \bar{E}_D \end{bmatrix} \right)$$

such that $\det\{\bar{E}_D\} \neq 0$ *and*

$$\begin{bmatrix} \hat{N}(z) \\ \hat{D}(z) \end{bmatrix} = \begin{bmatrix} \bar{C}_N \\ \bar{C}_D \end{bmatrix} [zI - \bar{A}]^{-1} \bar{B} + \begin{bmatrix} \bar{E}_N \\ \bar{E}_D \end{bmatrix}$$

then

(i) $\det\{\hat{D}\} \not\equiv 0$

(ii) $\hat{P} := \hat{N}\hat{D}^{-1}$ *is given by the state space representation* $[A, B, C, E]$ *with*

$$\begin{cases} A = \bar{A} - \bar{B}\bar{E}_D^{-1}\bar{C}_D \\ B = \bar{B}\bar{E}_D^{-1} \\ C = \bar{C}_N - \bar{E}_N\bar{E}_D^{-1}\bar{C}_D \\ E = \bar{E}_N\bar{E}_D^{-1} \end{cases} \tag{18}$$

(iii) $(\hat{N}, \hat{D})$ *is a rcf of* $\hat{P}$.

Proof: The factor $\hat{D}$ has a state space representation $(\bar{A}, \bar{B}, \bar{C}_D, \bar{E}_D)$ and due to the non-singular feedthrough matrix $\bar{E}_D$, $\hat{D}$ is always invertible having a state space representation given by $(\bar{A} - \bar{B}\bar{E}_D^{-1}\bar{C}_D, \bar{B}\bar{E}_D^{-1}, -\bar{E}_D^{-1}\bar{C}_D, \bar{E}_D^{-1})$ which proves (i). $\hat{N}$ has a state space representation $(\bar{A}, \bar{B}, \bar{C}_N, \bar{E}_N)$. Performing the series connection of $\hat{D}^{-1}$ and $\hat{N}$ in $\hat{P} = \hat{N}\hat{D}^{-1}$, basic matrix manipulation yields an extended state space representation, wherein n uncontrollable states can be omitted, where n is the dimension of $\bar{A}$. This leads to the state space representation given in (18), which proves (ii). From this, the matrices $\bar{A}$, $\bar{B}$, $\bar{C}_N$, $\bar{C}_D$ and $\bar{E}_N$ can be found from (18) leading to

$$\begin{cases} \bar{A} &= A - BK \\ \bar{B} &= B\bar{E}_D \\ \bar{C}_N &= C - EK \\ \bar{C}_D &= -K \\ \bar{E}_N &= E\bar{E}_D \end{cases}$$

making

$$\begin{aligned} \hat{N}(z) &= ([C - EK][zI - A + BK]^{-1}B + E)\bar{E}_D \\ &= \bar{N}(z)\bar{E}_D \in \mathbb{R}\mathcal{H}_\infty \\ \hat{D}(z) &= (-K[zI - A + BK]^{-1}B + I)\bar{E}_D \\ &= \bar{D}(z)\bar{E}_D \in \mathbb{R}\mathcal{H}_\infty. \end{aligned} \tag{19}$$

The factorization $(\bar{N}(z), \bar{D}(z))$ is proven to be a right coprime factorization in Nett *et al.* (1984). Since the factorization $(\bar{N}(z), \bar{D}(z))$ is post multiplied by a constant non-singular matrix $\bar{E}_D$ only, the factorization $(\hat{N}(z), \hat{D}(z))$ is a also a rcf, which proves (iii). □

The result of theorem 5.4 gives rise to a wide class of parametrizations needed to estimate a rcf $(N(\hat{\theta}), \hat{D}(\hat{\theta}))$, since it involves the parametrization of a stable, minimal state space representation $[\bar{A}, \bar{B}, \bar{C}]$ with $\bar{C}^T = [\bar{C}_N^T \ \bar{C}_D^T]$, wherein the direct feedthrough matrix of the factor $\hat{D}$ is restricted to be non-singular. Restricting the estimate to be stable and minimal can be enforced by using the specific parametrization of asymptotically stable systems as given in Ober (1991) and further elaborated in Chou (1994). This gives rise to an estimate of the factorization $(N(\hat{\theta}), \hat{D}(\hat{\theta}))$ which is guaranteed to be stable, minimal and balanced.

Using prediction error methods (Ljung, 1987) to estimate the state space matrices in theorem 5.4, a stable and minimal state space estimate with non-singular feedthrough matrix $\bar{E}_D$ is found in the generic case, which is due to the following facts. Firstly, the map from x onto $[y \ u]^T$ is defined to be stable, according to proposition 4.4. Secondly, the map from x onto u is given by $[I + CP_0]^{-1}[I + CP_x]D_x$ according to (13), which is non-singular by definition. In this way the matrices are parametrized by standard pseudo canonical (overlapping) forms (Gevers and Wertz, 1984) without stability or non-singularity condition. Finally it should be noted that the matrix operations given in (18) leads to model $\hat{P}$ with McMillan degree less than or equal to n, where n is simply the McMillan degree of the factorization $(\hat{N}, \hat{D})$ being estimated.

Conclusions

In this paper the filtering and parametrization issues involved in the usage of fractional representations in multivariable, approximate and feedback relevant identification of a possibly unstable plant operating under closed loop conditions have been discussed. It has been shown that any stable right coprime factorization of the plant can be accessed by the filtering of signals present in the closed loop system. The freedom in choosing the filter has been characterized by employing the knowledge of the controller present during the closed loop experiments.

Consequently, a stable right coprime fractional representation generated by the closed loop system and the filtering being used, can be estimated. In order to have a model with a prefixed McMillan degree, a specific class of parametrizations with the same McMillan degree can be used to estimate a stable right coprime factorization of the model.

Finally, the approximate and feedback relevant estimation of a fixed order linear time invariant model based on coprime factor identification leads to an additional constraint. This constraint is intrinsic in many schemes on feedback relevant identification but can be written down explicitly in case of the coprime factor identification. The constraint boils down to a relation between the filter used to gain access to the coprime factors of the plant and model being estimated. A possible solution to deal with the constraint by updating the filtering is presented here.

References

Bayard, D.S., Y. Yam and E. Mettler (1992). A criterion for joint optimization of identification and robust control. *IEEE Trans. Autom. Control, AC-37*, 986–991.

Bitmead, R.R. (1993). Iterative control design approaches. *Proc. 12th IFAC World Congress*, Vol. *9*, pp. 381–384.

Bongers, P.M.M. (1994). *Modeling and Identification of Flexible Wind Turbines and a Factoriza-*

tional Approach to Robust Control. Dr. Dissertation, Delft Univ. Technology, The Netherlands.

Boyd, S.P. and C.H. Barrat (1991). *Linear Controller Design – Limits of Performance.* Prentice Hall, Englewood Cliffs.

Chou, C.T. (1994). *Geometry of Linear Systems and Identification.* PhD Thesis, University of Cambridge, UK.

De Callafon, R.A. (1994). *Filtering and Parametrizations Issues in Feedback Relevant Identification based on Fractional Model Representations.* Report N–478, Mech. Engin. Systems and Control Group, Delft Univ. Technology.

De Callafon, R.A., P.M.J. Van den Hof and D.K. de Vries (1994). Identification and control of a compact disc mechanism using fractional representations. *Prepr. 10th IFAC Symp. System Identification*, Vol. 2, pp. 121–126.

Desoer, C.A. and W.S. Chan (1975). The feedback interconnection of linear time invariant systems. *J. Franklin Institute*, pp. 335–351.

Farison, J.B., R.E. Graham and R.C. Shelton (1967). Identification and control of linear discrete systems. *IEEE Trans. Autom. Control, AC-12*, 438–442.

Gevers, M. (1993). Towards a joint design of identification and control? In: H.L. Trentelman and J.C. Willems (Eds.), *Essays on Control: Perspectives in the Theory and its Applications*, pp. 111–151.

Gevers, M.R. and V. Wertz (1984). Uniquely identifiable state–space and ARMA parametrizations for multivariable systems. *Automatica, 20*, 333–347.

Hakvoort, R.G., R.J.P. Schrama and P.M.J. Van den Hof (1994). Approximate identification with closed–loop performance criterion and application to LQG feedback design. *Automatica, 30*, 679–690.

Hansen, F.R. (1989). *A Fractional Representation Approach to Closed Loop System Identification and Experiment Design.* PhD Thesis, Stanford University, Stanford, CA, USA.

Hjalmarsson, H., M. Gevers, F. de Bruyne and J. Leblond (1994*a*). Identification for control: closing the loop gives more accurate controllers. *Proc. 33rd IEEE Conf. Decision and Control*, Lake Buena Vista, FL.

Hjalmarsson, H., S. Gunnarsson and M. Gevers (1994*b*). A convergent iterative restricted complexity control design scheme. *Proc. 33rd IEEE Conf. Decision and Control*, Lake Buena Vista, FL.

Horowitz, I.M. (1963). *Synthesis of Feedback Systems.* Academic Press, New York.

Lee, W.S., B.D.O. Anderson, R.L. Kosut and I.M.Y. Mareels (1992). On adaptive robust control and control–relevant system identification. *Proc. Amer. Control Conf.*, Chicago, IL, pp. 2834–2841.

Lee, W.S., B.D.O. Anderson, R.L. Kosut and I.M.Y. Mareels (1993). On robust performance improvement through the windsurfer aproach to adaptive robust control. *Proc. 32nd IEEE Conf. Decision and Control*, San Antonio, TX, pp. 2821–2826.

Ljung, L. (1987). *System Identification: Theory for the User.* Prentice Hall Inc., Englewood Cliffs.

Nett, C.N., C.A. Jacobson and M.J. Balas (1984). A connection between state–space and doubly coprime fractional representations. *IEEE Trans. Autom. Control, AC-29*, 831–832.

Ober, R. (1991). Balanced parametrizations of classes of linear systems. *SIAM J. Control Optimiz., 29*, 1251–1287.

Rivera, D.E. and S. Bhatnagar (1993). Closed–loop system identification of restricted complexity models using iterative refinement. *Proc. Amer. Control Conf.*, pp. 1993–1994.

Schrama, R.J.P. (1992*a*). Accurate identification for control design: the necessity of an iterative scheme. *IEEE Trans. Autom. Control, AC-37*, 991–994.

Schrama, R.J.P. (1992*b*). *Approximate Identification and Control Design with Application to a Mechanical System.* Dr.Dissertation, Delft University of Technology, Mech. Eng. Systems and Control Group.

Schwartz, S.C. and K. Steiglitz (1971). The identification and control of unknown linear discrete systems. *Int. J. Control, 14*, 43–50.

Van den Hof, P.M.J. and R.J.P. Schrama (1993). An indirect method for transfer function estimation from closed loop data. *Automatica, 29*, 1523–1527.

Van den Hof, P.M.J. and R.J.P. Schrama (1994). Identification and control – closed loop issues. *Prepr. 10th IFAC Symp. System Identification*, pp. 1–13.

Van den Hof, P.M.J., R.J.P. Schrama, O.H. Bosgra and R.A. de Callafon (1993). Identification of normalized coprime plant factors for iterative model and controller enhancement. *Proc. 32nd IEEE Conf. Decision and Control*, San Antonio, TX, pp. 2839–2844.

Vidyasagar, M. (1985). *Control System Synthesis: A Factorization Approach.* Cambridge, MIT Press.

Zang, Z., R.R. Bitmead and M. Gevers (1992). Disturbance rejection: on–line refinement of controllers by closed loop modelling. *Proc. Amer. Control Conf.*, pp. 2829–2833.

Selected Topics in Identification, Modelling and Control
Vol. 7, December 1994

An instrumental variable procedure for the identification of probabilistic frequency response uncertainty regions[‡]

Richard G. Hakvoort and Paul M.J. Van den Hof

Mechanical Engineering Systems and Control Group
Delft University of Technology, Mekelweg 2, 2628 CD Delft, The Netherlands.

Abstract. A procedure is developed to identify probabilistic frequency response system uncertainty regions. The procedure utilizes time-domain measurement data and prior information about the system and the noise. There are no restrictions on the input signal, it may even be generated in closed loop. The system is assumed to be linear, time invariant, and a bound is assumed on the system's (generalized) pulse response parameters. The noise is assumed to be a realization of a stationary stochastic process, and independent of the input signal (in open loop operation) or an external reference signal (in closed loop operation). Frequency response confidence regions are constructed by explicitly evaluating the bias and variance errors of an instrumental variable estimate.

Keywords. uncertainty bounding identification, probabilistic uncertainty regions, instrumental variable model, bias and variance expressions

1 Introduction

For robust controller analysis and synthesis it is necessary to have available a bound on the model error, the difference between plant and nominal model. For example robust stability can be established if frequency response uncertainty regions are available. Many authors have considered the problem of deriving frequency response system uncertainty regions on the basis of measurement data and prior assumptions about system and noise. The two main different uncertainty bounding approaches are the deterministic and the stochastic approach.

Procedures to derive frequency response uncertainty regions based on deterministic prior assumptions are presented in, for example, De Vries and Van den Hof (1992), Hakvoort (1993, 1994a), Hakvoort and Van den Hof (1993), Lamaire *et al.* (1991) and Wahlberg and Ljung (1992). In particular the noise is assumed to behave worst-case deterministic. The resulting uncertainty regions are correct provided the prior information that is used is correct. Unfortunately in practice it is often rather difficult, if not impossible, to guarantee that the priors, such as assumed noise bounds, are correct.

The stochastic approach is represented by e.g. Bayard (1992), De Vries and Van den Hof (1993) and Ninness and Goodwin (1992). In this approach the noise is assumed to behave noisy, i.e. random and uncorrelated to the input signal. Besides that also prior assumptions about the system are made, which vary from deterministic, De Vries and Van den Hof (1993), to stochastic, Ninness and Goodwin (1992). Typically these procedures yield uncertainty regions which are correct with a certain specified probability, provided the prior assumptions that are made are correct.

In this paper a new procedure is presented to identify probabilistic frequency response uncertainty regions. The procedure involves the explicit calculation of the bias and variance errors of an IV (Instrumental Variable) estimate. A linear model parametrization in terms of general basis functions is used, see Heuberger *et al.* (1993) and Ninness

[‡]This paper is presented at the 33rd IEEE Conf. Decision and Control, Lake Buena Vista, FL, December 14-16, 1994.

(1993, Ch. 2). In this way approximate knowledge about pole locations of the unknown system can be incorporated by the choice of proper basis functions. In fact the present procedure is the statistical counterpart of the deterministic uncertainty bounding procedure described in Hakvoort (1994a). There are no restrictions on the input signal, it need for example not be sinusoidal. The basic assumption about the noise process is that it is stationary and independent of the input signal in open loop, or an external reference signal in closed loop. The probability density function of the noise process is arbitrary and not assumed to be known. Instead asymptotic results are derived with a central limit theorem.

The present approach is different from the one in Bayard (1992), where a multisinusoidal input signal is needed, and the noise is assumed gaussian with known noise generating filter. Unlike in Ninness and Goodwin (1992) no stochastic assumptions are made about the undermodelling part. In the approach of De Vries and Van den Hof (1993) a frequency domain approach is taken, and also a periodic input signal is needed.

The outline of the paper is as follows. In the next section the identification setting is described. Section 3 presents the instrumental variable estimate. In Section 4 the frequency response error of the IV model is evaluated, which leads to probabilistic frequency response system uncertainty regions. In Section 5 the results are discussed.

Because of space limitations all proofs have been omitted. These can be found in Hakvoort (1994b). In this reference also simulations and an application of the identification procedure to a multivariable industrial process can be found.

2 Identification Setting

Consider the linear, time-invariant, discrete time, causal and ℓ_∞-stable SISO system $G_0(z)$ represented by

$$G_0(z) = \sum_{k=0}^{\infty} g_0(k) P_k(z),$$

where $\{P_k(z)\}_{k=0,\ldots,\infty}$, is some specified set of basis functions given by

$$P_k(z) = \sum_{k'=0}^{\infty} p_k(k') z^{-k'}, \ k = 0, \ldots, \infty,$$

for given and known scalar pulse response parameters $p_k(k')$. These basis functions can for example chosen to be the pulse functions, or the Laguerre functions, or general orthonormal basis functions, see Heuberger *et al.* (1993) and Ninness (1993, Ch. 2). The (unknown) coefficients $g_0(k)$ can be considered as generalized pulse response parameters of the system $G_0(z)$.

Consider given input data $\{u(t)\}_{t=1,\ldots,N}$ and measured output data $\{y(t)\}_{t=1,\ldots,N}$ and the following input-output relation of the data generating system,

$$y(t) = G_0(q)u(t) + e_0(t), \ t = 1, \ldots, N, \quad (1)$$

where N denotes the measurement time and $\{e_0(t)\}$ is an unknown additive output noise. There are no restrictions on the input signal, basically it may be determined in open loop as well as in closed loop.

It is assumed that a signal $\{r(t)\}_{t=1,\ldots,N}$ is available, which is highly correlated with the input signal $\{u(t)\}$, but independent of the noise process $\{e_0(t)\}$. Let by definition $r(t) = 0$ for $t \leq 0$. Typically in open loop operation the signal $\{r(t)\}$ is equal to the input $\{u(t)\}$. In a closed loop environment an external reference signal $\{\bar{r}(t)\}$ can be used, or a filtered version of this signal, $r(t) = F(q)\bar{r}(t)$.

The following assumptions are made about the noise process $\{e_0(t)\}$.

Assumption 2.1 *The noise process $\{e_0(t)\}$ is stationary with auto-covariance function $R_{e_0}(\tau) = Ee_0(t+\tau)e_0(t)$, and it satisfies $e_0(t) = H_0(q)w_0(t)$ for some ℓ_2-stable $H_0(q)$, and where $\{w_0(t)\}$ is a sequence of independent random variables with zero mean values, variances λ_0, and bounded fourth moments.*

Note that the distribution of the noise process is arbitrary, and not assumed to be known. The following assumptions about $\{r(t)\}$ are made.

Assumption 2.2 *The signal $\{r(t)\}$ is a bounded deterministic quasi-stationary signal, hence its auto-covariance function*

$$R_r(\tau) = \lim_{N\to\infty} \frac{1}{N} \sum_{t=1}^{N} r(t+\tau)r(t)$$

exists $\forall\, \tau$.

In order to cope with unknown initial conditions the input signal in the past is assumed to be bounded by

$$|u(t)| \leq \bar{u}, \ \forall\, t \leq 0, \quad (2)$$

for some given $\bar{u}$. This bound may result from actuator constraints and need not be very tight as its influence on the identification result is restricted.

The coefficients $g_0(k)$ are assumed to be bounded by

$$|g_0(k)| \leq \bar{g}(k), \ k = 0, \ldots, \infty, \quad (3)$$

for given $\bar{g}(k)$. Moreover it is assumed that the bound $\bar{g}(k)$ shows exponential decay rate for k larger than some k^*, i.e.

$$\bar{g}(k) \leq M\rho^k, \ \forall\, k > k^*,$$

for some given $M \geq 0$ and $\rho < 1$. In Heuberger *et al.* (1993) it is discussed that such a bound exists when an arbitrary ℓ_∞-stable system is expanded in a general orthonormal basis.

The identification objective is to derive probabilistic uncertainty regions for the system's frequency response,

$$G_0(e^{i\omega}) = \sum_{k=0}^{\infty} g_0(k) P_k(e^{i\omega}).$$

The identification problem is tackled by splitting the transfer function $G_0(z)$ into two parts,

$$G_0(z) = \widetilde{G}_0(z) + \bar{G}_0(z), \tag{4}$$

$$\widetilde{G}_0(z) = \sum_{k=0}^{n} g_0(k) P_k(z), \; \bar{G}_0(z) = \sum_{k=n+1}^{\infty} g_0(k) P_k(z),$$

for some user-defined truncation value n.

Next deterministic uncertainty bounds will be determined for the tail $\bar{G}_0(e^{i\omega})$, using the deterministic prior bounds $\bar{g}(k)$ given in (3). And probabilistic uncertainty bounds will be derived for $\widetilde{G}_0(e^{i\omega})$, using variance expressions of an instrumental variable estimate. These variance expressions are based on the stochastic noise assumption 2.1. In the variance expressions the influence of the undermodelling part $\bar{G}_0(z)$ is properly taken into account. The sum of the deterministic uncertainty bounds for $\bar{G}_0(e^{i\omega})$ and the probabilistic uncertainty bounds for $\widetilde{G}_0(e^{i\omega})$ provides probabilistic uncertainty regions for the system $G_0(e^{i\omega})$.

Note that there generally is an optimal value for n. If it is chosen too small, the resulting bounds will be completely determined by the prior information (3), which is generally conservative. If it is chosen too large, the confidence regions for $\widetilde{G}_0(z)$ will be large as the variance increases with the number of parameters to be estimated. More will be said about this later.

3 The Instrumental Variable Estimate

Consider the parametrized model

$$G(z) = \sum_{k=0}^{n} g(k) P_k(z),$$

where $\{g(k)\}_{k=0,\ldots,n}$ are the model parameters. Define the model input signal $\widetilde{u}(t)$ as

$$\widetilde{u}(t) := \begin{cases} 0, & t \leq 0, \\ u(t), & t = 1, \ldots, N. \end{cases}$$

The model input-output relation is given by

$$\begin{aligned} y(t) &= G(q)\widetilde{u}(t) + e(t) = \\ &= \sum_{k=0}^{n} g(k) P_k(q) \widetilde{u}(t) + e(t) = \\ &= \sum_{k=0}^{n} g(k) w_k(t) + e(t), \end{aligned}$$

where $e(t)$ is the output error, and

$$w_k(t) := \sum_{k'=0}^{t-1} p_k(k') u(t-k'), \; k = 0, \ldots, n. \tag{5}$$

Next define the instrumental signals

$$v_k(t) := P_k(q) r(t) = \sum_{k'=0}^{t-1} p_k(k') r(t-k'),$$
$$k = 0, \ldots, n,$$

and the matrices

$$W(t) := \begin{bmatrix} w_0(t) \\ \vdots \\ w_n(t) \end{bmatrix}, \; V(t) := \begin{bmatrix} v_0(t) \\ \vdots \\ v_n(t) \end{bmatrix}.$$

Also denote

$$\widetilde{N} = N - t_s + 1,$$

for some integer $t_s \in [1, N)$, which is user-defined. The integer t_s represents the starting sample used in the IV estimate, and can be used to reduce the influence of the unknown initial conditions, as will become clear later.

Consider the basic IV estimate (Söderström and Stoica, 1989, p. 262; Ljung, 1987, p. 192/193),

$$\begin{bmatrix} \widehat{g}(0) \\ \vdots \\ \widehat{g}(n) \end{bmatrix} = \text{sol} \left\{ \frac{1}{\widetilde{N}} \sum_{t=t_s}^{N} V(t) e(t) = 0 \right\},$$

which is given by

$$\begin{bmatrix} \widehat{g}(0) \\ \vdots \\ \widehat{g}(n) \end{bmatrix} = \left[\frac{1}{\widetilde{N}} \sum_{t=t_s}^{N} V(t) W^T(t) \right]^{-1} \frac{1}{\widetilde{N}} \sum_{t=t_s}^{N} V(t) y(t). \tag{6}$$

Notice that in case of open loop operation, $r(t) = u(t)$, this is just a FIR least squares estimate for general basis functions. The estimated IV model is given by

$$\widehat{G}(z) = \sum_{k=0}^{n} \widehat{g}(k) P_k(z).$$

This identified model is used to construct frequency response uncertainty regions. This is done by explicitly calculating the bias and variance errors of the IV estimate.

4 Frequency Response Uncertainty Regions

An analysis is made of the frequency response identification error of the instrumental variable estimate. This then leads to frequency response confidence regions for the system $G_0(z)$.

4.1 The Frequency Response Error of the IV Model

Consider some frequency ω_j chosen arbitrarily in the interval $[0, \pi]$. Substitution of the parameter estimate (6) yields the frequency response of the IV estimate,

$$\begin{aligned}\widehat{G}(e^{i\omega_j}) &= \sum_{k=0}^{n} \widehat{g}(k) P_k(e^{i\omega_j}) = \\ &= \left[P_0(e^{i\omega_j}) \cdots P_n(e^{i\omega_j})\right] \cdot \\ &\quad \cdot \left[\frac{1}{\widetilde{N}} \sum_{t=t_s}^{N} V(t) W^T(t)\right]^{-1} \frac{1}{\widetilde{N}} \sum_{t=t_s}^{N} V(t) y(t). \quad (7)\end{aligned}$$

Define for $t = t_s, \ldots, N$ the signals $r_1(t)$ and $r_2(t)$ as

$$\begin{aligned}r_1(t) &:= \left[\mathrm{Re}\left(P_0(e^{i\omega_j})\right) \cdots \mathrm{Re}\left(P_n(e^{i\omega_j})\right)\right] \cdot \\ &\quad \cdot \left[\frac{1}{\widetilde{N}} \sum_{t=t_s}^{N} V(t) W^T(t)\right]^{-1} V(t), \quad (8) \\ r_2(t) &:= \left[\mathrm{Im}\left(P_0(e^{i\omega_j})\right) \cdots \mathrm{Im}\left(P_n(e^{i\omega_j})\right)\right] \cdot \\ &\quad \cdot \left[\frac{1}{\widetilde{N}} \sum_{t=t_s}^{N} V(t) W^T(t)\right]^{-1} V(t). \quad (9)\end{aligned}$$

These signals $r_p(t)$, $p = 1, 2$, are filtered versions of the signal $r(t)$, and they can be computed, as they only depend on known quantities. They play an essential role throughout the following derivation of IV model error bounds. Note that they depend on the frequency ω_j that has been chosen, but for notational convenience this dependency is not explicitly mentioned all the time.

Using (1) and (4) the output $y(t)$ can be written as

$$\begin{aligned}y(t) &= G_0(q)u(t) + e_0(t) = \\ &= \widetilde{G}_0(q)u(t) + \bar{G}_0(q)u(t) + e_0(t) = \\ &= \sum_{k=0}^{n} g_0(k) P_k(q) u(t) + \\ &\quad + \sum_{k=n+1}^{\infty} g_0(k) P_k(q) u(t) + e_0(t) = \\ &= \sum_{k=0}^{n} g_0(k) w_k(t) + a(t) + b(t) + e_0(t),\end{aligned}$$

where $w_k(t)$ is defined in (5) and

$$a(t) := \sum_{k=n+1}^{\infty} g_0(k) \sum_{k'=0}^{t-1} p_k(k') u(t-k'), \quad (10)$$

$$b(t) := \sum_{k=0}^{\infty} g_0(k) \sum_{k'=t}^{\infty} p_k(k') u(t-k'). \quad (11)$$

The signal $a(t)$ represents the response of the tail $\bar{G}_0(q)$. The signal $b(t)$ represents the response due to past input signals, the initial conditions. Using this the following alternative expression can be given for $\widehat{G}(e^{i\omega_j})$ given by (7),

$$\begin{aligned}\widehat{G}(e^{i\omega_j}) &= \frac{1}{\widetilde{N}} \sum_{t=t_s}^{N} (r_1(t) + i r_2(t)) y(t) = \\ &= \frac{1}{\widetilde{N}} \sum_{t=t_s}^{N} (r_1(t) + i r_2(t)) \cdot \\ &\quad \cdot \left(\sum_{k=0}^{n} g_0(k) w_k(t) + a(t) + b(t) + e_0(t)\right).\end{aligned}$$

The first term of this expression can be worked out as follows,

$$\begin{aligned}&\frac{1}{\widetilde{N}} \sum_{t=t_s}^{N} (r_1(t) + i r_2(t)) \sum_{k=0}^{n} g_0(k) w_k(t) = \\ &= \left[P_0(e^{i\omega_j}) \cdots P_n(e^{i\omega_j})\right] \cdot \left[\frac{1}{\widetilde{N}} \sum_{t=t_s}^{N} V(t) W^T(t)\right]^{-1} \\ &\quad \cdot \frac{1}{\widetilde{N}} \sum_{t=t_s}^{N} V(t) W^T(t) \begin{bmatrix} g_0(0) \\ \vdots \\ g_0(n) \end{bmatrix} = \\ &= \left[P_0(e^{i\omega_j}) \cdots P_n(e^{i\omega_j})\right] \begin{bmatrix} g_0(0) \\ \vdots \\ g_0(n) \end{bmatrix} = \widetilde{G}_0(e^{i\omega_j}).\end{aligned}$$

Next define for $p = 1, 2$,

$$d(p) := \sum_{t=t_s}^{N} r_p(t) a(t), \quad (12)$$

$$f(p) := \sum_{t=t_s}^{N} r_p(t) b(t), \quad (13)$$

which depend on the frequency ω_j as $r_p(t)$, $p = 1, 2$, depends on the frequency ω_j. Again using (4) this finally gives the following expression for the identification error,

$$\begin{aligned}&\widehat{G}(e^{i\omega_j}) - G_0(e^{i\omega_j}) = \\ &= \widehat{G}(e^{i\omega_j}) - \widetilde{G}_0(e^{i\omega_j}) - \bar{G}_0(e^{i\omega_j}) =\end{aligned}$$

$$= \frac{1}{\widetilde{N}}(d(1)+id(2)+f(1)+if(2)+$$
$$+\sum_{t=t_s}^{N}(r_1(t)+ir_2(t))e_0(t)) - \bar{G}_0(e^{i\omega_j}). \quad (14)$$

Basically all terms at the right-hand side of this expression are unknown. However, it appears possible to derive a probabilistic distribution for the term containing $e_0(t)$, using assumption 2.1. And the terms with $d(p)$, $f(p)$ and $\bar{G}_0(e^{i\omega_j})$ can be bounded using the prior information (2) and (3).

4.2 Auxiliary Results

In this subsection the various terms appearing in (14) are evaluated. Consider any bounded signal $\{r_p(t)\}$ and consider $\bar{d}(p)$, $\bar{f}(p)$ defined by (12), (13) respectively, with $a(t)$, $b(t)$ defined by (10), (11) respectively. Making use of (2) and (3), the following bounds can be derived,

$$|d(p)| \leq \bar{d}(p) :=$$
$$\sum_{k=n+1}^{\infty} \bar{g}(k) \left| \sum_{t=t_s}^{N} r_p(t) \sum_{k'=0}^{t-1} p_k(k')u(t-k') \right|, \quad (15)$$

which represents a computable bound for the tail contribution. And,

$$|f(p)| \leq \bar{f}(p) := \sum_{k=0}^{\infty} \bar{g}(k) \sum_{t'=0}^{\infty} \left| \sum_{t=t_s}^{N} r_p(t)p_k(t+t') \right| \bar{u}, \quad (16)$$

which represents a computable bound for the contribution of the unknown initial conditions. The actual computation of the expressions involve the evaluation of infinite sums. Due to the fact that $\bar{g}(k)$ shows exponential decay rate in k, and $p_k(k')$ shows exponential decay rate in k' the outcomes are finite. Computational aspects are considered in Hakvoort (1994b). Clearly $\bar{d}(p)$ will be small if n is chosen large, and $\bar{f}(p)$ will be small if t_s is chosen large.

The real and imaginary part of the frequency response of the tail, $\bar{G}_0(e^{i\omega_j})$, can be bounded as follows,

$$\left|\mathrm{Re}\left(\bar{G}_0(e^{i\omega_j})\right)\right| = \left|\mathrm{Re}\left(\sum_{k=n+1}^{\infty} g_0(k)P_k(e^{i\omega_j})\right)\right| \leq$$
$$\leq \sum_{k=n+1}^{\infty} \bar{g}(k)\left|\mathrm{Re}\left(P_k(e^{i\omega_j})\right)\right| := \delta(1), \quad (17)$$
$$\left|\mathrm{Im}\left(\bar{G}_0(e^{i\omega_j})\right)\right| \leq$$
$$\leq \sum_{k=n+1}^{\infty} \bar{g}(k)\left|\mathrm{Im}\left(P_k(e^{i\omega_j})\right)\right| := \delta(2). \quad (18)$$

Note that $\delta(1)$ and $\delta(2)$ are finite due to the exponential decay rate of $\bar{g}(k)$. Computational aspects of the evaluation of these infinite sums are considered in Hakvoort (1994b).

Next a key lemma is established with respect to the asymptotic distribution of $\sum_{t=t_s}^{N} r_p(t)e_0(t)$.

Lemma 4.1 *Suppose that $\{e_0(t)\}$ and $\{r(t)\}$ are independent and that they satisfy the assumptions 2.1 and 2.2 respectively. Consider the signals $\{r_1(t)\}$ and $\{r_2(t)\}$, given by $r_1(t) = F_1(q)r(t)$, $r_2(t) = F_2(q)r(t)$ for any ℓ_∞-stable linear filters $F_1(q)$ and $F_2(q)$. Denote*

$$\Lambda^N_{r_1r_2} := E\frac{1}{\widetilde{N}} \begin{bmatrix} \sum_{t=t_s}^{N} r_1(t)e_0(t) \\ \sum_{t=t_s}^{N} r_2(t)e_0(t) \end{bmatrix} \cdot$$
$$\cdot \begin{bmatrix} \sum_{t=t_s}^{N} r_1(t)e_0(t) & \sum_{t=t_s}^{N} r_2(t)e_0(t) \end{bmatrix},$$

and

$$\Lambda_{r_1r_2} := \lim_{N\to\infty} \Lambda^N_{r_1r_2}.$$

Also denote for $i,j = 1,2$,

$$R^N_{r_ir_j}(\tau) := \frac{1}{\widetilde{N}+\tau} \sum_{t=t_s}^{N+\tau} r_i(t)r_j(t-\tau),$$
$$\tau = -N+t_s, \ldots, 0,$$
$$R^N_{r_ir_j}(\tau) := \frac{1}{\widetilde{N}-\tau} \sum_{t=t_s}^{N-\tau} r_i(t+\tau)r_j(t),$$
$$\tau = 1, \ldots, N-t_s,$$

and $R^N_{r_i}(\tau) := R^N_{r_ir_i}(\tau)$, $i = 1,2$. Then

(i) $$\Lambda^N_{r_1r_2} = \sum_{\tau=-N+t_s}^{N-t_s} \frac{\widetilde{N}-|\tau|}{\widetilde{N}} R_{e_0}(\tau) \cdot$$
$$\cdot \begin{bmatrix} R^N_{r_1}(\tau) & R^N_{r_1r_2}(\tau) \\ R^N_{r_1r_2}(\tau) & R^N_{r_2}(\tau) \end{bmatrix}$$

(ii) $$\Lambda_{r_1r_2} = \sum_{\tau=-\infty}^{\infty} R_{e_0}(\tau) \begin{bmatrix} R_{r_1}(\tau) & R_{r_1r_2}(\tau) \\ R_{r_1r_2}(\tau) & R_{r_2}(\tau) \end{bmatrix}$$

(iii) $$\frac{1}{\sqrt{\widetilde{N}}} \begin{bmatrix} \sum_{t=t_s}^{N} r_1(t)e_0(t) \\ \sum_{t=t_s}^{N} r_2(t)e_0(t) \end{bmatrix} \xrightarrow{N\to\infty} \mathcal{N}(0, \Lambda_{r_1r_2}),$$

where $\mathcal{N}(0, \Lambda_{r_1r_2})$ denotes the Multivariate Normal distribution with mean 0 and covariance matrix

$\Lambda_{r_1r_2}$. *Moreover, if* $\Lambda^N_{r_1r_2}$ *is invertible,*

$$\textbf{(iv)} \quad \frac{1}{\widetilde{N}}\begin{bmatrix}\sum_{t=t_s}^{N} r_1(t)e_0(t) & \sum_{t=t_s}^{N} r_2(t)e_0(t)\end{bmatrix}\cdot \left(\Lambda^N_{r_1r_2}\right)^{-1}\begin{bmatrix}\sum_{t=t_s}^{N} r_1(t)e_0(t)\\ \sum_{t=t_s}^{N} r_2(t)e_0(t)\end{bmatrix} \xrightarrow{N\to\infty} \chi^2(2),$$

where $\chi^2(2)$ *denotes the Chi-square distribution with 2 degrees of freedom.*

The results given in (iii) and (iv) are asymptotic results, established using a central limit theorem. For finite N the given distributions are approximations of the true ones. However, extensive monte carlo simulations show that this approximation can be very good for small N already, see Hakvoort (1994b). Note that the expression for the covariance matrix in part (i) is a non-asymptotic result, it is correct for any N.

4.3 Frequency Response Confidence Regions

Using the results of the previous subsection a computable bound for the IV model error $\widehat{G}(e^{i\omega_j}) - G_0(e^{i\omega_j})$ is straightforwardly obtained. And as such a confidence region for the system's frequency response $G_0(e^{i\omega_j})$ is obtained. The bound is given in the following main theorem.

Theorem 4.2 *Consider the IV estimate (6) with frequency response* $\widehat{G}(e^{i\omega_j})$ *given by (7). Suppose that* $\{e_0(t)\}$ *and* $\{r(t)\}$ *are independent and that they satisfy the assumptions 2.1 and 2.2 respectively. Let* $\bar{d}(p)$, $p = 1, 2$, *and* $\bar{f}(p)$, $p = 1, 2$, *be given by (15) and (16) respectively, with* $r_1(t)$ *and* $r_2(t)$ *given by (8) and (9) respectively. Moreover, let* $\delta(p)$, $p = 1, 2$, *be given by (17) and (18).*

Let $c_{\mathcal{N},\alpha}$ *correspond to a probability* α *in the standard Normal distribution, such that, if* $x \in \mathcal{N}(0,1) \Rightarrow \text{prob}(|x| \leq c_{\mathcal{N},\alpha}) = \alpha$. *Let* $c_{\chi,\alpha}$ *correspond to a probability* α *in the Chi-square distribution with 2 degrees of freedom, such that, if* $x \in \chi^2(2) \Rightarrow \text{prob}(x \leq c_{\chi,\alpha}) = \alpha$.

Denote matrix-element (i,j) *of* $\Lambda^N_{r_1r_2}$ *as given in part (i) of Lemma 4.1 by* $\lambda^N_{r_ir_j}$. *Moreover introduce* $\Gamma = \begin{bmatrix}\gamma_{11} & \gamma_{12}\\ \gamma_{21} & \gamma_{22}\end{bmatrix}$ *as the square-root of the inverse of* $\Lambda^N_{r_1r_2}$, *provided this matrix is invertible, i.e.* $\Gamma^T\Gamma = \left(\Lambda^N_{r_1r_2}\right)^{-1}$. *Then, if* $N \to \infty$,

$$\textbf{(i)} \quad \left|\text{Re}\left(\widehat{G}(e^{i\omega_j}) - G_0(e^{i\omega_j})\right)\right| \leq$$

$$\leq c_{\mathcal{N},\alpha}\sqrt{\frac{\lambda^N_{r_1r_1}}{\widetilde{N}} + \frac{\bar{d}(1)}{\widetilde{N}} + \frac{\bar{f}(1)}{\widetilde{N}} + \delta(1)}, \ w.p. \geq \alpha,$$

$$\textbf{(ii)} \quad \left|\text{Im}\left(\widehat{G}(e^{i\omega_j}) - G_0(e^{i\omega_j})\right)\right| \leq$$

$$\leq c_{\mathcal{N},\alpha}\sqrt{\frac{\lambda^N_{r_2r_2}}{\widetilde{N}} + \frac{\bar{d}(2)}{\widetilde{N}} + \frac{\bar{f}(2)}{\widetilde{N}} + \delta(2)}, \ w.p. \geq \alpha.$$

And, if $\Lambda^N_{r_1r_2}$ *is invertible,*

$$\textbf{(iii)} \quad \begin{bmatrix}\text{Re}\left(\widehat{G}(e^{i\omega_j}) - G_0(e^{i\omega_j})\right)\\ \text{Im}\left(\widehat{G}(e^{i\omega_j}) - G_0(e^{i\omega_j})\right)\end{bmatrix}^T \Gamma^T\cdot \Gamma\begin{bmatrix}\text{Re}\left(\widehat{G}(e^{i\omega_j}) - G_0(e^{i\omega_j})\right)\\ \text{Im}\left(\widehat{G}(e^{i\omega_j}) - G_0(e^{i\omega_j})\right)\end{bmatrix} \leq$$

$$\leq \left(\sqrt{\frac{c_{\chi,\alpha}}{\widetilde{N}}} + \sqrt{\gamma_{11}^2 + \gamma_{21}^2}\left(\frac{\bar{d}(1)}{\widetilde{N}} + \frac{\bar{f}(1)}{\widetilde{N}} + \delta(1)\right) + \sqrt{\gamma_{12}^2 + \gamma_{22}^2}\left(\frac{\bar{d}(2)}{\widetilde{N}} + \frac{\bar{f}(2)}{\widetilde{N}} + \delta(2)\right)\right)^2, \quad w.p. \geq \alpha,$$

The parts (i) and (ii) of this theorem provide probabilistic bounds for the real and imaginary parts of the IV model error, and as such for the frequency response of the system $G_0(z)$. These may be combined into rectangular system confidence regions in the complex plane using Bonferroni's inequality (Manoukian, 1986, p. 49). In particular, if any complex-valued random variable x has the property that $\text{Re}(x) \leq a$, w.p. $\geq \alpha$, and $\text{Im}(x) \leq b$, w.p. $\geq \beta$, then $\text{Re}(x) \leq a \wedge \text{Im}(x) \leq b$, w.p. $\geq 1 - (1-\alpha) - (1-\beta)$.

Ellipsoidal system confidence regions are obtained with part (iii) of the above theorem, provided the matrix $\Lambda^N_{r_1r_2}$ is invertible. Note that this is generally the case, except for frequencies $\omega_j = 0, \pi$. For these frequencies the signal $\{r_2(t)\}$ is identically zero, as $\text{Im}\left(P_k(e^{i\omega_j})\right)$ appearing in (9) is zero. This very naturally means that for frequencies 0 and π there is no imaginary system uncertainty.

The first contribution to the frequency response uncertainty regions as specified in Theorem 4.2, corresponds to the variance of the IV model, due to the noise $\{e_0(t)\}$. The second contribution, with $\bar{d}(p)$, is due to the response of the tail $\bar{G}_0(q)$, and represents a bias contribution. The third contribution, with $\bar{f}(p)$, is due to the unknown initial conditions. Finally, the fourth contribution, with $\delta(p)$, corresponds to the frequency response of the tail $\bar{G}_0(q)$, and also represents a bias contribution.

The different error sources in the IV estimate can be clearly distinguished and traded-off. In particular the truncation value n can be used to make a trade-off between bias and variance. A larger value n means a smaller bias, but a larger variance. By trying different values an optimal value can be

determined. Similarly the integer t_s offers the possibility to trade-off the influence of initial conditions to the variance. A larger value t_s means a decrease of the error contribution $\bar{f}(p)$, but an increase of the variance, due to a decreasing $\widetilde{N} = N - t_s + 1$.

It is emphasized that the identification of the IV model is not a purpose in itself, but serves as a basis for the construction of system uncertainty regions. The design variables in the IV identification, such as the IV model order n, should not be used to obtain a tractable (low-order) nominal model, but should be tuned in such a way that the uncertainty regions are as small as possible. The identification of a good nominal model, suited for use in control design, is not the issue here.

Remark 4.3 *The probabilistic uncertainty regions given in Theorem 4.2 correspond to an explicit frequency domain variance and bias expression for an instrumental variable estimate $\widehat{G}(e^{i\omega_j})$. In case of open loop identification, if $r(t) = u(t)$, the IV estimate is identical to a FIR least squares estimate. The expressions have been derived for any set of basis functions, $\{P_k(z)\}_{k=0,\ldots,\infty}$. Also the contribution of the initial conditions and undermodelling are properly taken into account.*

In literature variance expressions are given for IV and FIR estimates, however mainly with respect to the parameter variance, assuming that the system is in the model set, and neglecting the influence of the initial conditions, see for example Ljung (1987, Ch. 9) and Söderström and Stoica (1989, Ch. 8). Some progress has been made in Hjalmarsson (1993) and Hjalmarsson and Ljung (1993), where for a different identification setting a procedure is presented to incorporate the influence of the bias when computing the variance.

Theorem 4.2 provides frequency response confidence regions for the unknown system $G_0(z)$. However, it appears that these can only be calculated if the auto-covariance function of the noise process is known, as $\Lambda^N_{r_1 r_2}$ given in part (i) of Lemma 4.1 contains $R_{e_0}(\tau)$, $\tau = -N + t_s, \ldots, N - t_s$. In Hakvoort *et al.* (1993) a procedure is described to estimate the auto-covariance function $R_{e_0}(\tau)$ from measurement data. In Hakvoort (1994b) it is shown, by means of monte carlo simulations, that this estimate is quite accurate, even if it is based on a small amount of data.

5 Discussion

In this paper an identification procedure has been developed which yields confidence regions for the frequency response of some stable LTI system. The procedure involves the explicit calculation of bias and variance errors of an IV or FIR least squares estimate. Important features of the identification procedure are:

- Essentially the procedure is stochastic. Probabilistic uncertainty regions are calculated based on data, deterministic system priors, and stochastic noise priors.
- The actual computations can be performed quite efficiently. No nonlinear optimizations are involved, as use is made of a linear system parametrization, and consequently there is no problem with local optima.
- The required prior information can be reliably estimated from data.
- There are no restrictions on the input signal, it need for example not be periodic. It is even not necessary that the input is generated in open loop.
- No order assumption about the system is made.
- The procedure is easily extendable to MIMO systems.
- Rough prior knowledge about the system, or more specifically pole-locations, can be incorporated by using generalized orthonormal basis functions.
- Unknown initial conditions are properly taken into account.
- The identification procedure is robust for noise outliers, and small errors in the prior information. This means for example that if the system has a small nonlinearity (measured in terms of its ℓ_∞-induced norm), the resulting uncertainty regions are just slightly erratic, and hence are still (approximately) valid.

On the other hand some drawbacks of the probabilistic uncertainty bounding identificiation procedure developed in this paper, are:

- Although all computations can be carried out efficiently and accurately, the identification procedure requires a lot of computations. This means that on-line application of the procedure seems infeasible.
- The procedure makes use of results which are asymptotic in the number of data. As in applications there are always finite-data records, the results might not be valid in practice. On the other hand, monte carlo simulations (Hakvoort, 1994b) show that the error caused by the finiteness of the number of data can be very small, even for small values of N. The acccuracy of the finite-data approximation depends on sev-

eral factors, such as the length of the pulse response of the noise generating filter, and the actual distribution of the noise process.

References

Bayard, D.S. (1992). Statistical plant set estimation using Schroeder-phased multisinusoidal input design. *Proc. Am. Contr. Conf.*, Chicago, IL, pp. 2988–2995.

De Vries, D.K. and P.M.J. Van den Hof (1992). Quantification of model uncertainty from data: input design, interpolation and connection with robust control design specifications. *Proc. Am. Contr. Conf.*, Chicago, IL, pp. 3170–3175.

De Vries, D.K. and P.M.J. Van den Hof (1993). Quantification of uncertainty in transfer function estimation: a mixed deterministic-probabilistic approach. *Prepr. 12th IFAC World Congress*, Sydney, Australia, Vol. 8, pp. 157–160.

Hakvoort, R.G. (1993). Worst-case system identification in H_∞: error bounds and optimal models. *Prepr. IFAC World Congress*, Sydney, Australia, Vol. 8, pp. 161–164.

Hakvoort, R.G. (1994a). A linear programming approach to the identification of frequency domain error bounds. *Prepr. SYSID'94, 10th IFAC Symp. on Syst. Id.*, Copenhagen, Denmark, Vol. 2, pp. 195–200.

Hakvoort, R.G. (1994b). *System Identification for Robust Process Control: nominal models and error bounds*, PhD. Thesis, Mech. Eng. Syst. and Contr. Group, Delft Univ. of Techn., The Netherlands.

Hakvoort, R.G. and P.M.J. Van den Hof (1993). Identification of model error bounds in ℓ_1- and H_∞-norm. *The Modeling of Uncertainty in Control Systems, Proc. 1992 Santa Barbara Workshop, Lecture Notes in Contr. and Inf. Sciences*, Springer Verlag, London, Vol. 192, pp. 139–155.

Hakvoort, R.G., P.M.J. Van den Hof and O.H. Bosgra (1993). Consistent parameter bounding identification using cross-covariance constraints on the noise. *Proc. 32nd IEEE Conf. Decision and Control*, San Antonio, TX, pp. 2601–2606.

Heuberger, P.S.C., P.M.J. Van den Hof and O.H. Bosgra (1993). A generalized orthonormal basis for linear dynamical systems. To appear in *IEEE Trans. Autom. Contr.*, abbreviated version in *Proc. 32nd IEEE Conf. Decision and Control*, San Antonio, TX, pp. 2850–2855.

Hjalmarsson, H. (1993). A model variance estimator. *Prepr. 12th IFAC World Congress*, Sydney, Australia, Vol. 9, pp. 5–10.

Hjalmarsson, H. and L. Ljung (1993). Estimating model variance in the case of undermodelling. *IEEE Trans. Autom. Contr., AC-37*, 1004-1008.

Lamaire, R.O., L. Valavani, M. Athans and G. Stein (1991). A frequency domain estimator for use in adaptive control systems. *Automatica, 27*, 23–38.

Ljung, L. (1987). *System Identification: Theory for the User*, Prentice-Hall, Englewood Cliffs, N.J.

Manoukian, E.B. (1986). *Modern Concepts and Theorems of Mathematical Statistics.* Springer Verlag, New York.

Ninness, B.M. (1993). *Stochastic and Deterministic Modelling*, PhD. Thesis, Univ. of Newcastle, Australia.

Ninness, B.M. and G.C. Goodwin (1992). Robust frequency response estimation accounting for noise and undermodelling. *Proc. Am. Contr. Conf.*, Chicago, IL, pp. 2847–2851.

Söderström, T. and P. Stoica (1989). *System Identification*, Prentice-Hall, U.K.

Wahlberg, B. and L. Ljung (1992). Hard frequency-domain model error bounds from least-squares like identification techniques. *IEEE Trans. Autom. Contr., AC-37*, 900–912.

Selected Topics in Identification, Modelling and Control
Vol. 7, December 1994

Identification and robust control design of an industrial glass tube manufacturing process

Dick de Roover and Richard G. Hakvoort

Mechanical Engineering Systems and Control Group
Delft University of Technology, Mekelweg 2, 2628 CD Delft, The Netherlands.

Abstract. A recently developed identification procedure is applied to measurement data of a multivariable industrial glass tube manufacturing process. Both a nominal model and probabilistic frequency response model error bounds are identified with this procedure. The nominal model is used to design an H_∞-controller. The model error bounds are used in a μ-analysis to assess robust stability of the designed controller before actual implementation.

Keywords. Industrial application, probabilistic uncertainty bounding identification, robust control design.

1 Introduction

In this paper the problem is discussed of identification and robust control design of a multivariable industrial glass tube manufacturing process. Due to increasing demands on the quality and quantity of the glass tubes a high performing controller has to be designed for the production process. Besides, the controlled system has to be robust against (severe) fluctuations of the dynamical behaviour of the uncontrolled process. The design of a robust controller requires the specification of a nominal model of the process dynamics and explicit error bounds on the frequency response of this model, see for example Maciejowski (1989), Morari and Zafiriou (1989). The modelling is done by using identification techniques based on time-series of several process parameters. The industrial process puts the following requirements on the identification procedure:

- The identification method has to be MIMO (multi-input multi-output) applicable, as the process is multivariable.
- The identification method has to be able to handle arbitrary input signals, as there is no complete freedom to do experiment design. During the identification experiments the production is lost, and therefore measurement time is very much restricted. In particular no sine-sweep experiments could be carried out.
- If not clear from physical insights, all prior information required has to be gathered from data.
- Because of the subsequent control-design step, and the necessity to implement a low-order controller, it is desirable to identify a reasonably low-order nominal model.

In literature many identification procedures are described which deliver a nominal model and explicit frequency response model error bounds, see for example Bayard (1992), De Vries (1992), De Vries (1993), Hakvoort (1994), Hakvoort and Van den Hof (1994), Lamaire *et al.* (1991), Ninness and Goodwin (1992), Wahlberg and Ljung (1992). Most of these methods appear not applicable to the industrial process at hand, either because the input signal is required to be sinusoidal, or because the procedure is intended for SISO (single input single output) systems.

In this paper the identification procedure described in Hakvoort (1994) is applied to the industrial glass tube manufacturing process because it does satisfy all of the requirements listed above. The procedure yields both probabilistic frequency response

system uncertainty regions, with the procedure described in Hakvoort and Van den Hof (1994), and a nominal model, with the curve fit procedure described in Hakvoort (1993). These are used to design a robust H_∞-controller. The glass tube manufacturing process has previously been considered in Backx and Damen (1992), Falkus *et al.* (1993), Murad *et al.* (1993), Overschee and De Moor (1993). However, in these papers no model error bounds have been identified or derived in some other way, and consequently no robust controllers could be designed, which account for the model error.

The outline of the paper is as follows. In Section 2 a description is given of the glass tube manufacturing process. In Section 3 the identification procedure is shortly described, and the identification results are presented. Next in Section 4 the control design procedure is described, and the resulting design is presented. Also a robust stability analysis is performed. Finally in Section 4.3 conclusions are drawn.

2 Process Description

The industrial process under consideration is a glass tube manufacturing process, schematically depicted in Figure 1. By direct electric heating, quartz sand

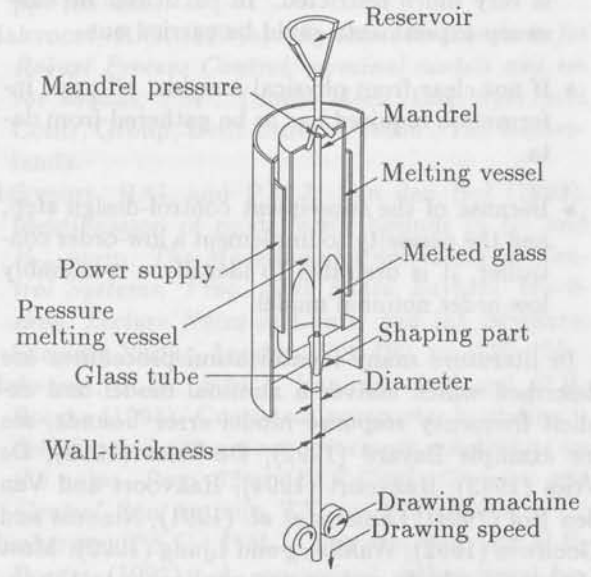

Fig. 1: Schematic overview of the glass tube manufacturing process.

is melted and flows down through a ring-shaped hole along the accurately positioned mandrel. Under pressure, gas is led through the hollow mandrel. The glass tube is pulled down due to gravity and supported by a drawing machine.

Shaping of the tube takes place at, and just below the end of the mandrel. The longitudinal shape of the tube is characterized by two important dimensions, which will be taken as outputs to be controlled: tube diameter (first output) and tube wall-thickness (second output). Both outputs are influenced by many process conditions such as:

- mandrel gas pressure,
- drawing speed,
- power applied to the furnace (temperature of the glass),
- melting vessel pressure,
- composition of raw materials.

Some of these have a small bandwidth (power and composition of raw materials), poorly influence the glass quality (composition of raw materials), or have extremely large delay times involved (power, melting vessel pressure and composition of raw materials). Therefore these are not well suited for control of the tube dimensions.

The mandrel pressure and the drawing speed influence the shaping of the tube in a most direct way. Transfers from these inputs to both wall-thickness and diameter have the largest bandwidth, the shortest delay times and permit, to some extent, independent manipulation of the outputs. The permitted ranges of these two process inputs allow a control of the tube dimensions over the full amplitude range of output disturbances and enable the production of a large variety of different products. Consequently these two are taken as controlling inputs. The drawing speed will be denoted as the first input, and the mandrel pressure as the second input.

Shaping of the glass tube clearly is a MIMO process with a high degree of interaction. Increase of the mandrel pressure results in an increase of the tube diameter and a decrease of the tube wall-thickness. Increase of the drawing speed causes a decrease of both diameter and wall-thickness. A physical model of this shaping part has been obtained by deriving the physical laws of the shaping process, describing the shaping of the tube in detail and over the full range of possible operating points, determined by various values of tube diameter and wall-thickness. However, this physical model is very complex and has physical parameters included with numerical values that are unknown for the different operating points. Therefore modelling is performed by means of black-box identification.

Basically the process is nonlinear. However, one operating point is considered. Stair-case experiments, i.e. experiments with the inputs being excited by steps of different amplitudes, indicate that

the process can very well be considered linear and time-invariant in the operating point, see for example De Roover (1993). Therefore there is no problem with using linear identification and control design techniques.

In the sequel only scaled data will be used, such that the original process data cannot be retrieved. This is because of the industrial confidentiality required.

3 Identification of a Nominal Model and a Model Error Bound

3.1 The Identification Procedure

An identification procedure is used that yields both a nominal model and frequency response model error bounds. The nominal model is used for model-based control design, and the model error bounds are used to assess robust stability before implementation of the controller. Basically the identification procedure consists of two steps:

1. In the first step probabilistic frequency response uncertainty regions are identified with the procedure described in Hakvoort and Van den Hof (1994). Consider the linear, time-invariant, causal and stable MIMO system denoted by $G_0(z)$. The entry of $G_0(z)$ corresponding to input j' and output i' is represented by

$$G_0^{i'j'}(z) = \sum_{k=0}^{\infty} g_0^{i'j'}(k) z^{-k},$$

where $g_0^{i'j'}(k)$ are the (unknown) pulse response coefficients. Consider given input data $\{u(t)\}$ and measured output data $\{y(t)\}$ and the following input-output relation of the data generating system,

$$y(t) = G_0(q)u(t) + e_0(t),\ t = 1, \ldots, N,$$

where q denotes the forward time-shift operator, N signifies the measurement time and $\{e_0(t)\}$ is an unknown additive output noise. In the error bounding procedure knowledge is required of the auto-covariance function of the noise process. In Hakvoort (1994) a procedure is presented to estimate this bound from measurement data. Besides, a bound $\bar{g}^{i'j'}(k)$ on the coefficients $g_0^{i'j'}(k)$,

$$\left| g_0^{i'j'}(k) \right| \leq \bar{g}^{i'j'}(k),\ \forall i', j',\ k = 0, \ldots, \infty.$$

In Hakvoort (1994) also a procedure is presented to estimate this bound from measurement data.

Next for a specified set of frequencies $\{\omega_j\}_{j=1,\ldots,l}$ probabilistic confidence regions for the system's frequency response $G_0^{i'j'}(e^{i\omega_j})$ are derived for each entry i', j'. This is performed by explicitly calculating the bias and variance errors of an instrumental variable estimate, see Hakvoort and Van den Hof (1994). Due to the fact that the real and imaginary part of the frequency response are considered separately, the resulting uncertainty regions are rectangular. The centers of these uncertainty regions constitute a nonparametric nominal estimate of the system's frequency response.

2. In the second step of the identification procedure a stable parametric nominal model is constructed with the frequency response curve fit procedure described in Hakvoort (1993). The curve fit problem concerns the minimization of

$$\max_{i',j',j} \left| \left(G^{i'j'}(\omega_j) - \widehat{G}^{i'j'}(e^{i\omega_j}) \right) \widetilde{W}^{i'j'}(\omega_j) \right|,$$

over stable $\widehat{G}(z)$ of some specified order, i.e. the minimization of the maximum amplitude of the weighted difference between a set of frequency response data and a parametric (low-order) model for a finite number of frequencies. Here $\{G^{i'j'}(\omega_j)\}_{j=1,\ldots,l}$ are the complex-valued frequency response data, in particular the centers of the frequency response uncertainty regions derived above. $\{\widetilde{W}^{i'j'}(\omega_j)\}_{j=1,\ldots,l}$ is a weighting function, which can be used to tune the frequency distribution of the fit error.

To reduce numerical complexity the MIMO identification problem is split into two MISO identification problems. Models are estimated for each output separately, and at the end these are combined into one MIMO model. More details of the identification procedure are given in Hakvoort (1994).

3.2 Identification Results

For identification purposes the following experiments have been carried out on the glass tube production process:

- A free-run experiment, i.e. output measurements without input excitation. This gives an indication of the output noise, and can be used to estimate the second order noise statistics, knowledge of which is required for the uncertainty bounding identification procedure, see Hakvoort and Van den Hof (1994).
- Stepresponse experiments. These can be used to accurately identify the low-frequent system dynamics.

- A PRBS experiment, i.e. the input signals are Pseudo Random Binary Sequences, and independent of each other. This excites the system uniformly in the entire frequency range of interest.
- An experiment where the input signals are filtered PRBS signals. The filter is a bandpass filter with high gain in the medium frequency range, which is considered important for the control application.
- One more unfiltered PRBS experiment, which is not used for identification, but for validation purposes.

The data have been preprocessed to make them suitable for identification purposes, i.e. outliers, trends and offsets have been removed, and the fast sampled data have been decimated to a sampling rate corresponding to the sampling rate for the discrete time controller.

The process contains large time delays, partly due to the physical time it takes before the glass tube reaches the measurement equipment. First these time delays are estimated and removed from the data. Due to the fact that MISO problems are considered, it is always possible to do this by shifting both input signals over the proper amount of samples. A correlation analysis on the basis of the white PRBS experiments, is applied to estimate the time delays. In Table 1 the delay times are given.

	input 1	input 2
output 1	5	7
output 2	10	12

Table 1: Time delays in number of samples.

Next the above sketched identification procedure has been carried out. The nominal model $\widehat{G}(z)$ (without delays) is shown in the Bode plot of Figure 2.

Rectangular confidence regions have been derived using the PRBS and the filtered PRBS experiments separately. Next the intersection of these confidence regions has been calculated. The resulting uncertainty regions are depicted in the Nyquist diagram of Figure 3, with the delays added, together with the frequency response of the nominal model $\widehat{G}(z)$. The confidence regions correspond to a 99.8%-confidence level. From this Nyquist diagram it is straightforward to calculate upper and lower bounds on the amplitude and the phase of the system's frequency response. These bounds, corresponding to the undelayed model, are depicted in Figure 2 as well.

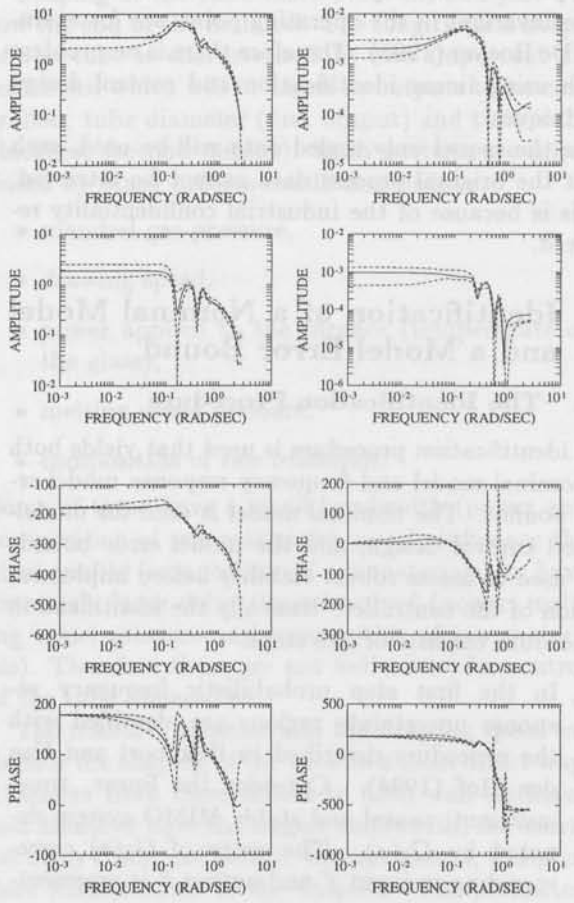

Fig. 2: Bode plot of the identified undelayed nominal model $\widehat{G}(z)$ (solid) and 99.8%-confidence intervals for the amplitude and phase (dashed). The entry in row i' and column j' corresponds to the transfer function from input $u_{j'}$ to output $y_{i'}$.

From Figure 3 a frequency dependent upper bound on the additive model error is easily derived as the worst-case distance from the nominal frequency response $\widehat{G}(e^{i\omega_j})$ to the rectangular uncertainty region for that frequency. In Figure 4 this upper bound on the model error is shown for each entry i', j', and corresponding to a confidence level of 99.8%.

The undelayed MISO model for the first output is of order 9. The undelayed model for the second output is also of order 9. The combined MIMO model with delays is of order 35. Due to similar dynamics for both outputs, there are redundant orders in this MIMO model. As a low-order model is desired for the control design application, this nominal model is reduced to order 15 with Hankel-norm model reduction, Glover (1984). This model reduction step has

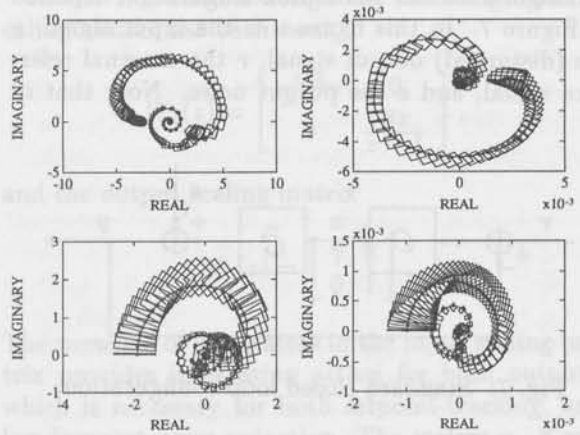

Fig. 3: Nyquist plot nominal model $\widehat{G}(z)$ (solid,$*$) and 99.8%-confidence regions (rectangulars) with the delays being added. The entry in row i' and column j' corresponds to the transfer function from $u_{j'}$ to $y_{i'}$.

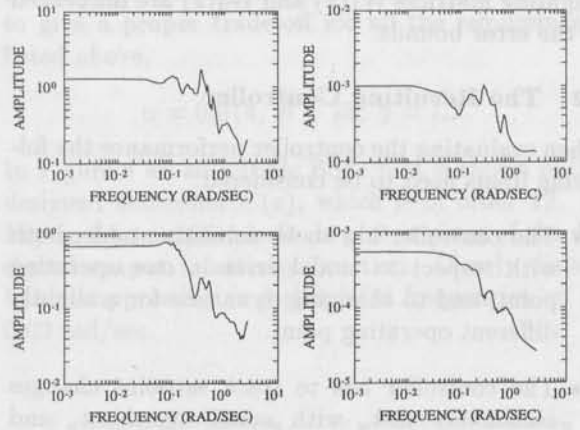

Fig. 4: Upper bound on the additive model error corresponding to a confidence level of 99.8%. The entry in row i' and column j' gives the additive model error bound for the transfer function from $u_{j'}$ to $y_{i'}$.

been carried out in such a way that no significant dynamics are lost.

Notice from Figure 2 that also high-frequent dynamics present in the process can be accurately modelled, this despite of the bad signal-to-noise-ratio at these frequencies. Other identification methods, such as standard prediction error and subspace methods, appear not capable of modelling so much detail in the high-frequency range. Compare Figure 2 for example with the identification results in Falkus *et al.* (1993), Overschee and De Moor (1993). If an attempt is made to identify high-order models with a prediction error method, then easily numerical problems in the nonlinear optimization occur because of the bad signal-to-noise-ratio. On the other hand, if a low-order model is identified, only the low-frequent dynamics are accurately modelled. Application of a high-pass filter in order to emphasize the high-frequent dynamics, again easily leads to numerical problems in a sens that (non-linear) minimization routines get stuck to local minima. The main reason for this failure is that both prediction error methods and subspace methods use a time-domain criterion in their optimization routines. In general for strictly proper systems the contribution of high-frequent process dynamics to a time series is only marginal and therefore hardly present in a time-domain based criterion. However for control design, and especially robust control design, these high-frequent process dynamics can be very important, and should therefore be accurately estimated as well.

Next the time-domain behaviour of the nominal model $\widehat{G}(z)$ is evaluated. In Figure 5 the measured and simulated step responses are shown; note the approximate linear behaviour of the system in one operating point. In Figure 6 measured and simulated responses are shown for the validation PRBS experiment, which has not been used in the identification. The time-domain fit appears very good both for the step response experiments as for the validation experiments, which gives confidence in the nominal model.

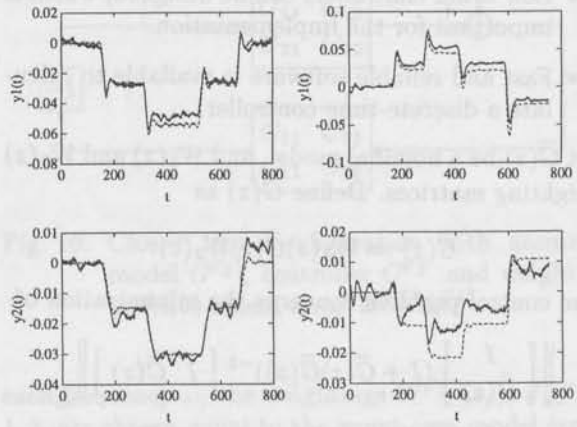

Fig. 5: Measured (solid) and simulated (dashed) stepresponses. The entry in row i' and column j' corresponds to the response of output $y_{i'}$ to step-excitation of input $u_{j'}$.

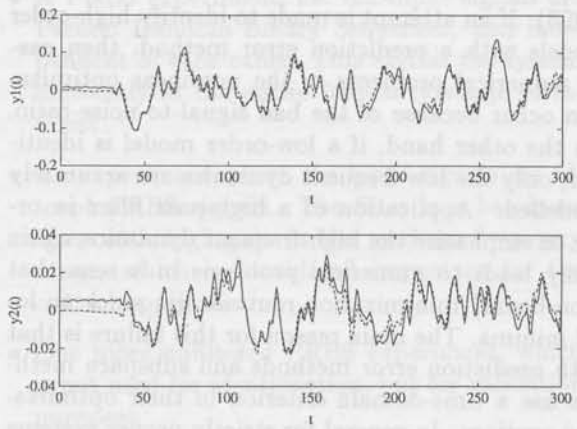

Fig. 6: Measured (solid) and simulated (dashed) responses on PRBS-excitation of both inputs for the validation experiment.

4 Robust Controller Design and Analysis

4.1 The Control Design Procedure

The H_∞-control design method described in Bongers (1994), Bongers and Bosgra (1990), McFarlane and Glover (1989) is used to design a model-based controller. The reasons for using this control design procedure are:

- The controller performance and robustness can easily be tuned by the use of simple (constant, diagonal) input and output weighting matrices.
- Low-order controllers can be designed, which is important for the implementation.
- Fast and reliable software is available to calculate a discrete-time controller.

Let $\widehat{G}(z)$ be a nominal model, and $W_1(z)$ and $W_2(z)$ weighting matrices. Define $\widetilde{G}(z)$ as

$$\widetilde{G}(z) := W_1(z)\widehat{G}(z)W_2(z).$$

The control problem concerns the minimization of

$$\left\| \begin{bmatrix} I \\ \widetilde{G}(z) \end{bmatrix} (I + \widetilde{C}(z)\widetilde{G}(z))^{-1} \begin{bmatrix} I & \widetilde{C}(z) \end{bmatrix} \right\|_\infty$$

over stabilizing $\widetilde{C}(z)$ of some specified order. The controller

$$C(z) := W_2(z)\widetilde{C}(z)W_1(z)$$

stabilizes $\widehat{G}(z)$ and achieves a certain performance and robustness, dependent on the choice of weighting matrices $W_1(z)$ and $W_2(z)$. The controller $C(z)$ is designed for the standard configuration depicted in Figure 7. In this figure u is the input signal, y the (disturbed) output signal, r the external reference signal, and e the output noise. Note that in

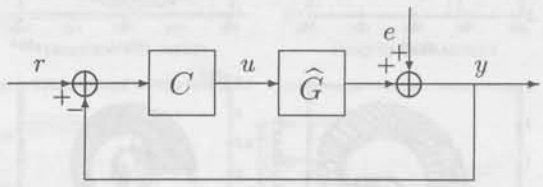

Fig. 7: Standard closed loop configuration.

the control design only use is made of the nominal model, and no direct use is made of the model error bounds. These error bounds are used later for stability robustness analysis of the resulting controller. Of course indirect use is made of the model error bounds in a sense that if no robust stability can be proven, a new nominal control design is performed, and in a sense that decisions upon the choices of the weighting matrices $W_1(z)$ and $W_2(z)$ are influenced by the error bounds.

4.2 The Resulting Controller

When evaluating the controller performance the following items need to be considered.

- The controller has to be robustly stable, both with respect to model error in one operating point, and to changing dynamics for a slightly different operating point.
- The controller has to track setpoint changes reasonably fast, with small overshoot, and without static error.
- Low-frequent and very-low-frequent noise, such as trends, should be removed by the controller as much as possible.
- High-frequent noise should not be amplified too much.
- The input signals to the system should be as smooth as possible, without large overshoots on setpoint changes.
- Both outputs have to be statically and dynamically decoupled as much as possible.

The items above constitute a rather qualitative measure for controller performance. Engineering interpretation is required to actually construct a controller which meets these requirements.

In the H_∞-control design the following input scaling matrix has been used,

$$W_2(z) = \begin{bmatrix} \frac{\alpha z}{z-1} & 0 \\ 0 & \frac{\beta z}{z-1} \end{bmatrix},$$

and the output scaling matrix

$$W_1(z) = \begin{bmatrix} \gamma & 0 \\ 0 & 1 \end{bmatrix}.$$

The presence of integrators in the input scaling matrix provides integrating action for both outputs, which is necessary for both setpoint-tracking, and low-frequent noise reduction. The scalars α, β and γ are used to tune the controller, such that acceptable performance and robustness are achieved, in accordance with the items listed above. The parameter γ is used to tune the relative importance of each output. The parameters α and β are used to tune the relative importance of each input, and to tune the bandwidth of the closed loop system. A larger value for α and β generally means a higher bandwidth. Finally the following values appeared to give a proper trade-off for all the requirements listed above,

$$\alpha = 0.014,\ \beta = 25,\ \gamma = 1.2.$$

In Figure 8 an amplitude Bode plot is shown of the designed controller $C(z)$, which is of order 12. In Figure 9 an amplitude Bode plot is given of the designed output sensitivity function. Clearly disturbance suppression is realized for frequencies up to 0.02 rad/sec.

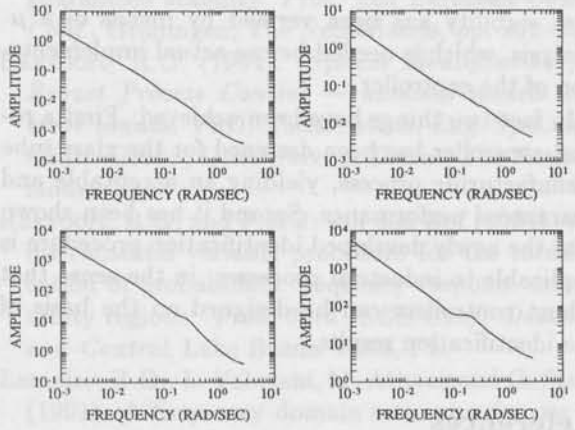

Fig. 8: Amplitude Bode plot of the designed controller $C(z)$. The entry in row i' and column j' corresponds to $C^{i'j'}(z)$.

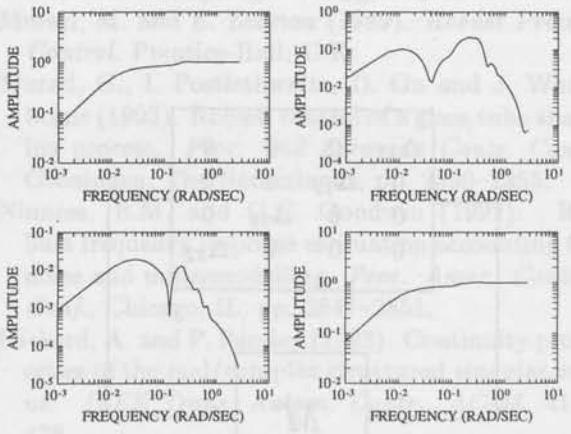

Fig. 9: Amplitude Bode plot of the output sensitivity function $S(z) = (I - \widehat{G}(z)C(z))^{-1}$. The entry in row i' and column j' corresponds to $S^{i'j'}(z)$.

4.3 μ-Stability Robustness Analysis

Before implementing the controller on the system, stability guarantees should be required. Therefore a robust stability analysis is performed, using the frequency dependent model error bound. Consider the closed loop configuration depicted in Figure 10. For

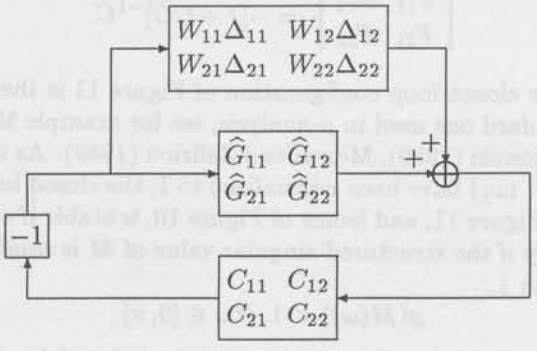

Fig. 10: Closed loop configuration with nominal model $\widehat{G}^{i'j'}$, controller $C^{i'j'}$ and weighted additive model error $W^{i'j'}\Delta^{i'j'}$

each frequency ω_j the weightings $W^{i'j'}(\omega_j)$, $i', j' = 1, 2$, are chosen equal to the worst-case model error bounds depicted in Figure 4. Hence the perturbations $\Delta^{i'j'}(\omega_j)$ are normalized to 1,

$$|\Delta^{i'j'}(\omega_j)| \leq 1,\ i' = 1, 2,\ j' = 1, 2,\ \forall \omega_j.$$

Straightforward manipulations show that the closed loop configuration of Figure 10 is stable if and only

if the closed loop configuration of Figure 11 is stable,

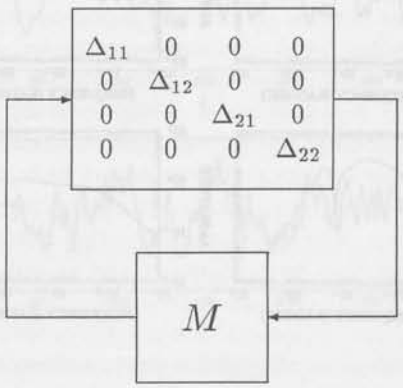

Fig. 11: Standard uncertainty configuration for μ-analysis

where the matrix M is given by:

$$M := \begin{bmatrix} F_{11}W_{11} & F_{11}W_{12} & F_{12}W_{21} & F_{12}W_{22} \\ F_{21}W_{11} & F_{21}W_{12} & F_{22}W_{21} & F_{22}W_{22} \\ F_{11}W_{11} & F_{11}W_{12} & F_{12}W_{21} & F_{12}W_{22} \\ F_{21}W_{11} & F_{21}W_{12} & F_{22}W_{21} & F_{22}W_{22} \end{bmatrix},$$

and $F^{i'j'}$, $i', j' = 1, 2$, is defined by

$$\begin{bmatrix} F_{11} & F_{12} \\ F_{21} & F_{22} \end{bmatrix} := -[I + C\widehat{G}]^{-1}C.$$

The closed loop configuration of Figure 11 is the standard one used in μ-analysis, see for example Maciejowski (1989), Morari and Zafiriou (1989). As the $\Delta^{i'j'}(\omega_j)$ have been normalized to 1, the closed loop of Figure 11, and hence of Figure 10, is stable if and only if the structured singular value of M is smaller than 1,

$$\mu(M(\omega)) < 1, \ \forall \omega \in [0, \pi].$$

For simplicity this requirement is replaced by the requirement,

$$\mu(M(\omega_j)) < 1, \ j = 1, \ldots, l,$$

assuming that the frequency grid $\{\omega_j\}_{j=1,\ldots,l}$ has been chosen suitably, such that the inter sample frequency behaviour causes no problems. This simplification is also supported by Packard and Pandey (1993), where it is shown that the structured singular value is a continuous function of frequency in case complex-valued perturbations are considered.

For each frequency ω_j, $j = 1, \ldots, l$, separately, $\mu(M(\omega_j))$ has been calculated. In Figure 12 the resulting μ-curve is shown. It appears that for all frequencies $\mu(M(\omega_j))$ is smaller than 1. Hence robust stability is concluded, and it is considered safe to actually implement the controller, as there is no danger of closed loop instability in the specific operating point of the process.

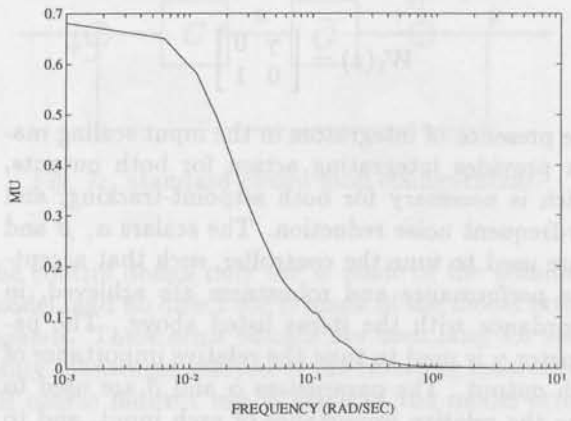

Fig. 12: $\mu(M(\omega_j))$ for $j = 1, \ldots, l$.

Conclusions

The identification procedure developed in Hakvoort (1994) has been applied to measurement data of an industrial glass tube manufacturing process. It appears possible to identify an accurate nominal model with the identification method applied. Moreover, also reliable frequency response model error bounds can be derived, which are not overly conservative. An H_∞-controller has been designed based on the nominal model. With the model error bounds robust stability has been verified by means of a μ-analysis, which is needed before actual implementation of the controller.

In fact two things have been achieved. First a robust controller has been designed for the glass tube manufacturing process, yielding an acceptable and guaranteed performance. Second it has been shown that the newly developed identification procedure is applicable to industrial processes, in the sense that robust controllers can be designed on the basis of the identification results.

References

Backx, T.C.P.M. and A.A.H. Damen (1992). Identification for control of MIMO industrial processes. *IEEE Trans. Autom. Contr., AC-37*, 980–986.

Bayard, D.S. (1992). Statistical plant set estimation using Schroeder-phased multisinusoidal input de-

sign. *Proc. Amer. Contr. Conf.,* Chicago, IL, pp. 2988–2995.

Bongers, P.M.M. (1994). *Modelling and Identification of Flexible Wind Turbines and a Factorizational Approach to Robust Control.* PhD. Thesis, Mech. Eng. Syst. and Contr. Group, Delft Univ. of Techn., The Netherlands.

Bongers, P.M.M. and O.H. Bosgra (1990). Low order H_∞ controller synthesis. *Proc. 29th IEEE Conf. Dec. and Contr..*, Honolulu, HI, USA, pp. 194–199.

De Roover, D. (1993). *Identification of a Glass-Bulb Production Process – A Comparison of Two Identification Methods.* Report TUD-WBMR-A-633, Delft University of Technology, The Netherlands, pp. 52–56.

De Vries, D.K. and P.M.J. Van den Hof (1992). Quantification of model uncertainty from data: input design, interpolation and connection with robust control design specifications. *Proc. Amer. Contr. Conf.,* Chicago, IL, pp. 3170–3175.

De Vries, D.K. and P.M.J. Van den Hof (1993). Quantification of uncertainty in transfer function estimation: a mixed deterministic-probabilistic approach. *Prepr. 12th IFAC World Congress,* Sydney, Australia, Vol. 8, pp. 157–160.

Falkus, H., A.A.H. Damen and A.C.P.M. Backx (1993). Identification of a tube glass production process: point vs. set estimation. *Proc. 2nd European Contr. Conf.,* Groningen, The Netherlands, pp. 2344–2349.

Glover, K. (1984). All optimal Hankel-norm approximations of linear multivariable systems and their L_∞-error bounds. *Int. J. Control, 39,* 1115–1193.

Hakvoort, R.G. (1993). Frequency domain curve fitting with maximum amplitude criterion and guaranteed stability. *Proc. 2nd European Contr. Conf.,* Groningen, The Netherlands, pp. 252–257.

Hakvoort, R.G. (1994). *System Identification for Robust Process Control — nominal models and error bounds.* PhD. Thesis, Mech. Eng. Syst. and Contr. Group, Delft Univ. of Techn., The Netherlands.

Hakvoort, R.G. and P.M.J. van den Hof (1994). An instrumental variable procedure for the identification of probabilistic frequency response uncertainty regions. *Proc. 33rd IEEE Conf. Decision and Control,* Lake Buena Vista, FL.

Lamaire, R.O., L. Valavani, M. Athans and G. Stein (1991). A frequency domain estimator for use in adaptive control systems. *Automatica, 27,* 23–38.

Maciejowski, J.M. (1989). *Multivariable Feedback Design.* Addison Wesley, U.K.

McFarlane, D.C. and K. Glover (1989). *Robust Controller Design Using Normalized Coprime Factor Plant Descriptions.* Lect. Notes Control Inform. Sc., Vol. 138, Springer Verlag, Berlin.

Morari, M. and E. Zafiriou (1989). *Robust Process Control.* Prentice-Hall, U.K.

Murad, G., I. Postlethwaite, D. Gu and J. Whidborne (1993). Robust control of a glass tube shaping process. *Proc. 2nd European Contr. Conf.,* Groningen, The Netherlands, pp. 2350–2355.

Ninness, B.M. and G.C. Goodwin (1992). Robust frequency response estimation accounting for noise and undermodelling. *Proc. Amer. Control Conf.,* Chicago, IL, pp. 2847–2851.

Packard, A. and P. Pandey (1993). Continuity properties of the real/complex structured singular value. *IEEE Trans. Autom. Contr., AC-38,* 415–428.

Van Overschee, P. and B. de Moor (1993). N4SID: subspace identification of a glass-tube manufacturing process. *Proc. 2nd European Contr. Conf.,* Groningen, The Netherlands, pp. 2338–2343.

Wahlberg, B. and L. Ljung (1992). Hard frequency-domain model error bounds from least-squares like identification techniques. *IEEE Trans. Autom. Control, AC-37,* 900–912.

Selected Topics in Identification, Modelling and Control
Vol. 7, December 1994

Closed loop system identification of an industrial wind turbine system and a preliminary validation result

Gregor E. van Baars

Mechanical Engineering Systems and Control Group
Delft University of Technology, Mekelweg 2, 2628 CD Delft, The Netherlands.

Abstract. Reliable dynamical simulation models of complete wind turbine systems are expected to be of great importance for the development of economically attractive wind turbine systems. Reliability is closely related to validity, which is difficult to assess from measurements and model simulation only. This is mainly due to fluctuations of the wind field corrupting the measurements. Application of system identification solves this problem because the noise model accounts for the (wind induced) disturbances and attention can be focussed to the deterministic part describing the dynamics which are the subject of validation. An industrial full size wind turbine system is available for identification experiments. This plant is a multivariable system. Experiments were restricted to a closed loop situation with existing single loop PI controllers. Plant models are identified from this closed loop data using a two step approach. In the preliminary validation stage the resulting identified model demonstrated qualitatively good agreement to the physical model (DUWECS code) of the wind turbine.

Keywords. system identification, closed-loop experiments, wind power plants, model validation

1 Introduction

Unfortunately, still a lot of faillures occur with modern wind turbine systems. Underestimation of fatigue problems is in many cases the main cause of demolished gears or broken rotor blades of a wind turbine system.

It is a generally accepted idea that the quality of *dynamical simulation models* used in the design and development phase of the complete wind turbine systems will play a crucial role in the improvement of wind turbine systems. For example, various dynamical load cases, which are expected to be critical for the system, are simulated with the model, and the simulation results are then used to evaluate whether or not the designed system has an acceptable dynamical behavior.

Testing a design through evaluation of dynamical load cases becomes increasingly important when the fatigue loading of the wind turbine system is considered. Clearly, the fatigue loading is related to the expected life time of the wind turbine system, and therefore directly connected to the economic viablility of wind energy systems for electrical power production, compared to conventional power production exploiting (non-renewable) fossile fuels like gas or coal.

Obviously, reliability of the design tools will depend heavily on the extent to which the simulation model has been *validated.* That is: How reliable and accurate are the models in their ability to simulate the phenomena that are expected to play an important role on the real system?

Since the dynamics of a wind turbine system are complex, validation of the physical models will be a complex and difficult problem. High validation requirements usually can not be met by just evaluating a comparison of measured data and simulations generated by the model. This is mainly due to the disturbing influence of the unknown wind field on the measurements. Suppose a very important

aspect of modeling has to be validated which only exhibits subtle dynamical responses during the experiments, while the wind induces large disturbances on the measurement of this phenomenon. In that case any comparison with simulation will fail because the human eye is unable to observe any deterministic match or mismatch between simulation and measurement simply because this is drowned in the disturbances.

To reduce the effect of disturbances often a technique called azimuthal binning is applied. This averaging technique obviously deteriorates the dynamical information in the measurement data, which we would like to preserve if possible.

System identification can help to solve the validation problem for several reasons. The most important one is that it provides a separation of deterministic and stochastic phenomena in the data. Therefore the wind induced disturbances need no longer to be averaged out but can be captured by the noise model. This allows for undisturbed evaluation of the quality of the identified deterministic part compared to noise-free simulation of the physical model.

Another important reason is that the result of identification is a model rather than a particular time series. For example, a decisive judgement about the model quality can be obtained by comparison of dynamical transfer functions of the experimental model and the simulation model (e.g. in the frequency domain).

Note that conventional validation techniques which exploit for example azimuthal binning cannot handle In the case of closed loop measurements conventional validation techniques are not able to extract reliable open loop behavior of the wind turbine system. Therefore validation can not be investigated properly. Several closed loop identification methods exist to deal with this situation and provide reliable open loop models.

Despite these reasons, application of system identification to wind turbine systems is, in general, not straightforward. However, previous research based on data measured from small scale test facilities, each of them emphasizing a specific part of the wind turbine system, was succesful using this approach (van Baars and Bongers,1992, van Baars and Bongers,1993).

This paper will pursue extension of the validation results of the physical simulation model. To make sure that the validation results are not system specific it is desirable to investigate several wind turbine systems of different size and configuration. Besides investigation of dedicated experimental research test facilities it is therefore also important to consider full scale industrial state of the art wind turbine sytems which are operating today. Integration of specific small scale experimental results and insights for a full scale industrial wind turbine will be essential in determining the value of the simulation model for practical situations (such as support of the design process of modern wind turbine systems and control systems).

The paper presents a project, which has been started recently, in the PWC wind farm located in Friesland (The Netherlands) consisting of 18 industrial wind turbines with rated power of 310 kW each. One of the wind turbines is available for experimentation. The wind turbine system can be influenced by input excitation at the electrical conversion system and pitching of the rotor blades. This means that validation involves a system with multiple inputs and multiple outputs.

A series of system identification experiments were designed and performed. During the experiments normal operation of the wind turbine was continued with the control and safety system unchanged. This means that identification is based on closed loop data. However, the parameters of the PI controllers in the loop are known.

The organization of this paper is as follows: In Section 2 a more detailed description will be given of the turbine and the data acquisition setup. Identification of wind turbine systems is the topic of Section 3. Attention will be paid at the consequences of the presence of controlers in view of the desire to identify the dynamics of the turbine system itself. In Section 4 validation of the DUWECS simulation model is briefly addressed. The paper ends with conclusions in Section 4.

2 Wind turbine systems

This section introduces some aspects of the wind turbine simulation model that is the subject for validation, and the particular wind turbine system which is used to obtain system identification measurements from.

2.1 Physical simulation model

The non linear simulation model that has to be validated with respect to its dynamics is described in Bongers *et al.* (1993), and Bongers (1990). Before its validity will be investigated in Section 4 some comments will be given here on the structure and contents of the model.

A modular structure has been chosen in which each part of the wind turbine system (rotor, transmission, electrical conversion system, and tower) are

modelled separately, each having their own inputs and outputs Fig. 1.

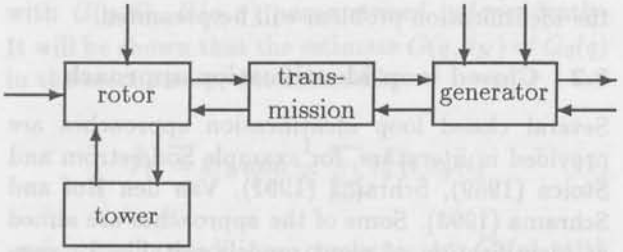

Fig. 1: modular structured simulation model

A model describing the dynamics of the complete wind turbine is then realized by connecting these submodels with each other. For each component different submodels are developed with modeling complexity ranging from simple to extremely complicated.

This setup allows for system case study with easy switching between various submodels and parameter variations. Evaluation of the differences this makes for the behavior of the complete system connects perfectly with the design supportive model useas mentioned in Section 1.

2.2 Experimental set up

The industrial wind turbine which will be used to validate the simulation model behavior with, is part of the PWC wind farm in Sexbierum, Friesland (the Netherlands). The wind turbines in this wind farm are industrial, variable speed, 3-bladed, 310kW machines.

The electrical conversion system consists of a synchronous generator with a rectifier, and inverter DC-link. The field excitation voltage of the synchronous machine and the delay angle of the rectifier can be utilized for control. The rotor has full span blade pitch control. A discussion about which signals can be considered as inputs and outputs will be given in Section 3.

The system is controlled by 4 SISO PI controlers (with known parameters) as can be seen from Fig. 2. The setpoint values for the rotational speed of the generator shaft are generated by block T, which has only very slow dynamics. This closed loop structure and declaration of the signals will be discussed in greater detail in Section 3.

During the experiments normal operation of the wind turbine was continued with the control and safety system unchanged.

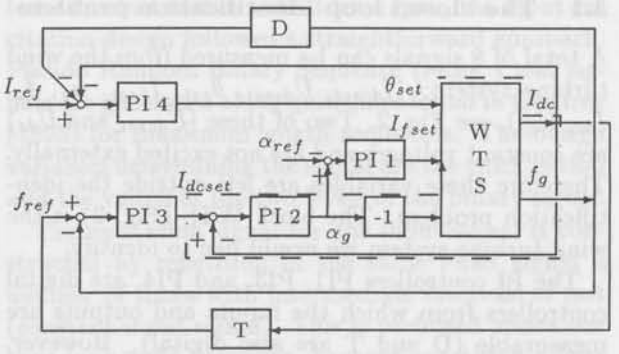

Fig. 2: present closed loop structure of wind turbine system

2.3 Data acquisition

To facilitate the process of designing and performing experiments a portable computer is equipped with data acquisition hardware and software (A/D, D/A, anti-aliasing filters with adjustable cut-off frequency). A patch panel was also configured to customize signals from the wind turbine system to make them suitable for measurement by the PC.

With this setup it is possible to generate test signals within MATLAB (1990), feed these signals to the system through D/A conversion, and measure the response of the system through A/D conversion with a specified sample frequency.

The measurements are directly available in the MATLAB environment. This allows for direct preliminary data analysis and, if necesssary, adjustments of the test signals. Consequently, the time span between the actual experiment and the evaluation of the quality of the measurements can be kept very short. The PC and data acquisition hardware and software is discussed in Huisman (1994)

3 Identification of wind turbine systems

System identification of the wind turbine system, introduced in the previous section, will now be addressed. The situation given in Fig. 2 will first be translated in a general closed loop identification configuration, which obviously involves the selection of inputs and outputs. A two step approach to the closed-loop identification problem at hand will be commented upon. Attention will be given to experiment design, and identification results will be presented.

3.1 The closed loop identification problem

A total of 8 signals can be measured from the wind turbine system: (I_{dcset}, U_{dcset}, θ_{set}, I_{fset}, α_g, f_g, I_{dc}, U_{dc}), see Fig. 2. Two of these (U_{dcset} and U_{dc}) are constant voltages and are not excited externally. Therefore these variables are left outside the identification problem. The block WTS (Fig. 2) is the wind turbine system we would like to identify.

The PI controllers PI1, PI3, and PI4, are digital controllers from which the inputs and outputs are measurable (D and T are also digital). However, PI2 is an anolog PI controller which is unaccessible for the measurement equipment. Therefore this controller is considered to be part of the wind turbine system (indicated by the dashed contour in Fig. 2).

This configuration is reformulated into the following closed loop situation, depicted in Fig. 3.

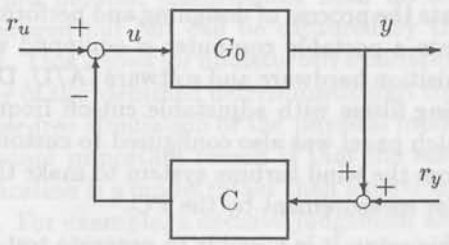

Fig. 3: closed loop situation

The wind turbine system is from now on equivalent to the system G_0, also called the *plant*. The PI controllers are lumped into the *controller* system C. The input vector u and output vector y of the plant are:

$$u = \begin{pmatrix} I_{dcset} \\ \theta_{set} \\ I_{fset} \end{pmatrix} \begin{matrix} : \textit{direct current setpoint} \\ : \textit{pitch angle setpoit} \\ : \textit{field excitation current} \end{matrix}$$

$$y = \begin{pmatrix} \alpha_g \\ f_g \\ I_{dc} \end{pmatrix} \begin{matrix} : \textit{delay angle rectifier} \\ : \textit{generator frequency} \\ : \textit{direct current} \end{matrix}$$

The vectors r_u and r_y indicate the external signals that can be fed into the loop, for example the excitation signals for identification experiments.

In case of a partial load operational condition the blade pitch angle controller PI4 will be fixed and therefore the number of input variables reduces to 2.

The closed loop identification problem boils down to identification of a model of the the plant G_0 based on measurements of the input signals u, the output signals y, which are excited by one of the external signals r_u or r_y. The result is an identified model $\hat{G}$ of the plant. In the next subsection a solution to the identification problem will be presented.

3.2 Closed loop identification approach

Several closed loop identification approaches are provided in literature, for example Söderström and Stoica (1989), Schrama (1991), Van den Hof and Schrama (1993). Some of the approaches are aimed at identification of plant models suitable for controller design or controller enhancement. However, in this paper the purpose of identification is to estimate a reliable open loop model from closed loop data.

In this paper the so called two stage identification method (Van den Hof and Schrama,1993) is applied to deal with the closed loop situation, which will briefly discussed.

Consider a data generating system that is defined as:

$$y(t) = G_0(q)u(t) + H_0(q)e(t) \tag{1}$$

with $H_0(q)e(t)$ the well known noise representation as a filtered white noise. The input signal is determined according to:

$$u(t) = r_u(t) - C(q)y(t) \tag{2}$$

Let us consider the sensitivity function of the closed loop system (1), (2),

$$T_0(q) = [1 + C(q)G_0(q)]^{-1} \tag{3}$$

Using T_0 we can rewrite equations (1), (2):

$$u(t) = T_0(q)r_u(t) - T_0(q)C(q)H_0(q)e(t) \tag{4}$$

$$y(t) = G_0(q)u(t) + H_0(q)e(t) \tag{5}$$

Since r and e are uncorrelated signals, and u and r are available from measurements, it follows from (4) that we can identify the sensitivity function T_0 in an open loop way. By again manipulating equations (4), (5), we can write:

$$u^r(t) := T_0(q)r_u(t) \tag{6}$$

$$y(t) = G_0(q)u^r(t) + \tag{7}$$

$$[I - G_0(q)T_0(q)C(q)]H_0(q)e(t) \tag{8}$$

Since u^r and e are uncorrelated, it follows from (8) that when u^r would be available from measurements, G_0 could be estimated in an open loop way, using the common open-loop techniques. Instead of knowing u^r, we have an estimate of this signal available through

$$\hat{u}^r_N(t) = \hat{T}_0(q)r_u(t) \tag{9}$$

Consider the model structure

$$y(t) = G(q,\theta)\hat{u}_N^r(t) + H(q,\eta)\varepsilon_y(t) \qquad (10)$$

with $G(q,\theta)$, $H(q,\eta)$ parametrized independently. It will be shown that the estimate $G(q,\hat{\theta}_N)$ of $G_0(q)$ in the second step, determined by

$$\hat{\theta}_N = \arg\min_{\theta,\eta} \frac{1}{N}\sum_{t=1}^{N} \varepsilon_y^T(t)\varepsilon_y(t) \qquad (11)$$

under weak conditions converges to $G_0(q)$ with probability 1.

This result is formalized in Van den Hof and Schrama (1993) which also gives the proofs and a characterisation of the bias distribution of the asymptotic model in case undermodelling is accepted.

In both steps of the identification procedure MIMO models will be estimated using the well known prediction error method by Ljung (1987) as implemented in the system identification toolbox of MATLAB .

3.3 Experiment design

Experiment design is aimed at gathering informative measurements from the system. This means that the data should provide enough information to identify accurate models which are suitable for the intended model use.

Several choices need to be made, preferrably in a way that they contribute as much as possible to the information contents in the measurements. However, some choices may be fixed due to practical limitations. For example, the available, measurable signals are fixed. To guarantee an active safety system, experiments are restricted to closed loop situation with the existing PI controllers.

Also the operational condition of the experiment can not be governed by experiment design, because it is just a function of the mean wind speed. We therefore can only hope for the wind speed to have the desired value.

The sample rate and the excitation signals r_u and r_y are the remaining experiment design choices, which are not fixed yet. The sample rate was chosen to be $100Hz$, which should be enough to cover the relevant dynamics (which are not expected to be important beyond $50Hz$). The anti-aliasing fitlers should have cut-off frequency of $50Hz$ or lower.

Since there are no prior measurements available, and experimentation opportunities were scarce and had to be finished within a short time span, the input excitation design followed a straightforward approach. Pseudo Random Binary Sequence (PRBS) test signals are generated along guidelines found in Godfrey (1993) for maximum length sequences. The design variables determining the signal are the clock period and the values of the two levels of the binary signal.

The excitation signal for one input signal is constructed by repetition of the same PRBS signal a number of times with intermediate intervals of rest (constant input signal). This is preferred above one very long PRBS sequence, because repetition allows for averaging the responses to the repeated PRBS , which reduces the noise. Besides, if the mean wind speed changes during one PRBS repetition this interval can be easily rejected and would be useless for identification.

The intervals with no excitation provide information about the free run closed loop dynamics and disturbances, which may be a useful reference for evaluation of how effective the input excitations have been.

The final input signal design shows 5 repetitions of a PRBS with a length of $51,2s$ and intermediate intervals of zero input during $10s$. This results in a typical identification experiment which takes approximately 5 minutes. The PRBS for excitation of I_{dcset} has a clock period of $0.05s$ and amplitude of $0.4V$ while I_{fset} was excited with an amplitude of $0.2V$ and clock period of $0.10s$.

3.4 Results

This subsection will present results which are obtained following the experiment design and identification approach described in the previous subsections. Attention will be focussed on only one transfer function of the multivariable wind turbine system. Similar results are obtained for the other transfer functions of the MIMO plant.

The measurement presented here originated from a partial load operational condition. As mentioned in Section 3.1 this means that the blade pitch controller $PI4$ is saturated which cancels the blade pitch angle as input for the plant.

A fragment of the measurement data is given in Fig. 4.

The 5 repetitions of PRBS excited intervals in the measurement data are already averaged.

The sample rate is reduced to $33Hz$ by decimation with a factor of 3. Therefore identified models describe dynamics up to $16Hz$.

With the two step procedure the quality of the final estimate depends heavily on the accuracy of the first step. Since no difficulties were encountered

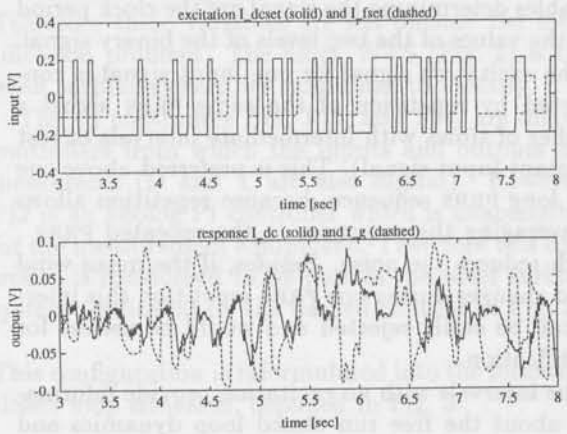

Fig. 4: measurement data: input excitation and output response

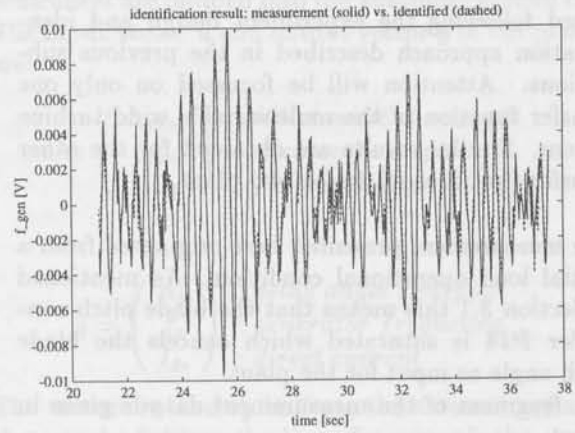

Fig. 5: identification result: measured generator frequency vs. identified model response

in the first step no results of this step are presented.

The second step estimates the plant transfer function. Acceptable models (2 inputs, 3 outputs) with ARX structure of order 7 per entry have been identified.

The transfer function from field excitation current I_{fset} to generator frequency f_g covers important dynamics of the generator system and is therefore very interesting from validation point of view.

The identification result for this transfer function is given in Fig. 5.

This looks good enough to be confident that the identified model represents the real life PWC wind turbine with respect to this input-output behavior. Therefore we can proceed and compare this model to the same transfer function derived from the physical model.

4 Validation of wind turbine system models

Validation is concerned with the question how well a physical model describes some aspects of the real world process. These aspects and the desired accuracy depend strongly on the application of the model once it has been succesfully validated.

Clearly, validation can only be investigated if enough information from the process is available. Referring to the previous section this is not critical here because, in principle, the same requirement needs to be satisfied in order to obtain reliable system identification results.

We would like to evaluate whether or not the physical model is capable of reproducing essentially the same dynamics as identified from the experimental set up. This means that we are satisfied, in first instance, if both models exhibit the same structural behavior in the frequency domain, without demanding a perfect match.

In other words the qualitative validation comes first. Such a structural resemblance affirms that the physical model provides proper modeling of the dynamical phenomena observed from the process.

Only if this stage is reached, it makes sense to adjust parameter values (those which were not completely known or had to be guessed) in the equations governing parts of the physical model. This is done in order to close the gap between the identified and the physical model. In other words the quantitative validation comes second.

In this section the identified transfer function will be compared with the transfer function derived by

linearization of the physical simulation model. In Fig. 4 the result is presented.

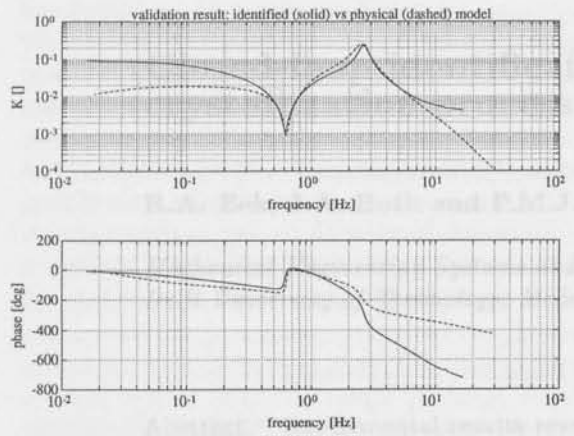

Fig. 6: validation result: transfer I_{fset} to f_g

The comparison is acceptable except for the very low frequencies. The fundamental resonance of the the dive train ($2.6Hz$) as well as the zero at $0.7Hz$ is modelled quite accurately.

The physical model seems to underestimate the low frequency gain, but despite this misfit no essential dynamics are missing in the physical model. It remains an issue for further research to determine whether parameter adjustment is able to bend the physical model towards the identified model. On the other hand it should be investigated how accurate the identified model is for the low frequencies (for example by evaluation of confidence intervals around the frequency response).

A strategy to proceed from here is twofold. The first and most obvious step is to investigate how sensitive the outcome of the simulation model is for slight variations in the physical parameters that are uncertain. The second step is to refine the identification result by design of new closed loop experiments based on the knowledge we have from our first attempt. New external excitation signals could be applied which alows for emphasizing certain frequency regions which are important for the identified model. In principle this could be repeated until the identification result cannot be improved anymore.

Conclusions

Valid physical models describing the dynamics of complete wind turbine systems may be very important. For example, in the design phase of the next generation wind turbine systems.

Due to disturbances induced by the presence of an unknown wind field, this validity is difficult to assess by straigthforward comparison of measurements and model simulation.

System identification helps in splitting the stochastic disturbances from deterministic data revealing dynamics from the process to be validated. In this way, a platform is created for comparison of identified models with models obtained from physical modelling.

This comparison of models allows for decisive answers to the validation problem. For example, frequency responses of both models show directly whether or not the physical model is capable of describing the same dynamics as identified from the plant.

This approach is applied to the identification of an industrial, full scale, wind turbine located in the northern part of the Netherlands.

Due to safety regulations, experiments were restricted to a closed loop situation with existing single loop PI controllers.

The identification followed a two step approach which successfully extracted accurate models of the process from the closed loop data.

Conventional model validation techniques which for example exploit azimuthal binning cannot handle closed loop data and do not result in reliable open loop behavior of the wind turbine system to be validated.

It is demonstrated that the physical model exhibits the same structural behavior as the dynamics which were identified from the wind turbine system. This preliminary validation results encourages to proceed with this approach.

Acknowledgements

The author thanks N.V. SEP for permission to experiment, and Herre van der Meulen explicitly for assistance and cooperation. I also thank Henk Huisman (TUDelft) because his skills and ideas to install and optimize the complete experimental set up, made it possible to finish the measurements just in time.

References

Bongers P.M.M. (1990). *DUWECS User's Guide, Delft University Wind Energy Conversion Simulation Program.* Delft University of Technology, The Netherlands.

Baars G.E. van, P.M.M. Bongers (1992). Flexible wind turbine model validation. *Wind Engineering, 16*, 247-256.

Baars G.E. van, P.M.M. Bongers (1993). System identification serving wind turbine model validation. *Proc. Windpower '93,*San Francisco, California, USA,274-280.

Bongers P.M.M., G.E. van Baars, Sj. Dijkstra, O.H. Bosgra (1993). *Dynamic Models for Wind Turbines.* Delft University, The Netherlands, TUD-MEMT-28, ISBN 90-370-0088-6.

Godfrey K. (1993). *Perturbation Signals for System Identification.* Prentice Hall.

Van den Hof P.M.J., R.J.P. Schrama (1993). An indirect method for transfer function estimation from closed loop data. *Automatica, Vol 28,* no. 6, *1523-1527.*

Huisman, H. (1994). Using a personal computer as a cheap tool for identification and control of wind turbines in the field. *Proc. European Wind Energy Conference EWEC'94,* Thessaloniki, Greece, October 10-14.

Ljung L. (1987). *System Identification: Theory for the User.* Prentice Hall, Inc. Englewood Cliffs, New Jersey.

MATLAB (1989). *Matlab User's Guide.* The Mathworks Inc., South Natick, MA, USA.

Schrama R.J.P. (1991). An open-loop solution to the approximate closed-loop identification problem. In: C. Banyasz, L. Keviczky (Eds.), *Identification and System Param. Estim. 1991.* IFAC Proceedings Series 1992, No. 3, pp. 761-766.

Soderstrom T., P. Stoica (1989). *System Identification.* Prentice Hall.

Selected Topics in Identification, Modelling and Control
Vol. 7, December 1994

Closed-loop identification of a continuous crystallization process

R.A. Eek, J.A. Both and P.M.J. Van den Hof

Mechanical Engineering Systems and Control Group
Delft University of Technology, Mekelweg 2, 2628 CD Delft, The Netherlands.

Abstract. Experimental results reveal that open-loop identification of continuous crystallization processes leads to poor results as the crystal size distribution (CSD) has a tendency to oscillate. Improved experimental conditions are achieved, using a simple single loop feedback controller. Identification of low order models, on the basis of closed-loop data, is studied using a nonlinear first principles (FP) model and linear multivariable input-output models. Two closed-loop identification methods are applied, one of which is recently introduced to provide accurate approximate models. Using the FP model, which includes a population balance and a set of empirical relations related to crystallization kinetics, a high order nonlinear model is obtained. A low order reduced and linearized version of this model is considered as initial model for the estimation of input-output models. Closed-loop identification and validation data is obtained from an evaporative pilot crystallizer. Both identified and physical models are validated in terms of time and frequency domain responses and are shown to provide accurate descriptions of the process dynamics.

Keywords. System identification, orthonormal basis functions, closed-loop experiments, crystallization.

1 Introduction

Crystallization from solution is a well established industrial purification and separation process, in which a solids fraction is derived from a solution. It is applied in continuous operation on a large scale, with production rates exceeding 10^6 tons/year for the production of bulk inorganic materials like sodium chloride, and ammonium-sulphate (a fertilizer), and organic materials like adipic acid (a raw material for nylon). On a small scale, crystallization is often applied batch wise to obtain high purity fine chemicals or pharmaceuticals, e.g. aspartame (a sweetener), and l-ascorbine (vitamin C).

A main characteristic of crystallization processes is that a distribution of differently sized particles is produced, which is characterized by the *crystal size distribution* (CSD). The CSD, is an important parameter as it determines the physical properties of both the wet crystal magma and the dried crystal product in bulk. An inappropriate CSD may result in a reduced performance of down stream solid-liquid separators and may cause caking of the final dried crystal product, yielding transportability and storage problems. In many cases these problems occur when the mean crystal size is low and when an excessive number of small crystals (*fines*) exists in the distribution.

Inappropriate CSD's may exist (temporarily) due to process disturbances, intrinsic physical feedback mechanisms, which can cause cycling of the CSD, and during plant start-up and shutdown. For these reasons the derivation of accurate (low order) dynamic models that can be used for CSD controller design is a major issue.

In the literature, experimental results on identification and control of crystallizers are scarce. This is mainly due to a lack of on-line measurement systems and the absence of reliable experimental e-

quipment, including sampling systems. In De Wolf and Van den Hof (1992), system identification techniques have been applied to estimate low order linear models from crystallization process input-output data directly. Miller and Rawlings (1992) present results on parameter estimation within a first principles model structure, including a method for the estimation of confidence intervals, based on batch crystallization experiments. A review of recent results on identification and control of crystallizers is given by Rawlings (1993).
In earlier work (Eek *et al.*, 1995), results from first principles modelling of continuous crystallizers and the estimation of empirical parameter values on the basis of start-up experiments are presented. The experimental data sets were obtained from the free start-up responses of a pilot crystallizer. Start-up responses are advantageous as they are readily available in historical databases, and give excitation of the process dynamics, without requiring additional external test signals. A main disadvantage, however, is that the resulting process response exhibits only the slow process dynamics within a wide (nonlinear) process output range. In practice, knowledge on the faster dynamics around the bandwidth of the system is important, as closed-loop stability and the performance of the closed-loop system are strongly determined in this frequency range. Another disadvantage is that the data contains no information on the combined effect of simultaneous process input disturbances, which may be important for multivariable controller design.
Therefore, it is desirable to perform multivariable identification experiments were the control relevant process dynamics are deliberately excited with uncorrelated, frequency rich, *test signals* (Ljung, 1987), which are added to the different process inputs simultaneously.

The purpose of this paper is to describe a procedure for the identification of low order dynamic models for the dynamics of a continuous crystallization process on the basis of experimental process input-output data. The intended use of the resulting models is predictive control. As both input-output models and first principles models have specific advantages and disadvantages, we will apply both and discuss their respective merits. In particular, a route will be outlined where a priori, -first principles- model knowledge is applied to obtain an initial estimate for the identification of input-output models.

The sequel of this paper starts with a short description of a first principles model. The results of an open-loop identification experiment are used to indicate the necessity to perform identification in closed-loop. Using a closed-loop controller, that effectively suppresses a prevailing oscillatory mode in the open-loop process, improved experimental conditions are established, A method for consistent model identification in a closed-loop fashion is described, and applied. Finally, estimated input-output models are validated with an independent data set and compared to the linearized and reduced version of the identified first principles model. On the basis of this, conclusions are drawn with respect to the applied identification approach and the validity of black-box and first principles models.

2 Process modelling

The main model assumptions are that the crystallizer is a single stage crystallizer, which is operated continuously, at ideal mixed, and isothermal conditions, and with a constant effective volume. Further it is assumed that the product slurry is removed unclassified, e.g. each particle has the same probability to enter the product discharge line, irrespective of its size. A fines segregation and destruction system is present for the removal of fines from the crystallizer volume. A forward light scattering technique is applied, on-line, to measure CSD dynamics in the main crystallizer volume.
The CSD is characterised by a *population density function* $n(x,t)$, which describes the number of particles per unit of slurry and per crystal size as a function of time. The first principles model that can be derived for this process comprises a first order partial differential equation for the CSD dynamics, an ordinary differential equation for the supersaturation of the mother liquor and several empirical relations for crystallization kinetics and particle classifiers. For details on the model and the process we refer to earlier work (Eek *et al.*, 1995).

2.1 The sensor model

Fraunhofer theory is used to develop a model for the recorded scattered laser light energy as a function of the CSD. The discretized version of this model is written as:

$$y = Hn, \tag{1}$$

with H the sensor model matrix, y the sensor output vector, which contains 31 values, e.g. y_i, $i = 1, \cdots, 31$, for the scattered laser light energy, and n a discrete population density, which is lumped on a finite set of equidistant crystal sizes.
The population density $n(x,t)$ contains information on both the shape of the CSD, and the solids fraction of the produced crystal slurry: $M_t(t) = \rho_c k_v \int_0^\infty n(x,t)x^3 dx$, where k_v is a shape factor and

ρ_c the density of the crystals. Multiplication of M_t with the actual product flow gives the yield of the process in produced solids mass per second. It is found that the total scattered light energy: $y_T = \sum_{i=1}^{31} y_i$, mainly correlates with the slurry density, for which accurate measurements are obtained from the independent density indicator. Therefore, the measured output vector elements y_i, $i = 1, \cdots, 31$, were normalized by subdividing each element with the total scattered energy y_T. The remaining vector, denoted as y_p, thus solely bears information on the shape of the CSD.

For stabilizing control, which we further discuss below, a sensitive parameter is required that is related to the number of fines in the CSD. Using the correlation matrix R of the sensor readings, which is estimated from $\hat{R} = E\{Y^T Y\}$, where E denotes the expected value, and where Y contains n_p output vectors y_p as its rows: $Y^T = \{y_{p1}, y_{p2}, \cdots, y_{pn}\}$, the major and minor directions in the sensor readings can be calculated from the eigenvalue decomposition of the correlation matrix. The following relation holds:

$$\hat{R}\,\Phi = \Phi\,\Lambda, \tag{2}$$

where the n_p columns of Φ: $\{\phi_1, \phi_2, \cdots, \phi_{n_p}\}$ are the non-zero normalized eigenvectors of $\hat{R}$ and Λ contains the n_p corresponding eigenvalues $\{\lambda_1, \lambda_2, \cdots, \lambda_{n_p}\}$ on its diagonal. If the eigenvectors and eigenvalues are sorted, so as to obtain the eigenvalues in decreasing order, the best linear combination of elements in y_p, representing the largest signal energy, is represented by the eigenvector ϕ_1, and the corresponding eigenvalue λ_1 then represents the relative signal energy in this specific signal direction. Clearly, the least significant signal direction is represented by the eigenvector ϕ_{n_p} and the eigenvalue λ_{n_p}. Omitting the least significant signal directions, a reduced representation of the measured output pattern y_p is obtained.

This decomposition is also known as the discrete version of the Karhuenen-Loéve expansion (Fukunage, 1972). Application to the measured light scattering data reveals that already 99.5 percent of the signal energy is grasped by the first 5 signal directions $\{\phi_1, \cdots, \phi_5\}$. It is found that projection of the signal y_p on the first principal signal direction $\{\phi_1\}$, results in a signal (denoted as y_{r1}), that is strongly related to the number density of fines and and has a low signal to noise ration. This signal is chosen as process output parameter as it has excellent properties to serve as an input for a stabilizing controller that acts on the fines removal system.

In addition to this signal the mean crystal size is chosen as an output parameter as it strongly determines the performance of downstream solid liquid separators. This parameter is calculated from the third and fourth moment of the distribution (Randolph and Larson, 1988):

$$X_{43} = \frac{\int_0^\infty n(x)x^4 dx}{\int_0^\infty n(x)x^3 dx} = \frac{m_4}{m_3} \tag{3}$$

When only small perturbations around the stationary distribution are assumed, this relation can be linearized, resulting in:

$$\Delta X_{43} = \frac{m_{4s}}{m_{3s}}\Delta m_4 - \frac{m_{4s}}{m_{3s}^2}\Delta m_3, \tag{4}$$

where m_{3s} and m_{4s} denote stationary moments. Lumping gives:

$$\Delta X_{43} = T_{43}\Delta n \tag{5}$$

with T_{43} a column vector containing the elements $\{a_1, a_2, \cdots, a_n\}$. given by:

$$a_i = \left[\frac{m_{4s}}{m_{3s}}x_i^4 - \frac{m_{4s}}{m_{3s}^2}x_i^3\right]\Delta x \tag{6}$$

Because only y_p is measurable we can calculate ΔX_{43}, (using (1)) from:

$$\Delta X_{43} = T_{43}H^{-1}\Delta y_p = T\Delta y_p. \tag{7}$$

The pseudo inverse H^{-1} is approximated from the singular value decomposition $H = U^T\Sigma^{-1}V$ (Golub and Van Loan, 1983), where the matrices U and V contain the n_u left, and n_v right singular vectors of the sensor model H, respectively, and Σ contains the corresponding singular values. As the matrix H is ill conditioned only the first n_r singular vectors are used in the inversion, which gives the following approximation: $T \approx T_{43}U_r\Sigma_r^{-1}V_r^T$, with $n_r < n_y$. It is found that n_r should be chosen to obtain a trade-off between bias and sensitivity to noise in the reconstructed signal y_p.

In summary, the (open-loop) process, which will be considered for identification, has three inputs and three outputs. A schematic overview is given by Fig. 1. As inputs the fines flow Q_f, the product flow Q_p and the total heat input P_t are taken. As outputs, the number density of fines y_{r1}, the mean crystal size X_{43} and the solids fraction M_t are chosen.

2.2 Derivation of low order linear models

To arrive at a low order linear model, the nonlinear distributed parameter model is lumped, linearized and reduced, consecutively. The reduced linear models can be used for control directly, or

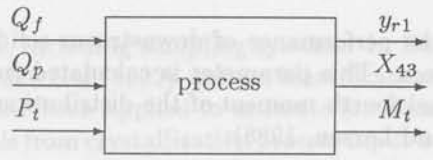

Fig. 1: Block scheme of open-loop process.

serve as an initial model for system identification, as will be described below. As described in Eek, *et al.*(1995b) the linearized model is a high order linear continuous time state-space model, given by:

$$\Delta\dot{z} = F\Delta z + G\Delta u, \qquad z_0 = z_s,$$
$$\Delta y = H\Delta z, \tag{8}$$

where Δ denotes a small perturbation around the stationary solution. For frequency domain analysis and model reduction a 100th order lumped and linearized model is used, while the nonlinear simulation is performed accurately with a 200th order lumped population balance model.

Reduction

A balanced model reduction method is applied to approximate the 100th order linearized state-space model with a low order linear model. The key problem with balanced model reduction is to find a balancing transformation (Moore, 1981). Assuming a linear time invariant state-space model $\{F, G, H\}$, a transformation $\{F, G, H\} \rightarrow \{T^{-1}FT, T^{-1}G, HT\}$ is a balancing transformation, if:

$$T^{-1}PT^{-T} = T^{-1}QT^{-T} = \Sigma, \tag{9}$$

where Σ is a diagonal matrix, containing the so-called Hankel singular values in decreasing order, and P and Q represent the controllability and observability Gramian of the system $\{F, G, H\}$, given by:

$$P = \int_0^\infty \exp^{Ft} GG^T \exp^{F^T t}\, dt \tag{10}$$

$$Q = \int_0^\infty \exp^{F^T t} H^T H \exp^{Ft}\, dt \tag{11}$$

A reduced order model $\{F_R, G_R, H_R\}$ is devised by taking the first n_r columns of T denoted as L and the first n_r rows of T^{-1} denoted as R. The reduced model with order n_r is then given by $\{F_R, G_R, H_R\} = \{LFR, LG, HR\}$.
Several methods can be employed to solve this problem. We used a frequency weighted balanced reduction method which employs a singular value decomposition of the observability and controllability

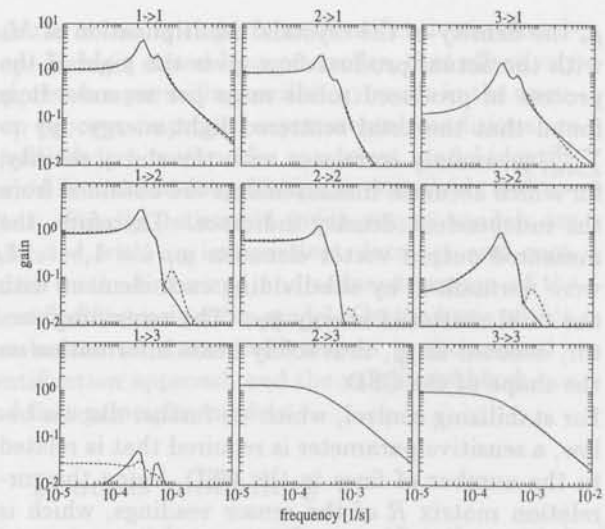

Fig. 2: Comparison of Bode amplitude plots for linear 100th order (solid), and reduced 5th order model (dashed) with i– >j denotes the tranfer relationship of the ith input to the jth output (see Fig. 1).

Gramians. With this method the fit of the reduced model can be favoured in the frequency range, which is relevant for control. It was found that the method is fast and robust, e.g, not sensitive to ill conditioned models. Besides, the algorithms are available as an easy to use Matlab toolbox, (Wortelboer, 1994).
It is found that 4th or 5th order models give good approximations of the process input output behaviour. In Fig. 2 a comparison is made between the Bode amplitude plots of a reduced 5th order and the full 100th order three input, three output model. No frequency weighting is applied in this example.

3 Open-loop plant behaviour

At first, the process dynamics were considered by applying excitation signals directly onto the process inputs, in an open-loop fashion. As test signals multi-sine signals where chosen for the fines removal rate Q_f, and the product removal rate Q_p, each containing 29 logarithmically spaced frequency components, with phase angles chosen according to Schroeder (1970), in order to minize the signal amplitudes. For every frequency in the first signal the second signal has the first harmonic next to it to obtain uncorrelated signals. In Fig. 3 the designed input signals, are depicted. An 45 hours lasting experiment, which will be referred to as RUN35, is performed with the pilot crystallizer. In Fig. 4, the first three signal modes, estimated according to (2), representing already 97.1 percent of the total signal energy, are given.

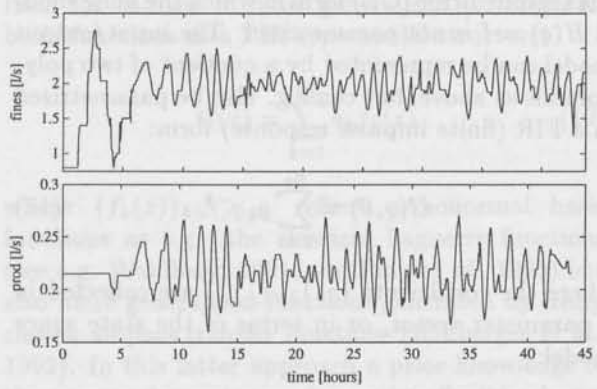

Fig. 3: Sinusoidal excitation signals used for open-loop identification after t>6 hrs, for fines flow Q_f (upper) and product flow Q_p.

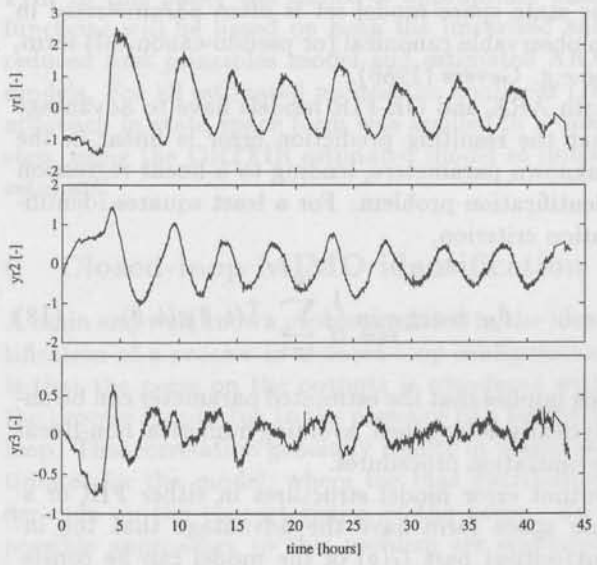

Fig. 4: First major three orthogonal signal components, obtained with open-loop identification; y_{r1} (upper), y_{r2} (middle), y_{r3} (lower).

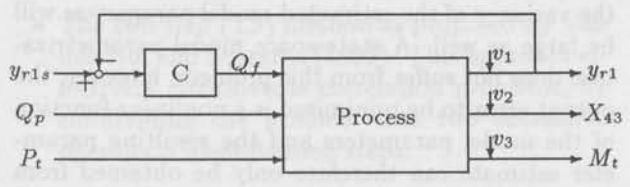

Fig. 5: Block scheme of closed-loop system.

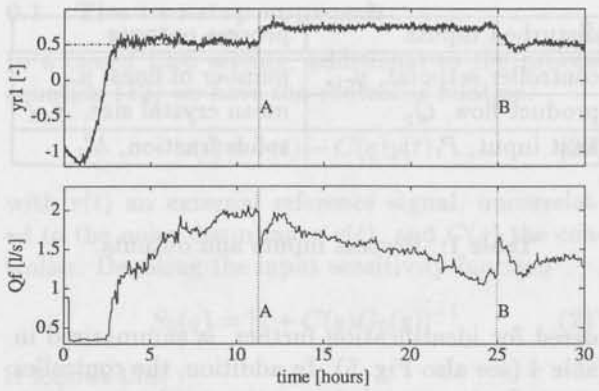

Fig. 6: Closed-loop responses to setpoint changes in y_{r1s} (dash-dotted): y_{r1} (upper) and Q_f (lower) at (A and B).

Visual inspection of the data directly reveals that the process output response is strongly dominated by slow cycling behaviour of the CSD with a time period of approximately 6 hours. Similar observations are reported in (Eek *et al.*, 1995). This behaviour may have been invoked from the non-stationary initial state of the process. From this result it is concluded that for application of a standard linear time invariant approach for process indentification, a closed-loop controller that effectively stabilizes the cycling behaviour is required.

4 Design of a stabilizing controller

Exercises with the nonlinear model revealed that stability of the CSD can easily be obtained by applying a single input single output (SISO) PI-control loop, which uses the weighted number of fines y_{r1} as its input, and the fines removal rate Q_f as its output. The resulting closed-loop control configuration is depicted in Fig. 5. Prior to the first closed-loop identification experiment, the ability of the controller to stabilize the start-up response of the crystallizer, and to follow step wise setpoint changes were evaluated experimentally. In Fig. 6, the responses of the controlled variable y_{r1} together with the manipulated variable Q_f, on the process start-up and two setpoint changes at A and B to the controller setpoint are given. Clearly, the system is stabilized within approximately 5 hours after start-up. Around 17 hours after start-up some unwanted disturbances have occurred in the process, which caused a gradually, ramp like, decrease of the manipulated variable as a function of time. The controlled variable, however, remains on its setpoint. The results indicate that this simple closed-loop configuration effectively dampens open-loop cycling of the CSD. The closed-loop process, which will be con-

disturbed inputs	process outputs
controller setpoint, y_{r1s}	number of fines, y_{r1}
product flow, Q_p	mean crystal size, X_{43}
heat input, P_t	solids fraction, M_t

Table 1: Process inputs and outputs.

sidered for identification further, is summarized in Table 4 (see also Fig. 5). In addition, the controller output Q_f is measured to estimate the open-loop process transfer-functions, following a method that is described in the next section. The signal y_{r1s} is the setpoint for the stabilizing controller, and $v(t)$ is a noise contribution.

5 Identification method

The system identification procedure includes the selection of an appropriate model set and a criterion of fit. On the basis of an informative set of process input-output data, the best model within the set is then searched for that minimizes the chosen criterion.

5.1 Model structures

Following Ljung (1987) the system to be identified is denoted as

$$y(t) = G_0(q)u(t) + v(t) \tag{12}$$

with $u(t)$, $y(t)$ the process input and output, G_0 a linear time-invariant system represented by its transfer function in the shift operator q, and $v(t)$ a stationary stochastic process represented by $v(t) = H_0(q)e_0(t)$. Here H_0 is the stable and stably invertible noise model, and e_0 is a white noise process. A corresponding model of this process is represented by the collection of transfer functions $(G(q,\theta), H(q,\theta))$, parametrized by some unknown parameter θ, and the corresponding one step ahead prediction error is given by:

$$\varepsilon(t,\theta) = H(q,\theta)^{-1}[y(t) - G(q,\theta)u(t)]. \tag{13}$$

The parametrization of the set of models considered $\{(G(q,\theta), H(q,\theta)),\ \theta \in \Theta\}$ can be done in several ways, among which the popular ARX parametrization represented by $G(q,\theta) = A(q,\theta)^{-1}B(q,\theta)$ and $H(q,\theta) = A(q,\theta)^{-1}$ with A, B polynomials in the shift operator q^{-1}, leading to the linear regression form:

$$\varepsilon(t,\theta) = A(q,\theta)y(t) - B(q,\theta)u(t). \tag{14}$$

An alternative way of parametrizing the models is the Output Error (OE) form in which the noise model $H(q) = I$ is not parametrized. The input/output model can be represented by a quotient of two polynomials as above, but can e.g. also be parametrized in a FIR (finite impulse response) form:

$$G(q,\theta) = \sum_{k=1}^{n_b} g_k q^{-k} \tag{15}$$

where the coefficients $\{g_k\}_{k=1,\cdots,n_b}$ are collected in a parameter vector, or in terms of the state space model:

$$x(t+1) = A(\theta)x(t) + B(\theta)u(t) \tag{16}$$

$$y(t) = C(\theta)x(t) + D(\theta)u(t). \tag{17}$$

In the latter form the transfer function $G(z)$ is given by $D+C(zI-A)^{-1}B$. To obtain a unique represenation of the transfer function within the set of models, the state space model set is often parametrized in an observable canonical (or pseudo-canonical) form, see e.g. Gevers (1986).

Both ARX and OE-FIR models have to advantage that the resulting prediction error is linear in the unknown parameters, leading to a linear regression identification problem. For a least squares identification criterion,

$$\hat{\theta}_N = \arg\min_{\theta\in\Theta} \frac{1}{N}\sum_{t=1}^{N} \varepsilon^T(t,\theta)\varepsilon(t,\theta) \tag{18}$$

this implies that the estimated parameter can be analytically determined, avoiding numerical non-linear optimization procedures.

Output error model structures in either FIR or state space form have the advantage that the input/output part $G(q)$ of the model can be consistently identified even if the noise model part $H(q)$ is misspecified, (Ljung, 1987).

However for FIR models the number of parameters to be estimated is generally large, especially when the underlying system dynamics is moderately damped and when the sampling rate is high in relation to the fastest process dynamics. Consequently, the variance of the estimated model parameters will be large as well. A state-space model parametrization does not suffer from this problem, however, the output error to be minimized is a nonlinear function of the model parameters and the resulting parameter estimate can therefore only be obtained from iterative numerical optimization procedures. Especially for high order multivariable process and large data sets the computational burden can be severe, besides possible convergence problems.

As an alternative, recently renewed interest has risen for the use of more generalized (orthogonal) basis functions in a FIR-type model structure:

$$G(z) = \sum_{k=1}^{n_b} b_k f_k(z) \qquad (19)$$

where $\{f_k(z)\}_{k=1,\cdots,\infty}$ reflect orthonormal basis functions as e.g. the classical Laguerre functions (see e.g. Wahlberg, 1991, and Finn *et al.*, 1993) but also more generalized functions generated by freely chosen all-pass transfer functions (Heuberger *et al.*, 1992). In this latter approach a prior knowledge of the process dynamics can be used to flexibly choose the basis functions so as to increase the speed of convergence of the series expansion (19). In this way the number of parameters to be estimated can be kept small, while retaining a high accuracy of the identified model (Van den Hof *et al.*, 1993).
The model structure (19) will be denoted as ORTFIR. In this paper the choice of appropriate basis functions will be based on both the linearized and reduced first principles model and estimated ARX models. For all estimated models the nonlinear OE approach in state space form was applied in a final step, using the ORTFIR estimated model as initial estimate.

6 Closed-loop MIMO identification

A main and well known problem related to the identification of a process in a closed-loop configuration is that the noise on the outputs is correlated with the process inputs due to the presence of a feedback loop. This correlation generally results in biased estimates for the model, where the bias distribution depends on the characteristics of the noise. Two possible approaches to this problem are employed in this paper:

- The direct identification (DI) method. This method fully ignores correlation between inputs and outputs and identifies directly on the basis of closed-loop process input and output data (Söderström and Stoica, 1989).
- The two step (TS) method as proposed by Van den Hof and Schrama (1993). This approach effectively circumvents correlation problems, by subdividing the problem into two successive open-loop identification steps.

Application of the direct approach is straightforward. The TS approach is shortly explained. We refer to Van den Hof and Schrama (1993) for further reading.

6.1 The two step approach

In a closed loop setting, additional to the process equation (12) we have the controller relation:

$$u(t) = r(t) - C(q)y(t) \qquad (20)$$

with $r(t)$ an external reference signal, uncorrelated to the noise disturbance $v(t)$, and $C(q)$ the controller. Denoting the input sensitivity function

$$S_0(q) = [I + C(q)G_0(q)]^{-1} \qquad (21)$$

it follows that

$$u(t) = S_0(q)r(t) - C(q)S_0(q)v(t). \qquad (22)$$

In the first step, using measurement data of $r(t)$ and $u(t)$ one identifies the transfer function S_0. This is an open-loop type of problem as r and v are uncorrelated. Next the estimate $S(q,\hat{\beta})$ is used to reconstruct a noise-free input signal:

$$\hat{u}_r(t) = S(q,\hat{\beta})r(t) \qquad (23)$$

that is used in the second step of the procedure when applying a model structure:

$$\varepsilon(t,\theta) = y(t) - G(q,\theta)\hat{u}_r(t). \qquad (24)$$

It can be shown that, provided the first step in the procedure is performed sufficiently accurate, this method can provide a consistent estimate of the plant dynamics in the second step.
Application to a MIMO process is reported in Van der Klauw *et al.*, (1994).

6.2 Design of a closed-loop experiment

Two closed-loop experiments for identification and successive model validation are performed with the pilot crystallizer. We refer to these experiments as RUN55 and RUN56. All three inputs of the closed-loop process, e.g: y_{r1s}, Q_p, and P_t (see also Fig. 5), have been excited with generalized binary noise sequences (GBN) which are introduced by Tulleken (1991). These signals switch (pseudo-) randomly between two fixed signal levels at discrete points in time. Choosing a switching probability between $0.5 < p < 1$ will provide more excitation in the low frequency range, conversely, choosing $0 < p < 0.5$ will increase the signal energy in the high frequency range. An important advantage of binary noise sequences is that the energy is roughly evenly distributed over the frequency range of interest, hence the maximum signal amplitude is lower. In addition, plant operators are most familiar with step wise or pulse wise signals.
The basic intervals for the GBN signals are chosen 20 minutes. The switching probability was chosen

process input	nominal value	amplitude
setpoint y_{r1s}	0.5 (RUN55), 0.5 (RUN56),	0.25 (RUN55), 0.20 (RUN56),
product flow	0.215, [l/s]	0.035, [l/s]
heat input	120, [KW]	30 , [KW]

Table 2: Nominal values and amplitudes of the GBN test signals.

$p = 0.7$. The real nominal signal values and their amplitudes are given in Table 6.2. From simulation tests it was found that the signal Q_f saturates easily. This problem is reduced by limiting the amplitude of the excitation signal. Moreover, this further legitimates the use GBN signals instead of sinusoidal excitation, which were used for the open-loop experiments.
The GBN signal for used for RUN55 was sufficiently uncorrelated with the signal for RUN56, while its frequency contents are comparable. For both experiments, a duration of 50 hours was chosen. This value roughly equals 8 times the dominant time constant in the system. The identification method is evaluated with input-output data generated with a low order linear model, which is derived from the simulation model. Using the designed input signals for RUN55, reveals that the original model can be recovered from the simulation data.

Data preprocessing

Proper treatment of the data, prior to the estimation of parameters, is a necessity to obtain consistent identification results (Ljung, 1987). The raw process data consists of measured values for the density recorded from the independent density sensor, with a sample time of 10 seconds, and the scattered light energy vectors, which are sampled with a frequency of 1 minute. The raw scattered light intensity vectors are averaged values from batches of 1000 sweeps each, which are recorded from the detector in approximately 5 seconds.
All scattered light energy patterns were corrected for the signal background (Eek *et al.*, 1995). The recorded light diffraction patterns are normalized by subdividing each element by the total scattered light energy. Signal outliers are removed by linear interpolation between good measurements that neighbour outliers. The fines density y_1 and the mean crystal size X_{43} are estimated from the normalized diffraction patterns, according to the method described above. All input and output signals are detrended. Finally, all detrended input and output signals are scaled to obtain an equal signal energy in terms of the signal 2-norm, and the sampling rate is decimated with a factor 5, to 1 sample per 5 minutes. The resulting set of 3 input and 3 output signals, each containing 600 data points, is described in Table 4.

Model verification

A model verification step is included to judge whether the estimated models are sufficiently accurate. Model verification is done in the time and frequency domain on the basis of the independent data set (RUN55). A scalar measure, denoted as the relative mean square (RMS) value is evaluated for assessing the quality of fit. This measure is calculated from:

$$RMS_i = \sqrt{\frac{\sum_{k=1}^{N}(y_i(k) - \hat{y}_i(k)) \times (y_i(k) - \hat{y}_i(k))}{\sum_{k=1}^{N} y_i(k) y_i(k)}} \tag{25}$$

with $\hat{y}$ the noise free simulated output and y the measured output.
In the frequency domain, models can be compared using their Bode amplitude and phase plots. In addition, the Bode plot may be compared to the empirical transfer-function estimate (ETFE), which is estimated from the input-output data directly. As discussed by Ljung (1987), interpretation of the ETFE should be done with care. From a simulation exercise we found that due to a low number (600) of data points in our input-output data set, a large bias in the low frequency range exists. This bias can be reduced to a certain extent by applying a narrow frequency window, however, at the expense of an increased variance in the estimate (see also Ljung, 1987).

7 Results and discussion

The excitation signals presented in the previous section were applied to identify the dynamics of the open-loop process, on the basis of closed-loop data. The data from RUN56 will be used for identification and of RUN55 for validation. During the validation experiment (RUN55) a relatively large density of inert gas bubbles were observed in the solution, due to air leakage into the (vacuum) crystallizer. As these bubbles are observed as particles by the sensor, the observed process trends are likely to be corrupted by this non quantified disturbance.

7.1 Results direct identification

Three state-space models in canonical observability form, with order 3, 4 and 5, were estimated directly on the basis of the input-output data from RUN56. Also an initial state and an offset were estimated,

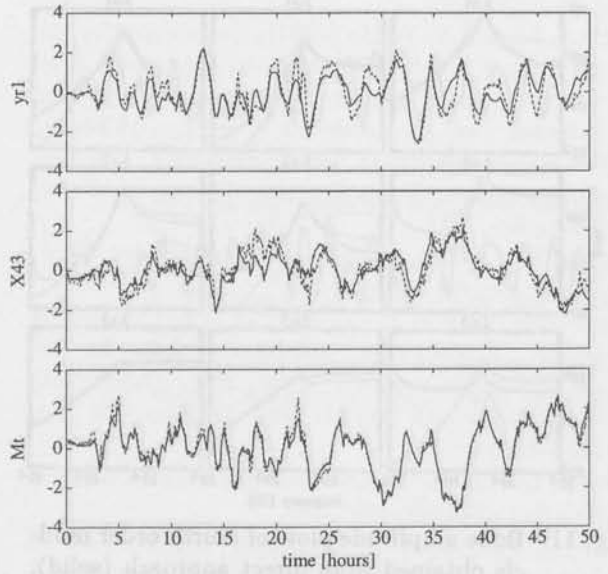

Fig. 7: Identification results of fourth order model (solid) estimated with direct identification method on data from RUN56 (dashed); fines density y_{r1} (upper), mean crystal size X_{43} (middle) and solids fraction M_t (lower).

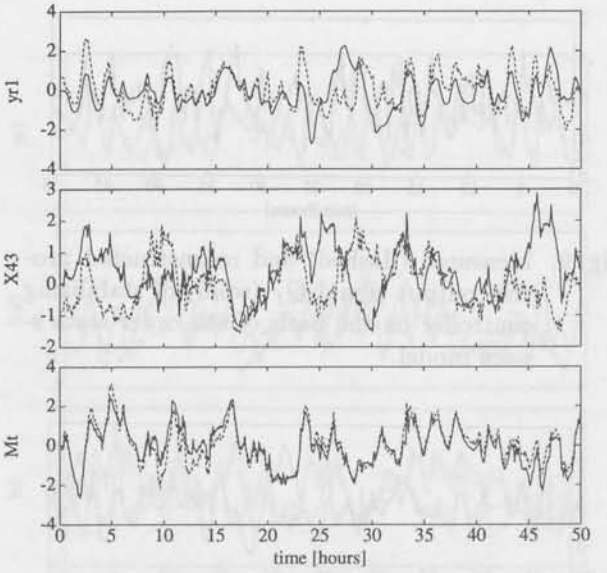

Fig. 8: Validation results of fourth order model (solid), estimated with direct identification on data from RUN56 (dashed), with uncorrelated data from RUN55; fines density y_{r1} (upper), mean crystal size X_{43} (middle) and solids fraction M_t (lower).

while the direct coupling matrix D in (17) was kept zero, hence in total 24, 31, and 38 parameters were estimated, respectively, on the basis of 600 input-output samples. The RMS values of the estimated models, for both the identification (denoted with "idf") and the validation (denoted as "val") experiment, are given in Table 7.3. The consistency of the model is checked by adding the (known) stabilizing feedback controller again to the estimated open-loop model and simulate the output response successively on the basis of the three (GBN) test signals. The resulting RMS values (denoted as "cl") are also provided in Table 7.3.

Checking the RMS values reveals that the fourth order model gives the best fit. In Fig. 7 and Fig. 8 the fit of this model on both the identification and the validation data set are given, respectively. Note that the first portion of the simulated signal trend in Fig. 8 is biased as the initial model state was kept zero.

The results show that reasonable fits are obtained. However, in the validation data set some large deviations are present. In particular in between 24 and 32 hours large deviations exist. As mentioned above, these deviations may be due to process disturbances, and the non-stationary initial state as well.

7.2 Results two step identification

Application of the first step of the two step identification procedure resulted in a 6th order state-space model in canonical observability form, for the input sensitivity model (21). Note that all three inputs of the process (see Fig. 5) had to be used in this step as all three affect the input Q_f. The known value for the proportional action of the controller was used to determine the coupling matrix D a priori. Also an initial state is estimated. With the sensitivity model a noise free output signal for the stabilizing controller is simulated. The measured and reconstructed output signal of the controller are given in Fig. 9. The RMS value corresponding to this fit is 0.25. This plots elucidates that the difference between the reconstructed and the measured controller output signal are small. This, however, does not necessarily imply that the result of the second step is equal to the result of the direct identification step. Below Bode plots of the estimated transfer functions are used to explore this difference further.

In the second step, again 3rd, 4th, and 5th order state-space models in canonical observability form were estimated in an open-loop fashion. However, for the controller output Q_f, the reconstructed controller output $\hat{u}_c$, which is obtained from the first step, is used. An initial state and an offset were also estimated, while the matrix D was kept zero.

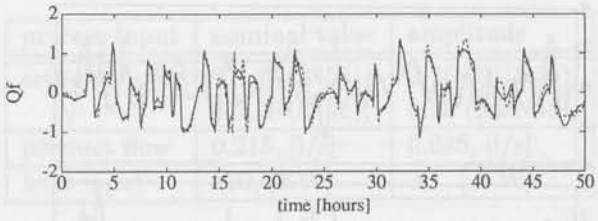

Fig. 9: Measured (dashed) and reconstructed process output signal Q_f (solid) of stabilizing controller on the basis of 6th order state space model.

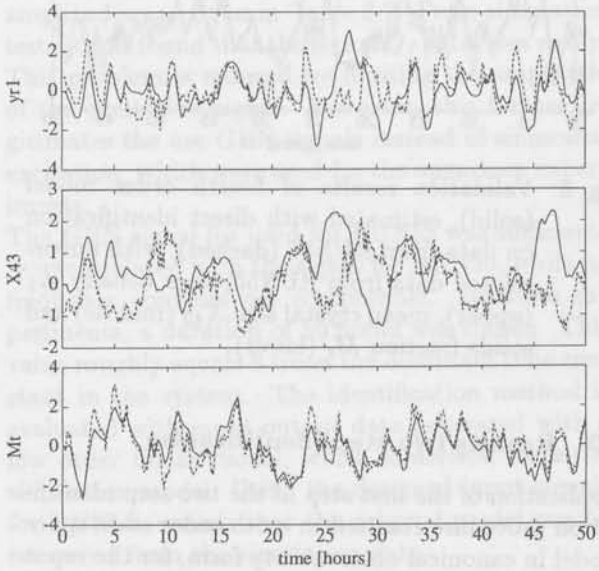

Fig. 10: Validation results of fourth order model (solid) estimated with 2 steps identification method on data from RUN55 (dashed), with uncorrelated data from RUN56; fines density y_{r1} (upper), mean crystal size X_{43} (middle) and solids fraction M_t (lower).

The RMS values of the residuals of the different models for both data sets are given in Table 7.3. Also for this model the estimated open-loop model is simulated in closed loop on the basis of the excitation signals. The resulting RMS values are also provided in Table 7.3. Also for this case a fourth order model seems to provide the best estimate of the open-loop process dynamics. The fit on the identification set strongly resembles the fit obtained with the direct approach. In Fig. 10, the fits on the validation sets are given At first hand, the RMS values and the time domain fits reveal a small difference between the DI and the TS model. However, if we compare the Bode plots of these models given in Fig. 11, a clear difference is observed, mainly in the region of high frequencies. The deviation of the DI model from the TS model exist mainly due to the

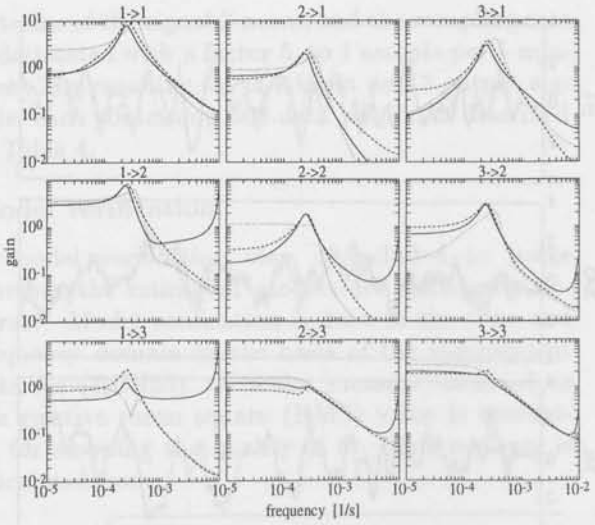

Fig. 11: Bode amplitude plots of fourth order models obtained from direct approach (solid), the two step approach (dashed), and the first principles model (dotted), with i− >j denoting the tranfer relationship of the ith input to the jth output (see Fig. 1).

existence of a correlation in the noise between the input-output signals used in the DI approach. This result confirms the importance of using the proposed TS approach instead of the DI approach.

7.3 Validation of the non-linear process model

One of the reasons for application of system identification was to obtain data for the evaluation of the nonlinear process model. The nonlinear process model was fitted on the data of RUN56 according to a method described in Eek *et al.*, (1995). The results showed that the model error was not sensitive to the model parameters $p_1, \cdots, p_{10}$, except the parameter p_3, which describes the constant nucleation rate. This parameter was adapted only slightly to improve the fit on the data.

From the nonlinear model 3rd, 4th and 5th order models were derived, according to the described method. The fits of the optimized nonlinear model and the reduced 4th order model on the identification data are given in Fig. 12 and on the validation data (RUN55) in Fig. 13. The RMS values of the output errors of the different models are provided in Table 7.3.

The fit on the output y_{r1} is better then the fit on output X_{43}. The latter exhibits a less regular response on the input excitation then the real process trend. Probably a dispersion effect that smoothens the particle waves when transported (by growth) over the crystal size domain is responsible for this.

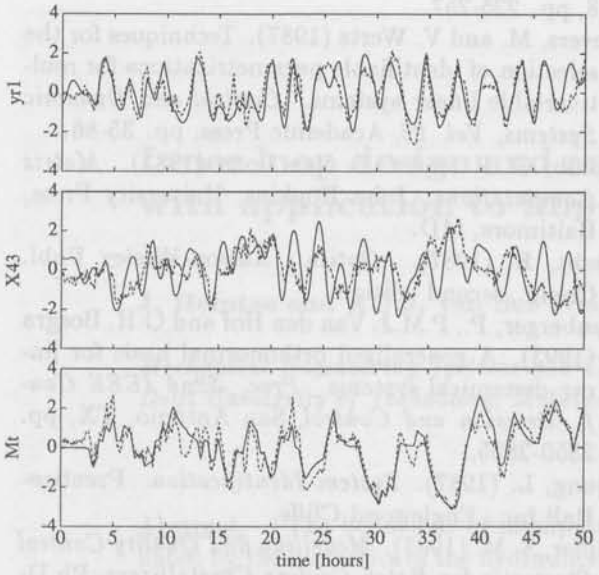

Fig. 12: Fit of nonlinear process model (solid) on measured data of RUN56 (dashed); fines density y_{r1} (upper), mean crystal size X_{43} (middle) and solids fraction M_t (lower).

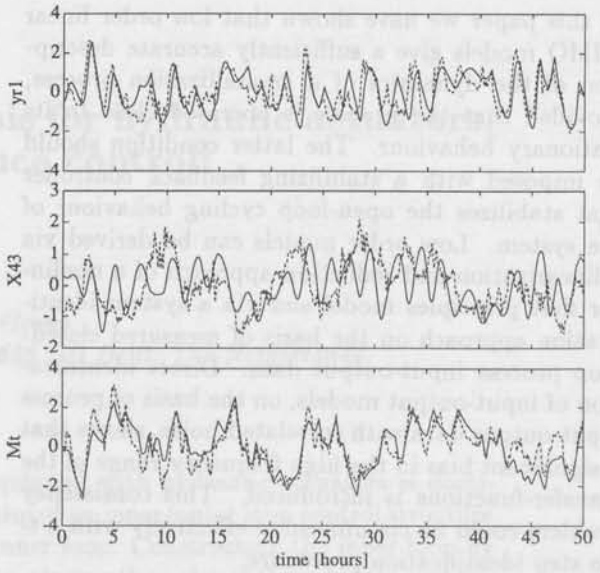

Fig. 13: Validation of full nonlinear process model (solid) on measured data of RUN55 (dashed); fines density y_{r1} (upper), mean crystal size X_{43} (middle) and solids fraction M_t (lower).

The dynamics of the solids fraction M_t is described with approximately the same accuracy as the input-output model. On the basis of the identification data set the first principles model does not perform significantly worse or better then the identified model. However, on the independent validation data set the nonlinear model performs significantly better.

In Fig. 11 also the Bode plot of a fourth order model obtained by linearizing and reducing the nonlinear model is added as a dotted line. As can be concluded also the linearized first principles model gives a reasonable fit on the data. The dynamics are reasonably comparable however the static gain differs from the identified models. It may be expected that the physical model gives a better description of the low order dynamics in the system then the black-box model. However, it should be noted that a proper estimate of the static gain is less important for most control applications as most controllers will have integral action which tailors the process outputs to a zero static deviation at infinite time.

As the first principles model also contains significantly less unknown parameters, less informative process data is needed, hence the method suits the industrial requirements better. Further improvement of the first principles model can be attained by incorporating models for mixing, and improved models for forward light scattering.

	RMS1			RMS2			RMS3		
	DI	TS	FP	DI	TS	FP	DI	TS	FP
	third order model								
idf	0.52	0.54	1.08	0.59	0.56	1.00	0.28	0.28	0.42
cl	0.57	0.55	1.22	0.78	0.92	1.11	0.30	0.32	0.47
val	1.00	1.10	1.11	1.29	1.52	1.22	0.50	0.55	0.65
	fourth order model								
idf	0.52	0.47	1.16	0.51	0.52	0.92	0.20	0.28	0.46
cl	0.57	0.50	1.66	0.86	0.86	0.98	0.24	0.29	0.46
val	0.99	1.13	1.15	1.40	1.42	1.25	0.42	0.49	0.63
	fifth order model								
idf	0.45	0.45	1.14	0.51	0.46	1.06	0.29	0.27	0.43
cl	0.51	0.46	1.26	0.94	0.67	1.22	0.44	0.33	0.48
val	0.96	1.24	1.21	1.26	1.59	1.40	0.52	0.58	0.63
	nonlinear model								
idf	0.65			1.17			0.46		
val	0.82			1.08			0.58		

Table 3: RMS values for y_{r1} (RMS1), X_{43} (RMS2) and M_t (RMS3), of directly estimated models (DI), the two-step approach (TS) and the first principles model (FP), on the basis of identification data (idf), identification data with the model in closed-loop (cl), and validation data (val).

Conclusions

In this paper we have shown that low order linear MIMO models give a sufficiently accurate description of the dynamics of a crystallization process, provided that the process is operated close to its stationary behaviour. The latter condition should be imposed with a stabilizing feedback controller that stabilizes the open-loop cycling behaviour of the system. Low order models can be derived via a linearization and reduction approach of a nonlinear first principles model and via a system identification approach on the basis of measured closed-loop process input-output data. Direct identification of input-output models, on the basis of process input-output data with correlated noise, shows that a significant bias in the high frequency range of the transfer-functions is introduced. This consistency problem could be circumvented effectively with a two step identification procedure.

Validation of the estimated models with an independent data set, shows that the nonlinear first principles model gives the best fit. The difference with the low order linear input-output models is, however, small.

Acknowledgements

The authors are indebted to Raymond de Callofon, and to the Dutch Foundation of Technology (STW), AKZO, DOW Chemicals, DSM, E.I. DuPont de Nemours, and Eastman Chemical Company for their financial support of the UNIAK research program.

References

De Wolf, S. and P.M.J. Van den Hof (1992). Identification of a pilot plant crystallization process with output error methods. In: C. Banyasz and L. Keviczky (Eds.), *Identif. and System Param. Estim. 1991. IFAC Symp. Series 1992, No. 3*, Pergamon Press, Oxford, UK, pp. 133-138.

Eek, R. A., Sj. Dijkstra and G.M. van Rosmalen (1995). Dynamic modeling of suspension crystallizers, using experimental process data. To appear in *AIChE Journal*.

Eek, R. A., H.A.A. Pouw and O.H. Bosgra (1995b). Design and experimental evaluation of stabilizing feedback controllers for continuous crystallizers. *Powder Technology*, February 1995.

Finn, C. K., B. Wahlberg and B.E. Ydstie (1993). Constrained predictive control using orthogonal expansions. *AIChE Journal, Vol. 39*, No. 11, pp. 1810-1826.

Fukunage, K. (1972). *Introduction to Statistical Pattern Recognition.* Academic Press, Chapter 8, pp. 225-257.

Gevers, M. and V. Wertz (1987). Techniques for the selection of identifiable parametrizations for multivariable linear systems. *Control and Dynamic Systems, Vol. 26*, Academic Press, pp. 35-86.

Golub, G. H. and C.F. Van Loan (1983). *Matrix Computations.* John Hopkins, University Press, Baltimore, MD.

Hecht, E. (1987). *Optics.* Adison-Wesley Publ. Comp., second edition.

Heuberger, P., P.M.J. Van den Hof and O.H. Bosgra (1993). A generalized orthonormal basis for linear dynamical systems. *Proc. 32nd IEEE Conf. Decision and Control*, San Antonio, TX, pp. 2850-2855.

Ljung, L. (1987). *System Identification.* Prentice-Hall Inc., Englewood Cliffs.

Miller, S. M. (1993). *Modelling and Quality Control Strategies for Batch Cooling Crystallizers.* Ph.D-Thesis, University of Texas, Austin.

Moore, B. C. (1981). Principal component analysis in linear systems: controllability, observability, and model reduction. *IEEE Trans. Automat. Contr. AC-26*, pp. 17-32.

Rawlings, J. B., S.M. Miller and W.B. Witkowski (1993). Model identification and control of solution crystallization processes: a review. *Ind. Eng. Chem. Res., Vol. 32*, pp. 1275-1290.

Söderström, T. and P. Stoica (1989). *System Identification.* Prentice Hall, Hemel Hempstead, UK.

Tulleken, H. J. A. F. (1990). Generalized binary noise test-signal concepts for improved identification-experiment design. *Automatica, Vol. 25*, No. 1, pp. 37-49.

Van den Hof, P. M. J. and R.J.P. Schrama (1993). An indirect method for transfer function estimation from closed loop data. *Automatica, Vol. 29*, No. 6, pp. 1523-1527.

Van den Hof, P. M. J., P.S.C. Heuberger and J. Bokor (1993). Identification with generalized orthonormal basis functions - statistical analysis and error bounds. *Prepr. 10th IFAC Symp. System Identification*, Copenhagen, Denmark, Vol. 3, pp. 207-212.

Van der Klauw, A. C., G.E. van Ingen, A. van Rhijn, *et al.*(1994). Closed-loop identification of a distillation column. *Proc. 3rd IEEE Conf. Comp. Control Applic.*, Glasgow, UK.

Wahlberg, B. (1991). System identification using Laguerre models. *IEEE Trans. Autom. Control, AC-36*, pp. 551-562.

Wortelboer, P. M. R. (1994). *Frequency-Weighted Balanced Reduction of Closed-Loop Mechanical Servo-Systems: Theory and Tools.* Ph.D-Thesis, Delft University of Technology, The Netherlands.

Selected Topics in Identification, Modelling and Control
Vol. 7, December 1994

Inner loop design and analysis for hydraulic actuators, with application to impedance control[‡]

J. Heintze and A.J.J. van der Weiden

Mechanical Engineering Systems and Control Group
Delft University of Technology, Mekelweg 2, 2628 CD Delft, The Netherlands.

Abstract. The behaviour of manipulators equipped with hydraulic actuators is dominated by the dynamics of the hydraulics. The aim of an inner/outer loop control structure is to mask these hydraulic dynamics with an inner loop. Constructing the inner loop by using the inverse of the actuator dynamics, or by placing the poles of the actuator system, is fundamentally different. An analysis of these two options concludes that a pole placement is the best choice. First results of an actual implementation of a proposed method on an industrial hydraulic drive system, shows the practical relevance of this controller.

Keywords. hydraulic rotary servo system, cascade Δp control, theoretical analysis, impedance control, experimental application

1 Introduction

Although most industrial robots are equipped with electrical actuators, in some occasions it is preferable to use hydraulic actuators. These are situations in which big loads have to be handled and available space for construction is limited (due to the excellent rate of dimension to delivered torque), or long linear strokes have to be realised (flight simulator systems). Generally speaking, these are direct drive situations with severe specifications on load, speed and/or accuracy.

An example is a Brick Laying Robot which is developed in cooperation with industry[1]. Target specifications for the design did include: a pay load of 100 kg, large range of operation (a circular sector of 1.4 rad with radius of 2.2 meters), transportation of the load within 3 seconds anywhere in the range of operation with 2-3 mm position accuracy. In addition the manipulator has to operate on a platform (diameter 2.8 meter) supported by a telescopic mast. Therefore severe limitations in size and weight of the manipulator where imposed.

One of the main differences between electrically driven robots and hydraulically driven robots, and subsequently the applied model based control design, is the significant presence of the actuator dynamics. In most of the control literature on (electrically driven) robots, actuator dynamics are not taken into account, e.g. Khosla (1990) and Whitney (1987). Hydraulic actuators do exhibit lightly damped dynamics. As these dynamics often dominate the behaviour of the manipulator, special attention for the hydraulic drive system is necessary (Heintze *et al.*, 1993).

To perform model based control design for nonlinear systems such as manipulators, techniques such as feedback linearization are often used. For example the well known Computed Torque technique (e.g. An *et al.* (1988)) is a feedback linearization method. Such a feedback linearization technique uses in some sense the inverse dynamics of the system (Slotine and Li, 1991). In case the model used at the control design is not an exact description of reality, the method hardly gives a clue about robustness. Especially in case of lightly damped systems (as hydraulically driven manipulators are), robustness problems can be expected (Boer, 1992).

[‡]This paper is also presented at the 4th IFAC Symposium on Robot Control, September 19-21, 1994, Capri, Italy.

[1]Eureka EU 377 FAMOS BRICK, Highly Flexible Automated and Integrated Brick Laying System.

The Brick Laying Robot in the hydraulic laboratory of the Mechanical Engineering Systems and Control Group, Delft University of Technology, is equipped with standard industrial hydraulic actuators and valves. This means: safety features in the hydraulic circuit, varying (Coulomb) friction due to industrial seals, uncertain internal leakage flow due to limited accuracy of construction and bearings, standard quality valves with uncertain behaviour (dynamic as well as static) in the centre position (which is exactly the range of operation in case of high precision positioning). Due to these difficult to describe phenomena, it is hard to produce an accurate model, which motivates the analysis in this paper.

In order to focus complete upon the dynamics of a hydraulic actuator, the analysis is performed for the one degree of freedom situation; an industrial hydraulic rotary vane actuator with an attached inertia.

First a short description of the model of the hydraulic system is given in section 2. In section 3 some comments are given regarding the division in inner and outer loop control. Section 4 is the main part of the paper, the theoretical analysis of the inner loop. Preliminary experimental results in section 5 will show the practical validity of a proposed method. Conclusions will conclude this paper.

2 Hydraulic actuator model

A short summary of the equations which describe a hydraulic rotary vane actuator with valve will be given. Detailed information concerning modelling and identification of these type of actuators can be found in Heintze *et al.* (1993).

The equation that describes the dynamic behaviour of the hydraulics is (with $s = \frac{d}{dt}$):

$$\Delta p\,(s + k_3) = -k_1 \dot{q}_a + k_2 i_{sc}\sqrt{1 \pm \Delta p} \qquad (1)$$

Δp is the pressure difference in the actuator, normalized with respect to the supply pressure given by the the pump, q_a is the actuator position in $[rad]$ (the dot means the time derivative), i_{sc} is the valve steering signal, normalized with respect to the maximum valve steering. $k_1 = F\Psi(q_a)$, $k_2 = \dot{q}_{max}k_1$, $k_3 = LP_v k_2$ ($k_1,\ k_2 > 0,\ k_3 \geq 0$). F is a constant depending upon the oil compressibility and the pressure delivered by the pump, $\Psi(q_a)$ is an position dependent parameter, $\dot{q}_{max}$ is the maximum achievable velocity of the actuator (reflecting the valve dimension in relation to the dimension of the actuator), and LP_v is a parameter concerning leakage flow inside the actuator. The position dependent parameters $k_{1,2,3}$ can be regarded as constants in one operational point. The term $\sqrt{1 \pm \Delta p}$ is due to the pressure dependency of the valve and can be regarded as an input nonlinearity, the ($\pm$) sign being opposite to the sign of i_{sc}.

The mechanical part of the model due to the load can be described by:

$$\begin{bmatrix} \dot{q}_a \\ \ddot{q}_a \end{bmatrix} = \begin{bmatrix} 0 & 1 \\ 0 & \frac{-w}{J_a} \end{bmatrix} \begin{bmatrix} q_a \\ \dot{q}_a \end{bmatrix} + \begin{bmatrix} 0 \\ \ddot{q}_{max} \end{bmatrix} \Delta p + \begin{bmatrix} 0 \\ \frac{1}{J_a} \end{bmatrix} (T_e + T_c) \qquad (2)$$

J_a in $[kgm^2]$ is the inertia attached to the actuator, w in $[Nms]$ is the viscous friction coefficient, $\ddot{q}_{max}$ in $[rad/s^2]$ is the maximum achievable acceleration of the actuator and reflects the dimension of the actuator in relation to the load attached to it, T_e in $[Nm]$ is the external torque, and T_c in $[Nm]$ is the Coulomb friction and/or stiction torque. The friction torque T_c is modelled as a constant torque during movement (opposing the direction of movement), and a varying 'stiction torque' during standstill, similar as described in e.g. Southward *et al.* (1991). The transfer function of only the mechanical part of the actuator is then given by:

$$\frac{q_a}{\Delta p} = \frac{\ddot{q}_{max}}{s\left(s + \frac{w}{J_a}\right)} \qquad (3)$$

Combining equations (1) and (2) the following description of the total actuator is obtained:

$$\begin{bmatrix} \dot{q}_a \\ \Delta p \end{bmatrix} = \frac{1}{OP} \begin{bmatrix} \ddot{q}_{max}k_2\sqrt{1 \pm \Delta p} & \frac{s+k_3}{J_a} \\ \left(s + \frac{w}{J_a}\right) k_2\sqrt{1 \pm \Delta p} & \frac{-k_1}{J_a} \end{bmatrix} \begin{bmatrix} i_{sc} \\ T_e + T_c \end{bmatrix} \qquad (4)$$

With $OP = s^2 + \left(\frac{w}{J_a} + k_3\right)s + \left(\frac{w}{J_a}k_3 + \ddot{q}_{max}k_1\right)$, the open loop characteristic polynomial. Taking q_a as output results in a third order model from steering current (i_{sc}) to position (q_a). The dynamics are then described by an integrator in series with a second order system, well-nigh always badly damped.

In the modelling process, we have made the following assumptions: 1] symmetrical actuator, 2] symmetrical critical-centre valve with turbulent oil flow and no valve dynamics, 3] laminar leakage flow, and 4] the mean pressure in each compartment is half the supply pressure. These are quite standard assumptions, see e.g. Viersma (1990). When modelling a linear hydraulic actuator, angular position and inertia transform into distance and mass respectively.

3 The inner/outer loop concept for hydraulically driven manipulators

Feedback linearization techniques, for example applied to nonlinear systems as manipulators, often

result in a so called inner/outer controller scheme. The inner loop used for the feedback linearization, transforms the dynamics of the manipulator to a set of SISO not coupled integrators. The outer loop is used to place the poles of the linear system, such that the desired controlled behaviour is obtained, regardless of the original manipulator dynamics (Slotine and Li, 1991). For example Computed Torque control (An *et al.*, 1988) is according to this concept.

With similar reasoning, an inner loop for hydraulic actuators can be used in order to mask the dynamics due to the hydraulic part of the system, and then an outer loop can be used to control the dynamics due to the mechanical part of the manipulator. This outer loop itself is also possibly composed of two parts: a (second inner) loop which for example performs a feedback linearization of the nonlinear dynamical behaviour of the mechanical part of the manipulator, and a (linear) outer loop designed such that a specific required behaviour of the by now totally feedback linearized system is obtained.

Although the primary interest is in the design and analysis of an inner loop specific for hydraulic actuators, an outer loop need to be chosen in order to have a fully controlled system when performing tests. As the inner/outer loop control strategy also fits for impedance control (Anderson and Spong, 1988), the outer loop controller is chosen to be of this kind.

Impedance control as described in Hogan (1985) aims at realizing a behaviour at the end effector of a manipulator such that this manipulator appears to be a passive system, in case of interaction of the end effector with an environment. Within a impedance control design method, there are free to choose design parameters which are directly characterizing the dynamics of this passive system, the so called target impedance.

Opting for a simple linear second order target impedance in the non contact situation only, i.e. an inertia, rotary damper and spring system, gives the outer loop control law:

$$\ddot{q}_t = \frac{K_t}{J_t}(q_0 - q_a) + \frac{B_t}{J_t}(\dot{q}_0 - \dot{q}_a) + \frac{T_{int}}{J_t} \qquad (5)$$

where J_t in $[kgm^2]$ is the target inertia, B_t in $[kgm^2/s]$ is the target damping, K_t in $[kgm^2/s^2]$ is the target stiffness, $q_0, \dot{q}_0$ are the reference position and velocity in $[rad], [rad/s]$, $q_a, \dot{q}_a$ are the actuator position and velocity, $\ddot{q}_t$ in $[rad/s^2]$ is the target actuator-acceleration, and T_{int} in $[Nm]$ is the interaction torque. $T_{int} = 0$ in this paper. The outcome $\ddot{q}_t$ of the outer loop (5) is the reference for an inner loop.

The above outer loop requires in principle the availability of the acceleration signal of the mechanical system, which can be considered as a severe handicap for practical application. However, the Δp signal is easy to measure in a hydraulic actuator, and is related to the acceleration by equation (2). Therefore the following target pressure difference is proposed:

$$\Delta p_t = \frac{\ddot{q}_t + \frac{w}{J_a}\dot{q}_a - \frac{1}{J_a}(T_e + T_c)}{\ddot{q}_{max}} \qquad (6)$$

where $(T_e + T_c)$ is the summation of a known or measured external torque, and a measured or estimated friction torque (for friction compensation). Although the non contact situation is examined, and no attempt to friction compensation is made, this term is included in the subsequent analysis to maintain a general setting. Equation (6) can be regarded as a 'second inner loop' as introduced above. In the next section the 'first inner loop' is introduced, followed by the main part of this paper: the analysis of this inner loop.

4 Inner loop analysis

The objective of the first inner loop (in the remainder simply called the inner loop) is to track the requested Δp_t as good as possible, such that the dynamics of the hydraulics will not disturb the overall behaviour of the manipulator. Two options for this problem will be treated.

One solution to this problem is to make the hydraulic dynamics fast by means of a cascade Δp controller, another solution is using the inverse dynamics of the hydraulics.

4.1 Introduction and first analysis of the inner loop

Cascade Δp controller

The basic idea of cascade Δp control is a direct feedback of $(\Delta p_t - \Delta p)$. In addition there is foreseen in a compensation of the valve signal due to the velocity present in the system[2], giving a controller of the form

$$i_{sc} = K_c\,(\Delta p_t - \Delta p) + K_v \dot{q}_a$$

This basic scheme was already used in Sepehri *et al.* (1990) (with K_c and K_v both constants), 'cascaded' with a Self-Tuning Regulator.

The value for K_v can be determined from equation (1) as:

$$K_v = \frac{1}{\sqrt{1 \pm \Delta p}}\frac{k_1}{k_2} = \frac{1}{\dot{q}_{max}\sqrt{1 \pm \Delta p}} \qquad (7)$$

[2] A hydraulic actuator is primarily velocity driven, i.e. a constant valve opening results in a constant (rotational) velocity.

The position dependency of the actuator completely drops out. In addition to a constant gain we see a cancellation for the input nonlinearity. The same input nonlinearity cancellation will be used at the pressure feedback, leading to the control law:

$$i_{sc} = \frac{1}{\sqrt{1 \pm \Delta p}} \left\{ K_c \left(\Delta p_t - \Delta p \right) + \frac{1}{\dot{q}_{max}} \dot{q}_a \right\} \quad (8)$$

Applying this controller to equation (4), the following description is obtained:

$$\begin{bmatrix} \dot{q}_a \\ \Delta p \end{bmatrix} = \begin{bmatrix} \frac{\ddot{q}_{max} k_2 K_c}{(s+\frac{w}{J_a})(s+k_3+k_2K_c)} & \frac{J_a^{-1}}{s+\frac{w}{J_a}} \\ \frac{k_2 K_c}{s+k_3+k_2K_c} & 0 \end{bmatrix} \begin{bmatrix} \Delta p_t \\ T_e+T_c \end{bmatrix} \quad (9)$$

Due to the velocity feedback K_v, the complex pole pair of equation (4) is decoupled into two real poles: one for the mechanical part and one for the hydraulics, see $entry_{[1,1]}$ of (9). Subsequently the hydraulics can be made fast with gain K_c (i.e. $K_c > 0$). Note, for example in $entry_{[2,1]}$ of (9), that the position of this fast pole, as well as the gain of the transfer are position dependent due to k_2 and k_3.

Inverse controller

The solution, which comes more naturally forward from the point of feedback linearization, is to use a controller which contains the inverse dynamics of the hydraulics:

Direct use of equation (1) gives the control law:

$$i_{sc} = \frac{k_1}{k_2\sqrt{1 \pm \Delta p}} \dot{q}_a + \frac{(s+k_3)\,\Delta p_t}{k_2\sqrt{1 \pm \Delta p}} \quad (10)$$

Note that the velocity compensation and the cancellation of the input non linearity are identical with the cascade Δp controller. Substitution of the above equation into equation (4) gives:

$$\begin{bmatrix} \dot{q}_a \\ \Delta p \end{bmatrix} = \begin{bmatrix} \frac{\ddot{q}_{max}}{s+\frac{w}{J_a}} & \frac{J_a^{-1}}{s+\frac{w}{J_a}} \\ 1 & 0 \end{bmatrix} \begin{bmatrix} \Delta p_t \\ T_e+T_c \end{bmatrix} \quad (11)$$

$\Delta p = \Delta p_t$ results due to the control law (10): the dynamics due to the hydraulics are cancelled. Compare also $entry_{[1,1]}$ of this matrix equation with equation (3). Left over are the dynamics due to the mechanical system, which will be taken care of by the second inner loop (see equation (15)).

Effect of input nonlinearity cancellation

In case that K_v and K_c are constants the following equation results instead of equation (9):

$$\begin{bmatrix} \dot{q}_a \\ \Delta p \end{bmatrix} = \frac{1}{CP} [A] \begin{bmatrix} \Delta p_t \\ T_e+T_c \end{bmatrix} \quad (12)$$

With:

$$[A] = \begin{bmatrix} \ddot{q}_{max} k_2 K_c \sqrt{1 \pm \Delta p}^{\,c} & \frac{s+k_3+k_2K_c\sqrt{1\pm\Delta p}^{\,c}}{J_a} \\ \left(s+\frac{w}{J_a}\right) k_2 K_c \sqrt{1 \pm \Delta p}^{\,c} & \frac{k_1}{J_a}\left(\sqrt{1 \pm \Delta p}^{\,v} - 1\right) \end{bmatrix}$$

and,

$$CP = \left(s+\tfrac{w}{J_a}\right)\left(s+k_3+k_2K_c\sqrt{1 \pm \Delta p}^{\,c}\right) + \ddot{q}_{max} k_1 \left(1 - \sqrt{1 \pm \Delta p}^{\,v}\right)$$

The term $\sqrt{1 \pm \Delta p}^{\,c}$ results when the input nonlinearity in the pressure loop is not compensated for, i.e. using in equation (8) a constant K_c instead of $K_c \left(\sqrt{1 \pm \Delta p}\right)^{-1}$. $\sqrt{1 \pm \Delta p}^{\,v}$ has an equivalent meaning for the velocity loop.

The effect of omitting the cancellation of the input nonlinearity in control parameter K_c only, is that the position of the fast pole, and the gains have become a function of Δp, but the decoupling between hydraulic- and load-system is still present. Using a constant velocity compensation (i.e. $\sqrt{1 \pm \Delta p}^{\,v}$ instead of 1) is destroying this decoupling. The two real poles can transform into a complex conjugate pole pair, of which the damping is uncertain; the pressure dynamics has become dependent upon the dynamics of the mechanical load. In addition, Δp will now be influenced by external torques, by the non-zero value of $entry_{[2,2]}$ of equation (12).

A similar analysis can be performed for the controller based on the inverse of actuator dynamics.

A first comparison of the two options for the inner loop

The first column of equations (9) and (11) differs by:

$$\frac{k_2 K_c}{s+k_3+k_2K_c} \quad (13)$$

In case of the cascade Δp controller the pressure reference is tracked via first order dynamics, which can be made fast with gain K_c, and will have static gain equal to 1 for $k_3 = 0$ or $K_c \to \infty$. However, at first sight it seems that the inverse controller is doing the best job.

Both controllers are utilizing exactly the same compensation for the velocity present in the system: a constant gain depending on actuator-valve characteristics plus a compensation for the input nonlinearity. For the pressure dynamics however, the inverse controller is cancelling a pole whereas the cascade Δp controller is placing a pole.

This will make a substantial difference in the case of a non exact pole-zero cancellation, especially when the location of such a pole is near the imaginary axis. And this is likely to be the case, as k_3 is

dependent upon the leakage parameter LP_v. This leakage parameter is kept as small as possible by design, and in addition, is hard to determine.

Furthermore, in the event that the velocity compensation is not perfect, the dynamics of the hydraulic and the mechanical part are not decoupled completely (see (12)). The pole-zero cancellation, as designed for by means of the inverse controller, will not take place ⇒ a zero near the imaginary axis and a rather undamped complex conjugate pole pair may result.

Moreover, the only knowledge necessary to implement the cascade Δp controller is the constant $\dot{q}_{max}$[3]. K_c can be adjusted either way, according to model studies or right on the spot! However for the implementation of the inverse controller knowledge about the non constant parameter k_3 is required, which essentially contains the complete parameter set of the hydraulic actuator model.

Note also that the inverse controller (10) is a non proper system. In case of practical implementation at least a fast enough first order system has to be added. (This will result in an equivalent description as (9), where equation (13) is replaced by the fast first order system.)

Also remarkable is that the inverse controller is using the Δp signal only for the input nonlinearity cancellation, and is not actual having Δp in a feedback loop. The cascade Δp controller is using the Δp signal in the feedback. One can say that the inverse controller relies more upon the model knowledge, and that the cascade Δp controller is using the actual process information to a larger extent.

At this point a preference for the cascade Δp inner loop controller is stated.

4.2 Influences of parameter uncertainty

Closing the second inner loop (6) in combination with the cascade Δp controller (8) as the first inner loop gives:

$$\begin{bmatrix} \dot{q}_a \\ \Delta p \end{bmatrix} = \begin{bmatrix} \frac{k_2 K_c}{CP_1} & \frac{(s+k_3)J_a^{-1}}{CP_1} \\ \frac{\left(s+\frac{w}{J_a}\right)k_2 K_c}{\ddot{q}_{max} CP_1} & \frac{-s\, k_2 K_c J_a^{-1}}{\ddot{q}_{max} CP_1} \end{bmatrix} \begin{bmatrix} \ddot{q}_t \\ T_e + T_c \end{bmatrix} \tag{14}$$

With $CP_1 = s^2 + s\left(\frac{w}{J_a} + k_3 + k_2 K_c\right) + \frac{w}{J_a} k_3$. The second inner loop combination with the inverse controller (10) gives:

$$\begin{bmatrix} \dot{q}_a \\ \Delta p \end{bmatrix} = \begin{bmatrix} s^{-1} & 0 \\ \frac{s+\frac{w}{J_a}}{\ddot{q}_{max}\, s} & -\frac{1}{P_s V_r} \end{bmatrix} \begin{bmatrix} \ddot{q}_t \\ T_e + T_c \end{bmatrix} \tag{15}$$

The resulting integrator for the mechanical part of the system gives a perfect tracking of the target acceleration $\ddot{q}_t$.

Replacing $\frac{k_2 K_c}{s^2 + s\left(\frac{w}{J_a} + k_3 + k_2 K_c\right) + \frac{w}{J_a} k_3}$ in equation (14) by an integrator s^{-1} gives equation (15), except for $entry_{[1,2]}$. Assuming that the viscose friction w (which is generally small) approaches to zero, the examination of the correspondence of the result using the inverse dynamics or the cascade Δp controller is equivalent to the question ($\overset{?}{\approx}$ indicates that similarity is questioned):

$$\frac{1}{s} \overset{?}{\approx} \frac{k_2 K_c}{s\,(s + k_3 + k_2 K_c)}$$

For[4], $k_3 \ll k_2 K_c$ the right hand side of the last equation becomes an integrator in series with a first order system. This first order system has a static gain 1, and can be made fast by the design parameter K_c.

With the same assumptions, $entry_{[1,2]}$ of equation (14) transforms to an integrator in series with a first order lead/lag filter, with a static gain $\ll 1$: $entry_{[1,2]} \approx \frac{(s+k_3)J_a^{-1}}{s(s+k_2 K_c)}$.

As the inner loops (6), (8) and (10) are based upon model parameters, it is interesting to analyze the influence of parameter uncertainties upon the dynamical behaviour of the controlled system. Only examination of the parameters of the hydraulic part is presented, i.e. parameter uncertainties in equations (8) and (10), and not in the second inner loop (6). The uncertainties are assumed to be bounded such that the inequalities under equation (1) are not violated, for example: $\varepsilon_{k_3} \geq -k_3$. A correct compensation of the input nonlinearity is assumed, as this influence is already analyzed in (12).

[3] $\dot{q}_{max} = \frac{\Phi_n}{V_r}$. V_r, which reflects the size of the actuator, is easy to measure and always specified accurately by the manufacturer of hydraulic actuators. The nominal valve flow Φ_n is dependent upon the supply pressure P_s, the maximum steering current i_{max}, and the valve constant C. The supply pressure is given by the pump and is easy to verify. A measure for the valve constant is also given by the manufacturer of hydraulic servo valves, and can be measured from quasi static experiments. But this "constant" can fluctuate considerably around the zero position of the valve ($i_{sc} = 0$, regarding this phenomena you can buy different qualities of valves), and tends to drop off for $i \to \pm i_{max}$. This drop off depends upon resistance of the oil flow from the valve to the actuator. In every control problem, the valve appears to be a critical subject.

[4] k_3 is dependent upon the leakage over the vane, LP_v. This parameter will normally have a small value. $k_2 K_c$ is designed to be large, in order to obtain fast dynamics of the hydraulic system, see (9).

Parameter uncertainties in the inverse inner loop controller

In control law (10) the parameters $\frac{k_1}{k_2} = \dot{q}_{max}^{-1}$, k_2 and k_3 have been used. As the cascade Δp controller only uses $\dot{q}_{max}$, the influence of an isolated uncertainty upon this parameter will be analyzed first. Further, to gain some more insight, the influence of an uncertainty ε for the parameters k_2 and k_3 separate is analyzed. Although it is clear that a combination of uncertainties will give some additive insights, the analysis mentioned above, is sufficient to compare the two options for the inner loop.

Suppose[5] $\underline{\dot{q}_{max,cntr} = \dot{q}_{max} + \varepsilon_{\dot{q}_{max}}}$, equation (11) transforms into:

$$\begin{bmatrix} \dot{q}_a \\ \Delta p \end{bmatrix} = \begin{bmatrix} \frac{\ddot{q}_{max}(s+k_3)}{CP_2} & \frac{(s+k_3)J_a^{-1}}{CP_2} \\ \frac{\left(s+\frac{w}{J_a}\right)(s+k_3)}{CP_2} & \frac{-J_a^{-1}k_1\varepsilon^n_{\dot{q}_{max}}}{CP_2} \end{bmatrix} \begin{bmatrix} \Delta p_t \\ T_e+T_c \end{bmatrix} \tag{16}$$

With $CP_2 = \left(s + \frac{w}{J_a}\right)(s + k_3) + \ddot{q}_{max}k_1\varepsilon^n_{\dot{q}_{max}}$ and $\varepsilon^n_{\dot{q}_{max}} = \frac{\varepsilon_{\dot{q}_{max}}}{\dot{q}_{max}+\varepsilon_{\dot{q}_{max}}}$. The in paragraph 4.1 mentioned influence of a not correct velocity compensation is recognized in equation (16). A zero due to the controller is introduced, and the dynamics of the hydraulic part is not decoupled from the dynamics of the mechanical part. CP_2 shows that this effect is not significant in case $\ddot{q}_{max}k_1\varepsilon^n_{\dot{q}_{max}} \ll \frac{w}{J_a}k_3$. However due to the fact that both, w and LP_v ($k_3 = LP_vk_2$) can be small, it might be that effect is significant. For $\varepsilon_{\dot{q}_{max}} < -\frac{w\,LP_v\dot{q}^2_{max}}{J_a\ddot{q}_{max}+w\,LP_v\dot{q}_{max}}$, the characteristic polynomial CP_2 will even have an unstable pole.

A similar analysis is done with the second inner loop (6) closed. Only the first column of (15) is influenced, $\frac{1}{s}$ is transformed into $\frac{(s+k_3)(\dot{q}_{max}+\varepsilon_{\dot{q}_{max}})}{s(s+k_3)(\dot{q}_{max}+\varepsilon_{\dot{q}_{max}})+\ddot{q}_{max}k_1\varepsilon_{\dot{q}_{max}}}$. For $-\dot{q}_{max} < \varepsilon_{\dot{q}_{max}} < 0$ this system will have unstable poles. For $\varepsilon_{\dot{q}_{max}} > 0$ the significance of this term is dependent upon the relative size of $\ddot{q}_{max}k_1\varepsilon_{\dot{q}_{max}}$.

Suppose $\underline{k_{2,cntr} = k_2 + \varepsilon_{k_2}}$, equation (11) transforms into:

$$\begin{bmatrix} \dot{q}_a \\ \Delta p \end{bmatrix} = \begin{bmatrix} \frac{\ddot{q}_{max}k_2}{\left(s+\frac{w}{J_a}\right)(k_2+\varepsilon_{k_2})} & \frac{J_a^{-1}}{s+\frac{w}{J_a}} \\ \frac{k_2}{k_2+\varepsilon_{k_2}} & 0 \end{bmatrix} \begin{bmatrix} \Delta p_t \\ T_e+T_c \end{bmatrix} \tag{17}$$

The parametric uncertainty ε_{k_2} introduces a (relative harmless) gain error in the first column of the matrix equation (11) (compare with equation (17)).

After closing the second inner loop, the elements of (15) have been multiplied by $\frac{s\,k_2}{s\left(k_2+\varepsilon_{k_2}\right)+\frac{w}{J_a}\varepsilon_{k_2}}$. The position of the pole of this first order system is uncertain, and is even unstable for $-k_2 < \varepsilon_{k_2} < 0$. In case of zero viscose friction ($w = 0$), the influence of ε_{k_2} reduces to a static gain error. $Entry_{[1,2]}$ of (15) becomes $\frac{\varepsilon_{k_2}J_a^{-1}}{s\left(k_2+\varepsilon_{k_2}\right)+\frac{w}{J_a}\varepsilon_{k_2}}$, introducing a coupling between the external torques and the velocity.

Suppose $\underline{k_{3,cntr} = k_3 + \varepsilon_{k_3}}$, equation (11) transforms into:

$$\begin{bmatrix} \dot{q}_a \\ \Delta p \end{bmatrix} = \begin{bmatrix} \frac{\ddot{q}_{max}\left(s+k_3+\varepsilon_{k_3}\right)}{\left(s+\frac{w}{J_a}\right)(s+k_3)} & \frac{J_a^{-1}}{s+\frac{w}{J_a}} \\ \frac{s+k_3+\varepsilon_{k_3}}{s+k_3} & 0 \end{bmatrix} \begin{bmatrix} \Delta p_t \\ T_e+T_c \end{bmatrix} \tag{18}$$

In this case the order of the system is increased: closing the first inner loop results in the addition of a stable first order lead/lag filter in the first column of matrix equation (18) (instead of just a gain as in (17)). This is due to the fact that the system pole $(s + k_3)$ is not cancelled correctly by the controller zero $(s + k_{3,cntr})$.

When closing the second inner loop the same controller zero is introduced, and a second order characteristic polynomial results. This polynomial has one unstable pole for all $\varepsilon_{k_3} > 0$. Equivalent to the uncertainty ε_{k_2}, $entry_{[1,2]}$ of (15) has become nonzero.

Parameter uncertainties in the cascade Δp inner loop controller

Control law (8) uses only the model parameter $\dot{q}_{max}$. Suppose $\underline{\dot{q}_{max,cntr} = \dot{q}_{max} + \varepsilon_{\dot{q}_{max}}}$, equation (9) transforms into:

$$\begin{bmatrix} \dot{q}_a \\ \Delta p \end{bmatrix} = \begin{bmatrix} \frac{\ddot{q}_{max}k_2K_c}{CP_3} & \frac{(s+k_3+k_2K_c)J_a^{-1}}{CP_3} \\ \frac{\left(s+\frac{w}{J_a}\right)k_2K_c}{CP_3} & \frac{-J_a^{-1}k_1\varepsilon^n_{\dot{q}_{max}}}{CP_3} \end{bmatrix} \begin{bmatrix} \Delta p_t \\ T_e+T_c \end{bmatrix} \tag{19}$$

With
$CP_3 = \left(s + \frac{w}{J_a}\right)(s + k_3 + k_2K_c) + \ddot{q}_{max}k_1\varepsilon^n_{\dot{q}_{max}}$ and $\varepsilon^n_{\dot{q}_{max}}$ as at equation (16). A comparison of this situation with the equivalent parameter uncertainty in the inverse controller (equation (16)) gives: There is not a zero, due to the controller, introduced in the first column of (19). The $entries_{[2,2]}$ are equivalent. And the zero which appears in $entry_{[1,2]}$ in both equations, is apparently not due to a zero in the controller. Note that in the case of the cascade Δp controller the location of this zero can be influenced. The characteristic polynomials CP_2 and CP_3 do have an equivalent structure,

[5] The subscript 'cntr' identifies the parameter used in the control law, without a subscript is the nominal value of the parameter. Just one parameter uncertainty at a time is being examined. For the other control parameters is assumed that they match the correct values.

but in case of the cascade Δp controller the position of the poles can be influenced by control parameter K_c. Stability in spite of the parameter uncertainty is determined by the following inequality: $\varepsilon_{\dot{q}_{max}} > -\frac{w(LP_v+K_c)\dot{q}^2_{max}}{J_a\ddot{q}_{max}+w(LP_v+K_c)\dot{q}_{max}}$. Therefore stability can be forced in case of certain bounded parameter uncertainty, with respect to the first inner loop.

Closing the second inner loop, only the poles of the characteristic polynomial have been disturbed (compared to (14), and the numerator of $entry_{[2,2]}$ has been transformed to $s\,k_2K_c + \ddot{q}_{max}k_1\varepsilon^n_{\dot{q}_{max}}$, which is non-minimum phase for $\varepsilon_{\dot{q}_{max}} < 0$. This system will be stable for: $\varepsilon_{\dot{q}_{max}} > -\frac{w\,LP_v\dot{q}^2_{max}}{J_a\ddot{q}_{max}+w\,LP_v\dot{q}_{max}}$. This condition is a little less restrictive as compared to the case with the inverse actuator dynamics controller.

Conclusions with respect to the parameter uncertainty analysis

Conclusions due to the above analysis are:

- Three different kinds of parameter uncertainties can introduce instability in case of the inverse controller. For the cascade Δp controller this is just the case for one parameter uncertainty.
- The conditions for stable behaviour are for the cascade Δp controller less severe.
- Parameter uncertainty in case of the cascade Δp controller will not result in the addition of (badly conditioned) dynamics after closing the second inner loop, as is the case with the inverse actuator dynamics controller.
- For both controllers it is advisable to use an estimated $\dot{q}_{max,cntr}$ which is larger than the real one, such that $\varepsilon_{\dot{q}_{max}} > 0$.

Note from equation (1) that the parameters $k_{1,2,3}$ are position dependent. Therefore uncertainties $\varepsilon_{k_{1,2,3}}$ can also be due to the operation of the actuator at a different position q_a, as the controller was designed for.

4.3 Extension of the cascade Δp inner loop

The dynamics of a hydraulic actuator, controlled with the cascade Δp controller (8) or the inverse controller (10) differs by the first order system of equation (13). Not only the pole of this system is varying with the position dependent parameters k_2 and k_3, but also the static gain. This static gain is approaching 1 for $k_3 \ll k_2K_c$.

Introducing a leakage compensation within the cascade Δp structure, gives instead of equation (13) the following difference with the inverse controller:

$$\frac{k_2K_c}{s+k_2K_c} \tag{20}$$

The complete cascade Δp controller inclusive leakage compensation becomes:

$$i_{sc} = \frac{1}{\sqrt{1\pm\Delta p}}\left\{K_c(\Delta p_t - \Delta p) + K_{LP_v}\Delta p + \frac{\dot{q}_a}{\dot{q}_{max}}\right\} \tag{21}$$

With $K_{LP_v} = LP_v$ in the nominal case. Instead of equations (9) and (14) the control law with leakage compensation results in:

$$\begin{bmatrix}\dot{q}_a\\ \Delta p\end{bmatrix} = \begin{bmatrix}\frac{\ddot{q}_{max}k_2K_c}{(s+\frac{w}{J_a})(s+k_2K_c)} & \frac{J_a^{-1}}{s+\frac{w}{J_a}}\\ \frac{k_2K_c}{s+k_2K_c} & 0\end{bmatrix}\begin{bmatrix}\Delta p_t\\ T_e+T_c\end{bmatrix} \tag{22}$$

and,

$$\begin{bmatrix}\dot{q}_a\\ \Delta p\end{bmatrix} = \begin{bmatrix}\frac{k_2K_c}{s\,CP_4} & \frac{J_a^{-1}}{CP_4}\\ \frac{(s+\frac{w}{J_a})k_2K_c}{\ddot{q}_{max}s\,CP_4} & -\frac{k_2K_cJ_a^{-1}}{\ddot{q}_{max}CP_4}\end{bmatrix}\begin{bmatrix}\ddot{q}_t\\ T_e+T_c\end{bmatrix} \tag{23}$$

with $CP_4 = \left(s + \frac{w}{J_a} + k_2K_c\right)$. A full compensation of the leakage dependent parameter k_3 is realized.

An equivalent robustness analysis as in paragraph 4.2 can be performed. The results in case that $\dot{q}_{max,cntr} = \dot{q}_{max} + \varepsilon_{\dot{q}_{max}}$ are similar to paragraph 4.2, but without the influence of k_3 (i.e., taking $k_3 = 0$ or $LP_v = 0$ give the equivalent equations and stability conditions).

The situation $LP_{v,cntr} = LP_v + \varepsilon_{LP_v}$ is of course similar to no leakage compensation ($\varepsilon_{LP_v} = -LP_v$). Therefore taking $LP_v = -\varepsilon_{LP_v}$ and consequently $k_3 = LP_vk_2 = -\varepsilon_{LP_v}k_2$ in equations (9) and (14) gives the equations concerning the analysis of the parameter uncertainty ε_{LP_v} of LP_v. As stability conditions we get: $K_c > \varepsilon_{LP_v}$ for the first inner loop, and $\varepsilon_{LP_v} < 0$ due to the second inner loop. Because of the second condition, the first condition will not be a problem as $K_c > 0$, see under equation (9). This stability condition is equivalent to the case of the inverse controller[6] (ε_{k_3}), but the effect of a nonzero ε_{LP_v} will be a shift of pole locations in stead of adding uncertain dynamics. In general the estimated value of the leakage coefficient ($LP_{v,cntr}$) must have a value less than the actual leakage coefficient (LP_v), such that $\varepsilon_{LP_v} < 0$.

The conclusion of this section is that leakage compensation can increase the performance of the cascade Δp controller at the expense of more model

[6] Although k_3, and consequently its uncertainty, is dependent upon 6 parameters, as ε_{LP_v} solely depends upon LP_v.

knowledge, and the introduction of an extra stability condition. The stability condition on $\dot{q}_{max}$ has become a little more restrictive with $\varepsilon_{\dot{q}_{max}} > 0$

5 Experimental results

This section presents the results of some preliminary experiments, performed on an industrial hydraulic rotary actuator with load and standard valve. The purpose is to show the practical applicability of the chosen control configuration, rather than a complete experimental validation of the proposed method. More information about the experimental setup, parameter estimation and model validation is reported in Heintze *et al.* (1993).

As a result of the analyses only the cascade Δp inner loop together with the impedance control outer loop is selected for implementation (i.e. equations (5), (6) and (8) or (21)).

First the influence of the control parameter K_{LP_v} is shown. In figure 1 a square wave reference is added to the Δp_t signal. Given are the pressure and the target pressure signals (i.e. '$entry_{[2,1]}$' of equation (9) or (22)), and the valve input. Along the Y-axis are scaled units, equivalent to equation (1). To minimize the influence of control laws (5) and (6), the amplitude of the square wave is chosen such that the actuator did not start moving, due to the friction inside the actuator. In figure 1a $K_{LP_v} = 0$ and in figure 1b K_{LP_v} is the estimated leakage parameter LP_v. Due to the leakage compensation a static gain of almost 1 for the pressure loop is realized, which does agree with equation (20). Note that:

1. The static error between Δp and Δp_t is caused due to a static position error, via equation (5).
2. Especially the recorded valve input signal seems rather noisy. But we are examining signals in the order of $\frac{1}{1000}$ of the maximum value.

In figure 2 K_c is increased compared to figure 1. According to equation (13) the pressure loop is faster than in figure 1, and the static error in figure 2a is smaller than in figure 1a. Addition of leakage compensation as represented in figure 2b, resulted again in a static gain of 1 for the pressure loop.

Figures 3 and 4 show that the cascade Δp controller does function well within the impedance control outer loop. Presented is the response upon a step-size input on q_0 (and $\dot{q}_0 = 0$). The input q_0 is the dotted line in the left upper subfigure. For the experiment presented in figure 3 is $K_t = 4460$, $B_t = 31.8$

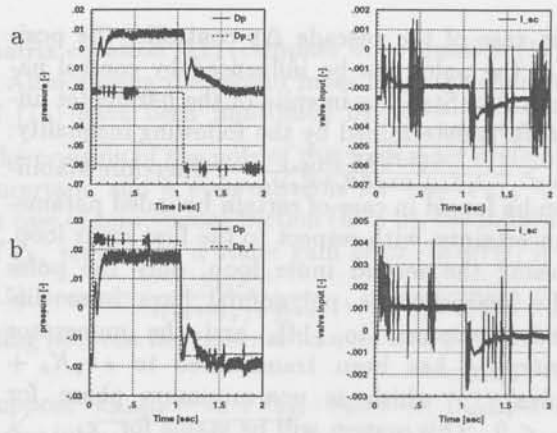

Fig. 1: Response of Δp upon a square wave on Δp_t, 'slow pressure loop'. Upper: $K_{LP_v} = 0$, lower: $K_{LP_v} = LP_{v,cntr}$.

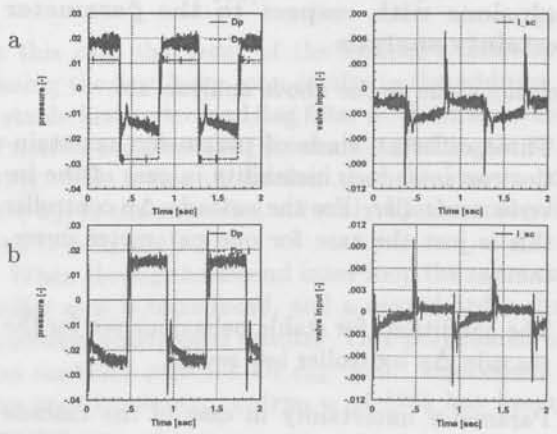

Fig. 2: Response of Δp upon a square wave on Δp_t, 'fast pressure loop'. Upper: $K_{LP_v} = 0$, lower: $K_{LP_v} = LP_{v,cntr}$.

and $J_t = 1$ implemented as target impedance, and for the experiment presented in figure 4 the target impedance was $K_t = 1225$, $B_t = 8.4$ and $J_t = 1$. For comparison, the simulated nominal response of the target impedance is given in the right lower corner. The three other subfigures represent measured data from the actuator. The cascade Δp controller had an identical adjustment for both experiments.

From these initial experiments is concluded that the position of the actuator is performing as requested by the different target impedances. The cascade Δp inner loop controller is performing well.

Conclusions

Based upon the description of a hydraulic actuator, two inner loop controllers have been formulated. A theoretical analysis towards the robustness prop-

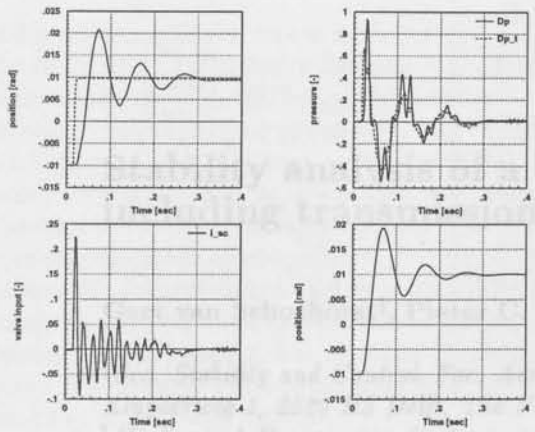

Fig. 3: Response upon a step on reference q_0, $K_t = 4460$, $B_t = 31.8$ and $J_t = 1$. In left upper plot, reference q_0 is $\cdots$, actual position q_a is $-$. Right lower: simulated response of target impedance.

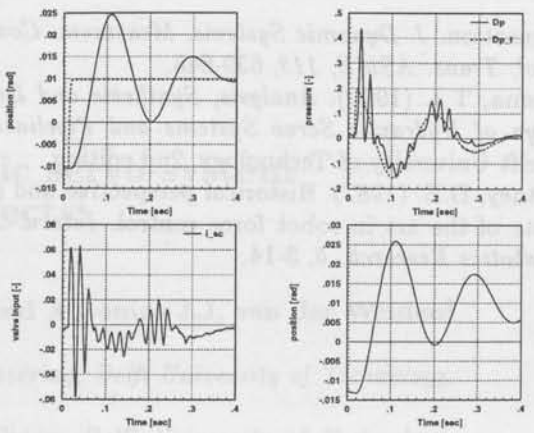

Fig. 4: Response upon a step on reference q_0, $K_t = 1225$, $B_t = 8.4$ and $J_t = 1$. In left upper plot, reference q_0 is $\cdots$, actual position q_a is $-$. Right lower: simulated response of target impedance.

erties of the proposed controllers, with respect to model parameter uncertainties, is performed. Preliminary experiments upon a actual hydraulic actuator have been executed. From this research it is concluded that:

- Inner loop control based upon cancellation of dynamics is sensitive to an inaccurate model used at the control design. This is very likely to result in poor or even unstable behaviour of the controlled system.

- The cascade Δp inner loop controller, which is placing the poles of the hydraulic system, is relatively easy to design and has better robustness properties than the inverse controller.

- An inner/outer loop control structure applied to hydraulic actuators is able to separate the hydraulic dynamics from the mechanical part. This gives the opportunity to perform further control design solely based upon the mechanical structure of the manipulator.

- Practical application of the cascade Δp inner loop within an impedance outer loop structure, does yield satisfactory behaviour.

Future research will include: a more elaborated experimental validation of the one degree of freedom situation, the application of the cascade Δp controller in an inner/outer structure to the Brick Laying Robot, the controlled execution of a task in which the manipulator is in contact with an environment, using the cascade Δp - impedance control combination.

References

An, C.H., C.G. Atkeson and J.M. Hollerbach (1988). *Model-Based Control of a Robot Manipulator*. The MIT Press.

Anderson, R.J. and M.W. Spong (1988). Hybrid impedance control of robotic manipulators. *IEEE Trans. Robotics and Automation, RA-4*, 549-556.

Boer, F.G. de (1992). *Multivariable Servo Control of a Hydraulic RRR-Robot*. PhD Thesis, Mechanical Engineering Systems and Control Group, Delft University of Technology.

Heintze, J., G. v. Schothorst, A.J.J. v.d. Weiden and P.C. Teerhuis (1993). Modeling and control of an industrial hydraulic rotary vane actuator. *Proc. 32nd IEEE Conf. Decision and Control*, San Antonio, TX, pp. 1913-1918.

Hogan, N. (1985). Impedance control: an approach to manipulation: Part 1-theory, part 2-implementation, part 3-applications. *J. Dynamic Systems, Measurem. Control, Trans. ASME, 107*, pp. 1-7, 8-16, 17-24.

Khosla, P.K. (1990). Recent advances in experimental robot control. In: G.E. Taylor (Ed.), *Kinematic and Dynamic Issues in Sensor Based Control*, NATO ASI Series, Vol. F57. Springer-Verlag, Berlin, pp. 161-178.

Sepehri, N., G.A.M. Dumont, P.D. Lawrence and F. Sassani (1990). Cascade control of hydraulically actuated manipulators. *Robotica, 8*, part. 3, pp. 207-216.

Slotine, J.-J.E. and W. Li (1991). *Applied Nonlinear Control*. Prentice-Hall Inc.

Southward, S.C., C.J. Radcliffe and C.R. MacCluer (1991). Robust nonlinear stick-slip friction com-

pensation. *J. Dynamic Systems, Measurem. Control, Trans. ASME, 113*, 639-645.

Viersma, T.J. (1990). *Analysis, Synthesis and Design of Hydraulic Servo Systems and Pipelines.* Delft University of Technology, 2nd edition.

Whitney, D.E. (1987). Historical perspective and state of the art in robot force control. *Intern. J. Robotics Research, 6*, 3-14.

Selected Topics in Identification, Modelling and Control
Vol. 7, December 1994

Stability analysis of a hydraulic servo-system including transmission line effects‡

Gert van Schothorst§, Pieter C. Teerhuis♯ and Antonius J.J. van der Weiden♯

§ *Sec. Stability and Control, Fac. Aerospace Engineering, Delft University of Technology, Kluyverweg 1, 2629 HS Delft, The Netherlands*
♯ *Mechanical Engineering Systems and Control Group, Delft University of Technology, Mekelweg 2, 2628 CD Delft, The Netherlands*

Abstract. In applications where high-performance control of long-stroke hydraulic actuators is required, such as in flight simulator motion systems, the dynamics of the transmission lines between the servo-valve and the actuator are relevant for control design. Insight into the coupled behaviour of the hydraulic control system is obtained by means of physical modelling of the transmission lines (by a modal approximation technique), the actuator and the servo-valve. The validated models lead to an explanation of potential stability problems encountered in a flight simulator motion system, namely that if the resonance peaks of the transmission line dynamics interfere with the phase shift of the valve dynamics, pressure difference feedback may violate stability margins.

Keywords. Hydraulic servo control, transmission line modelling, servo-valve dynamics, experimental validation.

1 Introduction

In a number of applications in the field of motion control, hydraulic actuators are preferred to electrical actuators, especially when long-stroke linear actuators are required. An application of these hydraulic actuators is the motion system of a flight simulator (Advani, 1993), where the desired stroke of the actuators may vary from .5 m to 2 m.

In order to improve the performance (and hence fidelity) of flight simulation, an increasing in the performance of the actuator control is also required, especially in the control of the actuator accelerations cq. forces over wide frequency ranges. For this reason, the actuator control will be based more and more on (high-frequency) force cq. pressure control loops, instead of the usual (middle-frequency) position servo control loops (Merrit, 1967; Viersma, 1990). Recent work in the area of hydraulic robot control shows a similar shift in control strategy, in the application of high-gain pressure feedback loops (Heintze, 1994).

A consequence of this shift in control strategy is, that high-frequency dynamics in the actuator behaviour become important where they were irrelevant before. Besides that, the application of long-stroke hydraulic actuators inherently introduces high-frequency dynamics, related to transmission line effects in the connection lines between valve and actuator.

In literature, transmission line dynamics, electro-hydraulic control systems and the combination of both have been extensively described. A clear historic overview of the research on transmission line dynamics, is given by Yang and Tobler (1991). They also present a modelling technique, which approximates the transmission line dynamics by minimal order linear models, in which the physical parameters are preserved. This so called "modal approximation technique" provides the possibility to physi-

‡This work has been carried out in the scope of the SIMONA-International Research Centre at Delft University of Technology. This paper was presented at the 3rd International Conference on Automation, Robotics and Computer Vision, Shangri-La, Singapore, November 9-11, 1994.

Par.	Description	Value; k=1	Value; k=2	Dim.
r_k	Radius circular line	$1\ 10^{-2}$	$0.8\ 10^{-2}$	$[m]$
A_{dk}	Line area (πr_k^2)	$3.14\ 10^{-4}$	$2.01\ 10^{-4}$	$[m^2]$
D_{nk}	Dissipation number	$6.05\ 10^{-4}$	$7.63\ 10^{-4}$	$[-]$
E	Effective bulk modulus of oil	$1.3\ 10^{9}$	$1.3\ 10^{9}$	$[kg/m^2]$
L_k	Line length	1.31	1.06	$[m]$
Z_{0k}	Line impedance constant	$3.41\ 10^{9}$	$5.36\ 10^{9}$	$[Ns/m^5]$
$\alpha_{k,1}$	Frequency modif. factor mode 1	1.03	1.02	$[-]$
$\alpha_{k,2}$	Frequency modif. factor mode 2	1.03	1.02	$[-]$
$\beta_{k,1}$	Damping modif. factor mode 1	7.0	8.0	$[-]$
$\beta_{k,2}$	Damping modif. factor mode 2	6.5	8.0	$[-]$
$\lambda_{k,1}$	Norm. natural frequency mode 1	$2.60\ 10^{3}$	$7.79\ 10^{3}$	$[rad]$
$\lambda_{k,2}$	Norm. natural frequency mode 2	$2.06\ 10^{3}$	$6.18\ 10^{3}$	$[rad]$
ν	Kinematic viscosity	$5.5\ 10^{-5}$	$5.5\ 10^{-5}$	$[m^2/s]$
ρ	Density of oil	900	900	$[kg/m^3]$
ω_{ck}	Viscosity frequency	.55	.86	$[1/s]$

Table 1: Transmission line parameters and values

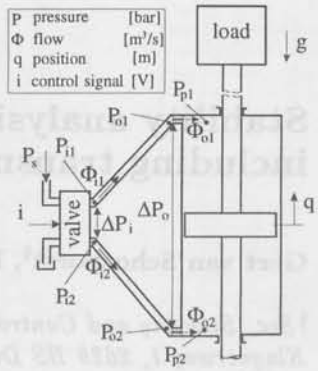

Fig. 1: Modelling of the servo-system setup

cally interpret the dynamic effects introduced by the transmission lines. This is important when these effects are included in the models of complete fluid networks, or other dynamic systems, like hydraulic control systems.

Concerning these latter systems, dynamic (and even non-linear) characteristics of hydraulic servo-systems have been thoroughly investigated and described by e.g. Merrit (1967), Viersma (1990) and Walters (1991). Apart from specific research on the dynamics of the electro-hydraulic servo-valve (Lin and Akers, 1991; Lebrun *et al.*, 1978), valve dynamics are often neglected in practical applications (Viersma, 1990), or approximated by low-order (experimental) linear models (Feuser, 1984; Watton and Tadmori, 1985; Watton, 1987).

In some of these practical applications, the combination of transmission line effects and the dynamics of hydraulic control systems is studied. For example, Ham (1982) studies the effect of supply line dynamics, while Watton and Tadmori (1985), and Watton and Tadmori (1988) deal with transmission lines coupled to underlapped servo-valves, and finally the behaviour of a hydraulic drive with transmission line effects is considered by Watton (1987). In the latter study, it is concluded that valve dynamics provide damping of the (oscillatory) fluid transients in hydraulic control systems.

The results presented in literature suggest no severe problems with transmission lines in hydraulic control systems. The application of a long-stroke actuator in a flight simulator motion system however showed stability problems when applying well known pressure feedback techniques (Merrit, 1967; Viersma, 1990). In this paper it will be shown and explained that transmission line dynamics, coupled to the hydraulic control system dynamics, cause severe stability problems when aiming at high-performance control of long-stroke hydraulic actuators.

In Section 2, a review of the relevant sub-systems models will be given, ending up with an integrated model for the complete servo-system. The validation of this model with experimental results will be described in Section 3. Based on this model, Section 4 discusses the main issue, namely the stability of the complete hydraulic servo-system under pressure feedback on behalf of high-performance control. Finally, Section 4.3 ends the paper with conclusions.

2 Hydraulic servo-system model

For the setup depicted in Figure 1, three sub-systems can be distinguished: the transmission lines, the actuator and the servo-valve. For each of these, a model description will be given, providing some physical interpretation. These sub-system models will be integrated into one model for the complete servo-system. The model parameters for this particular setup, are given in Table 1 and 2.

2.1 Transmission line model

For both transmission lines, which have differing geometries, linear models can be derived by a modal approximation technique. Here, the procedure described by Yang and Tobler (1991) will be adopted, because the physical parameters are preserved in the resulting approximating linear models. The basic idea is, that the (infinite dimensional) input/output description of a transmission line can be represented as an infinite product series of second order models. Each second order model then represents a mode of the transmission line dynamics. The modal approximation consists of a finite dimensional state-space model, obtained by taking into account a finite number of modes only.

In the approximation step, one essential choice has to be made, namely the number of (resonance)

modes per transmission line to be taken into account by the model. Preliminary analysis of the infinite dimensional model in the frequency domain showed resonance frequencies at about 200, 600, 1000 Hz and higher. Given a digital controller sample frequency of 5 kHz, and a servo-valve with relevant dynamics up to 500 Hz, it is assumed that first two modes (denoted by the index l, $l = 1, 2$) may be relevant for control design and analysis. With this choice, the dynamics of the two transmission lines (denoted by the index k, $k = 1, 2$) can be described by two fourth-order state-space models of the form (see Yang and Tobler, 1991):

$$\begin{aligned} \tfrac{1}{\omega_{ck}}\dot{x}_k &= A_k x_k + B_k u_k \\ y_k &= C_k x_k \end{aligned} \qquad k = 1,2 \tag{1}$$

where

$$\begin{aligned}
x_k &= \left[\begin{array}{cccc} P_{ok,1} & \Phi_{ik,1} & P_{ok,2} & \Phi_{ik,2} \end{array}\right]^T && k = 1,2 \\
u_k &= \left[\begin{array}{cc} P_{ok} & \Phi_{ik} \end{array}\right]^T && k = 1,2 \\
y_k &= \left[\begin{array}{cc} P_{ik} & \Phi_{ok} \end{array}\right]^T && k = 1,2 \\
A_k &= diag\left[\begin{array}{cc} A_{k,1} & A_{k,2} \end{array}\right] && k = 1,2 \\
A_{k,l} &= \left[\begin{array}{cc} 0 & -(-1)^{l+1} Z_{0k}\lambda_{k,l} \\ \frac{(-1)^{l+1}\lambda_{k,l}}{Z_{0k}\alpha_{k,l}^2} & -\frac{8\beta_{k,l}}{\alpha_{k,l}} \end{array}\right] && \begin{array}{l} k = 1,2 \\ l = 1,2 \end{array} \\
B_k &= \left[\begin{array}{cc} B_{k,1}^T & B_{k,2}^T \end{array}\right]^T && k = 1,2 \\
B_{k,l} &= \left[\begin{array}{cc} 0 & \frac{2Z_{0k}}{D_{nk}} \\ -\frac{2}{Z_{0k}D_{nk}\alpha_{k,l}^2} & 0 \end{array}\right] && \begin{array}{l} k = 1,2 \\ l = 1,2 \end{array} \\
C_k &= \left[\begin{array}{cccc} 1 & 0 & 1 & 0 \\ 0 & 1 & 0 & 1 \end{array}\right] && k = 1,2
\end{aligned}$$

and the viscosity frequency for line k defined by $\omega_{ck} = \nu / r_k^2$ (see Table 1).

Note, that there are two reasons for the specific choice of the states x_k, the inputs u_k and the outputs y_k in equation (1). First, the input-output description should be physically realizable and causal, which means that it is incorrect to choose both pressure and flow at one line end as inputs. Secondly, the transmission line models have to be integrated with the actuator and valve models, requiring this specific choice, as argued in Section 2.4.

The two most important line parameters in the expressions above, the dissipation number D_{nk}, and the line impedance constant Z_{0k}, are calculated as follows:

$$D_{nk} = \frac{L_k \nu}{c_0 r_k^2}; \qquad Z_{0k} = \frac{\rho c_0}{A_{dk}} \qquad k = 1,2 \tag{2}$$

with the sound velocity in the oil: $c_0 = \sqrt{\frac{E}{\rho}}$ in $[m/s]$.

The remaining parameters in the state-space model (1) are obtained by calculating the normalized (by ω_{ck}) modal undamped natural frequencies:

$$\lambda_{k,l} = \frac{\pi(l - \frac{1}{2})}{D_{nk}} \qquad \begin{array}{l} k = 1,2 \\ l = 1,2 \end{array} \tag{3}$$

For these frequencies $\lambda_{k,l}$, the factors $\alpha_{k,l}$ and $\beta_{k,l}$ can be determined from figures given in Yang and Tobler (1991). These frequency-dependent factors are introduced by Yang and Tobler (1991) to incorporate frequency-dependent friction in the model. For the setup to be considered here, they are given in Table 1.

Although equation (1) describes the transient properties of the transmission lines sufficiently accurate, steady-state accuracy is lost in general by modal approximations. In order to overcome this inaccuracy, a steady-state correction is proposed by Yang and Tobler (1991), which is actually an input modification that transforms the input matrix B_k in (1) into $B_k G_k$.

The correction matrix G_k, $k = 1, 2$ is found by setting the steady-state gain of the (input modified) modal approximation (1) equal to the steady-state gain of the infinite dimensional model. This can be shown to result in (Yang and Tobler, 1991):

$$\begin{aligned} G_k &= H_k^{-1}\left[\begin{array}{cc} 1 & 8Z_{0k}D_{nk} \\ 0 & 1 \end{array}\right] && k = 1,2 \\ H_k &= -\left(A_{k,1}^{-1}B_{k,1} + A_{k,2}^{-1}B_{k,2}\right) && k = 1,2 \end{aligned}$$

The procedure described in this Section, provides dynamic models of the first sub-system to be modelled, the transmission lines. Models for the other sub-systems, actuator and servo-valve, will be given in the following Sections.

2.2 Actuator model

When modelling the actuator, physical insight can be preserved, like in the case of the transmission line dynamics, by stating a model based on physical laws. For the symmetric actuator of Figure 1, with the variables defined in the Figure, the equation of motion of the piston is:

$$M_p \ddot{q} = A_p\left(P_{p1} - P_{p2}\right) - w_p \dot{q} - M_p g \tag{4}$$

while mass balances for the actuator compartments give state equations for the actuator pressures:

$$\begin{aligned} \dot{P}_{p1} &= \tfrac{E}{A_p(q_{max}+q)}\left(\Phi_{o1} - A_p\dot{q}\right) \\ \dot{P}_{p2} &= \tfrac{E}{A_p(q_{max}-q)}\left(\Phi_{o2} + A_p\dot{q}\right) \end{aligned} \tag{5}$$

and modelling a turbulent in-/outlet restriction for both actuator compartments gives the following relation:

Par.	Description	Value	Dim.
g	Gravity constant	10	$[m/s^2]$
q_{max}	Half the actuator stroke	.5	$[m]$
w_p	Viscous friction coeff.	500	$[Ns/m]$
A_p	Piston area	$2.5\,10^{-3}$	$[m^2]$
C_m	Manifold constant	$1.33\,10^{-12}$	$[m^8/Ns^2]$
C_v	Valve constant	$1.42\,10^{-6}$	$[m^2/V]$
K_p	Prop. feedback gain valve	.7	$[-]$
K_v	Velocity gain valve	1100	$[1/s]$
M_p	Mass of piston plus load	55	$[kg]$
P_s	Supply pressure	$1.4\,10^7$	$[N/m^2]$
β_v	Damping coeff. valve	.27	$[-]$
ω_{0v}	Natural freq. valve	$2.76\,10^3$	$[rad/s]$

Table 2: Actuator and valve parameters and values

$$P_{ok} = P_{pk} - \frac{\Phi_{ok}^2}{C_m} \qquad k = 1, 2 \quad (6)$$

The manifold constant C_m acts as a tuning parameter, which was determined by model validation. The numerical values for the parameters in equations (4), (5) and (6) are given in Table 2. It is clear, that these equations in fact constitute a dynamic state-space model of 4^{th} order.

2.3 Servo-valve model

For the two-stage electro-hydraulic servo-valve, which will be considered here, a similar modelling procedure as in the previous Section can be carried out. This results in a rather complex, non-linear model. Dependent on the specific valve applied, the dynamics of this model can be reduced to some specific third-order linear model structure (Schothorst *et al.*, 1994). For the Rexroth valve[1] with electrical feedback to be considered here, the open loop dynamics can be described by a second order system in series with an integrator. With the proportional electrical feedback loop, the following transfer function of the closed loop servo-valve is obtained:

$$\frac{d(s)}{i(s)} = \frac{K_p K_v}{\frac{1}{\omega_{0v}^2} s^3 + \frac{2\beta_v}{\omega_{0v}} s^2 + s + K_p K_v} \quad (7)$$

where the control signal i and the spool position d are both expressed in $[V]$ according to the experimental setup.

Assuming a critical centre, symmetric valve, with turbulent flows through the valve ports, the valve flows are non-linearly related to the spool position and the pressures at the valve ports by:

$$\Phi_{i1} = C_v \frac{|d|+d}{2} \sqrt{2\frac{P_s - P_{i1}}{\rho}} - C_v \frac{|d|-d}{2} \sqrt{2\frac{P_{i1}}{\rho}}$$
$$\Phi_{i2} = C_v \frac{|d|+d}{2} \sqrt{2\frac{P_{i2}}{\rho}} - C_v \frac{|d|-d}{2} \sqrt{2\frac{P_s - P_{i2}}{\rho}} \quad (8)$$

[1]Type no.: 4WS2EE10-45/75B2ET210Z8EM

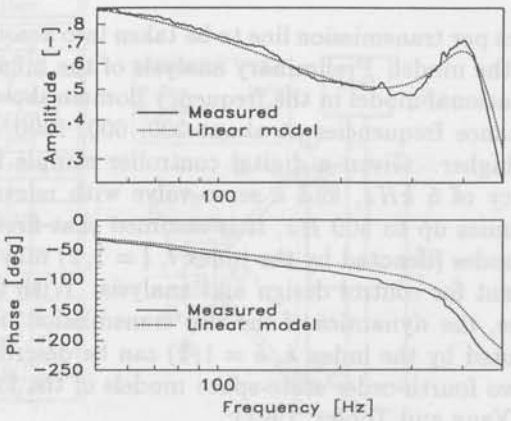

Fig. 2: Frequency response valve dynamics $\frac{d(s)}{i(s)}$.

where the reader is referred to Figure 1 for the variable definitions and to Table 2 for the parameter definitions and values.

2.4 Integration of the sub-system models

The sub-system models described in the previous Sections can be integrated into a complete model of the hydraulic servo-system, because the principle of the bilateral coupling in the physical systems has been taken into account while stating the sub-system models. That is why the actuator model, with an inertial character, has been defined with flows as inputs and pressures as outputs (eq. (5)). The valve flow relation (with a resistive character) has been defined with flows as outputs and pressures as inputs in order to avoid division by zero for zero valve displacement. Together with the specific input/output relations of Section 2.1 for the transmission lines, a correctly stated model of the complete hydraulic servo-system is available, by combining equations (1) - (8). See Oosterhout (1992) for a more detailed discussion of the integration of the transmission line models and the hydraulic servo-system models.

3 Model validation

Because the valve dynamics modelling plays an important role in the stability analysis of Section 4, the first part of the model validation consists of a comparison of the frequency response of the linear model for the valve dynamics (7) to the measured frequency response[2]. See Figure 2. Despite a discrepancy in the phase characteristic (possibly due to non-linearities or sensor dynamics), the fit is satisfactory, especially with respect to the amplitude.

[2]Obtained with HP 3562 A Dynamic Signal Analyzer; for all responses, an input amplitude of 1.5 % was applied

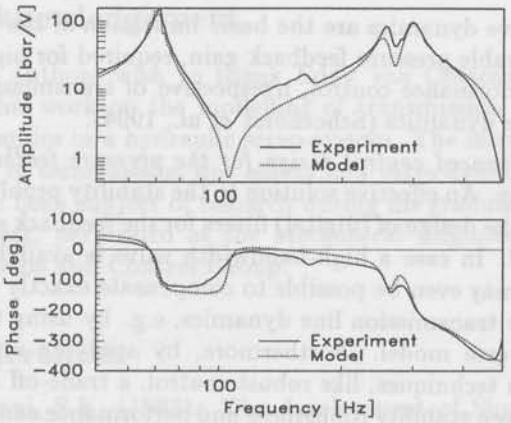

Fig. 3: Frequency response of pressure difference near the valve $\frac{\Delta P_i(s)}{i(s)}$.

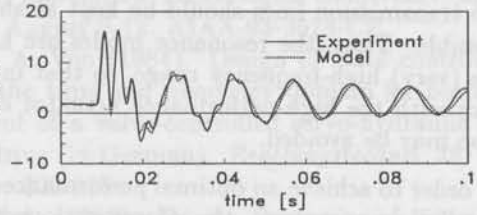

Fig. 4: Time response pressure difference ΔP_i on open loop step of 1.5 % on input i.

Given the validity of the valve dynamics model, the model of the remaining dynamics may be validated by comparing the model responses of the complete servo-system with experimental results. This has been done in both the frequency domain and in the time domain. The experiments were performed in open loop conditions[3], with the control signal i as input, and the measured pressure difference $\Delta P_i = P_{i1} - P_{i2}$ as output.

Comparison of the frequency responses in Figure 3 shows a good agreement, indicating that the main dynamic effects are modelled correctly. This especially holds for the three resonance peaks: the first one due to the natural frequency of the actuator, and the second and third peaks originating from transmission line 1 and 2 respectively.

The validation of the time responses in Figure 4 also shows satisfactory results. Although flow measurements were not provided in the experimental setup, the steady-state behaviour of the complete model was validated by performing steady-state pressure and velocity measurements, which agreed with expectations.

In short, the experimental validation yields sufficient confidence in the model, so that a further analysis of the system dynamics, based on the model, is justified.

[3] Drifting due to the integrating behaviour of the actuator was avoided by manual offset adjustment

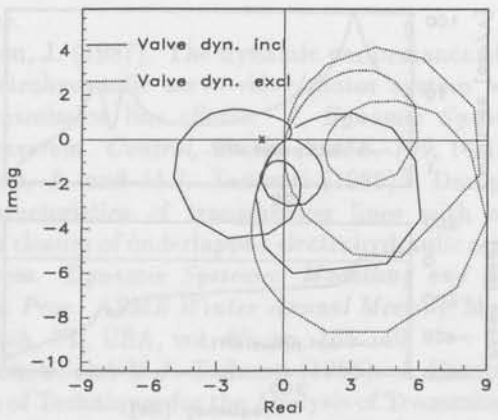

Fig. 5: Nyquist plot of $\frac{\Delta P_i(s)}{i(s)}$ (scaled by sensor gain), with and without valve dynamics in the model.

4 Stability closed loop servo-system

Slightly depending on the control strategy applied and the feedback signal used (Section 4.1), stability problems may occur due to the combination of transmission line dynamics and valve dynamics, as will be discussed in Section 4.2. A number of possible solutions to this problem will be given in Section 4.3.

4.1 Control strategy

In hydraulic servo control, the classical strategy of proportional actuator position feedback, plus some feedback loop for damping is widely used (Merrit, 1967; Viersma, 1990). The damping loop may then consist of either a pressure difference feedback loop, or an acceleration feedback loop.

For more recent applications of hydraulic servo control, high-performance force cq. pressure control loops are required (Section 1). This means that the gains for the pressure difference or acceleration feedback loops are very high compared to the classical situation.

Usually, pressure difference transducers are applied, because they are relatively robust, while accurate acceleration sensors are expensive. In the case of long-stroke actuators, the pressure difference will often be measured near the valve for practical reasons, so ΔP_i is used as a feedback signal.

4.2 Stability problem

The stability problem encoutered in the practical situation of proportional feedback of the pressure difference near the valve, ΔP_i, is easily explained by giving the open-loop frequency response of the

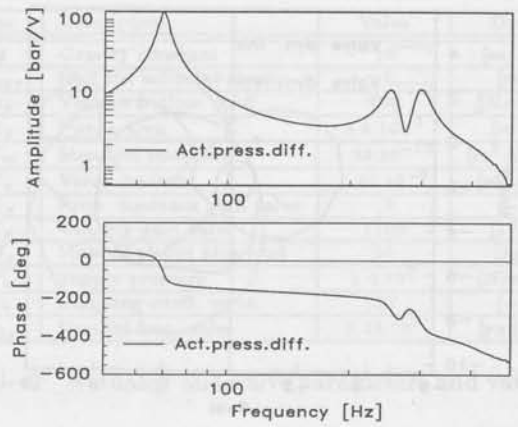

Fig. 6: Model frequency response $\frac{\Delta P_o(s)}{i(s)}$.

model (dashed line in Figure 3) in a Nyquist plot (solid line in Figure 5). For small feedback gains ($> .2$) the closed loop will already be unstable by the encirclement of the point (-1,0). This unstable behaviour was observed in practice.

The reason for this stability problem is clear: the combination of transmission line dynamics (resonance peaks) and valve dynamics (180^0 phase shift) causes problems by pressure feedback. This is illustrated by extracting the effect of the valve dynamics model (7) from the model response, resulting in the dashed line in Figure 5.

4.3 Solutions to the stability problem

With the new insight obtained into the dynamic properties of the hydraulic servo-system under pressure feedback, a number of solutions to the stability problem may be given:

- *Choice of the most suitable feedback signal.* In the case that the pressure difference at the actuator side of the transmission lines, $\Delta P_o = P_{o1} - P_{o2}$, is measured, the open loop model frequency response is given in Figure 6. A similar plot would be obtained for the acceleration $\ddot{q}$, which is directly related to ΔP_o by the inertia M_p in equation (4). Clearly, this type of response shows a high-frequency roll-off of 20 dB/dec, yielding a large amplitude margin and allowing for higher feedback gains. So, if it is possible, from a practical point of view, to measure ΔP_o or $\ddot{q}$, a higher overall performance can be achieved than in case of using ΔP_i.
- *Choice of the servo-valve.* A high performance valve will, in general, not solve the stability problems due to transmission line effects, as shown in this paper. In some cases a valve with a smaller bandwidth might yield wider stability margins, allowing for larger feedback gains. But, in general, valve dynamics are the basic limitation of the allowable pressure feedback gain, required for high-performance control, irrespective of transmission line dynamics (Schothorst *et al.*, 1994).
- *Advanced control design for the pressure feedback loop.* An effective solution to the stability problem is the design of (digital) filters for the feedback signal. In case a high-bandwidth valve is available, it may even be possible to compensate exactly for the transmission line dynamics, e.g. by using the inverse model. Furthermore, by applying modern techniques, like robust control, a trade-off between stability robustness and performance can be made.
- *Application of short transmission lines.* During the design of (long-stroke) hydraulic actuators, the transmission lines should be kept as short as possible. Thus, the resonance modes are kept in the (very) high-frequency range, so that interference with the high-performance actuator control loop may be avoided.

In order to achieve an optimal performance of the hydraulic servo-system, the aforementioned techniques have to be combined.

Conclusions

In applications where long-stroke hydraulic actuators are required, e.g. flight simulator motion systems, transmission line effects have to be taken into account in the control design. The transmission line dynamics can easily be incorporated in the model of the hydraulic servo-system by means of the modal approximation technique as proposed by Yang and Tobler (1991). Hereby, physical insight in the model is preserved.

By modelling the servo-system in this way, a good agreement with experiments is obtained, providing confidence in model based analysis and synthesis of control design strategies.

Concerning the design of high-performance pressure cq. force control loops, stability problems may be encountered for specific combinations of valve and transmission line dynamics. Solutions to this problem can be found in the actuator design, the choice and placing of transducers and the control design.

Future work

Future research will focus on the application of control techniques, which explicitly take the transmission line dynamics into account. Especially, robustness will be given more attention, as the resonance frequencies have been observed to vary with the actuator position.

Acknowledgement

The authors wish to thank Eddy van Oosterhout for his work on the modelling of transmission line dynamics in a hydraulic servo-system. The interaction of transmission line effects and valve dynamics have been subject of research during his graduation project, performed at the Mechanical Engineering Systems and Control Group.

References

Advani, S.K. (1993). The development of Simona: a simulator facility for advanced research into simulation techniques, motion system control and navigation system technoglogies. *Proc. of AIAA Flight Simulation Technologies Conference*, Montery, August 9-12. AIAA-93-3574-CP.

Feuser, A. Von (1984). Design of state controllers in the time and frequency domain for position control of a valve-controlled servo-hydraulic linear drive (in German). *Regelungstechnik 32*, vol. 9, pp. 309-316.

Ham, A.A. (1982). *On the Dynamics of Hydraulic Lines Supplying Servo-Systems.* PhD. Thesis, Delft University of Technology, Faculty of Mechanical Engineering.

Heintze, J. and A.J.J. van der Weiden (1994). Inner loop design and analysis for hydraulic acutator, with application to impedance control. *Proc. Fourth IFAC Symp. Robot Control*, September 19-21, Capri, Italy, pp. 401-406.

Lebrun, M., S. Scavarda and A. Jutard (1978). Computer simulation of a two-stage servo-valve (in French). *Automatisme, vol. 23*, March - April, pp. 84-95.

Lin, S.J. and A. Akers (1991). Dynamic analysis of a flapper-nozzle valve. *J. Dynamic Systems, Measurem. Control, Trans. ASME, 113*, 163-167.

Merrit, H.E. (1967) *Hydraulic control systems.* John Wiley & Sons, Inc.

Schothorst, G. van, O.P. van Wel, P.C. Teerhuis and A.J.J. van der Weiden (1994). Modeling of an electro-hydraulic servo-valve in view of high-performance hydraulic actuator control. To be published.

Oosterhout, E. van (1992). *Transmission Line Dynamics in Hydraulic Servo-Systems.* Report A-626, Mechanical Engineering Systems and Control Group, Delft University of Technology.

Viersma, T.J. (1990). *Analysis, Synthesis and Design of Hydraulic Servo-Systems and Pipelines* Delft University of Technology, Faculty of Mechanical Engineering, 2nd edition.

Walters, R.B. (1991). *Hydraulic and Electro-Hydraulic Control Systems.* Elsevier Applied Science.

Watton, J. (1987). The dynamic performance of an electrohydraulic servo-valve/motor system with transmission line effects. *J. Dynamic Systems, Measurem. Control, Trans. ASME, 109*, 14-18.

Watton, J. and M.J. Tadmori (1985). Damping characteristics of transmission lines with sudden closure of underlapped electrohydraulic servo-valves. *Dynamic Systems: Modelling and Control, Proc. ASME Winter Annual Meeting*, Miami Beach, FL, USA, vol. 85, pp. 135-140.

Watton, J. and M.J. Tadmori (1988). A Comparison of Techniques for the Analysis of Transmission Line Dynamics in Electrohydraulic Control Systems. *Applied Mathematical Modelling*, vol. 12, Butterworth Publishers.

Yang, W.C. and W.E. Tobler (1991). Dissipative modal approximation of fluid transmission lines using linear friction model. *J. Dynamic Systems, Measurem. Control, Trans. ASME, 113*, 152-162.

Selected Topics in Identification, Modelling and Control
Vol. 7, December 1994

Zero-ripple torque control in brushless DC motors

Henk Huisman

Mechanical Engineering Systems and Control Group
Delft University of Technology, Mekelweg 2, 2628 CD Delft, The Netherlands.

Abstract. The subject of zero-ripple torque control in Brushless DC Motors has gained importance due to the growing popularity of small electric motors in consumer electronic applications. A low number of phases and the occurrence of production tolerances give rise to low-frequency torque errors, which manifest themselves as relatively large position errors due to the low inertia of these small drives. With regard to the tight specifications of the controlled performance, reduction of these low frequent torque errors is desirable.
In literature, two main approaches have been demonstrated for the analysis and minimization of torque ripple. One approach is based on Fourier analysis, while the other uses calculus of variations to find optimal current waveforms.
In this paper, a new approach is presented for the determination of optimal current waveforms. The approach is based on an analysis of the back-emf's in the angular domain, and can be used even in the case when both the back-emf's and the stator resistances show asymmetry.
The new approach is compared to the Fourier method in a test case, and shows significant reduction in RMS and average values of the stator currents needed to generate a desired torque.

Keywords. Brushless DC motors; electrical torque ripple; current control.

1 Introduction

Due to their favourable characteristics, Brushless DC Motors (BLDCM's) are used more and more in applications where until recently classical Brush DC Motors (BDCM's) used to be common. Mostly, three-phase BLDCM's are used, as these offer the lowest complexity of the drive electronics.

BLDCM's are characterized by a trapezoidal back emf and square wave stator currents, whereas Synchronous Permanent Magnet Motors (SPMM's) feature sinusoidal back-emf and currents. In the sequel we will use BLDCM as a common denominator for both motor types.

Ideally, the interaction of the waves of the back-emf and the stator current in both cases leads to an electromagnetic torque which is constant, irrespective of the actual position of the rotor. However, these ideal wave shapes can not be realized in practice. On one side, a trapezoidal or sinusoidal back-emf is hard to realize with permanent magnets. Dually, ideal sinusoids or infinitely steep square wave currents are impossible to generate with a power converter with limited supply voltage and switching frequency.

Compared to BDCM's, three-phase BLDCM's often show a relatively large torque ripple. One reason for this behaviour is that the underlying assumptions of the motor behaviour (sine/sine or square/trapezoid) are violated. This being the case, the ripple is aggravated because of the relatively low number of phases compared to professional BDCM's, which feature at least 5 rotor phases. As a consequence of this torque ripple, a periodic position error will result. As long as the torque ripple has a relatively high frequency (large number of motor poles, and/or high rotation speed) and the driven mechanical system is stiff and has a large inertia, this position error will be small and can often be neglected. However, in the presence of possibly res-

onant mechanical structures, with small inertias and more stringent accuracy specifications, the problem of torque ripple gains relevance.

The reduction of torque ripple has been the subject of a number of recent papers, see Hanselman *et al.* (1992), Hung and Ding (1992), Hung and Ding (1993), Kempkes and Sattler (1993), Hanselman (1994). The dominant approach in these papers for the analysis of the problem has been to develop the well-known torque equation for a BLDCM in Fourier components, and use numerical analysis software to find the Fourier coefficients of the optimal stator currents. An inverse Fourier transform then yields the components of the optimal stator currents in the time domain.

A different approach has been advocated somewhat earlier in the German literature, see Grotstollen (1984), Schröder (1986), Schröder (1988). Here, an analytical optimization is made by means of calculus of variations, in order to obtain the optimal current waveforms. However, the derivation is somewhat more involved than the Fourier series approach, especially in the case of delta-connected windings. In this paper we will concentrate on the reduction of torque ripple due to an asymmetrical configuration of the BLDCM. Such an asymmetry could be caused by production tolerances, which can become a serious factor for miniature motors. It will be shown that even in the presence of such asymmetries, a constant torque can be generated if properly shaped asymmetrical currents are fed into the stator windings.

An important observation here is that the instantaneous value of the optimal stator currents is solely dictated by the instantaneous value of the derivative of the flux linkages. The actual speed of the motor, and the mechanical trajectory to follow are of no importance in this respect.

This observation is used for an alternative method to obtain the optimal stator currents in the time domain. This method is less complicated mathematically, and yields stator currents with a lower RMS value for the same torque, compared to the Fourier component approach.

The paper is structured as follows: Section 2 introduces a simplified model of the BLDCM. The most common sources of torque ripple are shown, together with their consequences for the position error. The torque equation of this model is then used in section 3 to derive optimal current waveforms. The derivation for the case of both asymmetrical back-emf's and stator resistances is performed using the computer algebra package Maple (Char *et al.*, 1991).

Section 4 elaborates on the treatment of reluctance and cogging torque components.

Section 5 shows the result of the application of the new derivation to a test case which has been presented in recent literature (Hung and Ding, 1992). The cases of floating and non-floating neutral are discussed separately. A comparison of the results to the cited test case shows that our derivation needs ca. 10% lower average current, and 7% lower RMS currents to obtain the same torque. The same result is obtained with the Fourier-based approach only if a very large (infinite) number of harmonics is taken into account, and this at the expense of significant computational effort. Some system aspects of the new derivation are discussed in section 6. The conclusions of this work are presented in section 6.

2 Model of the Brushless DC Motor

A possible realization of a Brushless DC Motor has been depicted in Fig. 1.

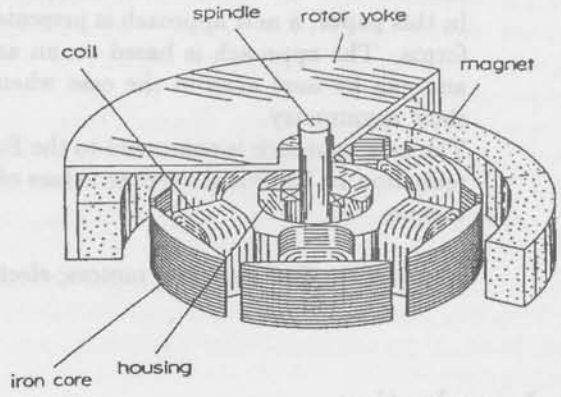

Fig. 1: Construction of a small BLDC Motor (taken from Nouws (1994))

The inner part of the construction shows the fixed stator windings. The outer part shows the cupped rotor, consisting of a ring-shaped permanent magnet, which is supported by the yoke. The six stator windings are pair-wise connected in series, and thus combined in three phases. The equivalent electrical circuit has been depicted in Fig. 2.

The circuit shown in Fig. 2 consists of 3 identical stator phases, each comprising a resistance R_{si}, and self- and mutual inductances which have been indicated symbolically with L and M. The stator phases each are powered by a voltage difference $U_{ia} - U_{ib}$. The lower part of the circuit shows the rotor winding, which has symbolically been powered with an ideal current source i_r. The rotor winding is cou-

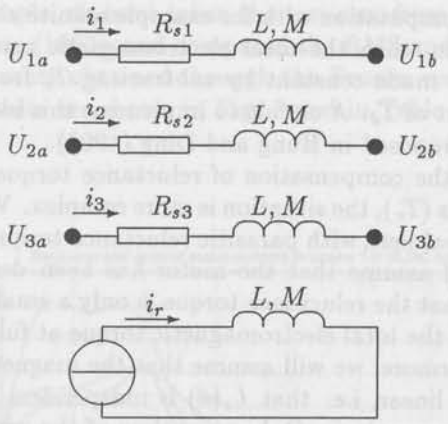

Fig. 2: Electrical circuit of a BLDC Motor

pled to the stator windings through their mutual inductances.

The electromagnetic torque in an electrical machine is dependent on the values of the stator and rotor currents. For a typical coil (pair) on stator or rotor, the following components can be distinguished:

- Cogging torque T_c, which depends on the square of the rotor current i_r and on the variation of the rotor self-inductances L_r versus the rotation angle θ: $T_c = \frac{dL_r}{d\theta} i_r^2$,
- Reluctance torque T_r, which depends on the square of the stator current i_s and on the variation of the stator self-inductances L_s versus θ: $T_r = \frac{dL_s}{d\theta} i_s^2$,
- Direct torque T_d, which depends on the product of stator and rotor currents and on the variation of the mutual inductance M versus θ: $T_d = \frac{dM}{d\theta} i_s i_r$.

In a BLDCM, the coil carrying rotor current is replaced by the field of permanent magnets. Consequently, the cogging torque will only depend on the geometry of the magnetic circuit, and can not be influenced once the motor has been realized. Reluctance torque can be influenced, but will often be negligibly small because of the presence of a constant differential permeability, due to the permanent magnets, along the air gap. For simplicity we will deal with the cogging and reluctance torque later. The direct torque production in a three-phase BLDCM can than be written as follows:

$$T_d = i_1 i_r \frac{dM_1}{d\theta} + i_2 i_r \frac{dM_2}{d\theta} + i_3 i_r \frac{dM_3}{d\theta} \qquad (1)$$

where the i_i denote the three stator currents, i_r the equivalent rotor current (modeled by a single winding), and the M_i denote the mutual inductances between the equivalent rotor winding and the three stator windings, respectively. Rewriting (1) leads to the following well-known equation for the direct torque:

$$T_d = \frac{e_1 i_1 + e_2 i_2 + e_3 i_3}{\Omega} \qquad (2)$$

where $\Omega = \frac{d\theta}{dt}$ denotes the mechanical angular frequency of the rotor, and the e_i represent the so called back-emf's, given by:

$$e_i = i_r \frac{dM_i}{dt} \qquad (3)$$

Note that the back-emf's have the dimension of a voltage. These voltages can be measured across the stator windings if the motor is rotating and the stator currents are zero.

The magnitude of the back-emf is proportional to the rotational speed, while the shape is determined by the angular derivative of the magnetization. For the common case where the back-emf's have a trapezoidal shape and the currents consist of 120 deg. square waves, a constant torque results. If, however, the shape of the back-emf's approaches a sine wave, or if a phase shift or amplitude error is present, significant torque ripple results.

3 Derivation of optimal current waveforms

In this section, we will assume that the position of the rotor axis θ is available with sufficient accuracy, either by direct measurement or by means of a state observer (see for example Brunsbach *et al.* (1993)).

For simplicity of notation, we will first introduce the shape functions E_i for the back-emf's as follows:

$$E_i(\theta) = \frac{e_i(\theta)}{\Omega} = i_r \frac{dM_i}{d\theta} \qquad (4)$$

Note that the E_i are only dependent on θ, i.e. the mechanical position of the rotor. Substitution of (4) in (1) yields:

$$T_d = E_1 i_1 + E_2 i_2 + E_3 i_3 \qquad (5)$$

Clearly, if a desired value of T_d is known, it is possible to obtain this value through an appropriate choice of the stator currents i_i as long as at least one of the E_i is nonzero, i.e. if a change in the magnetic field is linked to at least one of the stator coils.

If the three stator currents can be controlled independently, and all the E_i are nonzero, we can freely pick two of the i_i and then use (5) to compute the third current. Thus, in this case we have two degrees of freedom while selecting the currents.

Another case exists where the three stator phases are Wye-connected, and the sum of the three stator currents is forced to be zero:

$$i_1 + i_2 + i_3 = 0 \tag{6}$$

Still, in this case we can pick one of the currents, and use (5) and (6) to compute the third. Thus, in this case we have one degree of freedom. The freedom for picking one or two of the stator currents can be used to advantage to minimize the losses in the stator windings. These losses (P_{loss}) can be expressed as follows:

$$P_{loss} = R_1 i_1^2 + R_2 i_2^2 + R_3 i_3^2 \tag{7}$$

where the R_i denote the (not necessarily equal) resistances of the stator windings. The optimal stator currents for a certain torque can now be expressed as:

$$i_i = arg(min(P_{loss}(i_i))|(5)) \tag{8}$$

or

$$i_i = arg(min(P_{loss}(i_i))|(5)|(6)) \tag{9}$$

respectively. After some elementary algebra, which is performed in the appendix, the solutions to these equations can be found. For the case where no restrictions exist to the sum of the three currents we obtain for i_1:

$$i_1 = T_d \frac{R_{s2}R_{s3}E_1}{R_{s2}R_{s3}E_1^2 + R_{s3}R_{s1}E_2^2 + R_{s1}R_{s2}E_3^2} \tag{10}$$

For the Wye-connected stator the current in phase 1 is expressed by:

$$i_1 = T_d \frac{(R_{s2}+R_{s3})E_1 - (R_{s2}E_3 + R_{s3}E_2)}{R_{s1}(E_2-E_3)^2 + R_{s2}(E_3-E_1)^2 + R_{s3}(E_1-E_2)^2} \tag{11}$$

In both cases the equations for the other two currents can be found by simple rotation of indices. Clearly, these equations can be simplified considerably if equal stator resistances are assumed.

For an implementation, the shape functions E_i need to be measured, and the shapes of the stator currents i_i/T_d can be computed off-line and stored in a prom memory. After multiplication with T_d the setpoints for the three currents are then available. Examples of such systems have been given in Schröder (1988), Hanselman (1994).

4 Cogging and Reluctance Torque

So far, only the direct torque component of the BLDCM has been treated. If parasitic cogging and reluctance torque components are present, adjustments are needed.

Cogging torque T_c in a BLDCM depends only on the actual rotor position. Assuming that the value of $T_c(\theta)$ is known, either from measurements or from computation with for example a finite element program, then the total electromagnetic torque T can be made constant by subtracting T_c from the setpoint of T_d. A circuit to implement this idea has been proposed in Hung and Ding (1993).

For the compensation of reluctance torque components (T_r), the situation is more complex. We will only deal here with parasitic reluctance torques, i.e. we will assume that the motor has been designed such that the reluctance torque is only a small fraction of the total electromagnetic torque at full load. Furthermore, we will assume that the magnetic circuit is linear, i.e. that $L_s(\theta)$ is independent of the stator currents i_i. Only an outline of the proposed method will be given here, as the method is very similar to the one used to obtain (10) and (11).

Again, for brevity of notation, we start with defining shape functions F_i to represent the variation in the stator inductances:

$$F_i(\theta) = \frac{dL_{si}}{d\theta} \tag{12}$$

which are only dependent on θ. The sum of direct and reluctance torque can then be notated as follows:

$$T_d + T_r = E_1 i_1 + F_1 i_1^2 + E_2 i_2 + F_2 i_2^2 + E_3 i_3 + F_3 i_3^2 \tag{13}$$

The optimal currents for this situation are given by

$$i_i = arg(min(P_{loss}(i_i))|(13)) \tag{14}$$

for the case where the three stator currents can be controlled independently, or

$$i_i = arg(min(P_{loss}(i_i))|(13)|(6)) \tag{15}$$

for the Wye-connected stator. The actual computation of (14) and (15) is quite more involved, because of the quadratic terms in (13). We will not go into the intricacies here, but intend to deal with them in a future paper.

5 Comparison and Extensions

It is worthwhile to compare the computation effort of (10) and (11) to the approach presented in Hung and Ding (1993), where quite sophisticated matrix calculations are used to obtain almost the same result. With our method, the table for values of the i_i can be computed directly from the measured values of the stator resistances and the back-emf.

It can be shown that the solution via the Fourier approach is an approximation of the optimal waveforms as described by (10) or (11). Only when an infinite number of harmonics is taken into account, the Fourier solution converges to the same result. As

an example, we have taken the test case from Hung and Ding (1993), and computed the RMS and average currents obtained through the Fourier method. The results are shown in Fig. 3 and in Table 1.

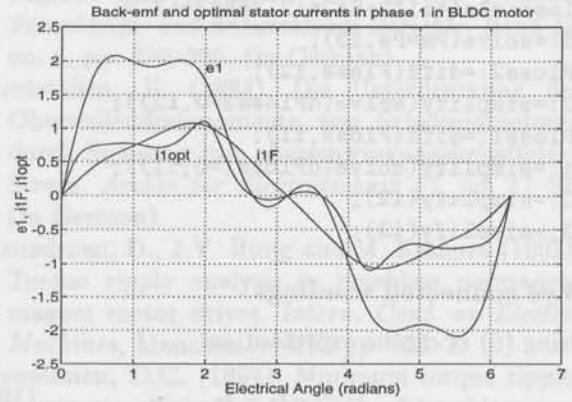

Fig. 3: Waveforms of e_1, i_1F (Fourier method) and $i_1$opt (new method)

Quantity	Fourier method	New method
i_1 average [A]	0.6481	0.5820
i_1 rms [A]	0.7232	0.6725

Table 1: Comparison of average and rms currents for both methods

Clearly, our simple calculation generates better currents with respect to the loading of the semiconductors and to losses.

More fundamentally, we have shown here that the optimal value for the stator currents can be obtained from 'local' data: for a certain rotor position only the values of the shape functions E_i *at this particular position* are relevant to the computation of the stator currents. Therefore, using data from all measured rotor positions for every sample of the optimal stator current seems to be a waste of effort. Inspection of the waveforms in Fig. 3 shows that the waveforms computed with the Fourier method in this example actually generate a negative torque around the zero crossing at $\theta = \pi$. To obtain the same net torque production, the other two stator phases will need more current: this is the main reason for the diminished efficiency.

6 Discussion

With regard to the material presented above, several questions and crosslinks come to mind. We will deal with them in a somewhat loose manner, the intention being more to draw attention to related topics and unsolved questions than to provide explicit solutions.

Limited supply voltage

One of the problems associated with current controlled PM machines is that at the end of the speed or torque range the current controllers will saturate due to the limited supply voltage.

It has been suggested in literature (Hanselman, 1994) that keeping the range of harmonics used in the stator currents low will result in lower consumption of the supply voltage range. Our work shows that selective addition of higher harmonics can be used to obtain a lower overall RMS content. We conclude that the best way to control the stator currents depends on the operating speed and torque load on the motor:

- As long as the supply voltage is not a limiting factor, use (10) or (11) to compute the optimal currents,
- If only one of the three current controllers saturates, compute the other two currents, using (5) and (6), to generate zero torque ripple,
- If two or more current controllers saturate, ripple-free generation of the desired torque is no longer possible.

It can be concluded that if lowest torque ripple is at a premium, it is worthwhile to design the motor such that the voltage limit is reached at the same speed or torque for all stator positions. In this way the torque ripple can be kept small up to the maximum design speed, and the magnetic circuit will be used to the fullest.

In practical applications, it will often be the case that torque ripple and the associated position error will be less important at high speeds than around standstill. One reason is that the frequency of the torque ripple will be much higher, resulting in lower position errors due to the integrating properties of the mechanical load. Furthermore, high ripple frequencies will often lie outside the bandwidth of the controlled system.

Optimum power factor

We like to point out here that the problem of finding optimal stator currents for a BLDCM is strongly related to determining currents which optimize

the power factor in multiphase power grids (Fischer, 1985*a*; Fischer, 1985*b*; Huisman and Haan, 1987). In fact, viewing the BLDCM as a generator of (negative) electrical power makes this relation quite obvious.

Conclusions

With today's availability of fast current control at substantial power levels, the torque production in BLDCM's can be precisely set to any desired level. In particular, constant torque operation, irrespective of the actual rotor position, is possible. In this paper, a simple method has been presented which permits to compute the optimal stator currents to achieve this. The computation method is based on calculus, and assumes that the waveforms of the back-emf's are known.

The method applies both to Wye-connected and independently excited motors. No assumptions are made regarding the symmetry of the three back-emf waveforms or the stator resistances, and therefore the method is especially suited for the computation of optimal currents for small motors which are more likely to show asymmetries due to production tolerances.

In an example, it is shown that the waveforms obtained with the new method have better properties with regard to power losses and semiconductor loading than the waveforms obtained through a Fourier series approach.

Appendix

In this appendix we will compute the optimal values for the stator currents both for the non-Wye (8) and Wye-connected (9) stator windings. For the computation, the symbolic package Maple (Char *et al.*, 1991) has been used. The relevant parts of the text files used in this package are shown after the actual equations.

non-Wye connected windings

Using (5) i_3 can be expressed as:

$$i_3 = \frac{T_d - E_1 i_1 - E_2 i_2}{E_3} \tag{16}$$

by substitution in (7) we obtain:

$$P_{loss} = R_1 i_1^2 + R_2 i_2^2 + R_3 \left(\frac{T_d - E_1 i_1 - E_2 i_2}{E_3} \right)^2 \tag{17}$$

To obtain an extreme, we set the derivative of P_{loss} to i_2 to zero, obtaining:

$$i_2 = -\frac{R_3 E_2 (-T + E_1 i_1)}{R_2 E_3^2 + R_3 E_2^2} \tag{18}$$

Now substitute this value for i_2 in (17), and set the derivative to i_1 to zero, to obtain the desired result (10).

Maple file for non-Wye connected windings

```
Pm:=omega*T;
Pe:=e1*i1+e2*i2+e3*i3;
Ploss:=Rs1*i1^2+Rs2*i2^2+Rs3*i3^2;
i3:=solve(Pm=Pe,i3);
dPloss2:=diff(Ploss,i2);
i2:=simplify(solve(dPloss2=0,i2));
dPloss1:=diff(Ploss,i1);
i1:=simplify(solve(dPloss1=0,i1));
i2:=simplify(i2);
i3:=simplify(i3);
```

Wye connected windings

Using (6) i_3 can be expressed as:

$$i_3 = -i_1 - i_2 \tag{19}$$

by substitution in (7) we obtain:

$$P_{loss} = R_1 i_1^2 + R_2 i_2^2 + R_3 (-i_1 - i_2)^2 \tag{20}$$

Using (5) i_2 can be expressed as:

$$i_2 = -\frac{T_d - E_1 i_1 - E_3 i_1}{E_3 - E_2} \tag{21}$$

Substitution of this value in (20), and computation of the extreme for i_1 produces the desired result (11).

Maple file for Wye connected windings

```
Pm:=omega*T;
Pe:=e1*i1+e2*i2+e3*i3;
Ploss:=Rs1*i1^2+Rs2*i2^2+Rs3*i3^2;
Sigmai:=i1+i2+i3;
i3:=solve(Sigmai=0,i3);
i2:=solve(Pm=Pe,i2);
dPloss:=diff(Ploss,i1);
i1:=simplify(solve(dPloss=0,i1));
i2:=simplify(i2);
i3:=simplify(i3);
```

References

Brunsbach, B.J., G. Henneberger and Th. Klepsch (1993). Position Controlled Permanent Excited Synchronous Motor without Mechanical Sensors. *Proc. European Power Electronics Conf.*, Brighton, UK, vol. 6, pp. 38–43.

Char, B.W., K.O. Gedels, G.H. Gonner, B.L. Leang, M.B. Monagan and S.M. Watt (1991). *Maple V Library Reference Manual.* Springer Verlag.

Fischer, H.D. (1985*a*). Leistungsbegriffe fur Mehrphasensysteme. Teil I: Die Leistungsbegriffe nach Buchholz und nach Quade. *Siemens Forschungs- und Entwicklungs Berichte Band 14 nr 5*, Springer Verlag, pp. 245–251. (In German).

Fischer, H.D. (1985*b*). Leistungsbegriffe fur Mehrphasensysteme. Teil II: Vergleich der Leistungsbegriffe nach Buchholz und Quade. *Siemens Forschungs- und Entwicklungs Berichte, Band 14*, no. 6, pp. 299–305. (In German).

Grotstollen, H. (1984). Die Unterdruckung der Oberwellendrehmomente von Synchronmotoren durch Speisung mit oberschwingungsbehaftetem Strom. *Archiv für Elektrotechnik 67*, pp. 17–27. (In German).

Hanselman, D., J.Y. Hung and M. Keshura (1992). Torque ripple analysis in brushless permanent magnet motor drives. *Intern. Conf. on Electric Machines*, Manchester, UK, pp. 823–7.

Hanselman, D.C. (1994). Minimum torque ripple, maximum efficiency excitation of brushless permanent magnet motors. *IEEE Trans. Industrial Electronics, vol. 41*, no.3, pp. 292–300.

Huisman, H. and S.W.H. de Haan (1987). General control method for high-frequency multiphase power converters. *Proc. Power Conversion International*, Munich, Germany, pp. 201–219.

Hung, J.Y. and Z. Ding (1992). Minimization of torque ripple in permanent magnet motors: a closed form solution. *IEEE Intern. Conf. on Industrial Electronics*, San Diego, CA, pp. 459–463.

Hung, J.Y. and Z. Ding (1993). Design of currents to reduce torque ripple in brushless permanent magnet motors. *IEE Proceedings-B, vol. 140*, pp. 260–266.

Kempkes, J. and Ph.K. Sattler (1993). Comparison of true running at different concepts of controlling brushless dc-motors. *Proc. European Power Electronics Conf.*, Brighton, UK, Vol. V, pp. 15–20.

Nouws, A.C.A.M. (1994). *Modelling and Simulation of a Hard Disk Drive for a Study of the Start-up Behaviour*. M.Sc.-Thesis. Philips Electronics.

Schröder, M. (1986). *Hochtouriger Bürstenloser Positionierantrieb mit Extrem Geringer Momentenwelligkeit*. Ph.D-Thesis. University of Stuttgart, Germany. (In German).

Schröder, M. (1988). Einfach anzuwendendes Verfahren zur Unterdruckung der Pendelmomente dauermagneterregter Synchronmaschinen. *etz Archiv, Band 10, Heft 1*. pp. 15–8. (In German).

Selected Topics in Identification, Modelling and Control
Vol. 7, December 1994

Predictive servo control through optimal feedforward compensation

D. de Roover

Mechanical Engineering Systems and Control Group
Delft University of Technology, Mekelweg 2, 2628 CD Delft, The Netherlands.

Abstract. This paper considers the servo problem of tracking a known reference trajectory in the presence of (deterministic) disturbances. Solving this problem by designing a suitable feedforward signal is favourable, as this leaves the closed loop dynamics unaltered. An algorithm is developed which not only solves this problem, but also yields an optimal solution under constraints on the input and output signals. Prediction of the output signal is used to calculate an optimal feedforward signal that minimizes the difference between this prediction and the desired reference trajectory according to some criterion. A simulation example explains the ability of the method, which easily trades-off constraint handling against performance specifications.

Keywords. Trajectory tracking; disturbance rejection; prediction; optimal feedforward; constraint handling.

1 Introduction

In this paper the classical servo problem is considered: tracking a known reference trajectory in the presence of (deterministic) disturbances. It is well recognized that the influence of deterministic disturbances can only be eliminated effectively if the controller encloses a model of these disturbances, as stated by the *internal model principle*. During the past decades numerous techniques have been developed which are based upon this principle, e.g. the well-known servo compensator, developed by Davison (1972) and formalized by Francis and Wonham (1976). If an exact model of the reference- and/or disturbance dynamics is included, the servo compensator provides both asymptotic tracking of the reference signal and asymptotic rejection of the disturbance signal. The disability of this method is the non-robustness of the compensator in the face of modeling errors. Besides, the order of the compensator increases rapidly with each mode of the included model, which limits its practical pertinence.

In the late seventies, Richalet *et al.* (1978) and Cutler and Ramaker (1980) simultaneously introduced the concept of *model based predictive control*, developed in industry, which turned out to be extremely powerful in a sense that tracking performance was optimized in the presence of (deterministic) disturbances by means of easily tunable algorithms. Moreover constraints on input and output signals could easily be handled. Since then the number of applications and the number of papers on this subject have increased rapidly though the basic elements of each 'new' algorithm remained unaltered, see for example Clarke *et al.* (1985), De Keyser and Van Cauwenberghe (1985) and Richalet and Papon (1985). The main inutility of this approach is its computationally involveness, because at each sampling instant a (constrained) optimization problem has to be solved.

Halfway the eighties two related control strategies were developed, known as *learning* and *repetitive* control, which focussed on the suppression of purely periodic disturbances, by adding a filtered version of the servo error to the control loop; an internal model of the periodic disturbance is used to properly design the learning/repetitive controllers, see e.g. Arimoto *et al.* (1984), Kavli (1992), Moore *et al.* (1992), Tomizuka (1987) and Chew and Tomizuka (1990). The main difference between these two tech-

niques is that a learning controller is implemented off-line by iteratively updating a feedforward signal over a finite time horizon (external model technique) while a repetitive controller is placed inside the loop, hence constituting an extension of the controller dynamics (internal model technique). Both techniques provide asymptotic tracking and disturbance rejection. The most important limitation of learning control is that it is restricted to a repeated reference trajectory requiring initial conditions to be the same during each cycle. Its main advantage is the idea of generating near to optimal feedforward signals, which leave the closed loop dynamics unaltered. The main shortcoming of a repetitive controller equals that of a servo compensator, namely the non-robustness against errors in the modelling of periodic disturbances.

From a completely different point of view, *input shaping* techniques have been developed which design optimal point-to-point trajectories for a servo mechanism, based on an accurate model of this system; only the steering of the servo mechanism from one position to another is considered without taking external disturbances acting on the system into account, see e.g. Singer and Seering (1989) and Bhat and Miu (1990,1991). The begin- and end-position are assumed to be given in this case, while the designer has the freedom to choose the intermediate trajectory. In general this freedom is used to suppress residual vibrations, caused by excitation of flexible system modes. In la Bastide (1994) it is shown that learning and repetitive control can be regarded as a kind of iterative input shaping techniques where the reference signal is adjusted such that the output of the system equals the desired output asymptotically.

In this paper an algorithm is developed which combines several aspects of the previously mentioned methods. If an arbitrary reference trajectory, a model of the system and a model of the disturbance affecting the system are given, an optimal feedforward signal is computed which minimizes the difference between the given reference trajectory and a prediction of the output of the system, according to some criterion. The prediction is based on a nominal model of the system and a model of the disturbance. If the disturbance is a stochastic process, *k-step-ahead* prediction of the noise is used. If on the other hand the disturbance is deterministic, a Kalman filter is used to reconstruct the disturbance. Moreover, due to its finite time nature, the procedure is able to handle constraints on input and output signals in a natural way, which contributes to its practical pertinence; actuator constraints and performance aspects can easily be specified in this way.

The remainder of this paper consists of a mathematical description of the problem and a formal derivation of the forementioned algorithm. The procedure is illustrated with a simulation example. Finally some conclusions are drawn.

2 Formulation of the Servo Problem

Assume that the true process output y_0 is generated by:

$$y_0(t) = P_0(q)u(t) + d(t),$$
$$t = -\infty, \ldots, -1, 0, 1, \ldots, \infty, \qquad (1)$$

where $P_0(q)$ is the transfer function from u to y_0 with q being the forward time shift operator, $u(t)$ is an input signal applied to the process, and $d(t)$ is an (unknown) disturbance signal acting on the process. Furthermore the following assumptions are made:

Assumption 2.1 *A set of sampled measurements* $\{y_m(t-k), u_m(t-k)\}$, $k = 0, \ldots, M$, *is available.*

Assumption 2.2 *A model of the true process* $\hat{P}_0(q) = \sum_{k=0}^{M} \hat{p}_0(k)q^{-k}$, *where* $\hat{p}_0(k), k = 0, \ldots, M$ *are the pulse response coefficients of the model*[1], *is available.*

Assumption 2.3 *A (desired) reference trajectory* $y_r(t+k)$, $k = 1, \ldots, N$, *is available.*

Assumption 2.4 *Depending on the character of the disturbance* $d(t)$, *one of the following assumptions is made:*

1. *If* $d(t)$ *is a stochastic process, it is assumed to be generated by* $d(t) = H(q)n(t)$, *where* $H(q)$ *is a known stable, LTI, monic transfer function and* $n(t)$ *is white noise with zero mean and finite covariance.*

2. *If* $d(t)$ *is a deterministic process, it is assumed to be generated by a known autonomous system* $d(t) = C_d n(t), n(t+1) = A_d n(t)$, $n(0) = n_0$, *where* $n(t)$ *is a state-vector at time* t *with initial state* n_0; A_d *and* C_d *are appropriate state-space matrices, with the eigenvalues of* A_d *on or outside the unit circle in the z-plane.*

The servo problem that is considered here is the minimization of the difference between the reference trajectory $y_r(t+k)$ and the output of the true process $y_0(t+k)$ in the presence of the disturbance $d(t+k)$ over the interval $\{t+k\}, k = 1, \ldots, N$, by

[1] Note that not only pulse response models will do but any model (like state space), as long as it can be used to compute predictions

choosing a suitable input signal $u(t+k)$. More formally the following objective function has to be minimized:

$$J_p = \| y_r - y_0 \|_p^p = \sum_{k=1}^{N} | y_r(t+k) - y_0(t+k) |^p, \tag{2}$$

where $\| \cdot \|_p$ denotes the signal $p-$norm. The feedforward signal that minimizes (2) is given by:

$$u_{ff} = \min_{u(t+k)} J_p, \quad k = 1, \ldots, N$$
$$\text{subject to:} \tag{3}$$
$$Au(\cdot) \leq b,$$

where A and b are respectively a matrix and a vector specifying the constraints on u and y_0; constraints on u can be directly specified, while contstraints on y_0 can enter indirectly via equation (1) by choosing $A = \pm P_0$.

Note that in principle any norm can be used in (2), but in most cases the 2-norm is used which measures the energy of the difference between the desired and the true output signal.

3 Derivation of the Predictive Feedforward Controller

Though equations (2) and (3) allow a clear formulation of the problem, it can never be solved in this way because the true output signal y_0 is unknown for future time instants. The best that can be done is to make a prediction of the output over the time interval $\{t+k\}, k = 1, \ldots, N$, using knowledge of the system and the disturbance signal. According to (1) future values of y_0 consist of 2 parts namely a controlled response $y_c(t+k) = P_0(q)u(t+k)$ and a free response $y_f(t+k) = d(t+k)$. A prediction of the controlled response is easily obtained by applying the future input signal u (to be computed) to the model $\hat{P}_0(q)$ of the true process:

$$\hat{y}_c(t+k) = \hat{P}_0(q)u(t+k), \quad k = 1, \ldots, N, \tag{4}$$

where $\hat{y}_c$ denotes a prediction of y_c.

A prediction of the free response is somewhat more complicated and depends on the nature of the disturbance. As becomes clear above, two situations can be distinguished:

1. $d(t)$ is a stochastic process, generated by $d(t) = H(q)n(t)$ where $n(t)$ is zero-mean white noise with finite covariance. A fairly general description for $H(q)$ is the ARMA model $H(q) = C(q)/D(q)$, with $C(q)$ and $D(q)$ polynomials in q. In order to make a prediction of $d(t)$ over k steps, the filter $H(q)$ needs to be split up into a part $E_k(q)$ that convolutes over the interval $\{t+1, t+k\}$ and a part $F_k(q)$ that convolutes over the interval $\{-\infty, t\}$. The polynomials $E_k(q)$ and $F_k(q)$ can be found by solving the following Diophantine equation:

$$C(q) = E_k(q)D(q) + q^{-k}F_k(q).$$

Substituting this in $d(t) = C(q)/D(q)n(t)$ gives:

$$d(t) = E_k(q)n(t) + q^{-k}\frac{F_k(q)}{D(q)}n(t),$$

or:

$$d(t+k) = E_k(q)n(t+k) + \frac{F_k(q)}{C(q)}d(t). \tag{5}$$

Hence a k-step ahead prediction of the free response is given by:

$$\hat{y}_f(t+k) = d(t+k \mid t) = \tfrac{F_k(q)}{C(q)}d(t), \quad k = 1, \ldots, N. \tag{6}$$

Equation (6) can be computed if there is knowledge of $d(t-k)$, $k = 0, \ldots, M$ but in general this will not be the case. However, we can make an estimate of it by using the measured data-set:

$$\hat{d}(t-k) = y_m(t-k) - \hat{P}_0(q)u(t-k), \quad k = 0, \ldots, M. \tag{7}$$

If there is no measurement noise and if the model $\hat{P}_0(q)$ equals the true system P_0, $\hat{d}(t-k)$ will equal $d(t-k)$. Else these corruptions should be regarded as noise contributions, and the prediction will be affected.

2. $d(t)$ is a deterministic process, generated by the autonomous system $d(t) = C_d n(t), n(t+1) = A_d n(t)$, $n(0) = n_0$. Because of the deterministic nature of the noise, a Kalman filter can be used to estimate the state $n(t-k)$ for $k = 0, \ldots, M$ from the measured data-set:

$$\hat{n}(t-k+1) = A_d\hat{n}(t-k) + K[\hat{d}(t-k) - C_d\hat{n}(t-k)], k = 0, \ldots, M, \tag{8}$$

where K is the Kalman gain, and $\hat{d}(t-k)$ is obtained from equation (7).

Now the estimated state at time $t(k=0)$ is used as initial condition for the prediction of the state over the future time interval $\{t+k\}, k = 1, \ldots, N$:

$$n(t+k \mid t) = \hat{n}(t+k) = A_d^k\hat{n}(t), \quad k = 1, \ldots, N.$$

Finally, the prediction of the free response is obtained by:

$$\begin{aligned}\hat{y}_f(t+k) = &\ d(t+k \mid t) = C_d n(t+k \mid t) \\ = &\ C_d A_d^k \hat{n}(t), \ \ k = 1, \ldots, N \end{aligned} \quad (9)$$

Adding the prediction of the controlled response (4) and the prediction of the free response (6) or (9) gives a prediction of y_0:

$$\hat{y}_0(t+k) = \hat{y}_c(t+k) + \hat{y}_f(t+k), \ \ k = 1, \ldots, N. \quad (10)$$

The problem defined by (2) and (3) can now be recasted into a solvable one:

$$\hat{J}_p = \| \, y_r - \hat{y}_0 \, \|_p^p = \sum_{k=1}^{N} | \, y_r(t+k) - \hat{y}_0(t+k) \, |^p. \quad (11)$$

The feedforward signal that minimizes (11) is then given by:

$$\begin{aligned} \hat{u}_{ff} = \min_{u(t+k)} \hat{J}_p, \ \ k = 1, \ldots, N \\ \text{subject to:} \\ Au(\cdot) \leq b, \end{aligned} \quad (12)$$

Two important points should be noted here. First, the computed feedforward signal is optimal for the 'real' system if the predicted output of the system equals the real system output. This stems from the fact that the optimization is performed for the prediction and the outcome is implemented on the real process. However, the question remains how good or how bad the calculated feedforward is in case the predicted output does not match the real system output, or under what condtions the predicted output will equal the real output. The following proposition, based on the triangular inequality for signal norms, formalizes the first question:

Proposition 3.1 *Given a process according to equation (1) and a prediction of the process output according to equation (10). Consider the criteria J_p and $\hat{J}_p$ given by respectively equations (2) and (11). Then a lower- and an upper bound for J_p are given by:*

$$\begin{aligned} \left(\left(\hat{J}_p \right)^{\frac{1}{p}} - \| \, y_0 - \hat{y}_0 \, \|_p \right)^p \leq J_p \leq \\ \left(\left(\hat{J}_p \right)^{\frac{1}{p}} + \| \, y_0 - \hat{y}_0 \, \|_p \right)^p, \end{aligned} \quad (13)$$

where: $\| \, y_0 - \hat{y} \, \|_p$ denotes the p-norm of the prediction error.

Proof: See appendix □

Remark 3.2 *The result stated in proposition 3.1 cannot be calculated a priori because the value of y_0 is unknown. However, it can be used to check after implementation of the feedforward signal whether the optimization based on the prediction was close to the optimization of the 'real' criterion. It can also be used to check convergence of $\hat{J}_p$ to J_p in case an iterative procedure of refining the feedforward signal is followed, where refining can be obtained e.g. by increasing the number of measurements used for prediction after each iteration.*

The following lemma states under what condition $\hat{J}_p$ converges to the criterion J_p:

Lemma 3.3 *Given a process according to equation (1) and a prediction of the process output according to equation (10). Consider the criteria J_p and $\hat{J}_p$ given by respectively equations (2) and (11). Then:*

$$\lim_{\|y_0 - \hat{y}_0\|_p \to 0} \hat{J}_p = J_p. \quad (14)$$

Proof: This follows immediately from propostion 3.1 by taking the limits of the lower- and upper-bound for $\| \, y_0 - \hat{y}_0 \, \|_p \to 0$. □

This result is rather trivial, but it can be used to specify convergence for a number of specific situations as considered in this paper. The following theorem formalizes this result:

Theorem 3.4 *Given a process according to equation (1) and suppose the assumptions 2.1,...,2.4 are satisfied. Also given a prediction of the process output according to equations (4),(6), (9) and (10). Consider the criteria J_p and $\hat{J}_p$ given by respectively equations (2) and (11). Now the following holds true:*

i. If $\hat{y}_c(t+k) = y_c(t+k) \ \forall k = 1, \ldots, N$, and $\hat{y}_f(t+k) = y_f(t+k) \ \forall k = 1, \ldots, N$, then:

$$\hat{J}_p = J_p. \quad (15)$$

ii. If $\exists \ k \in [1, \ldots, N]$, s.t. $\hat{y}_c(t+k) \neq y_c(t+k)$ and $\hat{y}_f(t+k) = y_f(t+k) \ \forall k = 1, \ldots, N$, then:

$$\lim_{\|\Delta_0 u\|_p \to 0} \hat{J}_p = J_p, \quad (16)$$

with $\Delta_0 = P_0 - \hat{P}_0$.

iii. If $\hat{y}_c(t+k) = y_c(t+k) \ \forall k = 1, \ldots, N$, and $\exists \ k \in [1, \ldots, N]$ s.t. $\hat{y}_f(t+k) \neq y_f(t+k)$, then:

a. if $d(t) = H(q)n(t)$ according to assumption 2.4.1, then:

$$\lim_{\|E_k n\|_p \overset{k=1..N}{\longrightarrow} 0} \hat{J}_p = J_p. \quad (17)$$

b. if $d(t) = C_d n(t), n(t+1) = A_d n(t)$, $n(0) = n_0$, *according to assumption 2.4.2, and* $n(t)$ *is reconstructed using the Kalman filter given in equation (8), then:*

$$\lim_{\|(A_d - KC_d)^k \tilde{n}_0\|_p \xrightarrow{k=1..N} 0} \hat{J}_p = J_p, \qquad (18)$$

with $\tilde{n}_0 = \tilde{n}(t) = n(t) - \hat{n}(t)$, $(k = 0)$.

iv. If $\exists\, k \in [1, \ldots, N]$ *s.t.* $\hat{y}_c(t+k) \neq y_c(t+k)$ *and* $\exists\, l \in [1, \ldots, N]$ *s.t.* $\hat{y}_f(t+l) \neq y_f(t+l)$, *then:*

a. if $d(t) = H(q)n(t)$ *according to assumption 2.4.1, then:*

$$\lim_{\|\Delta_0 u\|_p, \|E_k n\|_p \xrightarrow{k=1..N} 0} \hat{J}_p = J_p. \qquad (19)$$

b. if $d(t) = C_d n(t), n(t+1) = A_d n(t)$, $n(0) = n_0$, *according to assumption 2.4.2, and* $n(t)$ *is reconstructed using the Kalman filter given in equation (8), then:*

$$\lim_{\|\Delta_0 u\|_p, \|(A_d - KC_d)^k \tilde{n}_0\|_p \xrightarrow{k=1..N} 0} \hat{J}_p = J_p. \qquad (20)$$

Proof: See appendix □

Remark 3.5 *The conditions stated in part ii. and iv. of theorem 3.4 are rather stringent and not very useful in practice. However, there are situations where these conditions can be loosened. For example in learning control, where a reference trajectory is repeated a number of times, one of the basic assumptions is that the initial conditions are the same at the start of each new cycle. This means that the contribution of the undermodeling (i.e. the mismatch between the model* $\hat{P}_0$ *and the system* P_0*) to the servo- error has to be the same each new cycle. This in fact means that, considered over a number of cycles, the contribution of the modeling error becomes periodic with period-time equal to the period-time of the cycle. In that case this part of the error due to undermodeling fulfills assumption 2.4.2 which means that it can be regarded as a part of the free-response, instead of a deterioration of the controlled response. Hence the proposed procedure should follow an iterative scheme of updating the prediction over a number of cycles, and hence improving upon the computed feedforward signal.*

Remark 3.6 *In assumption 2.4.1 it is assumed that* $n(t)$ *has zero mean, which is more realistic than requiring the norm of* n *to tend to zero which means that* n *should tend to zero. Hence in the stochastic setting of assumption 2.4.1, it seems to be more convenient to use conditional expectations instead of norms. In that case the conditions in parts iii.a. and iv.a. of theorem 3.4 can also be loosened. However, such a stochastic setting seems to be less useful in practice, because k-step ahead prediction for large k is rather inaccurate as a stochastic process innovates each time sample. This limits the application of the developed algorithm in such a stochastic setting* [2].

Remark 3.7 *The condition stated in parts iii.b and iv.b of theorem 3.4 depends on the choice of the Kalman gain* K*. If* K *is chosen such that the eigenvalues of* $A_d - KC_d$ *are inside the unit circle (i.e.* $A_d - KC_d$ *is stable), e.g. by solving* K *from an algebraic Riccati equation, then convergence will take place, and the speed of convergence depends on the position of the eigenvalues inside the unit circle.*

The second comment on the developed algorithm is that the optimization of the feedforward signal should be performed each time either the reference trajectory or the disturbance signal changes. For example as mentioned in remark 3.5 most learning control schemes assume a fixed reference trajectory and a fixed disturbance signal during each cycle. In that case under certain convergence condtions, optimality of the feedforward signal is reached asymptotically (i.e. with the number of cycles tending to infinity), while the newly developed algorithm needs only one cycle to reach the optimal feedforward signal. Note again that in case $n(t)$ is a stochastic process the disturbance signal changes every sampling instant, which means that the optimization has to be performed each cycle.

4 Simulation Example

In this section a simulation example is given based on the theory of the foregoing sections. From remarks 3.5 and 3.6 it is clear that at this moment application of the developed algorithm in case of undermodeling and/or stochastic disturbances is limited. Hence to show the applicability of the method we consider in this simulation example case *iii.b.* of theorem 3.4. The true system is considered to be a SISO double integrator: $P_0(s) = 1/s^2$. After discretizing this system the 'bang-bang' type of input signal shown in figure 1 is applied to the undisturbed system resulting in a 3rd order smooth polynomial, which will be taken as the desired reference trajectory $y_r(t+k)$, $k = 1, \ldots, 61$. The constraints on the actuator output u are assumed to be

[2] Note that in model-based-predictive control a stochastic setting will cause less problems because in that case each sampling instant the optimization is performed, and at each sampling instant the prediction is corrected with new measurements.

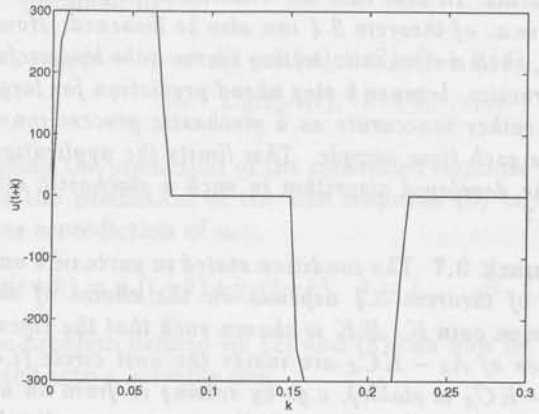

Fig. 1: Applied input signal $u(t+k)$

a limitation of its amplitude of ± 300 and let's specify that the system output may deviate only $\pm 1e^{-3}$ in amplitude over the last 10 samples of the reference trajectory, i.e. $y_r(t+k) - 1e^{-3} \leq y_0(t+k) \leq y_r(t+k) + 1e^{-3}$, $k = 52, \ldots, 61$. Moreover the output of the system is corrupted with a mixed deterministic/stochastic disturbance shown in figure 2. The deterministic part of the disturbance con-

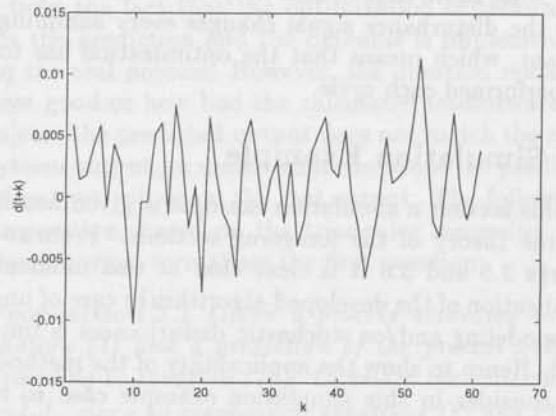

Fig. 2: Disturbance signal $d(t+k)$

sists of two sinusoids with frequencies 17 and 40 Hz. respectively, and a steady state error. The stochastic part constitutes normally distributed white noise with zero mean and covariance $\sigma_n^2 = 1e-5$. A spectrum of the composite disturbance is shown in figure 3; indeed the three deterministic peaks can clearly be distinguished from the random part. The level of the spectrum of the random part is approximately

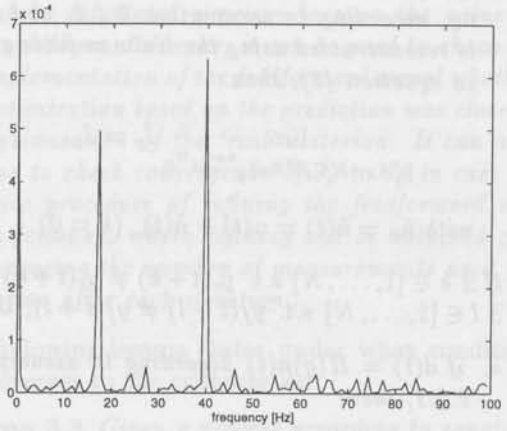

Fig. 3: Spectrum of the disturbance signal

$2e^{-5}$.

In order to simulate a real-time application, the disturbance signal is generated over a number l of cycles, $l = 1, \ldots, 10$), and the optimization of the feedforward signal is performed a number of times, each time taking a new disturbance realization into account, and also trying to improve the prediction of the disturbance by taking former disturbance realizations into account, compare remark 3.5.

According to section 2 the following assumptions are made:

- In the first iteration the set of measurements are taken to be $\{y_m(t-k), u(t-k)\}$, $k = 0, \ldots, 60$ to be $\{y_0(t-k), u(t-k)\}$, $k = 0, \ldots, 60$.
- As mentioned above, a model of the true system is taken to be the system itself, i.e. $\hat{P}_0(q) = P_0(q)$.
- As stated above, the desired reference trajectory is taken to be the one shown in figure 2.
- According to assumption 2.4.2, the disturbance is assumed to be generated by the following (continuous) autonomous system:

$$\dot{n} = \begin{bmatrix} \boxed{\begin{matrix} 0 & 1 \\ -a_1^2 & 0 \end{matrix}} & \begin{matrix} 0 & 0 \\ 0 & 0 \end{matrix} & \begin{matrix} 0 \\ 0 \end{matrix} \\ \begin{matrix} 0 & 0 \\ 0 & 0 \end{matrix} & \boxed{\begin{matrix} 0 & 1 \\ -a_2^2 & 0 \end{matrix}} & \begin{matrix} 0 \\ 0 \end{matrix} \\ \begin{matrix} 0 & 0 \end{matrix} & \begin{matrix} 0 & 0 \end{matrix} & \boxed{0} \end{bmatrix} n(t)$$

$$d(t) = [\,1\ 0\ 1\ 0\ 1\,]\, n(t),$$

where: a_1 and a_2 constitute the frequencies $2\pi 17$ and $2\pi 40$ respectively. Hence 2 states for

each sinusoid and 1 state for the steady state error[3] are needed to model the disturbance.

After discretization, this disturbance model is used to compute a Kalman filter by solving an algebraic Riccati equation. In turn this Kalman filter is used to reconstruct the disturbance state $n(t-k)$, $k = 0, \ldots, 60$ from the set of measurements. Thereafter, the state n at time t is used to predict the values of $d(t+k)$, $k = 1, \ldots, 61$. Using this prediction, the reference trajectory $y_r(t+k)$, $k = 1, \ldots, 61$ and the model $\hat{P}_0(q)$ a feedforward signal is computed according to formulas (11) and (12) by solving:

$$\hat{u}_{ff} = \min_{u(t+k)} \sum_{k=1}^{61} | \, y_r(t+k) - \hat{y}_0(t+k) \, |^2, \quad (21)$$

subject to:
$Au(\cdot) \leq b$

with A and b a matrix and a vector specifying the appropriate constraints on $u(t+k)$ and $y_0(t+k)$, $k = 1, \ldots, 61$. This problem can be solved numerically using *quadratic programming* techniques. If a solution exists it is always optimal due to the convexity of the problem. Figure 4 shows this computed optimal feedforward signal. It is seen that the input signal bumps against its constraints several times. A spectrum of this signal also shows emphasis on the frequencies of the disturbance signal (not shown here). Figure 5 shows the difference between the reference trajectory y_r and the output $\hat{y}_0$, simulated

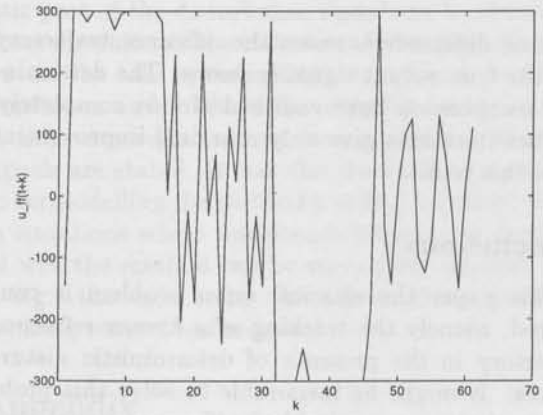

Fig. 4: Computed optimal feedforward signal u_{ff}; 1st iteration

[3]Notice that this state is precisely the model of an integrator which agrees with the well known fact that a controller should inhibit an integrator in order to cancel steady state disturbances

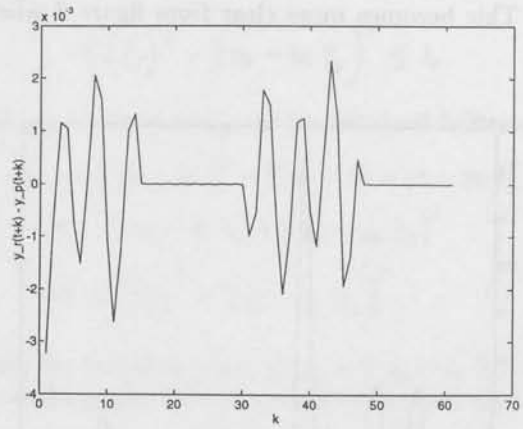

Fig. 5: Simulated difference between $y_r(t+k)$ and $\hat{y}_0(t+k)$

with the computed feedforward signal and the predicted disturbance signal. Wee see that this output perfectly matches its specifications.The constraints on the last 10 samples of the reference trajectory are perfectly fulfilled.

However, in practice the predicted output will not exactly match the true output. This is simulated by also showing the difference between the reference signal and the true output induced by the feedforward signal and the *true* disturbance signal including the stochastic part and the prediction error. This difference is shown in figure 6. Though

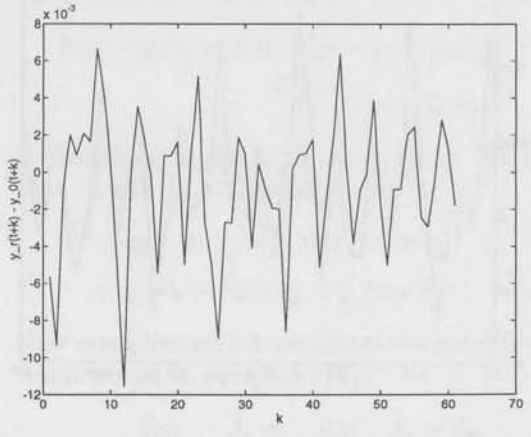

Fig. 6: True difference between $y_r(t+k)$ and $y_0(t+k)$

this difference is not as small as the simulated difference, the influence of the deterministic components

has tremendously decreased (about 100 times smaller). This becomes more clear from figure 7 where

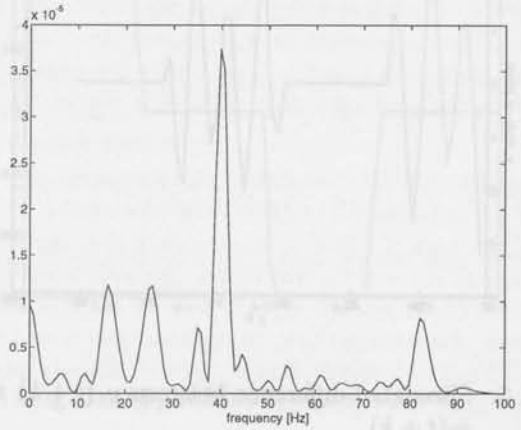

Fig. 7: Spectrum of the true difference between $y_r(t+k)$ and $y_0(t+k)$; 1st iteration

the spectrum of the true difference between y_r and y_0 is shown. It is seen that after only one iteration, the residual disturbance has almost reduced within the level of the stochastic part of the original disturbance.

This succes is only due to the fact that the prediction of the deterministic part of the disturbance matches the true deterministic disturbance, as was shown in section 3. Figure 8 shows the true disturbance, its deterministic component and the prediction of the deterministic part. It is seen that the prediction is a rather good description of the true disturbance, despite the influence of the stochastic part. However, by using more iterations, the prediction might be better as the estimation has not converged completely yet. After 2 iterations the prediction almost equals the true deterministic part of the disturbance (not shown). It is seen that the estimation has converged within very acceptable bounds. This is emphasized by figure 9 where the spectrum of

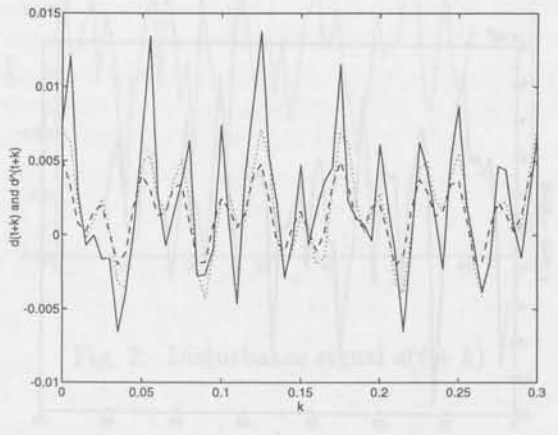

Fig. 8: Real disturbance(–), deterministic part(···) and predicted one(- -); 1st iteration

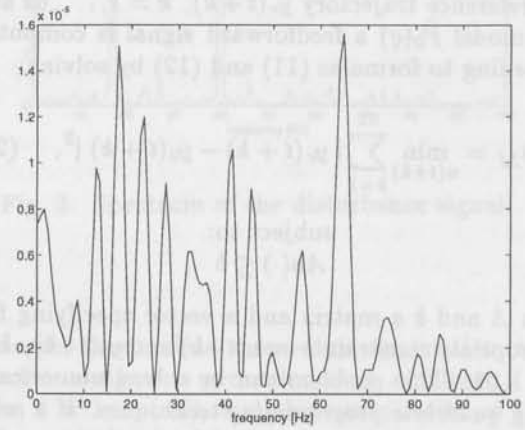

Fig. 9: Spectrum of the true difference between $y_r(t+k)$ and $y_0(t+k)$; 2nd iteration

the true difference between the reference trajectory and the true output signal is shown. The deterministic components have vanished almost completely. Further iterations give only marginal improvement upon this result.

Conclusions

In this paper the classical servo problem is considered, namely the tracking of a known reference trajectory in the presence of deterministic disturbances. It might be favourable to solve this problem by designing a suitable feedforward signal that leaves the closed loop system dynamics unaltered. Given this problem an algorithm has been developed which not only solves the problem but also optimizes the problem under constraints of both input and output signals. Prediction of the deterministic components of the disturbance is used to design a feedforward signal that minimizes the difference between a desired reference signal and a prediction of the system output according to some criterion. A simulation example showed the action of the procedure in case of deterministic disturbances and without taking undermodelling into account.

Compared with the classical 'servo-compensator' and the 'repetitive controller' in case periodic dis-

turbances are considered, the newly developed algorithm differs in implementation aspects. Whereas the former two techniques extend the closed loop *dynamics*, the latter one yields only the implementation of a feedforward *signal*. Compared with learning and repetitive control techniques, the newly proposed technique is able to handle not only periodic disturbances (with period-time equal to the cycle time), but also a general class of disturbances according to assumption 2.4, though in case of stochastic disturbances its application is limited as the prediction of stochastic disturbances over large intervals is not very good in general. Moreover an optimal feedforward signal is computed at once, while optimality in case of learning control is obtained asymptotically. Like model-based-predictive control techniques, the proposed algorithm can easily handle constraints on input- and output signals. Thus it can be an easy tool for trading-off constraints and performance specifications, always computing an optimal solution. Whether the optimal solution based on a prediction of the system output is an optimal solution in practice, heavily depends on the quality of the prediction. If the prediction matches the true output signal, the calculated optimal solution is also optimal for the true output signal. If the prediction does not completely match the true signal, still an extensive reduction of the deterministic part of the disturbance signal can be obtained. Formal results on the influence of the prediction error on the true optimization are derived, and also conditions under which the criterion based on predictions converges to the criterion based on the true signals are stated. It was also shown that in case of undermodelling the method has limited value. Only in situations where undermodelling can be predicted well the method can be succesfully applied; this is e.g. the case under the assumptions stated in learning control techniques.

Appendix

Proof of proposition 3.1

Consider the criterion $\hat{J}_p$ given by equation (11):

$$\hat{J}_p = \| y_r - \hat{y}_0 \|_p^p = \| y_r - y_0 + y_0 - \hat{y}_0 \|_p^p.$$

Now raising both sides to the power $1/p$ and using the triangular inequality gives:

$$\begin{aligned}\left(\hat{J}_p\right)^{\frac{1}{p}} &\leq \| y_r - y_0 \|_p + \| y_0 - \hat{y}_0 \|_p \\ &= (J_p)^{\frac{1}{p}} + \| y_0 - \hat{y}_0 \|_p.\end{aligned}$$

Rearranging this equation and raising both sides to the power p gives the lowerbound for J_p:

$$\left(\left(\hat{J}_p\right)^{\frac{1}{p}} - \| y_0 - \hat{y}_0 \|_p\right)^p \leq J_p.$$

The upperbound on J_p can be obtained likewise:

$$\begin{aligned}J_p &= \| y_r - y_0 \|_p^p = \| y_r - \hat{y}_0 + \hat{y}_0 - y_0 \|_p^p \\ &\leq \left(\| y_r - \hat{y}_0 \|_p + \| \hat{y}_0 - y_0 \|_p\right)^p \\ &= \left(\left(\hat{J}_p\right)^{\frac{1}{p}} + \| \hat{y}_0 - y_0 \|_p\right)^p.\end{aligned}$$

Using the fact that $\| \hat{y}_0 - y_0 \|_p = \| y_0 - \hat{y}_0 \|_p$ completes the proof of the result stated in equation (13).

Proof of theorem 3.4

i. $\boxed{\hat{y}_c = y_c, \hat{y}_f = y_f \Rightarrow \hat{J}_p = J_p}$

This part is rather trivial and can be obtained by substituting equation (10) into equation (11):

$$\hat{J}_p = \| y_r - \hat{y}_0 \|_p^p = \| y_r - \hat{y}_c - \hat{y}_f \|_p^p.$$

Now using the fact that $\hat{y}_c(t+k) = y_c(t+k)$ and $\hat{y}_f(t+k) = y_f(t+k)\ \forall k \in [1, \ldots, N]$ yields the result stated in equation (15):

$$\| y_r - y_c - y_f \|_p^p = \| y_r - y_0 \|_p^p = J_p.$$

ii. $\boxed{\hat{y}_c \neq y_c, \hat{y}_f = y_f \Rightarrow \lim_{\|\Delta_0\|_p \to 0} \hat{J}_p = J_p}$

Substituting equation (10) in the expression for the prediction error gives:

$$\begin{aligned}\| y_0 - \hat{y}_0 \|_p &= \| y_c + y_f - \hat{y}_c - \hat{y}_f \|_p \\ &\overset{\hat{y}_f = y_f}{=} \| y_c - \hat{y}_c \|_p.\end{aligned}$$

Substituting equation (4) and using the fact that P_0 and $\hat{P}_0$ are linear gives:

$$\begin{aligned}\| y_0 - \hat{y}_0 \|_p &= \| P_0 u - \hat{P}_0 u \|_p \\ &= \| (P_0 - \hat{P}_0) u \|_p = \| \Delta_0 u \|_p.\end{aligned}$$

Now using lemma 3.3 completes the proof of the result stated in equation (16):

$$\lim_{\|y_0 - \hat{y}_0\|_p \to 0} \hat{J}_p = \lim_{\|\Delta_0\|_p \to 0} \hat{J}_p = J_p.$$

iii. $\boxed{\begin{array}{c}\hat{y}_c = y_c, \hat{y}_f \neq y_f \Rightarrow a.\ \lim_{\|E_k n\|_p \overset{k=1..N_0}{\longrightarrow}} \hat{J}_p = J_p \\ b.\ \lim_{\|(A_d - KC_d)^k \tilde{n}_0\|_p \overset{k=1..N_0}{\longrightarrow}} \hat{J}_p = J_p\end{array}}$

a. Substituting equation (10) in the expression for the prediction error and using the fact that $\hat{y}_c = y_c$, gives:

$$\| y_0 - \hat{y}_0 \|_p = \| y_c + y_f - \hat{y}_c - \hat{y}_f \|_p \overset{\hat{y}_c = y_c}{=} \| y_f - \hat{y}_f \|_p. \quad (22)$$

Substituting equation (6) in equation (22) gives:

$$\| y_0 - \hat{y}_0 \|_p \overset{k=1..N}{=} \| d - \frac{F_k}{C} d_0 \|_p \overset{k=1..N}{=} \| d - d + E_k n \|_p \overset{k=1..N}{=} \| E_k n \|_p,$$

with: $d_0 = d(t)$ $(k = 0)$. Again using lemma 3.3 gives the result stated in equation (17):

$$\lim_{\|y_0 - \hat{y}_0\|_p \to 0} \hat{J}_p = \lim_{\|E_k n\|_p \overset{k=1..N}{\to} 0} \hat{J}_p = J_p.$$

b. From equation (9) it follows that:

$$y_f(t+k) - \hat{y}(t+k) = C_d n(t+k) - C_d \hat{n}(t+k).$$

Substituting this expression in equation (22) and denoting $\tilde{n}(t+k) = n(t+k) - \hat{n}(t+k)$, gives:

$$\| y_0 - \hat{y}_0 \|_p = \| C_d \tilde{n} \|_p.$$

Using equation (8) it follows that:

$$\| y_0 - \hat{y}_0 \|_p \overset{k=1..N}{=} \| C_d (A_d - K C_d)^k \tilde{n}_0 \|_p$$

where $\tilde{n}_0 = \tilde{n}(t)$ $(k = 0)$. Finally using lemma 3.3 the desired result of equation (18) is obtained:

$$\lim_{\|y_0 - \hat{y}_0\|_p \to 0} \hat{J}_p = \lim_{\|(A_d - K C_d)^k \tilde{n}_0\|_p \overset{k=1..N}{\to} 0} \hat{J}_p = J_p.$$

iv.

$$\hat{y}_c \neq y_c, \hat{y}_f \neq y_f \Rightarrow$$
$$a.\ \lim_{\|\Delta_0\|_p, \|E_k n\|_p \overset{k=1..N}{\longrightarrow} 0} \hat{J}_p = J_p$$
$$b.\ \lim_{\|\Delta_0\|_p \|(A_d - K C_d)^k \tilde{n}_0\|_p \overset{k=1..N}{\longrightarrow} 0} \hat{J}_p = J_p$$

a., b. This proof can easily be constructed by combining the proofs of part *ii.* and part *iii.*.

References

Arimoto, S., S. Kawamura and F. Miyazaki (1984). Bettering Operation of Robots by Learning. *J. Robotic Systems, Vol. 1*, 123-140.

Bhat, S.P. and D.K. Miu (1990). Precise point-to-point positioning control of flexible structures. *Trans. ASME J. Dynamic Systems, Measurement, and Control, Vol. 112*, 667-674.

Bhat, S.P. and D.K. Miu (1991). Solutions to point-to-point control problems using Laplace transform technique. *Trans. ASME J. Dynamic Systems, Measurement, and Control, Vol. 113*, 425-431.

Chew, K.K. and M. Tomizuka (1990). Steady-state and stochastic performance of a modified discrete-time prototype repetitive controller. *Trans. ASME J. Dynamic Systems, Measurement, and Control, Vol. 112*, 35-41.

Clarke, D.W., P.S. Tuffs and C. Mohtadi (1985). Self-tuning control of a difficult process. *Proc. 7th IFAC Symp. Ident. and System Param. Est.*, York, U.K., pp. 1009-1014.

Cutler, C.R. and B.L. Ramaker (1980). Dynamic matrix control – a computer control algorithm". *Proc. JACC*, San Francisco, CA.

Davison, E.J. (1972). The output control of linear time-invariant multivariable systems with unmeasurable arbitrary disturbances. *IEEE Trans. Automat. Contr., AC-17*, 621-630.

Francis, B.A. and W.M. Wonham (1976). The internal model principle of control theory. *Automatica, 12*, 457-465.

Kavli, T. (1992). Frequency domain synthesis of trajectory learning controllers for robot manipulators. *J. Robotic Systems, 9*, 663-680.

Keyser, R.M.C. de, and A.R. van Cauwenberghe (1985). Extended prediction self-adaptive control. *Proc. 7th IFAC Symp. Ident. and System Param. Est.*, York, U.K., pp. 1255-1260.

La Bastide, S.L.C. (1994). *Exact Point-to-Point Control of Periodically Disturbed Mechanical Systems: a Survey of Literature.* Delft Univ. Techn./Philips Research Lab., The Netherlands, Unclassified Report 008/94.

Moore, K.L., M. Dahleh and S.P.Bhattacharyya (1992). Iterative learning control: a survey and new results. *J. Robotic Systems, 9*, no. 5, pp. 563-594.

Richalet, J., A. Rault, J.L. Testud and J. Papon (1978). Model predictive heuristic control: applications to industrial processes. *Automatica, 14*, 413-428.

Richalet, J. and J. Papon (1985). Industrial applications of internal model control. *Proc. 7th. IFAC-IMACS Conf. Digital Comp. Applic. to Process Control*, Vienna, Austria.

Singer, N.C. and W.P. Seering (1989). Design and comparison of command shaping methods for controlling residual vibration. *Proc. 1989 IEEE Conf. Robotics and Automation*, pp. 888-893.

Tomizuka, M. (1987). Zero phase error tracking algorithm for digital control. *Trans. ASME J. Dynamic Systems, Measurement, and Control, Vol. 109*, 65-68.

CONTENTS Volume 7, December 1994

TU Delft
Delft University of Technology